REPORT DOCUMENTATION PAGE

Form Approved OMB No. 0704-0188

PLEASE DO NOT RETURN YOUR FORM TO THE ABOVE ADDRESS.

1. REPORT DATE *(DD-MM-YYYY)*	2. REPORT TYPE	3. DATES COVERED *(From – To)*
13-10-2006	Final Report	1 April 2003 - 03-Apr-07

4. TITLE AND SUBTITLE

Artificial Ionospheric Turbulence and Radio Wave Propagation (Sura - HAARP)

5a. CONTRACT NUMBER
FA8655-03-D-0001, Delivery Order 0001

5b. GRANT NUMBER

5c. PROGRAM ELEMENT NUMBER

6. AUTHOR(S)

Dr. Vladimir L Frolov

5d. PROJECT NUMBER

5d. TASK NUMBER

5e. WORK UNIT NUMBER

7. PERFORMING ORGANIZATION NAME(S) AND ADDRESS(ES)

Radio Physical Research Institute (NIRFI)
25 Bol'shaya Pecherskaya St
Nizhny Novgorod 603600
Russia

8. PERFORMING ORGANIZATION REPORT NUMBER

N/A

9. SPONSORING/MONITORING AGENCY NAME(S) AND ADDRESS(ES)

EOARD
PSC 821 BOX 14
FPO AE 09421-0014

10. SPONSOR/MONITOR'S ACRONYM(S)

11. SPONSOR/MONITOR'S REPORT NUMBER(S)
CRDF 02-9001

12. DISTRIBUTION/AVAILABILITY STATEMENT

Approved for public release; distribution is unlimited.

13. SUPPLEMENTARY NOTES

14. ABSTRACT

This report results from a contract tasking Radio Physical Research Institute (NIRFI) as follows: The objectives of the project were: (i) integrated experimental, theoretical and computer simulation studies of non-linear plasma phenomena, produced in the upper ionosphere by powerful HF radiation and giving rise to plasma density irregularities with a wide range of cross-field (relatively to geomagnetic field lines) scales from centimeters to tens of kilometers, (ii) investigation of an influence of these irregularities on characteristics of HF and VHF radio waves passed through the ionosphere disturbed volume, and (iii) control for long distance propagation of HF radio waves through an ionosphere wave-guide channel by means of radio wave scattering from small-scale field-aligned irregularities.

15. SUBJECT TERMS

EOARD

16. SECURITY CLASSIFICATION OF:			17. LIMITATION OF ABSTRACT	18, NUMBER OF PAGES	19a. NAME OF RESPONSIBLE PERSON
a. REPORT	b. ABSTRACT	c. THIS PAGE			GEORGE W YORK, Lt Col, USAF
UNCLAS	UNCLAS	UNCLAS	UL	164	19b. TELEPHONE NUMBER *(Include area code)* +44 (0)20 7514 4354

FINAL REPORT

(1) Title Page

Title: **Artificial Ionospheric Turbulence and Radio Wave Propagation (Sura – HAARP)**

Project Director: Vladimir Leont'evich Frolov

Institute: Radiophysical Research Institute (NIRFI), 603950 Russia, Nizhny Novgorod, B.Pecherskaya St. 25.

CRDF project number: RPO-1334-N0-02.

Reporting period: August 2003 – November 2006.

2) Nomenclature Page

AIT – artificial ionospheric turbulence;
PW – pump wave;
ASSI – artificial small-scale field-aligned irregularities (striations);
IDV – ionosphere disturbed volume;
MOF_F – maximum observed frequency for F-region propagation;
LFM – linear frequency modulation;
DFS – Doppler frequency shifts;
SEE – stimulated electromagnetic emission;
d-SEE – diagnostic SEE;
Δf^-, Δf^+ – negative and positive frequency shifts in the SEE spectra relative to PW frequency;
nf_{ce} – gyroharmonic frequency (n – gyroharmonic number, $f_{ce} \approx 1.3 – 1.35$ MHz in the ionospheric F_2 layer over the Sura facility).

Emission components in SEE spectra:

DM – downshifted maximum;
BC – broad continuum;
NC_{th} – thermal narrow continuum;
NC_p – ponderomotive narrow continuum;
BUM – broad up-shifted maximum;
BUM-1, BUM-2 – first and second BUM components;

(3) Summary Page

The main objectives of the project are: (1) integrated experimental, theoretical and computer simulation studies of non-linear plasma phenomena, produced in the upper ionosphere by powerful HF radiation and giving rise to plasma density irregularities with a wide range of cross-field (relatively to geomagnetic field lines) scales from centimeters to tens of kilometers, (2) investigation of an influence of these irregularities on characteristics of HF and VHF radio waves passed through the ionosphere disturbed volume (IDV), and (3) control for long distance propagation of HF radio waves through an ionosphere wave-guide channel by means of radio wave scattering from small-scale field-aligned irregularities (the SURA–HAARP experiment). In the framework of the project 8 heating campaign at the Sura facility have been carried out in all. Obtained in this campaign experimental data as well as data obtained in earlier performed measurements allowed to study in detail the following points: (i) space distribution of small-, middle-, and large-scale irregularities in the IDV; (ii) peculiarities of both artificial ionosphere turbulence (AIT) evolution and transport processes in the upper (F-region) ionosphere when short pulse pumping is used for ionosphere modification; (iii) influence of small-scale field-aligned irregularities (striations) on generation of stimulated electromagnetic emission (SEE); (iv) some features of the magnetic zenith effect; (v) ionospheric effects of geomagnetic disturbances; (vi) peculiarities of HF radio wave long distance propagation. Using the software elaborated for modeling of radio paths for the SURA–HAARP experiment, necessary calculations and estimations for this experiment have been done. In March and May 2006 two sessions of measurements in the framework of the SURA–HAARP experiment were carried out.

Besides, it was performed experiments aimed at the study of features of artificial ionosphere disturbances, which are generated by nonlinear mixing of two HF waves at frequencies higher than F_2-region critical frequency (f_{0F2}) but when difference between them is below of f_{0F2} (ionosphere heating at the local plasma frequency by beating two high-power electromagnetic waves). In these experiments the bispectral method was used for the spectral analysis of received signals. New experiments aimed at the study of AIT features when additional X-mode pumping is used were also performed.

Experimental results, obtained in the framework of the project, give new knowledge about AIT features and allow elaborating in more details its empirical models, as well as to study peculiarities of HF radio wave long distance propagation under different ionospheric conditions.

(4) Introduction

It should be mentioned that the work on the project is based on previously performed investigations of AIT features, which have allowed to establish dependences of low-frequency AIT properties on PW power, frequency, and polarization, on duration of PW radiation, as well as on turbulence gyrofeatures. Basing on these results some opportunities to control of spectral characteristics of artificial low-frequency AIT in heating experiments were suggested by Frolov V.L. (Control of spectral characteristics of artificial low-frequency ionosphere turbulence. // International J. Geomagnetism and Aeronomy, 2003. V.4, No.2, pp.159-165). The following three tasks were announced as the main objectives of the presented project:

T1. Integrated experimental and theoretical studies of non-linear plasma phenomena, produced in the upper ionosphere by powerful HF radiation and giving rise to plasma density irregularities in a wide range of cross-field (relatively to geomagnetic field lines) scales from centimeters to tens of kilometers.

T2. Investigation of the influence of these irregularities on characteristics of HF and VHF radio waves passed through the IDV.

T3. Control of long distance propagation of HF radio waves through an ionosphere wave-guide channel by means of radio wave scattering from small-scale field-aligned irregularities (the SURA–HAARP experiment).

It is clear that the systematic creation of AIT with controllable and repeatable properties in the ionosphere, irradiated by HF powerful radio waves, provides an advanced approach for solving many problems (including announced above), as well as possibilities to develop new radio physical diagnostics and to model a set of natural processes. At present the ionosphere is increasingly used as a nature plasma laboratory in which active plasma experiments are performed. The major attention of the ionospheric plasma lies in its large degree of homogeneity. Besides, the ionospheric plasma laboratory may be regarded as wall-less if the ionospheric scale length largely exceeds the scale lengths of the respective processes under consideration. This condition is usually satisfied.

Basing on numerous investigations performed till now, it has been well stated that the AIT occurs due to the development of ponderomotive and thermal (resonance) parametric instabilities, and involves HF electrostatic plasma waves (Langmuir, upper hybrid, electron Bernstein) and LF disturbances, in particular field-aligned plasma density irregularities in a wide range of cross-field scales ($l_\perp$) from centimeters to tens of kilometers. The AIT is manifested in a number of phenomena observable from the ground. This opens up opportunities to study fundamental properties of turbulence generation and evolution in magnetized plasmas and to develop new technologies for monitoring of the Earth ionosphere. Furthermore, the AIT is easy adaptable to modeling a set of natural processes observing in space plasmas. Many effects occur in ionosphere heating experiments. They comprise: (i) generation of plasma density irregularities together with growth of the electron temperature in the IDV and expansion of plasma perturbations along geomagnetic field lines, (ii) anomalous absorption and phase variations of HF probing waves sounding the IDV, as well as scattering and refraction of radio waves propagating through it, (iii) the electron acceleration by the AIT, which causes, in its turn, optical and UHF radio emissions and additional ionization of the ionosphere plasma, (iv) generation of the SEE, occurring as a result of conversion of HF-induced electrostatic waves into electromagnetic waves, etc. These phenomena are closely connected with each other and require integrated studies. It should be noted that dramatic changes of the AIT features is observed when the pump frequency is close to an electron cyclotron harmonic frequency. They are of special interest because to date many AIT gyro features are not well understood yet.

The project is related to the decision of the following problems:

1) To develop, on the basis of experimental data, advanced physical models for the generation mechanisms of the irregularities with scales from about of one meter to tens of kilometers with consideration of a mutual influence of irregularities with different scale lengths on their generation and of peculiarities of their formation when: (i) the pump frequency is close to an electron cyclotron harmonic frequency, (ii) generation of irregularities is carried out under underdense heating conditions, and (iii) X-mode powerful wave is used for pumping.
2) To determine scopes for the control over the spatial spectrum of the artificial irregularities employing elaborated complex schemes for ionosphere pumping.
3) To study transport processes in the upper ionosphere, leading to expansion of low-frequency turbulence up and down from its generation region.
4) To apply modern data processing techniques with the aim to obtain better time, frequency, or space resolution in ionosphere modification experiments.
5) To study, using the Sura and HAARP facilities, features of long distance propagation of HF radio waves in an ionosphere wave-guide channel employing radio wave scattering from small-scale field-aligned irregularities (ASSI) for excitation of a wave-guide and its control.

The work on all these problems is subject to the goal: to give better understanding of AIT properties and to study an influence of the AIT on HF and VHF radio wave propagation.

(5) Technical Description and Work Accomplished

During the reported period 8 heating campaigns at the Sura facility were performed in all, description of which is given in five Technical Reports presented earlier. Experiments performed during these campaigns were focused on the study of different AIT features including the study of the space structure of the IDV using a variety of diagnostic methods for ionosphere probing. For AIT diagnostic the following methods and techniques were used in our experiments:

(i) tomography and scintillation measurements using satellite's beacons;
(ii) ionosound measurements;
(iii) sounding of the IDV by O-mode and X-mode probing waves;
(iv) stimulated electromagnetic emission measurements;
(v) field-aligned scattering measurements;
(vi) oblique chirp-sounding of the IDV;
(vii) artificial airglow measurements;
(viii) bispectral method for the analysis of signals received from the IDV by multi-frequency pumping.

Below the main results obtained in the framework of the project are presented with short comments. All of them are divided into five groups:

(I) Features of artificial ionosphere turbulence (AIT).
(II) Radio tomography and scintillation studies of ionosphere electron density modification.
(III) Features of transport processes in the upper ionosphere.
(IV) Results of field-aligned scattering experiments.
(V) Results of the SURA–HAARP experiment.

Most of results obtained in the framework of the project are already published (see List of References in #8). It is why results presented below are given only with short comments.

5.1 Features of artificial ionosphere turbulence (AIT)

5.1.1. Features of the ponderomotive (NC_p) and thermal (NC_{th}) narrow continuum components in SEE spectra

Almost two decades ago it was discovered that a powerful HF heater wave of ordinary polarization, injected vertically from the ground into the ionosphere F-region, gives rise to secondary electromagnetic waves, occurring as a result of various wave-plasma processes, including the conversion of HF electromagnetic waves into electrostatic waves and vice versa. Emissions of this type were termed Stimulated Electromagnetic Emissions (SEEs). By now the SEE has become a very useful tool for the study of nonlinear processes in ionospheric interaction experiments, because both the short time scale ponderomotive nonlinearities, giving rise to Langmuir turbulence, and the long time scale thermal nonlinearities, leading to the excitation of large- and small-scale plasma density irregularities, are involved in the SEE generation. Once the generation mechanism of a SEE component is identified, one can obtain information on both the background state of the ionospheric plasma and the nonlinear processes in question by observing the SEE evolution and variations of the SEE features under different conditions realized in the experiments. The SEE has also been shown to be of potential importance as a diagnostic of geophysical processes.

The major emission components on the downshifted side of the SEE spectra are the "downshifted maximum" (DM), downshifted from the pump frequency, f_0, by approximately $\Delta f^- \approx 9 – 15$ kHz, the "broad continuum" (BC), extending up to $\Delta f^- \approx 60 – 120$ kHz below the DM, and the "narrow continuum" (NC), occurring in the frequency range between the DM and the pump frequency, showing a rapid decrease of the intensity with increasing Δf^-. The major components on the up-shifted side are the "up-shifted maximum" (UM), which is a narrow peak at frequencies of about $\Delta f^+ \approx 7 – 12$ kHz, the "broad up-shifted maximum" (BUM), occurring in the SEE spectra at frequency shifts $\Delta f^+ \approx 15 – 150$ kHz when f_0 is close to or slightly above harmonics n of the electron cyclotron frequency f_{ce} ($f_{ce} \approx 1.3 – 1.35$ MHz in the F layer over the Sura facility, depending on the pump wave reflection height, $h_{ref} \approx 200 – 300$ km), and the "broad up-shifted structure" (BUS), occurring at frequency shifts $\Delta f^+ \approx 10 – 100$ kHz for f_0 far above nf_{ce}. Here and below we use the notations Δf^- and Δf^+ to denote, respectively, negative and positive frequency shifts in the SEE spectra relative to the pump wave (PW) frequency f_0.

In contrast to the DM, BC, BUM, and BUS, for which empirical models have been elaborated in the past few years; the study of the NC has not been completed yet. This is because several different emission components were initially taken as one component named the "continuum". Later it was found that in the initial stage of pumping (during a few tens of milliseconds following HF wave turn on in the plasma) an emission component occurs in the lower sideband of the pump wave with an intensity strongly (~ 1 – 2 dB/kHz) decreasing with increasing downshift from f_0. The generation of this SEE component is associated with the development of the parametric decay instability (PDI). This emission component was named the ponderomotive NC, NC_p, implying that it is produced by the ponderomotive nonlinearity. Further, the NC, observed in the stationary SEE spectra, is produced by the thermal parametric (resonance) instability (TPI). This emission component was named as the thermal NC, NC_{th}. Until recently, empirical models for these SEE components have not been elaborated yet. Fig. 1 in [1] (see list of references in section 8 of the report and pdf-files of the published papers attached to the report) demonstrates temporal evolution of SEE spectrum and its transition from ponderomotive emission components to thermal components.

Basing on experiments carried out at the Sura facility [1], the following empirical model for the NC_p has been elaborated.

1. The generation of the NC_p occurs in the plasma resonance layer near the PW reflection altitude due to the PDI. A significant enhancement of the NC_p generation is observed when the pump power is above of about $P_{eff} \approx 10 - 15$ MW ERP. Excitation of the TPI and of field-aligned small-scale irregularities (striations) of thermal origin leads to a suppression of the NC_p as a result of anomalous absorption of HF energy a few km below the PW reflection height.
2. After the PW switch-on in the plasma and the development of the striction self-action a few milliseconds later, the NC_p intensity increases rapidly, having a maximum in the time interval 2 – 20 ms, depending strongly on pump power and ionospheric conditions.
3. At the initial stage of the NC_p development its maximum spectral intensity at $\Delta f^- \approx 4$ kHz for $P_{eff} \geq 30$ MW ERP is more than 10 dB higher than the maximum spectral intensity of the DM, which is the most prominent emission component in the stationary SEE spectrum. In the quasi-steady state of the NC_p development its spectrum often has a nearly exponential form with a constant slope of about 1 dB/kHz in the frequency shift range $\Delta f^- \leq 20 - 30$ kHz. The spectral width of the NC_p increases with growing PW power.
4. The magnitude of the e-folding decay time, τ_d, for the NC_p varies over a wide range from ~ 0.7 ms to 4 – 5 ms, depending on PW power, frequency shift, pumping scheme, stage and level of the AIT development, and showing strong diurnal variations. The maximum value, $\tau_d \approx 5$ ms, which is in good agreement with the damping time of Langmuir waves by Coulomb collisions, is observed under nighttime conditions when a rather low power, $P_{eff} \leq 10$ MW ERP, is used for the pumping.
5. Experiments performed near an electron cyclotron harmonic have shown that the plasma waves involved in the NC_p generation do not possess any significant gyro features, in distinction to the thermal SEE components (DM and BC), which show a crucial dependence of their properties on the PW frequency when the latter is close to a gyroharmonic frequency. This result can be considered as additional evidence that the NC_p is generated slightly below the PW reflection level where Langmuir waves propagate almost along geomagnetic field lines and thus do not depend strongly on the geomagnetic field.

The generation of the NC_p may be interpreted in terms of the strongest products of the PDI through the following processes:

a) scattering of the monochromatic electromagnetic O-mode pump wave into primary Langmuir waves from ion-acoustic waves;
b) decay of the primary Langmuir waves into secondary Langmuir waves through the cascading process in an electrostatic PDI which is responsible for the formation of the Langmuir turbulence spectrum;
c) re-conversion of the secondary Langmuir waves into electromagnetic waves (SEE) escaping the ionosphere disturbed volume.

It should be mentioned that a quantitative analysis of the NC_p generation has not been performed yet.

Basing on experiments carried out at the Sura facility [2], the following empirical model for the NC_{th} has been elaborated.

1. The generation of NC_{th}, as well as DM and BC, occurs due to the thermal (resonance) parametric instability (TPI) somewhat below the PW reflection height in a region where PW frequency is of about of the upper hybrid resonance frequency. Fig. 1 in [2] demonstrates the spectral form of the NC_{th}. Its generation is accompanied by excitation of field-aligned small-scale irregularities (striations). Integral intensity of the NC_{th} is close to or even higher than DM integral intensity. The basic characteristics of the NC_{th} are very similar to analogous DM ones. Among them are: magnitudes of their thresholds;

strong influence of striations on their features; dependences of their intensity on PW frequency, PW power, and antenna beam position relatively to the geomagnetic field; gyro features; typical times of their development after PW switch-on; generation of these SEE components when PW frequency is slightly below of the F2-region critical frequency (f_{0F2}) but the upper hybrid resonance frequency for the PW still remains below f_{0F2}.

2. The intensity of the NC_{th}, as for DM, has a maximal level in a PW frequency range from 5 to 7 MHz and it is fast reduced outside of this range (see Fig. 2 in [2]).
3. The form of NC_{th} spectra is often very similar to the spectral form of DM and its satellites (DM1 and DM2) for their low-frequency flanks.
4. When a PW frequency is very close to a gyroharmonic frequency and suppression of TPI and SEE thermal components (DM, BC, and NC_{th}) are observed, in a frequency range below the PW frequency it is registered the NC_p.

The generation of the NC_{th} may be interpreted through the following processes:

a) scattering of the monochromatic electromagnetic O-mode pump wave into primary upper hybrid waves from striations;
b) decay of the primary upper hybrid waves into secondary upper hybrid waves through the cascading process in an electrostatic PDI which is responsible for the formation of the upper hybrid turbulence spectrum;
c) re-conversion of the secondary upper hybrid waves into electromagnetic waves (SEE) escaping the ionosphere disturbed volume.

It should be mentioned that a quantitative analysis of the NC_{th} generation has not been performed yet.

The results are presented in [1,2,25] (according to the list of references presented in section 8 of the report).

5.1.2. The study of the aspect angle dependence for some SEE components

In this section of the report it is presented results of measurements of SEE features performed at the Sura heating facility in experiments when the HF pump beam was tilted in the geomagnetic field plane with 2- or 4-degree-step from 20° north to 20° south. Under conditions of our measurements this angle range includes the geographic zenith (vertical), the geomagnetic zenith (~19°), and the critical (Spitze) angle (~6°).

It has been revealed (see Fig. 1 in [3]) that the greatest emission intensity for such SEE components as the down-shifted maximum (DM) and the broad continuum (BC) was observed when the pump wave (PW) was beamed to 8 – 12° southward from the vertical, where the strongest striation intensity is also observed (Zyuzin V.A. et al. // Izv. Vuzov Radiofizika, 1988. Vol. 31, pp.622-624 (in Russian)). Performed calculations have shown that the PW, launched at the angle of ~10° southward from the vertical, will propagate along the geomagnetic field line at the upper hybrid resonance height. In such a situation amplification of plasma pumping takes place due to the magnetic zenith effect (Gurevich A.V., Zubin K.P., and Carlson H. // Izv. Vuzov Radiofizika, 2005. Vol. 48, pp.722-787 (in Russian)).

As it was stated by Frolov V.L. et al. (Phys. Rev. Lett., 1998. Vol.81, pp.1630-1633), the BUM actually consists of two separate components, BUM-1 and BUM-2, the first of which is generated in the immediate vicinity of an electron cyclotron harmonic frequency when suppression of striation generation takes place. The second component is generated when PW frequency is higher than a gyro harmonic frequency. Basing on experimental results, obtained in our pump beam scanning experiments in the cases when PW frequency was close to or slightly

higher than 4^{th} or 5^{th} electron cyclotron harmonic frequency, it was found that the BUM-1 is generated only if the angle of the pump beam is not larger than 8° from the vertical, whereas BUM-2 does not show any evident angular dependence in the angle range used. Taking into account of 10-degree pump beam width, this angle is in reasonable good agreement with the critical angle. The latter gives strong ground to suppose that the BUM-1 is generated only if the O-mode PW reaches the plasma resonance height. That can be realised only under conditions when the PW does not exert strong anomalous absorption on striations. Taking into consideration all mentioned above, it is reasonable to suppose that a mechanism of the BUM-1 generation has to be connected with the parametric decay instability development in the plasma resonance region.

These results are presented in [3,13].

5.1.3. Effects observed by a nonlinear interaction of two O-mode powerful radio waves in magnetized plasmas (in the ionosphere)

In this section of the report it is presented results obtained in two-frequency heating experiments [4] performed at the Sura heating facility still in 1993, but which could not be explained long time due to absence of an empirical model for BUM generation. The measurements were carried out by modification of the ionosphere F-region using two O-mode PWs with the effective radiated power $P_{eff} \approx 20$ MW for each and at frequencies close to 4^{th}, 5^{th}, or 6^{th} harmonic of the electron gyro frequency ($f_{ce} \approx 1.3 - 1.35$ MHz in our measurements). A frequency shift between PW frequencies was varied from a few kHz to 100 – 160 kHz and the measurements were carried out in a frequency range of about ± (50 – 150) kHz relatively to $n \cdot f_{ce}$. Diagnostics of HF-induced plasma perturbations was performed by means of detecting steady state SEE spectra, which were registered when one from two or both PWs were alternately used for pumping. In comparison with one frequency pumping, it is determined peculiarities of SEE features for different emission components when two-pump frequency scheme was used. It was revealed the effect of enhanced generation of the BUM, induced by the PW at the higher frequency, with strong simultaneous suppression of the BUM, induced by the second lower frequency PW. We have also studied behavior of the intensity of the DM under different experimental conditions and found that some variations of its intensity with changing of PW frequencies around of a gyro harmonic frequency cannot be directly connected with variations of characteristics of HF-induced small-scale field-aligned irregularities (striations). It must be emphasized here that features of phenomena observed in the two-frequency heating experiments depend strongly on the frequency shift between PW frequencies and a gyroharmonic frequency, as well as on the gyroharmonic number being more pronounced at $n = 4$.

These results are presented in [4].

5.1.4. Spectral characteristics of backscatter from artificial ionosphere turbulence when the pump frequency is close to the 4^{th} electron gyro harmonic

The experiments reported in this section of the report were carried out at the Sura heating facility on August 19, 2004 [5]. Measurements of field-aligned scattering from striations were used to study spectral features of scattered signals when a PW frequency, f_0, was close to the forth electron gyroharmonic frequency, $4f_{ce}$, in the interaction region between PW and F-layer ionosphere plasma. O-mode powerful waves were injected vertically in the ionosphere with the effective radiated power of ~ 150 MW. Sounding signals were radiated at frequencies 9996 and 14996 kHz by the precise-time radio station located near Moscow. In the scattering geometry used in the experiments a striation scale length in perpendicular to a geomagnetic field line direction $l_\perp$ is of about 11 m and 16 m respectively for the higher and lower sounding

frequencies. Scattered signals were detected at receiving sites placed near Rostov-na-Donu and Kharkov (UTR-2 radio telescope).

In measurements a value of $4f_{ce}$ is determined with an accuracy better than ± 5 kHz by means of the SEE taking into account the fact that the DM in SEE spectra is completely suppressed when $f_0 \cong n\, f_{ce}$ (n – gyroharmonic number) as well as some properties of the BUM. SEE measurements were carried out by means of a HP 3885A spectrum analyzer at a receiving site located near the Sura facility.

The experiments were arranged in the following way. Each observational cycle was started with finding $4f_{ce}$. Basing on the ionosphere conditions, we then chose a frequency range of about 80 – 100 kHz enveloping $4f_{ce}$ for radio wave transmissions and step-by-step changed the transmitter frequency with a step of 20 kHz, but in so doing one of the PW frequencies had always to be very close to $4f_{ce}$. The transmission timing at each sequential pump frequency was 105 s on, 15 s off. The pause time of 15 s gave us enough time to switch to the next pump frequency during the pump-off periods. Such a diagnostic scheme allowed us to study the temporal evolution of the scattered signal intensity after PW turn-on/-off at different PW frequencies in a gyroharmonic frequency range with optimal resolution in the backscatter spectral measurements. During each cycle of the abovementioned frequency scanning we kept diagnosing ionosphere conditions with the SEE observations to follow variations in the electron gyro frequency caused by changes in natural ionosphere conditions. This allowed us to promptly correct the magnitude of $4f_{ce}$ and to define the frequency range for the next scanning cycle. The duration of one observational cycle was about 10-12 minutes. From 19:00 to 21:00 LT we ran in total 8 cycles in the $4f_{ce}$ frequency range. The day of August 19, 2004 was geomagnetically quiet with $K_p \approx 1$.

In Fig. 5 and 6 in [5] it is presented several examples of spectra of scattered signals at different PW frequencies obtained in two best cycles of measurements. In Fig. 5 it is shown spectra registered by means of UTR-2 antenna array simultaneously at both sounding frequencies 14996 and 9996 kHz (cycle T = 16:00 – 16:12 LT, $4f_{ce} \cong 5360$ kHz); in Fig. 6 it is shown spectra obtained at sounding frequency 14996 kHz simultaneously in both receiving sites Kharkov and Rostov-na-Donu (cycle T = 16:28 – 16:40 LT, $4f_{ce} \cong 5340$ kHz). It can be clearly seen that, compared to frequencies below $4f_{ce}$, a noticeable spectral broadening occurs when PW frequencies was close to or above $4f_{ce}$.

An analysis of experimental data allows drawing the following conclusions:

1. Broadening of backscatter spectra is already registered when $f_0 \cong 4f_{ce}$, where suppression of generation of both resonance instability and striations takes place but generation of the first BUM component (BUM-1) occurs (V.L. Frolov et al. // Phys. Rev. Lett., 1998. Vol. 81, pp. 1630-1633). A maximal width of the frequency spectrum is registered at a frequency offset $\delta f = f_0 - 4f_{ce} \approx 20 - 40$ kHz, which corresponds to the most effective generation of the second BUM (BUM-2) component in the SEE spectra and to the most effective excitation of the electron Bernstein modes, and spectra become more narrow at higher PW frequencies.
2. The frequency spectrum of the scattered signals can be represented as a composition of narrow- and wide-band spectral components. It should be emphasized that the narrow-band backscatter component carries the major part of the backscatter power, which is about an order of magnitude higher than the wide-band one.

Below features of these components are considered in details.

Features of the narrow-band spectral component.

a) Its intensity keeps almost constant during 15s-pause of pumping, it follows that its decay time was longer than 15 s. It is a reason why we cannot say anything about temporal evolution features of the narrowband component basing on data obtained in the experiment.
b) Its width, being reached to the end of 105s-pulse of pumping and determined by the spectral intensity level of –20 dB relatively to its maximal level, depends slightly on $\delta f = f_0 - 4f_{ce}$ being of about 0.5 Hz at $\delta f \cong 0$, ~1 Hz at $\delta f = 20$ kHz, ~0.75 Hz at $\delta f = 40$ kHz, and ~0.7 Hz at $\delta f = 60$ kHz. Notice, the frequency spectrum width for $f_0 < 4f_{ce}$ was of about 0.3 Hz in the measurements.
c) Spectral flanks for the narrow-band component have exponential dependence on the frequency shift with the rate of about 20 – 40 dB/Hz, with a lower rate at negative frequency shifts.

Features of the broad-band spectral component.

a) Its typical growth time after PW switch-on after 15s-pause is of about of 0.5 – 1 s.
b) Its width, being reached to the end of 105s-pulse of pumping and determined by the spectral intensity level of +20 dB relatively to an equipment noise level, depends strongly on $\delta f = f_0 - 4f_{ce}$. For 11m-striations it is of about 5 Hz at $\delta f \cong 0$, ~ 9 Hz at $\delta f = 20$ kHz, ~ 12 Hz at $\delta f = 40$ kHz, and ~ 10 Hz at $\delta f = 60$ kHz. Thus, the widest spectra occur at $\delta f \approx$ 40 kHz. For 16m-striations the frequency offset δf, at which the widest spectra are observed, is somewhat smaller being ~ 20 – 30 kHz. It has been found that just after PW switch-on the spectral width is of 2 – 3 Hz higher than 15 – 20 s later at a quasi steady state level of scattering.
c) Spectral flanks for the broad-band component have exponential dependence on the frequency shift with the rate of about 6 – 10 dB/Hz at $\delta f = 40$ kHz, with a lower rate at negative frequency shifts.
d) A typical decay time for the broad-band component is of ≤ 1 s, this value is much longer than 50 – 70 ms reported by P.V. Ponomarenko et al. (J. Geophys. Res., 1999. Vol. 104(A5), pp. 10,081-10,087).
e) As it follows from simultaneous measurements at 14996 and 9996 kHz, the spectral width is in inverse proportion to the striation scale length $l_\perp$ (or in direct proportion to the value of striation *k*-vector).

Basing on experimental data considered above we can conclude that for both narrow- and broad-band spectral components the broadening of backscatter spectra is already observed when PW frequencies is very close to gyroharmonic, and maximal spectral width for them is registered at the frequency offset $\delta f = f_0 - 4f_{ce} \approx 20 - 40$ kHz where the second BUM component (BUM-2) has the highest intensity. Because for the broad component typical decay time is not longer than 1 s, which is much shorter than decay time of decameter striations after PW switch-off, that is of about 10 – 20 s, we can state with assurance that the broadening of backscatter signal spectra does not determine by a drift velocity of striations in ionosphere plasma.

These results are presented in [5,15,21].

5.1.5. Features of artificial small-scale field-aligned irregularities (striations) during sunset time period

Currently for sounding of the IDV a diagnostic scheme for SEE measurements is often employed (Kagan L.M. and Frolov V.L. // J. Atmos. Terr. Phys., 1996. Vol.58, pp.1465-1474). In such a scheme timing a few minutes on / a few minutes off for PW radiation is used to create the artificial ionosphere turbulence and to obtain the SEE as a product of it. In pauses of pumping short (≤ 20 ms) HF radio pulses are additionally radiated at a frequency close to PW frequency. If HF-induced striations exist in the IDV some time after the end of pumping in CW mode, 20-

ms radiation can produce emissions of the thermal SEE components (NC_{th}, DM, and BC), temporal evolution of which allows to made some conclusions about striation features. Such a scheme of measurements is called as the diagnostic SEE (DSEE). It was stated by Frolov V.L. et al. (Radiophysics and Quantum Electronics, 1994. Vol.37, NO.7, pp.593-603) that typical times of DSEE evolution increase strongly from a few seconds to a few tens of seconds after the sunset. It cannot be excluded that this effect is a result of keeping of striation intensity at a rather high level due to the pulse energy radiated in a pause of pumping in CW mode. To verify this hypothesis in March 2004 and in August 2005 we performed together with DSEE measurements field-aligned scattering measurements, for which signals of the Moscow precise time station at frequencies of 9996 and 14996 kHz were used for IDV sounding; scattered signals were registered at a receiving point located near Rostov-na-Donu.

It has been found that a value of the typical decay time for 14 – 20 m striations after switch-off of pumping in CW mode was of about 6 – 10 s both before and after the sunset time. The independence of the decay time values on the observation period shows that the revealed strong variations of DSEE typical times are not directly connected with changes in striation evolution, as it is usually assumed. In the experiments we decreased in some measurements the duration of pulse radiation from 20 mc to 200 μc. Such decreasing causes the striation development time after PW switch-on to a longer value (30 – 40 s instead of 15 – 20 s). It means that the pulse radiation even with 20-ms pulses in a pause of pumping in CW mode exerts a strong influence on striation evolution. Basing on experimental data, we can conclude that the sharp changing in the value of the typical DSEE times corresponds more to the sunset time on the Earth surface but not in the ionosphere F-region.

These results are presented in [17].

5.1.6. Preliminary results of ionosphere heating by beating two high-power pumps at the local plasma frequency

Experiments aimed at the study of features of ionosphere disturbances, which are generated by nonlinear mixing of two HF waves at frequencies higher than F_2-region critical frequency (f_{0F2}) but when difference between them is below of f_{0F2} (ionosphere heating by beating two high-power pumps at the local plasma frequency), have been carried out in August and September 2005 and in March 2006 using the field-aligned scattering method for AIT detection and the bispectral method for an analysis of HF signals produced in the IDV. At present we have not solid data in these measurements and new measurements with the use of improved heating scheme have to be carried out.

5.2. Radio tomography and scintillation studies of ionospheric electron density modifications.

For the first time at the Sura heating facility in August 2002 experiments on investigation of the space structure of the IDV were carried out using the satellite radio tomography method, which is an effective, modern and inexpensive method to produce maps of electron plasma density covering a wide region of the ionosphere within a relatively short time [6]. The ray (phase) tomography, applied in ionosphere modification experiments, gives maps of large electron density structures with scales from several km to about a hundred of km. Since the tomographic receivers can also record the amplitude scintillations of the satellite signals, features of mid-scale irregularities (from hundred meter to a few kilometers in size in perpendicular to a geomagnetic field-line direction) can be also investigated.

Amplitude scintillations of 150 MHz signal and variations of 400 and 150 MHz differential phase from Russian orbiting satellites passing over the IDV were registered. Three tomographic receivers were installed under the disturbed region on a chain lying approximately along a satellite pass moving from the north, thereby making it possible to study the temporal features and the spatial electron density distribution both in the F and E regions, within and outside the main lobe of the heating antenna. The central site (the Sura facility), the southern site Sechenovo and the northern site Arya were spaced by about 100 km (Sechenovo-Sura) and 150 km (Sura-Arya) between. In total, more than 300 records of signals from satellite beacons were registered under both day and night conditions, from which 20 records were made when the satellite line of site crossed the HF-disturbed region. The receivers registered radio signals from Russian navigational satellites flying at about 1000 km, the inclination of their orbits is 83º and the orbital period is 105 min. The receivers recorded the signals during 18 min for each satellite pass (± 9 min from the time of closest approach to the IDV). Only passes of satellites with such a high elevation that they could cross the ionospheric region illuminated by the main lobe of the heating facility were used in the tomographic analysis. Southward passes of such satellites lie close along to the receiver chain, which makes it possible to determine the electron density of the ionosphere in the vertical plane above the chain. A mobile automatic receiving system has been constructed in Polar Geophysical Institute. It is capable to measure the relative phase between the VHF and UHF waves and the amplitude of the VHF signal. During the experiment the Sura facility was operated in CW mode at 4.3 MHz for about 14 – 20 minutes when satellites were over the IDV. The facility transmitted radiation either vertically or the antenna beam was tilted by 12º to the south, that was close to the direction, for which the powerful wave has to be close to the geomagnetic line at the upper hybrid resonance height for the PW (see section 1.2).

Basing on experimental data obtained in the August 2002 heating campaign it has been stated (see Fig. 2,3 in [6]) that:

1) HF heating considerably affects the ionosphere resulting noticeable changes in the electron density distribution practically throughout the ionosphere body up to heights of about of 600 km, which are much higher than the F layer peak altitudes.
2) Artificial large-scale plasma density irregularities occupy a large region in the horizontal direction of about of 300 km, which is much wider than the ionosphere area illuminated by the main lobe of the heating antenna.
3) In the night-time ionosphere under quiet magnetic conditions the generation of artificial wave-like structures of plasma density with peak values of electron density fluctuations of $(0.2 – 0.4)\cdot 10^{11}$ $1/m^3$ with scale-lengths of 50 – 100 km were revealed in a wider region than the ionosphere illuminated area.
4) When the antenna beam was tilted by 12° to the south, the strongest depletions with a negative plasma density variation $\Delta N_e/N_{e0} \approx 20\%$ was observed inside the illuminated area.

Detail studies of the scintillation and phase data obtained in the measurements have shown that:

1) Enhancement of phase and amplitude fluctuations is observed when the propagation of satellite signals through the IDV is close to the geomagnetic field line direction. It means that irregularities with scales close to the Fresnel zone (~ 1 km in our case) are extended along the geomagnetic field.
2) Fluctuation patches, observed in scintillation data, are accompanied with strong gradients of the total electron contents, which is associated with large-scale irregularities well detected by means of tomography reconstructions.
3) Increase in the amplitude scintillations corresponds to the low-density region located inside of the area illuminated by the heating antenna beam. It follows that plasma density irregularities with scale length $l_\perp \approx 0.1 – 1$ km, which produce amplitude scintillations of satellite signals, are mainly concentrated inside this region.

Dependence of spectral behavior of phase variations and amplitude scintillations on the angle ψ between line of sight and geomagnetic field has been analyzed. It has been found existence of quasi-periodical structures with characteristic scales of 20 – 30 km along the satellite trajectory (in N-S direction) and revealed that the saturation region in amplitude scintillation spectra is shifted to higher frequency with decrease of ψ. Processing the experimental data has shown that a value of the spectral power index decreases with the increase of scintillation frequency. Moreover, in phase fluctuation spectra can be often resolved two regions with different index values: $p \geq 3$ for spectral frequency $\nu \leq 1$ Hz and $p \leq 2$ for $\nu \geq 1$ Hz.

The tomography and scintillation observations described here have clearly demonstrated a simultaneous existence near the magnetic zenith direction of large-scale irregularities and a great number of bunch-scale ($l_\perp \approx 0.1 - 1$ km) irregularities. According to the magnetic zenith effect theory [Gurevich et al., Phys. Lett. A, 2002. V.305, p.264], developed relating to a new non-linear process — self-focusing on striations, a powerful pump wave is trapped in soliton-like bunch structures and propagates along the Earth's magnetic field in the magnetic zenith direction. Strong ohmic heating of the ionospheric plasma by the trapped wave leads to the creation of large-scale irregularities as well.

The obtained results indicate that combination of the satellite radio tomography and scintillation measurements are the effective diagnostic technique giving valuable information on features of plasma density perturbations HF-induced in the upper ionosphere. New tomography measurements were carried out at the Sura facility in August 2005. Obtained here experimental data are in process now.

These results are presented in [6,7,14,18].

5.3. Features of transport processes in the upper ionosphere

5.3.1 Experiments carried out at heights below the F_2 peak altitude

In the paper (Frolov et al., Radiophys. and Quntum Electron., 2002. Vol.45, pp.109-128) it had been analyzed measurements of the velocity at which the artificial plasma turbulence, induced in the regions of resonance interaction between PW and plasma, spreads along a geomagnetic field line. It had been found that in the upper (F-region) ionosphere the spread velocity was usually higher than the ion thermal velocity and that in many cases this velocity was close to and sometimes even much higher than the electron thermal velocity ($V_{Te} \approx 2 \cdot 10^7$ cm/s under conditions of our measurements). That is easily observable by a short-pulse modification with pump pulse duration shorter than 3 s. Basing on these experimental results, in measurements presented below we used predominantly PW radiation with pulse duration of $\tau_p = 0.025 - 1$ s and pulse repetition period of $T_p = 1 - 10$ s. Such timing we shall assign to the short-pulse pumping.

The experimental results discussed in this section of the report were obtained in measurements at the Sura facility during 2003 – 2005 employing the so-called additional pumping scheme [8,9]. In such a scheme one from three modules of the Sura facility is used to radiate a diagnostic wave, which produces the diagnostic SEE (d-SEE). The second powerful wave (pump wave, PW), which is radiated by another two Sura modules at another frequency, is used here as an external source of intensive plasma disturbances. Propagating along geomagnetic field lines and changing conditions of d-SEE generation these disturbances are responsible for appearance of variations in both d-SEE spectral characteristics and its intensity. Because in the additional pumping scheme two spaced disturbed volumes are formed in the ionosphere F-region, it allows

to study influence of different turbulence component on features of interaction of HF powerful radio wave with ionosphere plasma and to estimate velocity of the disturbances along geomagnetic field lines basing on a delay time between the appearance of PW-produced disturbances at d-SEE generation level and the time of switching on the PW taking into account at that a turbulence growth time.

It has been found that in d-SEE temporal evolution four stages can be derived:

1. Emission intensity decreasing within 5 – 10 ms after PW switch on.
2. Following growth of emission intensity within 20 – 40 ms after PW switch on, which can be continued some time after PW switch off.
3. Following fast (for ≤ 100 ms) relaxation of PW-initiated emission intensity.
4. Slower restoring of d-SEE intensity to a level, which corresponds to the case when the ionosphere is pumped by means of the diagnostic wave only.

The first three stages we assign to the manifestation of fast processes in AIT evolution observed at the initial stage of PW-plasma interaction when short-pulse pumping is used for ionosphere modification. It is important to note that plasma disturbances, resulting in fast d-SEE intensity variations, have velocities along a magnetic field line that are close to and sometimes even much higher than the electron thermal velocity $V_{Te} \approx 2 \cdot 10^7$ cm/s.

Basing on analysis of the experimental data obtained, the following conclusions can be made:

1) The fast-time variations of the diagnostic emission intensity occurring just after PW switch-on, -off cannot be connected with evolution of HF-induced small-scale irregularities (striations).
2) It is most likely that appearance of these fast d-SEE intensity variations is connected with field-aligned flows of thermal and suprathermal electrons HF-induced in the IDV. Such suprathermal electrons are as a result of their acceleration due to development of the ponderomotive parametric instability.
3) Secondary turbulence, which is directly chargeable for the d-SEE features, is generated near a diagnostic wave reflection height by action of suprathermal electrons HF-accelerated in the IDV. These electron flows, due to short-circuit currents excited simultaneously in HF disturbed and background plasma, can also stimulate generation of secondary ionosphere disturbances far from regions of PW-plasma resonance interaction. It should be mentioned that generation of large-scale density irregularities outside of the region, in which the main part of HF energy is absorbed, has been recently confirmed in satellite tomography experiments performed at the Sura facility (see part 5.2 of the report).
4) Ionosphere modification for a time interval of 50 – 100 ms with the effective radiated power of about of 50 MW is sufficient to produce visible changes in d-SEE intensity at distance up to $\Delta h \approx 20 – 25$ km from PW reflection height. Without results were our experimental efforts to reveal some variations in d-SEE intensity if 25-ms pulses were used for pumping.

Basing on the experimental data obtained in the measurements with short- and long-time modifications of ionosphere F-region plasma, the method of investigation of features of transport processes in the upper ionosphere has been elaborated.

These results are presented in [8,9,16,24].

5.3.2 Preliminary results of the SURA-DEMETER experiment.

The goal of the experiment was to study at the height of the DEMETER orbit (h = 710 km) features of AIT induced by interaction of O-mode powerful radio waves with ionosphere F-

region plasma. Satellite board equipment was used for measurements of such turbulence characteristics as electron and ion density and temperature variations, plasma noises at a plasma frequency of background plasma, as well as for detection of ELF, VLF and whistler waves.

Modification of ionosphere plasma occurred by the Sura heating facility in April – September 2005. It was successfully carried out 11 heating séances. In 8 séances the satellite was over the Sura facility and in 3 séances the satellite was near the magnetic conjugation point relatively to the facility location. In each heating séance the Sura facility operated in CW mode for 15 min starting 10 min before the time of the closest point of the satellite trajectory to the center of HF-disturbed magnetic tube.

It should be noted that measurements performed either under daytime conditions or when the satellite was over the conjugate point did not show for the present any sensible variations of the turbulence parameters studied. When ionosphere modifications were carried out in evening hours (T = 22:00 – 22:40 LT) under the condition when PW frequency was somewhat below of F_2-layer peak plasma frequency, the following HF-induced turbulence features were revealed by the satellite equipment:

1) It was unambiguously detected variations of temperature and velocity for ions in a region of about of ± 400 km around of the closest point of a satellite trajectory to the center of HF-disturbed magnetic tube. In some instances variations of electron temperature and density were also registered.
2) The analysis of HF spectral data has not shown any HF-produced variations. It is most likely that the intensity of HF-induced plasma noise at frequencies close to an electron plasma frequency, which can be enhanced by electrons accelerated in the IDV, was below of an analyzer sensitivity level.
3) The analysis of VLF spectral data has shown that specific spectral structures are often observed for an electric field component in a frequency range of about of 10 – 15 kHz, and these structures are characterized, as a rule, by an increasing in time of their peak frequency.
4) The analysis of ELF spectral data has shown presence of multiform structures, which are observed everywhere over all frequency range from 0 to 1200 Hz and their characteristics depend strongly on a field component. Their duration is from a part of second till a few seconds. Some of them show drift in time of their peak frequency.

Unfortunately, a limited number of experimental data, obtained in 2005 in the framework of the SURA-DEMETER experiment and presented here, as well as the weak repetition of events registered, cannot allow us to carry out more detail classification of phenomena observed. The SURA-DEMETER experiments have been continued in 2006. Obtained experimental results are in process now.

This part of work was carried out in collaboration with Dr. M. Parrot and Dr. J.L. Rauch (LPCE, CNRS, Orleans, France).

These results are presented in [23].

5.4. Results of field-aligned scattering experiments

5.4.1 The study of peculiarities of HF radio wave long-distance propagation

First investigations of controlled HF-wave long-distance propagation on the basis of a chirp sounder by the use of HF ionosphere pumping to produce the AIT, in which radio waves can be

scattered and escape a wave-guide due to artificial field-aligned scattering, were carried out more than 10 years ago by V.P. Uryadov et al. (J. Atmos. Terr. Phys., 1995. Vol. 57, pp.1263-1271). Experiments were conducted using the path Khabarovsk (chirp sounder) – Sura (heating facility) – Temryuk (receiving site). In these experiments it was found that in a case when considerable negative gradients of the F-region critical frequency of about of – (0.02 – 0.1) MHz/100 km taken place for the radio wave path, in particular due to the solar terminator, the trapping of radio waves into ionosphere wave-guide occurred at frequencies exceeding by 1 – 2 MHz of the maximum observed frequency (MOF) for hop modes. It should be mentioned that the experiments were performed in March 1991 under conditions of maximum solar activity when f_{0F2} critical frequencies were so much high that the Sura facility could modify the ionosphere during night hours (that is needed for such measurements) and radio waves, trapped in the ionosphere wave-guide, can escape it by means of field-aligned scattering from artificial small-scale irregularities (ASSI).

Experiments conducted in the framework of the project and discussed here were carried out in August, 2003, 2004 and in March 2004, 2005 at the radio wave paths Khabarovsk – Sura – Rostov-na-Donu with length of about 6700 km and Irkutsk – Sura – Rostov-na-Donu with length of about 4500 km using chirp-sounders located near Khabarovsk (47.5°N, 134.5°E) and Irkutsk (51.8°N, 104°E) and operated with a frequency rate of 100 kHz/s. The ionosphere was modified by the Sura heating facility. PW was radiated vertically or with inclination of 10 – 12° to the south and cycled, as a rule, 5 min – on, 5 min – off. Scattered from ASSI radio waves were registered at a receiving point located near Rostov-na-Donu (47.3°N, 39.7°E).

It was assumed that trapping of HF radio waves into an ionosphere wave-guide channel would be achieved by their refraction on a negative plasma density gradient naturally produced in the upper ionosphere when the solar terminator intersects the radio wave path. In our case it should be occurred in nighttime. Because the possible lowest frequency for the Sura facility is 4.3 MHz, experiments could be carried out only in evening hours as long as F_2-layer critical frequency was higher than the lowest facility frequency (as a rule, till T = 21:00 – 22:00 LT). Modeling, performed for evening conditions of pumping, has shown that a value of the negative plasma density gradients for the paths used in these experiments was not large enough for trapping radio waves into an ionosphere wave-guide channel. It is a reason why in these measurements artificial field-aligned scattering of hop modes, propagating in the Earth-ionosphere channel, was only observed at frequencies of about or somewhat below of the maximum observed frequency for F-region propagation (MOF_F).

According experimental results obtained at the radio wave path Irkutsk – Sura in August 2003, 2004, in the absence of the necessary negative plasma density gradient the presence of a sporadic E-layer on the way of radio wave propagation is of considerable importance in appearance of radio waves at F-region heights over the Sura facility at frequencies higher than MOF_F [10]. Modeling performed for such conditions has shown that the first hop for radio waves at frequencies higher than MOF_F was formed by their reflection from E_s and the top of the second hop was in the vicinity of the IDV (see Fig. 7 in [11]). In this case scattered signals were registered in a frequency range of 19.5 – 22 MHz, or at frequencies which are of 2 – 3 MHz higher than MOF_F. If a sporadic E-layer was absent during the measurements on a way of radio wave propagation, scattered signals were registered only in a frequency range of 10 – 11.5 MHz, whereas MOF_F was of about 16 MHz.

These results are presented in [10,20].

5.4.2 *Frequency dependence HF wave back scattering from artificial small-scale irregularities (ASSI).*

Measurements presented in this section of the report were carried out during August 2004 heating campaign at the Sura facility using a wide-band HF transmitter located near Moscow and operated in a pulse mode in a frequency interval from 4 to 12 MHz. It has been found that for such a short path (~ 500 km) artificial field-aligned scattering is observed only in a rather narrow frequency range from ~ 8 to ~ 10 MHz which is significantly determined by refraction of radio waves in the ionosphere. Such a scheme of measurement can be successfully used to control parameters of artificial scattering from decameter ASSI.

These results are presented in [22].

5.4.3. *Ionospheric effects of the magnetic storm on August 18-22, 2003 according to the data of HF sounding of AIT*

The interest to such a problem is due to the needs of practical HF radio communication and over-horizon radiolocation, and, on the other hand, to abilities to study the formation mechanisms of short-wave field at long-distant paths in quiet and disturbed ionosphere. Results discussed in this section of the report were obtained in heating experiments carried out in August 2003 during various phases of a magnetic storm [11]. Russian (in Khbarovsk and Irkutsk) and foreign (in England) chirp-sounders were used for AIT sounding. Besides, signals of the RVM precise-time station (Moscow) at a frequency of 9996 kHz were also used in a scheme of a Doppler HF radar at the path Moscow — Sura — Rostov-na-Donu for diagnostics of artificial small-scale field-aligned irregularities (striations). The AIT was created in the ionosphere F-region by the Sura heating facility.

The experiment was carried out on August 18 – 22, 2003 from 20:00 till 24:00 LT (LT = UT+4^h). Following radio paths were used in measurements: Khabarovsk — Sura — Rostov-na-Donu, Irkutsk — Sura — Rostov-na-Donu and Inskip (England) — Sura — Rostov-na-Donu. The Sura facility radiation was cycled 5 min-on, 5 min-off starting at $00^h00^m00^s$ of each hour. The O-mode PW was radiated at a frequency f_0 close to the critical frequency of the ionosphere, f_{0F2} ($f_0 \le f_{0F2}$). The chirp-sounders in Khabarovsk and in Irkutsk started sounding cycles at 0, 5, 10,...55 min of each hour with the following parameters: 4 MHz was the starting frequency, 30 MHz was the end frequency with the frequency-sweep rate of 100 kHz/s.

Fig. 5 in [11] (the left-hand panel) demonstrates examples of the variations in the frequency Doppler shift during the operation of the heating transmitter and after its switching off under the conditions of relatively quiet ionosphere (on August 19) and during the magnetic storm (on August 20-22). It shows that the sonograms of the Doppler spectra of the scattered signals, obtained under different geophysical conditions, differ significantly from each other. For example, in the séance at 19:00 UT on August 19 (Fig. 5a) the Doppler frequency shifts for the direct (DS) and scattered (SS) signals are close to each other: the difference is about 1.2 Hz, so the Doppler spectrum of DS is practically overlapped on the Doppler spectrum of SS. In the period of the magnetic substorm on August 20 – 22 the Doppler shift of the frequency (DSF) of the scattered signal reached values of about 8 – 10 Hz (see the left-hand panel of Fig. 5c). It is worth noting that in the magnetically-disturbed period sporadically appearing trains of quasi-periodical modulation of DSF of the scattered signal with a period of ~ 40 – 60 s and amplitude reaching 2 Hz (see the left-hand panel of Fig. 5b-5d in [11]) were observed. No quasi-periodic variations were observed in the Doppler spectrum of the scattered signal on a relatively quiet day on August 19 (see Fig. 5a). It should be noted that no such variations were registered also in the Doppler spectrum of the direct signal in all the days of observations.

Using the Doppler measurements for the bistatic location of the HF radar one can determine the drift velocity of the irregularities responsible for the field-aligned scattering of radio waves in the direction orthogonal to the magnetic field along the bisecting line of the angle formed by the directions from the scatter region to the transmitter and receiver of the sounding signal: $V_{dr} = (\lambda \Delta F_D) / 2\sin(\theta_s/2)$, where λ is the wavelength, ΔF_D is the Doppler frequency shift, and θ_s is the scattering angle. Estimations have shown that in the relatively quiet ionosphere (on August 19) the measured north-east component of the velocity was of ~ 20 m/s. During the magnetic storm (August 20-22) the measured direction of the drift velocity was changed to the south-west one and the velocity magnitude increased up to ~ 186 m/s, that is up to the values typical to the high-latitude ionosphere. Estimations of the electric field based on the velocity of the **E**×**B** drift have shown an increase in the value of the electric field in the upper ionosphere from ~ 1 mV/m under quiet conditions up to ~ 8.6 mV/m during the magnetic storm. It is due to that during a magnetic storm the formation of the magnetosphere-ionosphere current systems, causing an increase of the electric fields at ionospheric heights, occurs in the upper ionosphere. This leads to the increase in drift velocity of the plasma density irregularities up to values of ~ 186 m/s.

The trend in the form of the DSF (Fig. 5b, the left-hand panel) may be due to the variations in the electric field vector (both by the magnitude and direction) at F-region heights during the development and recovery phases of the ionospheric effects of the magnetic storm. The occurrence of trains of quasi-periodical variations in DSF of the HF signals in the magnetically disturbed period manifests a presence of wave processes in the IDV containing artificial small-scale field-aligned irregularities (striations). This effect may be caused by transverse magneto hydrodynamics (MHD) waves playing the determining role in the activity of the natural pulsations of the geomagnetic field. By they periodicity (~ 40 – 60 s) the observed variations in DSF are close to the geomagnetic pulsations of the Pc3-4 types. By this means the obtained experimental data are indicative of a natural source of the MHD waves in the magnetically disturbed period, which is responsible for the appearance of the quasi-periodic oscillations of the Doppler frequency shift in scattered signals.

Obtained experimental results have shown, that HF sounding of the AIT can serve as an effective tool for diagnostics of a response of the middle-latitude ionosphere to a magnetic storm.

These results are presented in [11,12,19].

5.5. Results of the SURA-HAARP experiment

5.5.1. *Results of modeling and calculations for the SURA-HAARP experiment*

One of the main task of the project is carrying out the SURA-HAARP experiment, in the framework of which HAARP has to be used for excitation of wave-guides modes of HF radio waves through the field-aligned scattering of test waves, whereas the Sura facility has to be used to ensure of escaping excited guide waves from a wave-guide channel. An over-simplified scheme of this experiment is shown in Fig. 1 (see Fig. 1 – 5 in Appendices). Modeling and calculations of HF wave propagation in an ionosphere wave-guide channel for the SURA-HAARP experiment have been performed for a path: Kodiak SuperDARN radar – HAARP – Sura – Rostov-na-Donu (receiving site) by the use of a elaborated software basing on the IRI model and taking into account predictions of ionosphere conditions. The Kodiak SuperDARN radar was chosen as a sounding transmitter. In Fig. 2 an example of calculations for a sounding frequency 12 MHz of earth intersections of rays, scattered at a possible interval of heights (150 – 200 km) over the Sura facility, are presented under March 2006 conditions when the experiment was first performed (here two rays show directions from Sura to HAARP (upper ray) and to the SuperDARN radar (lower ray)). Basing on the calculations performed, it has been determined

that an ionospheric wave-guide along a path between HAARP and Sura has to exist at a time interval T ≈ 04 – 06 UT, and found that optimal sounding frequencies for this path lie in a frequency range from 10 to 12 MHz.

5.5.2. *Results of the March-2006 Sura-HAARP experiment*

The first Sura-HAARP experiment was carried out on March 27 – 31, 2006 (on March 26 – 30 Gakona LT) from 04 till 06 UT. Every day HAARP was radiated at frequency 3.2 MHz with the ERP P = ???? in a mode 5 min – on, 5 min – off, beginning 01 min after the hour. The Sura facility was radiated at frequency 4.3 MHz with the ERP P = 80 MW in a mode 10 min – on, 10 min – off beginning 09 min after the hour. In such a schedule we had the time intervals when HAARP and Sura radiated singly or together. To produce more intense artificial field-aligned small-scale irregularities, generated by a powerful HF wave, the heating beam for HAARP was directed towards the geomagnetic zenith and the heating beam for Sura was directed towards 12° to the south from the vertical, at which generation of the strongest AIT is observed (see section 5.1.2 of the report).

It is important to separate different propagation modes at the stage of obtained data processing. As a sounding transmitter it was used the Kodiak SuperDARN radar, which operated in its typical mode with running 3 or 6 a second dwell time on each of 16 beam directions using three fixed frequencies 8075 kHz (13995 kHz), 9990 kHz, and 12120 kHz for radiation respectively during time intervals 00 – 20 min, 20 – 40 min, and 40 – 60 min of each an hour. Besides, it was used a pulse code for radar operation. Unfortunately, the repetition period for the radar pulse sequence was not fixed, that does not give us an opportunity for coherent averaging received signals during the experiment. It is clear that such a schedule is not wholly satisfactory for the experiment.

In such a situation it was performed digitizing of received signals during of all 2-hour session with a rate of 50 kHz. After each session it is calculated a correlation function R(t) between the signals and sequence of 7 pulses used for radiation by the SuperDARN radar. It is suggested that a expected signal is absent if R(t) ≤ 0.3. At the next stage for the cases when R(t) ≥ 0.3 it is calculated averaged energy *E* during time intervals when the SuperDARN pulses were radiated. In Fig. 3 and 4 it is presented two typical examples of registered signals at a frequency f = 9990 kHz obtained on March 27 when the radar was operated in the normal sound mode (T = 05:20 UT, the initial time of registration) and on March 30 when the radar was operated in the fast sound mode (T = 05:20 UT, the initial time of registration). In both instances it is clearly seen the schedule of SuperDARN radar radiation with more intensive received signals for more western beams; in some instances it was observed more uniform energy distribution in relation to different radar beams.

For testing the HAARP – Sura path we also used a chirp-sounder in Magadan, location of which is more close to this path. It has been determined that frequencies, signals at which were registered in Nizhny Novgorod, were in a frequency range from 12 to 15 MHz.

In Fig. 5 we present an example of signals received in the Sura-HAARP experiment on March 30, 2006. In the session presented here HAARP was operated from 60s till 360s and from 660s till 960s; the Sura facility was operated from 540s till 1140s. It can be seen noticeable enhancement of the correlation coefficient R(t) during joint operation of HAARP and Sura. It is important that the enhancement is observed only for SuperDARN radar beams oriented to IDV over HAARP. It should be mentioned that it is a single case. In other cases we received analogous signals but with no so clear heating effect as presented in Fig. 5. Unfortunately, our

attempts aimed at additional more detail processing experimental data obtained do not yet any positive results. The reasons of that are the far from ideal schedule of the experiment in the frame of which we could not use methods of Doppler selection of received signals. It is due to short times when a SuperDARN radar beam was oriented to the ionosphere disturbed volume and absence of rigorous periodicity in the pulse sequence used the radar radiation. It does not allow us to say with full confidence that we observed twice-scattered signals.

5.5.3. *Results of the May-2006 Sura-HAARP experiment*

The second part of the Sura-HAARP experiment was carried out on May 16 – 19, 2006 (on May 15 – 18 for Gakona LT). According to calculations made, experiments were carried out from 05 till 07 UT at sounding frequencies from ~ 12 to ~ 18 MHz. Every day HAARP was radiated at frequency 3.2 MHz in a mode 5 min – on, 5 min – off, beginning 01 min after the hour. The Sura facility was radiated at frequency 4.3 MHz a mode 7 min – on, 3 min – off beginning 00 min after the hour. During this experiment the SuperDARN radar beam was oriented to IDV over HAARP at all times. The latter extends the capabilities of revealing twice-scattered signals. It should be mentioned also that on May 16 and 17 ionosphere conditions were very quite ($K_p = 0 – 1$); moderate magnetic disturbances were observed on May 18 and 19 ($K_p \approx 3$). Besides, strong sporadic-E layers were often observed during 3 days from 4; that was not good for measurements.

Results obtained in the May SURA-HAARP experiment are presented in 4 tables separately for each day of measurements. One can say with confidence that in some occasions twice-scattered signals have been registered, especially on May 17, which was the best day for results obtained, when sporadic-E layers did not observed over the Sura facility.

Table 1.

May 16

Time, UT	5:00	5:10	5:20	5:30	5:40	5:50	6:00	6:10	6:20	6:30	6:40	6:50
f_{0F2}, MHz (S) f_{Es}	4.8	4.8	4.8	4.9 4.35st	5.0 5.0st	5.0 5.0nt	5.1 5.2st	5.1 4.8st	5.2 4.5st	5.2 4.6st	5.1 3.5st	5.4 3.5st
f_{0F2}, MHz (H) f_0E_s	4.2			4.2 3.0st			4.2 3.2st			4.2		4.2 4.0st
f_1=12120 kHz	—			—			—			—		
f_2=13995 kHz		$\times_H$ $\times_S$			$\times_H$ $\times_S$			$\times_H$ $\times_S$			$+_{H(?)}$ $+_{S(?)}$	
f_3=16258 kHz			$\times_H$ $+_S$			$\times_H$ $\times_S$			$\times_H$ $\times_S$			$\times_H$ $\times_S$

Marks used in tables:
st – semitransparent E_s
nt – nontransparent E_s
_H – HAARP

_S – Sura

×– there is not any influence of Sura and HAARP pumping

+ – there is an influence of Sura and HAARP pumping

Table 2.

May 17

Time, UT	5:00	5:10	5:20	5:30	5:40	5:50	6:00	6:10	6:20	6:30	6:40	6:50
f_{0F2}, MHz (S) f_{Es}	5.1	5.1	5.3	5.2	5.2	5.4	5.4 3.4	5.4 3.4	5.4	—	5.25	5.4
f_{0F2}, MHz (H) f_0E_s	4.6			3.35			4.2			4.0		3.55
f_1=18043 kHz	$+_{H(?)}$ $+_{S(?)}$			$\times_H$ $\times_S$			$+_{H(?)}$ $+_S$			$+_{H(?)}$ $+_{S(?)}$		
f_2=13995 kHz		$\times_H$ $\times_S$			$+_H$ $+_S$			$\times_H$ $\times_S$			$+_{H(!)}$ $+_S$	
f_3=16258 kHz			$\times_H$ $+_S$			$+_H$ $+_S$			$\times_H$ $\times_S$			$+_{H(!)}$ $+_S$

Table 3.

May 18

Time, UT	5:00	5:10	5:20	5:30	5:40	5:50	6:00	6:10	6:20	6:30	6:40	6:50
f_{0F2}, MHz (S) f_{Es}	4.0	4.5	4.7 4.5st	4.9 5.2st	4.7nt	4.9 4.0nt	4.9 3.7nt	4.8nt	5.0nt	5.0nt	5.6nt	5.2nt
f_{0F2}, MHz (H) f_0E_s	4.4 9.0st			4.25 8.8st			4.1 10st			3.9 7.0st		3.7 10st
f_1=18043 kHz	$+_H$ $+_S$			$+_{H(!)}$ $+_S$			$\times_H$ $\times_S$			$+_{H(?)}$ $+_{S(?)}$		
f_2=13995 kHz		$+_H$ $+_S$			$+_{H(?)}$ $+_{S(?)}$			$\times_H$ $\times_S$			$\times_H$ $\times_S$	
f_3=16258 kHz			$\times_H$ $\times_S$			$\times_H$ $\times_S$			$\times_H$ $\times_S$			$\times_H$ $\times_S$

Table 4.

May 19

Time, UT	5:00	5:10	5:20	5:30	5:40	5:50	6:00	6:10	6:20	6:30	6:40	6:50
f_{0F2}, MHz (S) f_{Es}	5.2nt	5.2nt	5.4nt	5.2nt	5.3nt	4.5 3.7nt	4.8 4.2nt	4.8 4.6nt	5.0nt	5.4nt	4 4.5nt	5.0nt
f_{0F2}, MHz (H) f_0E_s	4.3 4.5st			3.9			3.2			3.0		3.0
f_1=18043 kHz	—			$\times_H$ $\times_S$			$+_{H(?)}$ $+_{S(?)}$			$\times_H$ $\times_S$		
f_2=13995 kHz		$+_{H(!)}$ $+_S$			$+_{H(?)}$ $+_{S(?)}$			$\times_H$ $\times_S$			$\times_H$ $\times_S$	
f_3=16258 kHz			$+_{H(!)}$ $+_S$			$+_{H(?)}$ $+_{S(?)}$			$\times_H$ $\times_S$			$\times_H$ $\times_S$

We have estimated signal strength by twice scattering and found that, if the values of scattering cross sections for the Sura and HAARP are of about of $(1 – 3)\cdot10^7$ m^2, SuperDARN-radar effective radiated power is 200 kW, and absorption of wave energy in a wave-guide is of about 20 dB, the signal amplitude on the receiver input have to be of about 0.03 – 0.1 μV. That is not than a few times higher than our instrument sensitivity corresponding strength of the received signals. Notice, the sensitivity can be strongly improved if would be possible to use coherent methods of signal processing. For that the fixed period of seven-pulse sequence for SuperDARN radar radiation has to be used.

6. Results and Conclusions

A powerful electromagnetic wave in O-mode, impinging upon the ionospheric plasma with a frequency below the maximum F-region plasma frequency, induces the generation of artificial ionospheric turbulence (AIT) in regions of resonance interaction pump wave with plasma. Two lines of investigations have been central to the work performed under the present project:

1) The study of AIT features and peculiarities of turbulence generation under different ionospheric conditions.
2) An influence of HF-induced field-aligned small-scale irregularities (striations) on propagation of HF and VHF radio waves.

Among main results obtained in the framework of the project we would like to note the following.

1. We have studied the spectral properties and the temporal evolution of the last SEE components previously poor explored, namely: ponderomotive narrow continuum NC_p and thermal narrow continuum NC_{th} [1,2]. Now we can conclude that features of all main SEE components have been studied in detail. Based on elaborated empirical and theoretical models, new methods for testing of the low- and high-frequency ionospheric turbulence, both natural and artificial origin, have been suggested and used in our experiments. By these methods it has been studied features of a nonlinear interaction of two O-mode powerful radio waves in the magnetized plasmas (in the ionosphere) [4], features of

transport processes in the upper ionosphere including some peculiarities of generation of secondary ionospheric turbulence far from the region of PW-plasma resonance interaction, which is stimulated by primary HF-induced plasma turbulence [8,9]. The SEE was also used for the search of artificial perturbations induced in the ionosphere by two high-power pumps at the local plasma frequency. This is a new way in our active experiments in the ionosphere.

2. On the base of tomography and scintillation measurements, we have studied the spatial structure of the ionosphere disturbed volume [6,7]. It has been stated that: a) HF-produced plasma density variations with scale-lengths $l_{\perp} \approx 20 - 100$ km are observed up to heights of about of 600 km and occupy a large region in the horizontal direction of about of 300 km, which is much wider than the ionospheric area illuminated by the main lobe of the heating antenna; b) increase in the amplitude scintillations corresponds to low density regions located inside of the area illuminated by the heating antenna beam, it follows that plasma density irregularities with scale length $l_{\perp} \approx 0.1 - 1$ km, which produce amplitude scintillations of satellite signals, are mainly concentrated inside this regions; c) the obtained experimental results have clearly demonstrated an existence the magnetic zenith effect at middle-latitudes. First results obtained by the use of micro satellite board equipment showed that substantial plasma disturbances are well revealed at heights of 700 km.
3. Using the additional pumping scheme in ionosphere heating experiments, it has been studied in detail AIT evolution at the initial stage of PW-plasma interaction and stated that: a) the fast-time variations of the diagnostic emission intensity occurring just after PW switch-on, -off cannot be concerned with evolution of HF-induced small-scale irregularities (striations); b) it is most likely that appearance of these fast d-SEE intensity variations are connected with field-aligned flows of thermal and suprathermal electrons HF-induced in the ionosphere disturbed volume; c) the secondary turbulence, which is directly chargeable for the d-SEE features, is generated near a diagnostic wave reflection height by action of suprathermal electrons HF-accelerated in the ionosphere disturbed volume; d) due to short-circuit currents, excited simultaneously in HF disturbed and background plasma, these electron flows, can also stimulate generation of secondary ionosphere disturbances far from the region of PW-plasma resonance interaction [8,9].
4. Using the Doppler measurements for the bistatic location of the HF radar it can be possible to determine the drift velocity of the irregularities responsible for the field-aligned scattering of radio waves from striations [10,11]. Our measurements have shown that in the quiet ionosphere the measured velocity is of ~ 20 – 50 m/s and during a magnetic storm it increases up to ~ 200 m/s, which is close to the values typical in the high-latitude ionosphere. Estimations of the electric field based on the velocity of the $\mathbf{E}\times\mathbf{B}$ drift have shown an increase in the value of the electric field in the upper ionosphere from ~ 1 mV/m under quiet conditions up to ~ 10 mV/m during a magnetic storm. It has been found that under magnetically disturbed conditions quasi-periodical variations with a period of about of 60 s occur in Doppler frequency shifts (DSF) of the HF signals. Such variations in the DSF of the scattered signal indicate to the natural source of the MHD waves responsible for their appearance.
5. It has been considered conditions for the trapping of radio waves into ionosphere wave-guide and shown that for middle-latitudes paths such trapping is realized in a case when considerable negative gradients of the F-region critical frequency takes place for the radio wave path, in particular due to the solar terminator. It means that artificially induced escaping of wave-guide modes by the use of the Sura facility is possible only in nighttime; in this case the F-region critical frequency has to be higher than 4.3 MHz, that is the lowest frequency for Sura operation. Such conditions can be realized only during the period of the maximum solar activity.
6. The SURA-HAARP experiment was carried out in March and May 2006. In spite of definite complications positive results were obtained: It was received twice-scattered

signal, intensity of which is in good agreement with estimations made for the path Kodiak SuperDARN radar — IDV over HAARP — IDV over Sura — receiving point (near Rostov-na-Donu).

7. Future Work Recommended

In our opinion, a new work has to be focused, first of all, on experiments related to HF wave long-distance propagation when HAARP and Sura are used for the control of such propagation. It is what we did in the framework of the SURA-HAARP experiment. Additionally, we can use the chirp-sounders in Khabarovsk and Irkutsk, as well as others chirp-sounders operated in word-net, to organize additional paths for such investigations. It would be very interesting to carry out experiments during 2007 – 2010 years (during transition from minimum to maximum of solar activity) to study influence of ionospheric conditions on features of long-distance propagation of HF waves.

Notice, the sensitivity of our equipment in a case of receiving of SuperDARN signals could be strongly improved if coherent methods for signal processing would be possible to use. For that the fixed period of seven-pulse sequence for SuperDARN radar radiation has to be stated. It could be suggested here 2 opportunities: 1) to use the radar only in the radiation mode with 10ms fixed period to exclude an influence of signal processing by radar equipment on the schedule of the SuperDARN operation; 2) to stay longer fixed period for radiation (for example, 15 – 20 ms) when processing of received signals will not occur any influence on the radar operation period.

In the framework of the investigation of AIT features it would be interesting to study in more details: 1) peculiarities of generation of artificial irregularities with different scale lengths far from resonance region of interaction of the pump wave with ionospheric plasma (from ~ 100 km to outer ionosphere) and 2) peculiarities of AIT generation when a pump wave frequency is close to a gyroharmonic frequency. New experimental data obtained here will be important for further development of AIT empirical models.

8. References

Papers

1. Frolov V.L., Sergeev E.N., Komrakov G.P., Stubbe P., Thide B., Waldenvik M., Veszeley E., and Leyser T.B. The ponderomotive narrow continuum (NC_p) component in stimulated electromagnetic emission spectra. // J. Geophys. Res., 2004. Vol.109, A07304, doi:10.1029/2001JA005063.
2. Frolov V.L., Nedzvetski D.I., Sergeev E.N., Stubbe P. On properties of the thermal narrow-continuum component in the spectrum of artificial ionospheric radiation. // Radiophys. and Quantum Electron., 2005. Vol.48, NO.12, pp.901-918.
3. Frolov V.L., Nedzvetski D.I., Komrakov G.P. Features of excitation of artificial radiation of the ionosphere affected by an oblique high-power radio wave. // Radiophys. and Quantum Electron., 2005. Vol.48, NO.9, pp.661-672.
4. Frolov V.L., Sergeev E.N., Thide B., and Shorokhova E.A. Experimental studies of the effects observed during the nonlinear interaction of two high-power radio waves in a magnetoplasma. // Radiophys. and Quantum Electron., 2005. Vol.48, NO.2, pp.110-133.
5. Kagan L.M., Nicolls M.J., Kelley M.C., Frolov V.L., Belikovich V.V., Bakhmet'eva N.V., Komrakov G.P., Nedzvetski D.I., Yampolski Yu. M., Koloskov A.V., Zalizovski A.V., Galushko V.L., Kasheev S.B., Blagoveshenskaya N.F., Kornienko V.A., Borisova T.D., Gurevich A.V., Vertogradov G.G., Vertogradov V.G., Trondsen T.S., Donovan E. Optical

and RF diagnostics of the ionosphere over the Sura facility. Review of results. // Radiofizika and Radioastronomiya (Ukraina), 2006 (in press).
6. Tereshchenko E.D., Khudukon B.Z., Gurevich A.V., Zybin K.P., Frolov V.L., Myasnikov E.N., Muravieva N.V., Carlson H.C. Radio tomography and scintillation studies of ionospheric electron density modification caused by a powerful HF-wave and magnetic zenith effect at mid-latitudes. // Physics Letters A, 2004. 325, pp381-388.
7. Myasnikov E.N., Muravieva N.V. Spectral features of electron density disturbanses excited at middle latitudes by the "Sura" heating facility. // Radiophys. and Quantum Electron., 2006. (in preparation for publication).
8. Frolov V.L., Komrakov G.P., Nedzvetski D.I., Rapoport V.O., Sergeev E.N., Shorokhova E.A., Stubbe P. On effects observed by upper ionosphere modification with powerful short-pulse radiation. // Radiophys. and Quantum Electron., 2006. Vol.49, NO.8 (in press).
9. Frolov V.L., Groves K.M. On peculiarities of artificial ionosphere turbulence development outside of region of resonance interaction of powerful radio waves with of the F-region ionosphere plasma. Intern. J. Geomagn. and Aeronom., 2006 (submitted for publication).
10. Uryadov V.P., Vertogradov G.G., Vertogradov V.G., Ponyatov A.A. and Frolov V.L. Radar observations of artificial ionospheric turbulence during a magnetic storm. // Radiophys. and Quantum Electron., 2004. Vol.47, NO.9, pp.646-661.
11. Uryadov V.P., Vertogradov G.G., Vertogradov V.G., Ponyatov A.A., Frolov V.L. Ionospheric effects of the magnetic storm on 18-22 August 2003 according to the data of HF sounding of the artificial ionospheric turbulence. // International Journal of Geomagnetism and Aeronomy. 2004. Vol.5, No.1, GI1007.

Abstracts

12. V.P. Uryadov, G.G. Vertogradov, V.G. Vertogradov, V.L. Frolov, V.I. Kurkin, and G.I. Litovkin. Ionospheric effects of magnetic storms observed by means of oblique sounding in HF-modified ionosphere. // RF Ionospheric Interactions Workshop, 18-21 April 2004, Sante Fe, New Mexico, USA. Summary of presentations, pp.1106 – 1113.
13. V.L. Frolov and D.I. Nedzvedski. The study of the aspect angle dependence for some SEE components. // RF Ionospheric Interactions Workshop, 18-21 April 2004, Sante Fe, New Mexico, USA. Summary of presentations, pp.1102 – 1105.
14. Tereshchenko E.D., Khudukon B.Z., Gurevich A.V., Zybin K.P., Frolov V.L., Myasnikov E.N., Muravieva N.V., Carlson H.C. Magnetic zenith effect at mid-latitudes. Radio tomography and scintillation studies of ionospheric electron density modification caused by a powerful HF-wave. // RF Ionospheric Interactions Workshop, 18-21 April 2004, Sante Fe, New Mexico, USA. Summary of presentations, pp.1159 – 1166.
15. V.L. Frolov, S.M. Grach, E.N. Myasnikov, E.N. Sergeev, G.G. Vertogradov and V.P.Uryadov. Review of modification experiments with the Sura heating facility. // VI International Suzdal URSI Symposium, Moscow, October 19-21, 2004. Book of Abstracts, p.8.
16. V.L. Frolov, E.N. Sergeev, D.I. Nedzvedski, and P. Stubbe. Studying the features of transport processes in the upper ionosphere by means of HF-induced artificial ionosphere turbulence. // VI International Suzdal URSI Symposium, Moscow, October 19-21, 2004. Book of Abstracts, p.37.
17. G.G. Vertogradov V.G. Vertogradov, V.L. Frolov and V.P. Uryadov. Features of artificial small-scale field-aligned irregularities during the sunset time period. // VI International Suzdal URSI Symposium, Moscow, October 19-21, 2004. Book of Abstracts, p.55.
18. E.N. Myasnikov V.L. Frolov, N.V. Muravieva, E.D. Tereshchenko, B.Z. Khudukon. Spectral features of electron density disturbances excited by the "Sura" heating facility. // VI international Suzdal URSI Symposium, ISS-04, Moscow, October 19-21, 2004. Book of Abstracts, p.21.

19. Uryadov V.P., Vertogradov G.G., Vertogradov V.G., Frolov V.L. Diagnostics of the ionospheric effects of magnetic storm with help of Doppler HF radar. // Proc. of XXI Russian Conference on Radio Wave Propagation. Russia, Yoshkar-Ola, Mari State Technical University, 25-27 May 2005. Book of Abstracts, Vol.2, pp.160-164.
20. Uryadov V.P., Vertogradov G.G., Vertogradov V.G., Ponyatov A.A., Frolov V.L., Kurkin V.I., Litovkin G.I. Influence of the artificial ionospheric turbulence on long-distance propagation of HF waves. // Proc. of XXI Russian Conference on Radio Wave Propagation. Russia, Yoshkar-Ola, Mari State Technical University, 25-27 May 2005. Book of Abstracts, Vol.2, pp.155-159
21. Frolov V.L., Nedzvetski D.I., Yampolski Yu. M., Koloskov A.V., Zalizovski A.V., Galushko V.L., Kasheev S.B., Vertogradov G.G., Vertogradov V.G., Blagoveshenskaya N.F., Kornienko V.A., Kagan L.M., Kelley M.C. Spectral features of field-aligned scattering from striations under conditions when a pump wave frequency is close to a gyroharmonic frequency. // Proc. of XXI Russian Conference on Radio Wave Propagation. Russia, Yoshkar-Ola, Mari State Technical University, 25-27 May 2005. Book of Abstracts, Vol.2, pp.179-182.
22. Kalichev A.A., Kim V.Yu., Panchenko V.A., Polimatidi V.P.,Uryadov V.P., Frolov V.L., Ponyatov A.A. Radar investigation frequency dependence of radio wave back scattering from artificial ionospheric disturbances. // Proc. of XXI Russian Conference on Radio Wave Propagation. Russia, Yoshkar-Ola, Mari State Technical University, 25-27 May 2005. Vol.2, pp.88-92.
23. Frolov V.L., Rapoport V.O., Parrot M., Rauch J.L. Preliminary results of the SURA-DEMETER experiment. 36th COSPAR Scientific Assembly. Beijing, China, 16-23 July, 2006. Abstract: COSPAR2006-A-00351.
24. Frolov V.L., Nedzvetski D.I., Sergeev E.N. Artificial ionosphere turbulence features related to short-pulse modifications of ionosphere F_2-region. 36th COSPAR Scientific Assembly. Beijing, China, 16-23 July, 2006. Abstract: COSPAR2006-A-00352.
25. Frolov V.L., Nedzvetski D.I., Sergeev E.N. Features of the NC_{th} in SEE spectra. 36th COSPAR Scientific Assembly. Beijing, China, 16-23 July, 2006. Abstract: COSPAR2006-A-00657.

9. Appendices

a) Figures 1 – 5.
b) Electronic copies of principal published papers.
These data will be sent as additional letters.

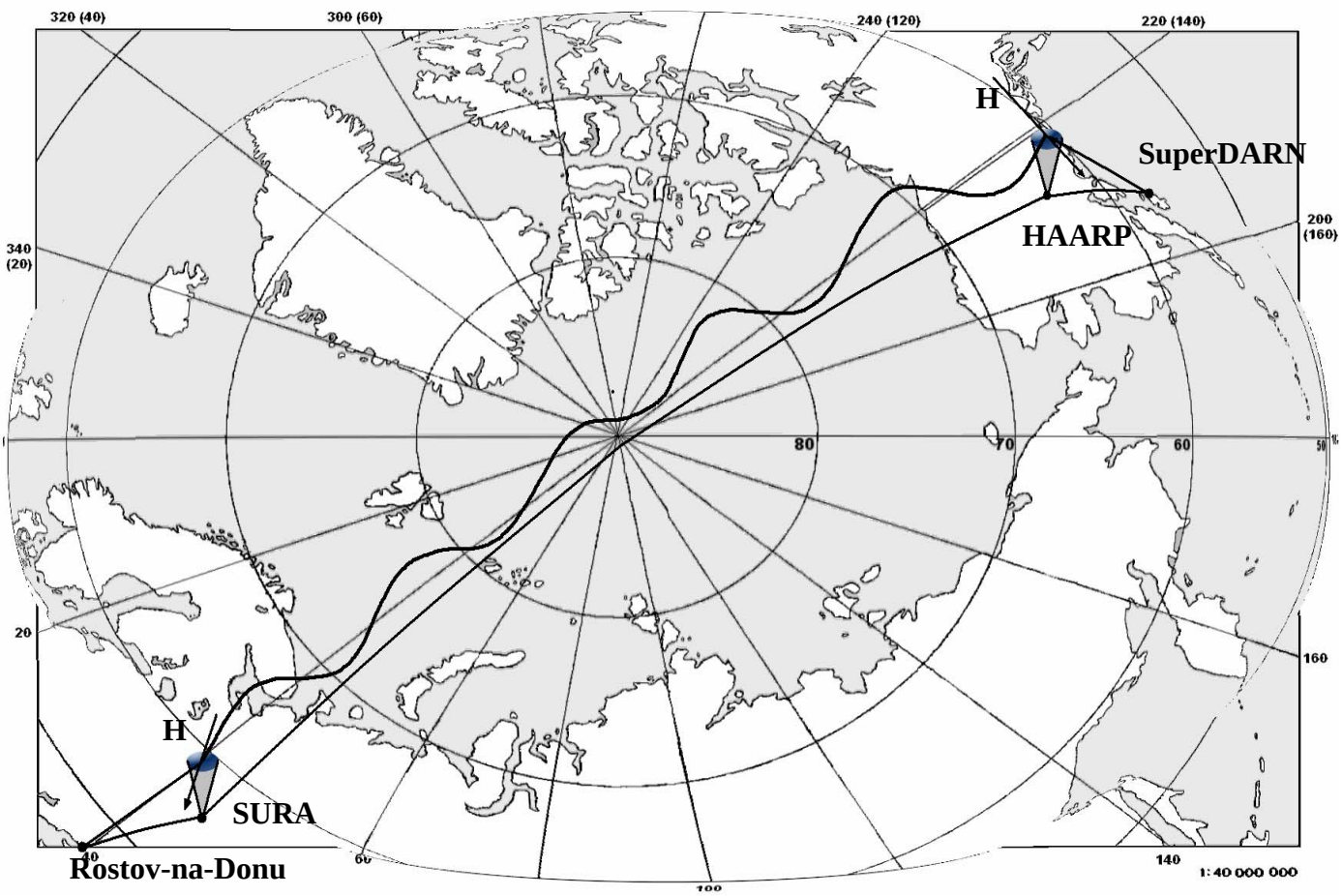
320 (40)
300 (60)
240 (120)
220 (140)
H
SuperDARN
HAARP
200
(160)
340
(20)
80
70
60
20
160
H
SURA
Rostov-na-Donu
140
1:40 000 000

Fig. 1

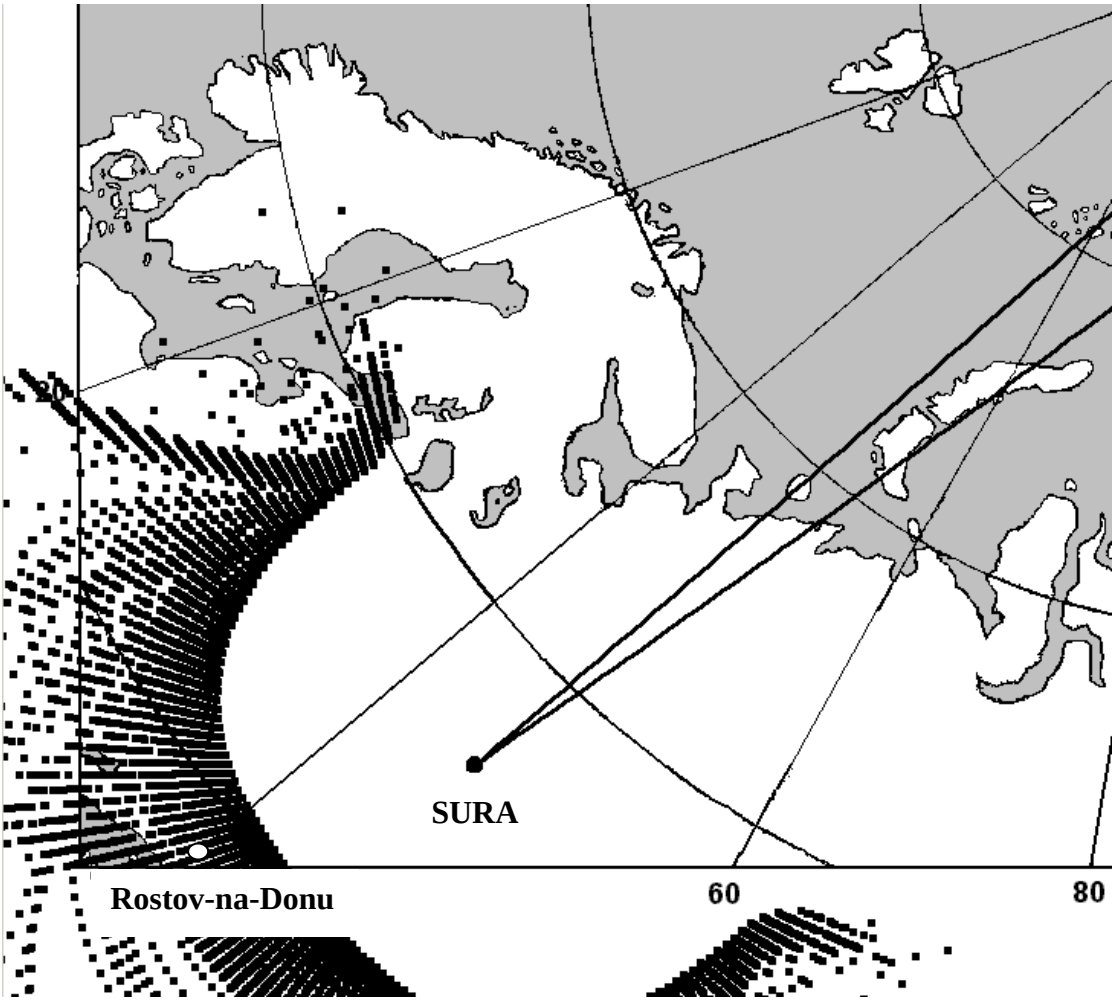

Fig. 2

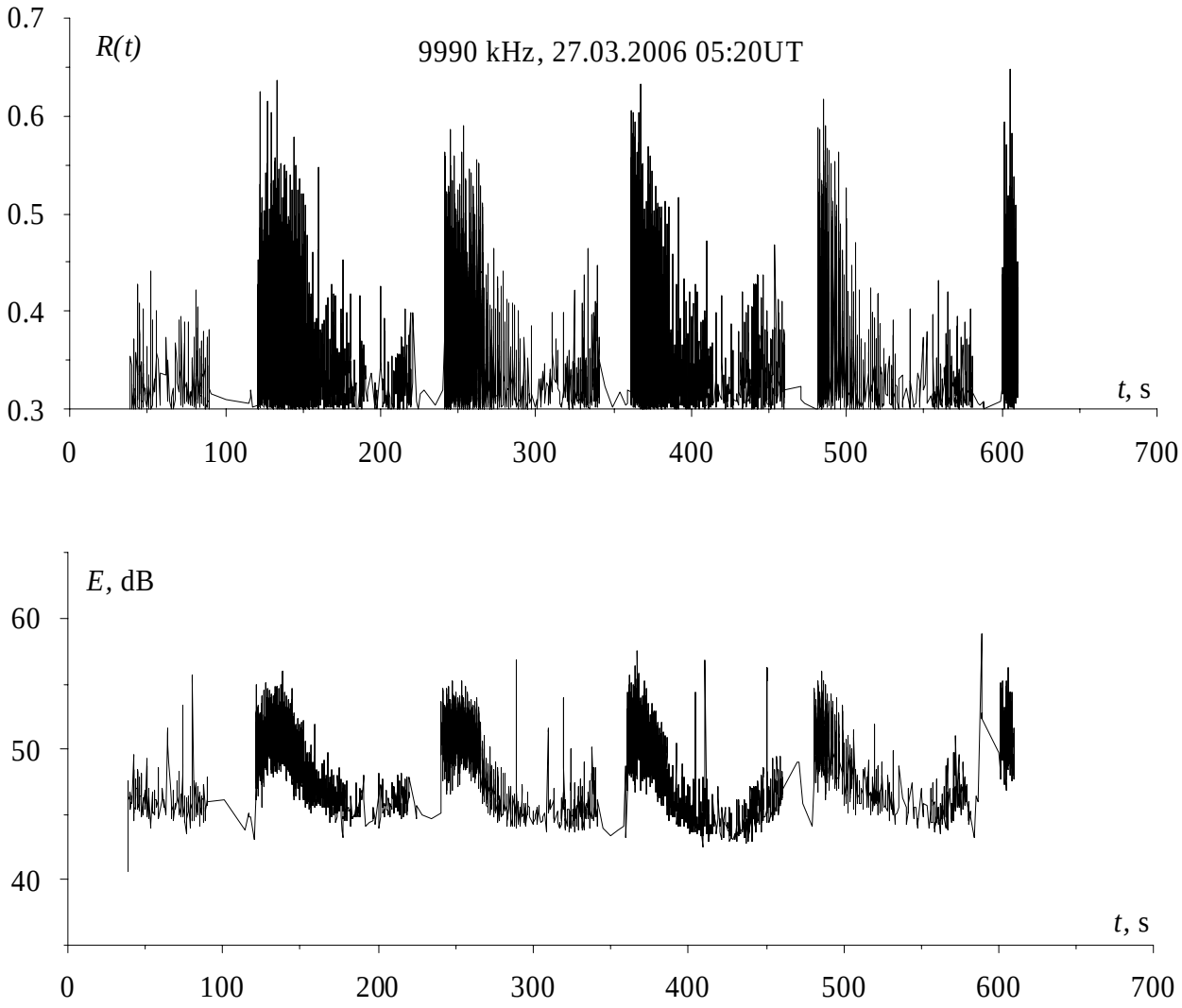
R(t)
9990 kHz, 27.03.2006 05:20UT
0.7
0.6
0.5
0.4
0.3
t, s
0
100
200
300
400
500
600
700
E, dB
60
50
40
t, s
0
100
200
300
400
500
600
700

Fig. 3

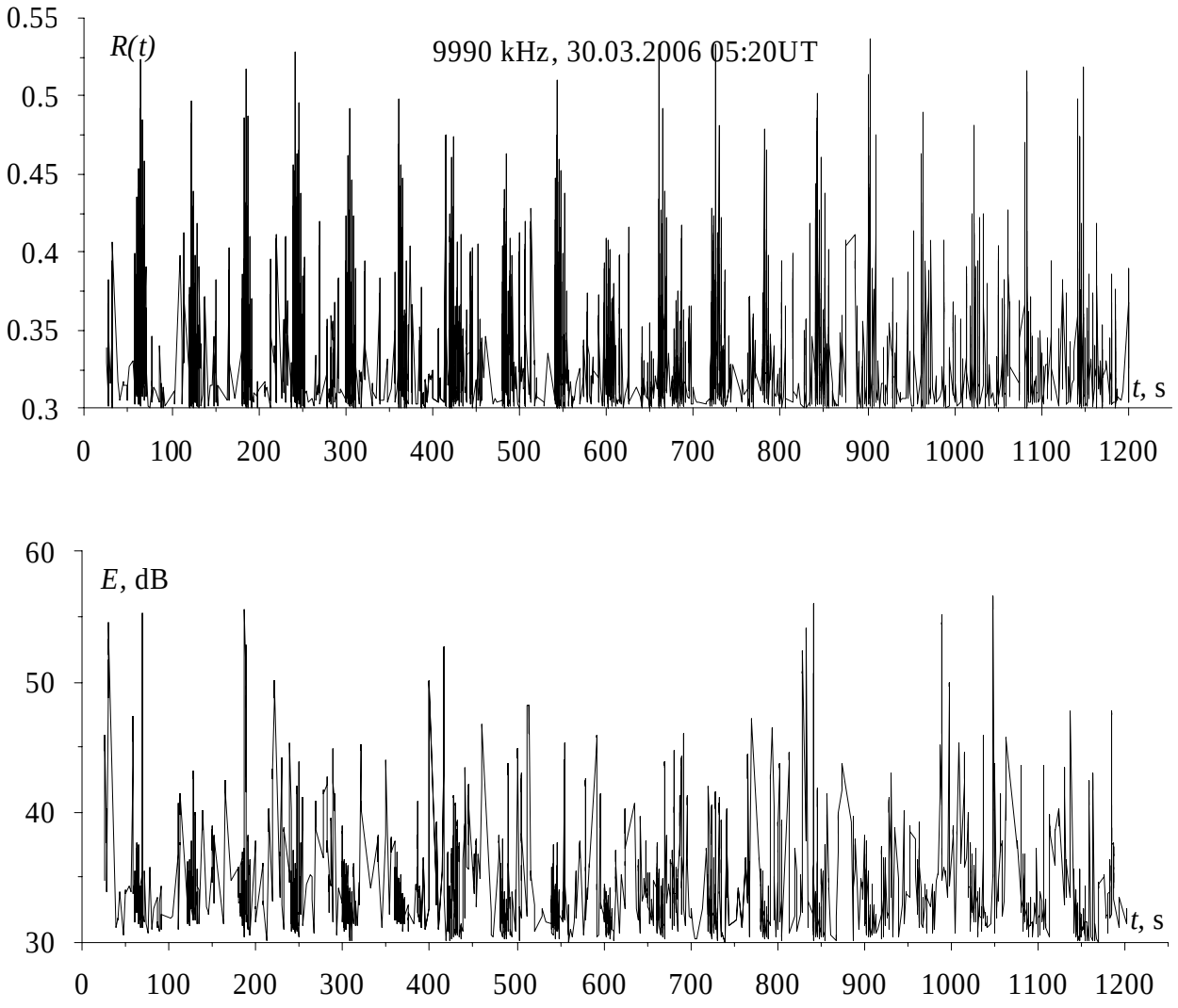
0.55
0.5
0.45
0.4
0.35
0.3
R(t)
9990 kHz, 30.03.2006 05:20UT
t, s
0
100
200
300
400
500
600
700
800
900
1000
1100
1200
60
50
40
30
E, dB
t, s
0
100
200
300
400
500
600
700
800
900
1000
1100
1200

Fig. 4

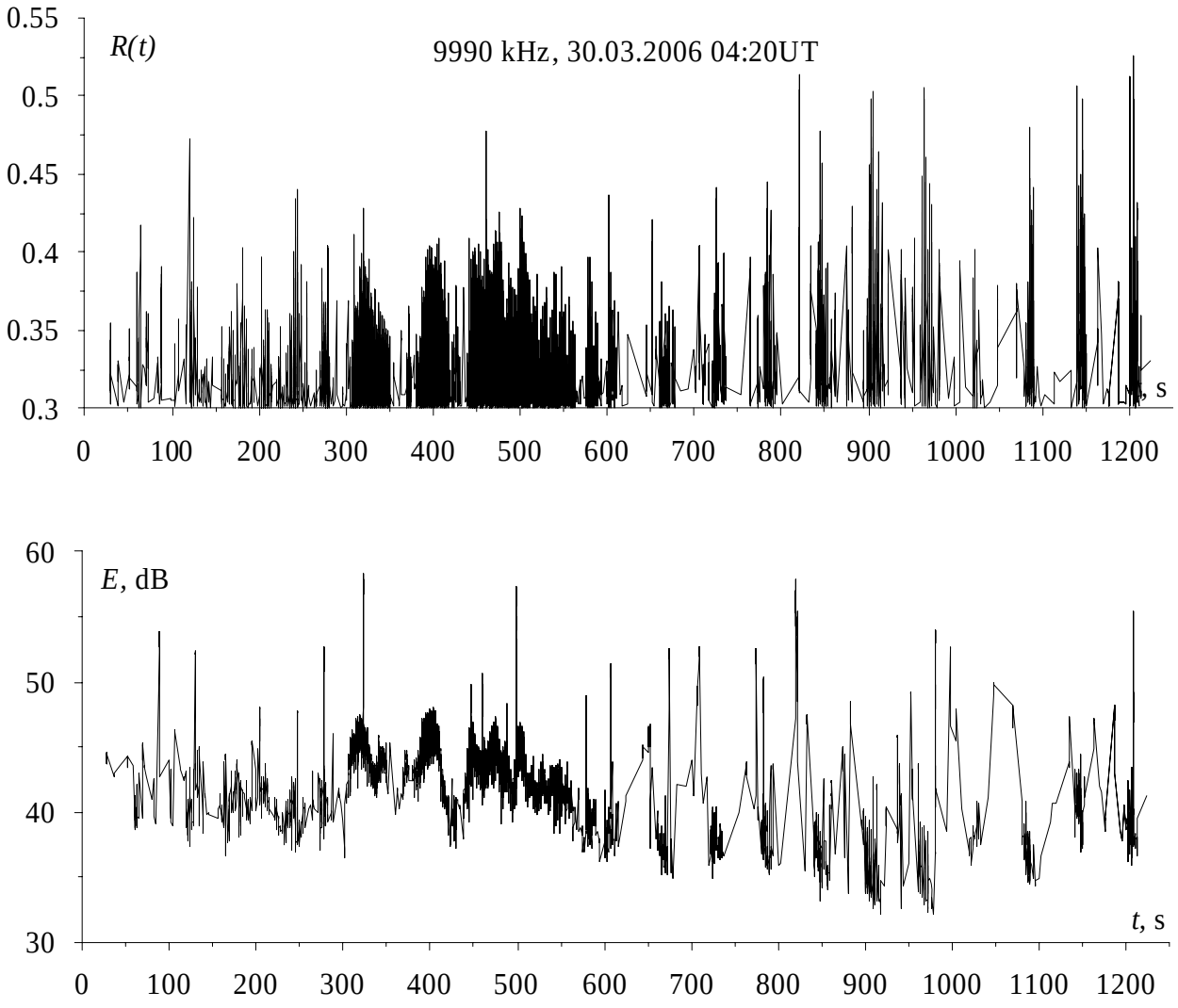
R(t)
9990 kHz, 30.03.2006 04:20UT
0.55
0.5
0.45
0.4
0.35
0.3
0
100
200
300
400
500
600
700
800
900
1000
1100
1200
t, s
E, dB
60
50
40
30
t, s

Fig. 5

Ponderomotive narrow continuum (NC_p) component in stimulated electromagnetic emission spectra

V. L. Frolov, E. N. Sergeev, and G. P. Komrakov
Radiophysical Research Institute (NIRFI), Nizhny Novgorod, Russia

P. Stubbe
Max-Planck-Institut für Aeronomie, Katlenburg-Lindau, Germany

B. Thidé, M. Waldenvik, E. Veszelei, and T. B. Leyser
Swedish Institute of Space Physics, Uppsala, Sweden

Received 10 August 2001; revised 11 February 2002; accepted 18 December 2003; published 13 July 2004.

[1] We present experimental results concerning the ponderomotive narrow continuum (NC_p) in stimulated electromagnetic emission spectra, generated in the ionospheric *F* region plasma by a powerful O mode electromagnetic wave. It is found that the generation of the NC_p is determined by the development of the parametric decay instability in the initial stage of the interaction of the HF pump wave with the plasma. The dependence of the NC_p temporal and spectral characteristics on pump power, pump frequency, time of day, and pump schedule as well as its gyrofeatures are considered. A possible mechanism for the NC_p generation is discussed. *INDEX TERMS:* 2403 Ionosphere: Active experiments; 7839 Space Plasma Physics: Nonlinear phenomena; *KEYWORDS:* HF-heating, ionosphere modification, plasma instabilities, HF-induced stimulated electromagnetic emissions

Citation: Frolov, V. L., E. N. Sergeev, G. P. Komrakov, P. Stubbe, B. Thidé, M. Waldenvik, E. Veszelei, and T. B. Leyser (2004), Ponderomotive narrow continuum (NC_p) component in stimulated electromagnetic emission spectra, *J. Geophys. Res.*, *109*, A07304, doi:10.1029/2001JA005063.

1. Introduction

[2] Almost 2 decades ago, it was discovered that a powerful HF heater wave of ordinary polarization, injected vertically from the ground into the *F* region of the ionosphere, gives rise to secondary electromagnetic waves [*Thidé et al.*, 1982], occurring as a result of various wave-plasma processes, including the conversion of HF electromagnetic waves into electrostatic waves and vice versa. Emissions of this type were termed Stimulated Electromagnetic Emissions (SEEs). A similar phenomenon, namely the generation of emissions stimulated by a short-pulsed powerful wave in the HF modified ionosphere, was found by *Belikovich et al.* [1981] and termed later Diagnostic Stimulated Electromagnetic Emission (DSEE) [*Erukhimov et al.*, 1988; *Frolov et al.*, 1994]. By now, the SEE has become a very useful tool for the study of nonlinear processes in ionospheric interaction experiments because both the short timescale ponderomotive nonlinearities, giving rise to Langmuir turbulence, and the long timescale thermal nonlinearities, leading to the excitation of large-scale and small-scale plasma density irregularities, are involved in the SEE generation (see, for example, *Erukhimov et al.* [1988], *Frolov* [1991], *Waldenvik* [1994], and the review by *Stubbe and Hagfors* [1997] and by *Leyser* [2001] and the papers referenced therein). Once the generation mechanism of a SEE component is identified, one can obtain information on both the background state of the ionospheric plasma and the nonlinear processes in question by observing the SEE evolution and variations of the SEE features under different conditions realized in the experiments. SEE has also been shown to be of potential importance as a diagnostic of geophysical processes [*Kagan and Frolov*, 1996; *Sergeev et al.*, 1997].

[3] SEE has been extensively investigated at the ionospheric modification facility in Tromsø, Norway [*Stubbe et al.*, 1984, 1994; *Leyser et al.*, 1990], at several Soviet/Russian facilities [*Boiko et al.*, 1985; *Erukhimov et al.*, 1987b; *Leyser et al.*, 1993; *Frolov*, 1995; *Frolov et al.*, 1999a], at the facility in Fairbanks, Alaska [*Armstrong et al.*, 1990; *Cheung et al.*, 1997], and at the facility in Arecibo, Puerto Rico [*Thidé et al.*, 1989, 1995]. SEE in its stationary state, typically reached after tens of seconds following the HF pump wave switch-on, shows a number of distinct spectral features, many of which were named by *Stubbe et al.* [1984]. The major emission components on the downshifted side of the SEE spectra are the "downshifted maximum" (DM) and the "downshifted peak" (DP) [*Stubbe et al.*, 1984], downshifted from the pump frequency, f_0, by approximately $\Delta f^- \simeq 9-15$ kHz and $\Delta f^- \simeq 2$ kHz, respectively, the "broad continuum" (BC) [*Boiko et al.*, 1985; *Leyser et al.*, 1993], extending up to $\Delta f^- \simeq 60-120$ kHz below the DM, and the "narrow continuum" (NC) [*Leyser et al.*, 1993; *Frolov et al.*, 1997a], occurring in the frequency range between the DM and the pump frequency, showing a rapid decrease of the intensity with increasing Δf^-. The major

0148-0227/04/2001JA005063$09.00

components on the upshifted side are the "upshifted maximum" (UM) [*Stubbe et al.*, 1984], which is a narrow peak at frequencies of about $\Delta f^+ \simeq 7-12$ kHz, the "broad upshifted maximum" (BUM) [*Stubbe et al.*, 1984, 1994; *Leyser et al.*, 1990, 1993; *Frolov et al.*, 1996, 1998], occurring in the SEE spectra at frequency shifts $\Delta f^+ \simeq 15-150$ kHz when f_0 is close to or slightly above harmonics n of the electron cyclotron frequency f_{ce} ($f_{ce} \simeq 1.3-1.35$ MHz in the F layer over the Sura facility, depending on the pump wave reflection height, $h_{ref} \simeq 200-300$ km), and the "broad upshifted structure" (BUS) [*Frolov et al.*, 1997b, 2000], occurring at frequency shifts $\Delta f^+ \simeq 10-100$ kHz for f_0 far above nf_{ce}. Here and below we use the notations Δf^- and Δf^+ to denote, respectively, negative and positive frequency shifts in the SEE spectra relative to the pump wave (PW) frequency f_0. The emission intensity for these SEE spectral components exceed, as a rule, natural and man-made noise levels by more than 10 dB and can be easily detected on the ground using a simple receiving antenna. The appearance of different spectral emission components depends strongly on the ionospheric conditions, the pump frequency (f_0), and the pump power [*Leyser et al.*, 1990, 1993; *Stubbe et al.*, 1994; *Sergeev et al.*, 1998; *Wagner et al.*, 1999]. In particular, the measurements performed have shown dramatic changes of the steady-state SEE spectra for small variations of f_0 around nf_{ce}. Based on the fact that the DM is not developed when $f_0 \cong nf_{ce}$, the gyroharmonic resonance condition can be found with a precision of a few kHz [*Leyser et al.*, 1994]. Such a DM property, as well as the spectral characteristics of the BC and BUM components [*Leyser et al.*, 1993; *Stubbe et al.*, 1994; *Frolov et al.*, 1998], is usually used in our experiments to determine the position of f_0 relative to nf_{ce}.

[4] In contrast to the DM, BC, BUM, and BUS, for which empirical models have been elaborated in the past few years (see the papers referenced above), the study of the NC has not been completed yet. This is because several different emission components were initially taken as one component named the "continuum" [*Stubbe et al.*, 1984]. Later, based on investigations of the SEE temporal evolution [*Boiko et al.*, 1985; *Erukhimov et al.*, 1987b, 1988; *Frolov*, 1991; *Waldenvik*, 1994], it was found that in the initial stage of pumping (during a few tens of milliseconds following HF wave turn on in the plasma) an emission component occurs in the lower sideband of the pump wave with an intensity strongly ($\sim$1–2 dB/kHz) decreasing with increasing downshift from f_0. As stated by *Erukhimov et al.* [1988], the generation of this SEE component is associated with the development of the parametric decay instability (PDI) [*Vas'kov and Gurevich*, 1973; *Fejer and Kuo*, 1973; *Alber et al.*, 1974; *Perkins et al.*, 1974; *Gurevich*, 1978]. This emission component was named the ponderomotive NC, NC_p [*Frolov*, 1991] (or the fast NC following by *Leyser* [2001]), implying that it is produced by the ponderomotive nonlinearity. Further, for the steady state, the continuum was found to be separated into two distinct spectral features, namely, the narrow continuum (NC) extending approximately 10–20 kHz below f_0 and the broad continuum (BC) having frequency components extending up to about 100 kHz below f_0 [*Leyser et al.*, 1993]. As stated by *Frolov et al.* [1997a], the NC, observed in the stationary SEE spectra, is produced by the thermal parametric (resonance) instability (TPI) [*Vas'kov and Gurevich*, 1975; *Grach et al.*, 1977; *Gurevich*, 1978; *Das and Fejer*, 1979]. This emission component was named by *Frolov et al.* [1997a] the thermal NC, NC_{th}. Hence by now three different SEE components (BC, NC_p, and NC_{th}) have been identified within the continuum. Such a separation of the continuum into three different components has required a revision of the available experimental data. The first effort on this way was made by *Frolov et al.* [1997a]. However, new data, obtained in past few years, give reason to continue this work.

[5] In the present paper we focus mainly on the NC_p features because an empirical model for this SEE component has not been elaborated yet. To fill this gap, we summarize experimental results obtained at the Sura heating facility (Nizhny Novgorod, Russia) during many heating campaigns in the years 1988 to 1999 and published in part by *Frolov* [1991, 1995], *Frolov et al.* [1997a, 1997c, 1999a, 1999b], and *Sergeev et al.* [1994, 1998, 1999]. For generality, we also use some experimental data of our earlier measurements carried out at the Zimenki (Nizhny Novgorod) [*Karashtin et al.*, 1986; *Erukhimov et al.*, 1987a] and Gissar (Dushanbe, Tadzhkistan) [*Erukhimov et al.*, 1987b] facilities. This is done with the goal to give the reader a comprehensive picture of NC_p features, as well as to present experimental results which have been published earlier in Soviet/Russian journals not easily accessible in western countries. The elaboration of an empirical model for the NC_p is important for the development of new methods employing the SEE as diagnostics of HF-induced ionospheric turbulence. It should be emphasized here that the NC_p, being generated slightly below the pump wave reflection height due to ponderomotive nonlinearities, makes it possible to investigate Langmuir turbulence, supplementing the incoherent scatter radar (ISR) technique, as demonstrated by *Thidé et al.* [1995]. In contrast to the NC_p, the DM and BC are determined by the excitation of upper hybrid (UH) waves and small-scale field-aligned irregularities (striations) in the UH resonance region [*Grach*, 1985; *Leyser et al.*, 1990; *Stubbe et al.*, 1994; *Gurevich et al.*, 1997; *Mjølhus*, 1998]. By this means, different types of artificial ionospheric turbulence (AIT) can be investigated simultaneously in one experiment by the measurement of different SEE components (mainly DM, BC, and NC_p). This represents the major advantage of the SEE method over the ISR method, where the latter is limited by the use of nearly vertical antenna beams which make the study of UH turbulence features impossible.

[6] The organization of the paper is as follows. In section 2 the experimental arrangement is outlined, including a brief description of the diagnostic equipment employed in our measurements. In section 3 the general features of the major SEE components, observed in the lower sideband, are characterized. Experimental results concerning the features of the NC_p are shown in section 4. In section 5 we present experiments in which an additional heating scheme is used. An empirical model for the NC_p, as well as a comparison of SEE results with ISR results, is presented in section 6. Concluding remarks are given in section 7.

2. Experimental Arrangement

[7] The majority of the experiments discussed in this paper were conducted at the Sura heating facility of the

Radiophysical Research Institute (NIRFI), Nizhny Novgorod, Russia (geographic coordinates, 56.13°N, 44.1°E). The magnetic dip at *F* region heights is 71°. The Sura facility comprises three HF broadcast transmitters, each of them producing a maximum continuous output power of 250 kW in the frequency range 4–25 MHz. Each transmitter is connected to its own subantenna array with dimensions 100 × 300 m^2, elongated in the E–W direction. Each subantenna array consists of four rows of 12 wideband crossed dipoles operating in the frequency range 4.3–9.5 MHz. This three-module configuration allows to radiate independently up to three pump waves of either left or right circular polarization with different frequencies, powers, and timing. When all three subantenna arrays are combined into one (12 × 12 crossed dipoles), the facility is capable of producing an effective radiated power (ERP) of 120 MW at 4.3 MHz which increases up to 280 MW at 9.3 MHz, corresponding to a pump intensity of about 0.5–1 mW/m^2 at 200 km altitude if absorption in the lower ionosphere is disregarded. The antenna beam can be steered in the geomagnetic meridian plane within the range ±40° off vertical.

[8] The diagnostic equipment at the Sura facility, placed at a receiving site situated approximately 1 km off the heater, is designed for (1) measurements of pump wave self-action effects, (2) SEE spectral and temporal evolution measurements, and (3) measurements of the anomalous absorption of probing waves sounding the disturbed ionospheric volume. The diagnostic facility comprises a wideband receiving antenna and different types of receivers and recorders. The receiving antenna consists of 12 crossed dipoles operating in the frequency range 4.5–6 MHz with approximately 15 dB gain; it is also used at higher frequencies but with lower efficiency. With this setup, it is possible to separate HF signals with O-mode, X-mode, or linear polarization. When required, a choke quartz filter, tuned to the pump wave (PW) frequency, is used to attenuate the received PW signal by about 20–30 dB. This is important for measurements of SEE features at small ($|\Delta f| \leq 7$ kHz) frequency shifts.

[9] The SEE spectra and the pump wave signals are monitored with a computer-controlled HP-3585A spectrum analyzer operating in sweep mode. The temporal resolution of such spectral measurements is, as a rule, a few seconds. To study faster processes in the PW and SEE evolution, we use eight receivers with frequency bands of 0.3–3 kHz. One of the receivers is always tuned to the PW frequency, and the others are tuned to characteristic parts of the SEE spectrum. In such measurements the highest temporal resolution is about 0.3 ms, corresponding to a 3 kHz Gaussian filter. The detected signals are stored by means of a computerized data acquisition system or are recorded in analogue form by a seven-channel, high-speed tape recorder for further digital processing. One of the remaining seven receivers is usually tuned to the DM frequency range because the appearance of the DM is associated directly with the presence of striations with cross-field scales $l_\perp \leq$ 20–30 m, HF-induced in the disturbed ionospheric volume by the TPI. In this respect the DM serves as a point of reference in our SEE measurements aiming at diagnosing the AIT. Besides, the DM can be used for finding the gyroharmonic frequency by the way of determining the pump frequency range in which the DM is strongly suppressed or absent [*Leyser et al.*, 1994; *Stubbe et al.*, 1994; *Frolov et al.*, 1998].

[10] During the heating campaign in September 1991, a purpose-built wide dynamic range receiver, equipped with a quadrature detector to receive the entire signal, was used to study SEE features [*Waldenvik et al.*, 1993; *Waldenvik*, 1994]. The baseband in-phase and quadrature phase signals were directly sampled to storage media. The nominal sampling rate used was 200 kHz. The response of the receiving system to a step-like input signal is a sharp overshoot that vanishes within, at most, 3 ms. Thus the first few milliseconds of data after the arrival of the sky wave, as well as after pump wave switch-off, may contain erroneous information, and was therefore discarded in the data analysis. Since typical e-folding growth and decay times for the high-frequency turbulence evolution are not longer than a few milliseconds [*Wong et al.*, 1983; *Djuth et al.*, 1986; *Sergeev et al.*, 1997, 1998; *Cheung et al.*, 2001], this technique does not allow to study, by means of SEE, the fastest stage in the parametric decay processes.

[11] To study the features of the NC_p, which have typical growth times less than 10–20 ms [*Erukhimov et al.*, 1988; *Sergeev et al.*, 1998], we used a scheme of short-pulse radiation for the PW with pulse duration $\tau_p \simeq 10$–200 ms and interpulse period $T_p \simeq 1$–10 s ($Q = T_p/\tau_p \simeq 50$–100) to ensure that the pulse pump power, averaged over the pulse repetition period, $\langle \tilde{P}_{eff} \rangle = \tilde{P}_{eff,p}/Q$, does not exceed the threshold value for the TPI development, $\tilde{P}_{th\ TPI}$, which is about 0.5–1 MW ERP [*Frolov et al.*, 1997c]. "Cold start" conditions are thus realized in the experiments. Notice that we take into account here the power decrease by one-way wave absorption in the ionospheric *D* and *E* layers and determine a corrected power, denoted by $\tilde{P}_{eff}$, which is appropriate for application to *F* region modification effects.

[12] Since the SEE has a noise nature, averaging is needed to decrease strong fluctuations of the emission intensity. An averaging of the SEE intensity over 10–50 pulse data sets with subsequent subtraction of the background noise is usually done in the data processing, especially when emission relaxation features are studied. Results of this procedure are presented in Figures 3, 5, 6, and 10. Besides, by recognizing that the usual duration of the measurements should not be longer than 5–10 min because of possible variations of the ionospheric conditions and, in consequence, of the experimental conditions, an upper limit for the pulse repetition period of 10–20 s should be used.

[13] It should be emphasized that in studying the features of the NC_{th}, DM, and BC, which have typical growth times of a few seconds [*Boiko et al.*, 1985; *Leyser et al.*, 1993], we often use a quasi-continuous mode for the PW radiation with short off times (typically 20 ms) every 100–200 ms [*Sergeev et al.*, 1997]. Since the intensity of the small-scale striations remains nearly constant during such short off periods, the SEE behavior is mainly determined here by evolution of the HF plasma turbulence. Such a quasi-continuous mode for PW radiation is employed to obtain a high temporal discrimination (every 100–200 ms) of the SEE characteristics during each heating cycle, and to investigate the high-frequency turbulence evolution at its different development stages. On the other hand, such a heating scheme allows to obtain well-averaged SEE signals at the steady state stage

over the quasi-continuous heating period (100–200 ms) and to determine with high accuracy variations in the magnitudes of typical growth and decay times for the high-frequency electrostatic turbulence. By using such a heating scheme, the ionospheric modification lasts, as a rule, 2–3 min with a subsequent 7–8 min off period to ensure a truly "cold start" for the next pumping cycle.

[14] In some measurements we use a so-called additional heating scheme, in which radiation of two different pump waves is employed [*Frolov*, 1995]. One of them is the O-mode pump wave which is used for the SEE excitation and, in turn, for AIT diagnostics. Its power is chosen weak but sufficient to excite an unsaturated turbulence level, which has the ability to respond flexibly to an additional external action. One transmitter of the facility is used for this purpose. The second powerful (heating) wave may be either in O-mode or X-mode polarization. It is used to create additional ionospheric perturbations whose influence on the AIT is indicated by changes in the SEE features. One or two transmitters of the facility are employed for this radiation. Such a scheme of additional heating allows to separate the influence of different factors on the AIT generation and evolution by varying the polarization, power, frequency, and timing of the second wave.

[15] Another experimental scheme consists in sounding the disturbed ionospheric volume by short HF pulses. It was found that the growth time even for SEE components of thermal origin (DM and BC, first of all) is of the order of a few milliseconds if the low-frequency ionospheric turbulence (striations) has been HF-induced by previous modification with continuous or quasi-continuous pumping, lasting a few minutes [*Erukhimov et al.*, 1988; *Frolov et al.*, 1994]. This allows to measure SEE features using short (~10–20 ms) powerful (~10 MW ERP) pump pulses with frequencies both close to and far from the PW frequency. The emission observed as ionospheric response to the sounding wave pulse has been named the diagnostic SEE (DSEE) [*Erukhimov et al.*, 1988]. Naturally, under conditions of well-developed striations, DSEE and SEE spectra are copies of each other. The studies performed have shown that applying such a scheme of pulse pumping to different starting conditions can induce either the ponderomotive part of the narrow continuum (NC_p) when the unperturbed ionosphere is modified (so-called cold-start conditions) or thermal SEE components (such as DM or BC) when a preconditioned ionosphere with well-developed striations is used (so-called preconditioned turn-on). The term "preconditioned" means that previous O-mode heating has been applied to excite the artificial ionospheric turbulence. In this case the long-time DSEE behavior after PW switch-off represents primarily the evolution of artificial small-scale irregularities, since the collisional damping time of HF-induced plasma waves amounts to a few milliseconds [*Sergeev et al.*, 1998]. A detailed description of the DSEE technique, including the selection of diagnostic wave parameters, can be found in the work of *Frolov et al.* [1994].

[16] For routine monitoring of the F_2 layer critical frequency, f_{0F_2}, and of the level of natural or artificial ionospheric disturbances, an ionosonde collocated with the Sura facility is used. When the situation requires, the ionosonde is employed in fixed frequency mode as a low power pulse transmitter to determine the magnitude of the linear absorption in the lower ionosphere and to calculate the reduction of the HF power transported into the upper ionosphere. Such measurements are necessary when the true value of the threshold power for the processes in question is to be determined, or when experimental results, obtained under different ionospheric conditions, are to be compared.

3. Some General Features of the SEE Evolution in the Lower Sideband of the PW Frequency

[17] For a better visualization of the different evolution stages of the SEE components of interest here (DM, BC, and NC, first of all), we give a brief summary of some principal experimental results concerning their general spectral and dynamical behavior when the PW frequency is far away from electron cyclotron harmonics. These earlier experimental results will serve as a reference for the new results to be presented in the subsequent sections.

3.1. Spectral Features of the SEE

[18] Figure 1 shows a sequence of emission spectra, measured at times $t \simeq 0.01$, 0.05, 0.1, 0.2, 0.5, 1, 2, and 4 s (Figures 1a–1h, respectively) after the PW switch-on in the plasma. Here the zero offset frequency corresponds to the PW frequency $f_0 = 5828$ kHz, which is suppressed in the receiver by about 80 dB in the frequency band ±60 Hz around the carrier by means of a low-frequency narrow-band rejection filter [*Waldenvik*, 1994]. The time intervals to which the spectra belong are labeled in the upper left corner of the panels. In this experiment the heater was operated 10 s on, 50 s off (for short we shall use below a notation of the form [+10 s; −50 s]) with pump power $\tilde{P}_{eff} = 30$ MW ERP. Notice that in all spectra shown in Figure 1 and below there is a large number of narrow spikes. These are due to interfering HF radio stations.

[19] From Figure 1 it is clearly seen that for $t \leq 0.5$ s the lower sideband of the SEE spectrum consists solely of the ponderomotive part of the narrow continuum (NC_p), the spectrum of which extends from f_0 down to $\Delta f^- \simeq 40$ kHz with a slope of about 1 dB/kHz. The spectrum at $t = 1$ s shows the appearance of the BC, extending up to $\Delta f^- \simeq 100$ kHz and having an exponential spectral form with a slope of about 0.3 dB/kHz without any discrete structures. The DM appears only slightly in the emission spectrum here, but at $t \geq 2$ s it is the dominant feature with its spectral maximum downshifted approximately 12 kHz from $f_0 = 5828$ kHz, with a discreteness of more than 5 dB over the BC. The NC_{th} can be observed here between f_0 and the DM in the frequency range $\Delta f^- \leq 5–7$ kHz as an emission rapidly decreasing in intensity with the increase in Δf^-. Such temporal evolution and spectral features of the SEE are typical when the PW frequency lies in the frequency range between the 4th and 5th gyroharmonic where the thermal emission components have their highest stationary intensities [*Frolov et al.*, 2001]. The spectrogram in the lower panel represents the SEE intensity as a function of frequency and time, showing at one glance all features of the SEE temporal evolution discussed above.

3.2. Some Remarks on the SEE Temporal Evolution

[20] Figure 2 displays results of simultaneous measurements of the evolution of artificial small-scale field-aligned

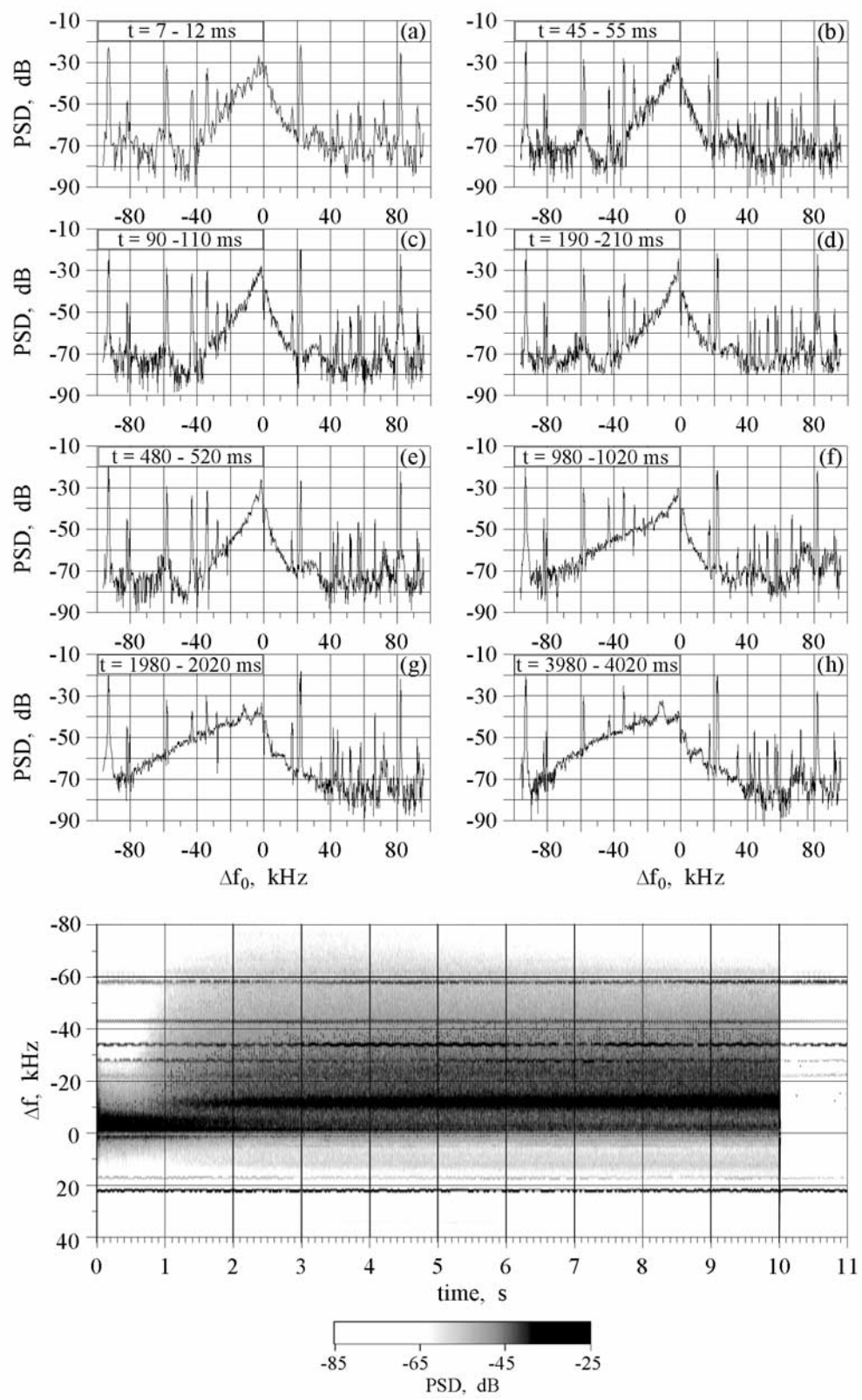

Figure 1. Sequence of emission spectra, measured around t = 0.01, 0.05, 0.1, 0.2, 0.5, 1, 2, 4 s after PW switch-on in the plasma (Figures 1a–1h, respectively) in a 10 s on, 50 s off pumping mode with pump frequency f_0 = 5828 kHz and ERP power $\tilde{P}_{eff}$ = 30 MW. The spectrogram in the lower panel represents the SEE intensity as a function of frequency shift (with respect to pump frequency) and time after switch-on. The measurements were performed on 25 September 1991 at T = 1330–1350 LT.

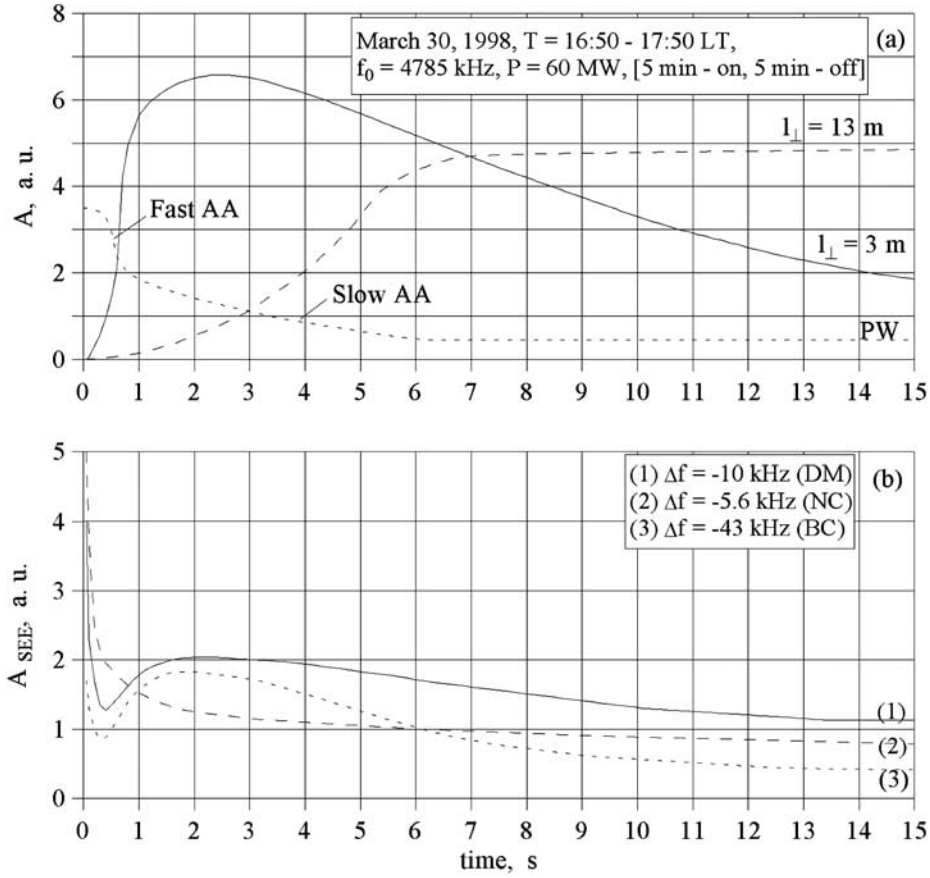

Figure 2. Simultaneous measurements of (1) temporal evolution of artificial small-scale field-aligned irregularities (striations) with scale lengths $l_\perp$ = 3 and 13 m perpendicular to the magnetic field, obtained in field-aligned scatter experiments (Figure 2a); (2) behavior of the PW sky signal (Figure 2a); (3) SEE temporal evolution after PW switch-on at the three frequency shifts Δf^- = 5.6, 10, and 43 kHz, corresponding to the NC, DM, and BC (Figure 2b). For the purpose of clarity, all curves presented here have been smoothed by hand over the random amplitude-time fluctuations of the received signals to bring out the systematic features. The measurements were performed on 30 March 1988 at T = 1650–1750 LT, with pump frequency f_0 = 4785 kHz, ERP power P_{eff} = 150 MW and 5 min on, 5 min off pumping mode.

irregularities (striations) with scale lengths $l_\perp$ = 3 and 13 m across the magnetic field, obtained by means of the field-aligned scattering technique (Figure 2a), the behavior of the PW sky signal (Figure 2a), and the SEE temporal evolution at the three frequency shifts Δf^- = 5.6, 10, and 43 kHz, corresponding to the NC, DM, and BC (Figure 2b). For the purpose of clarity, all curves in Figure 2 are smoothed by hand over the random amplitude-time fluctuations of the received signals to bring out the systematic features. The measurements were performed on 30 March 1988 in the eveningtime with f_0 = 4785 kHz and P_{eff} = 150 MW ERP [*Frolov*, 1991].

[21] From the data presented in Figure 2a we can conclude that the fast stage of the anomalous absorption (FAA) development, which is characterized by a strong decrease in the sky PW amplitude after $t = \tau_{FAA} \simeq 0.3$–0.5 s (curve labeled PW), is accompanied by the growth of the 3-m irregularities, while dekameter irregularities control the slow stage of the AA, during which a noticeable decrease in the intensity of the 3-m irregularities is also observed (see also *Frolov et al.* [1997c] as a reference source). The SEE temporal evolution presented in Figure 2b shows initial short-time peaks at $t \leq 0.3$ s in the emission intensities at all three frequency shifts Δf^- = 5.6, 10, and 43 kHz, which are associated here with the generation of the ponderomotive NC (NC_p); the emissions, observed at these frequency shifts for longer times of the SEE evolution, represent the thermal NC (NC_{th}), DM, and BC, respectively [*Frolov et al.*, 1997a]. It is significant that the NC_p intensity decreases abruptly during the first 100 ms of pumping, i.e., before the FAA development and the growth of the 3-m irregularities (see also subsection 4.2 below). In these experiments, as well as in other measurements [*Erukhimov et al.*, 1988], it has been found that the development of the TPI and the growth of the intensity of the striations leads to a suppression of both the PDI and the NC_p. This will be clearly demonstrated by additional heating experiments described in section 5. The direct correlation between striations and SEE represents the basis for using SEE measurements as a new diagnostic method to study features of small-scale irregularities, both of artificial

and natural origin [*Erukhimov et al.*, 1988; *Frolov et al.*, 1994; *Kagan and Frolov*, 1996; *Sergeev et al.*, 1999].

4. Features of the Ponderomotive Narrow Continuum

4.1. Spectral Characteristics

[22] Returning to Figure 1, Figures 1a–1e represent the temporal evolution of the NC_p during the first 500 ms of modification. On the basis of these data we can conclude that the NC_p has its maximum intensity and widest spectrum (extending up to $\Delta f^- \simeq 40$ kHz) after about 10 ms following PW switch-on in the plasma. For longer times ($10 \le t \le 500$ ms) some decrease in the emission intensity by 6–10 dB (so-called short-time overshoot) is observed, together with a narrowing of the NC_p spectrum. We use the terms short-time (timescale of a few tens of milliseconds) and long-time (timescale of a few seconds) overshoot in place of miniovershoot and main overshoot, as introduced by *Showen and Kim* [1978], to reflect more correctly their physical nature, associated with ponderomotive and thermal plasma processes, respectively. Notice that the NC_p maximum spectral intensity observed here at $\Delta f^- \simeq 1$–2 kHz is about 5 dB higher than the DM spectral intensity (see Figure 1h), which is the most intensive emission in stationary SEE spectra for $f_0 \ge 4.0$ MHz. The experiments considered here, as well as earlier measurements [*Boiko et al.*, 1985; *Erukhimov et al.*, 1988; *Frolov et al.*, 1997a], have shown that in the frequency range $0 < \Delta f^- < 40$ kHz the NC_p spectral intensity decreases strongly with increasing Δf^-, having a constant slope of about 1 dB/kHz (up to 2 dB/kHz in some other cases).

4.2. Temporal Development

[23] Studies of the NC_p temporal development in the initial stage of interaction of the PW with the ionospheric plasma, results of which are presented in Figure 3 were performed on 17 June 1994 (T = 1910–1940 LT) with $\tilde{P}_{eff}$ varied in 3 dB steps from full power (60 MW ERP) down to −15 dB [*Frolov et al.*, 1997a]. In these measurements the pump scheme [+0.2 s; −9.8 s] was used to ensure cold start conditions in each subsequent PW switch-on, with the possible exception of the case $\tilde{P}_{eff}$ = 60 MW ERP for which the PW power, averaged over a pump pulse period, $\langle \tilde{P}_{eff} \rangle \simeq 1$ MW ERP, was high enough to create a preconditioning effect that could affect the time development of the SEE. The SEE temporal evolution in the experiment was studied at two frequency shifts, Δf^- = 13 kHz (curves 1) and 20 kHz (curves 2). Besides, the intensity of the ionospherically reflected PW was also recorded during the heating cycle, and its temporal evolution is represented here by the curves labeled PW.

[24] From the data shown in Figure 3 it can be clearly seen that for all pump powers used, the NC_p experiences a short-time overshoot, more pronounced for smaller frequency shifts. The steady-state intensity of the NC_p, reached within about 100 ms, is several times smaller than the maximum intensity at times $t_{\max} \simeq 10$–50 ms. The $t_{\max}(\tilde{P}_{eff})$ dependence is shown in Figure 4a (curves marked by −13 and −20 kHz), which can be well represented by a power law in the form $t_{\max} \propto \tilde{P}_{eff}^{-\eta}$, where $\eta \simeq 0.4$–0.5. The time $t_{\max}$ increases by approximately a factor of 1.3 with an increase of Δf^- from 13 to 20 kHz. These data show also that the time of NC_p formation is about 5–40 ms, where shorter times correspond to higher pump powers. For both frequency shifts the dependence of the NC_p intensity on the pump power is shown in Figure 4b for two states, first when the emission reaches its maximum level (solid lines) and second for the quasi-stationary state after the short-time overshoot (dashed lines). It can be seen that a substantial enhancement of the NC_p generation for both these states occurs when $\tilde{P}_{eff} \ge 15$ MW ERP, which is manifest in the sharp increase of the emission intensity and the broadening of its spectrum.

[25] These measurements enable us also to compare directly the NC_p features with the development of the PDI. The latter shows its existence in the form of a strong (up to 20 dB) decrease in the ionospherically reflected PW intensity within $t \simeq 1$–10 ms, which is the result of an energy transfer from the electromagnetic pump into the electrostatic decay products. This phenomenon is known as striction self-action, SSA [*Erukhimov et al.*, 1982; *Frolov et al.*, 1997c], or as short timescale anomalous absorption [*Fejer and Kopka*, 1981; *Stubbe et al.*, 1982]. We prefer to use the term SSA for the ponderomotive absorption and the term AA for the anomalous absorption due to the TPI, in order to have two distinctly different names for these two different phenomena. It has been stated that the threshold power of the SSA, $\tilde{P}_{th\ SSA}$, is about 2 MW ERP ($E_{th\ SSA} \simeq 0.4$–0.5 V/m) at $f_0 \simeq 6$ MHz and that $E_{th\ SSA} \propto f_0^{3/2}$ if the reflection altitude of the PW, h_{ref}, is higher than 200 km [*Erukhimov et al.*, 1987b]. On the basis of PDI theories [*Vas'kov and Gurevich*, 1973; *Alber et al.*, 1974; *Perkins et al.*, 1974], the frequency dependence of the SSA threshold is obtained as $E_{th\ SSA} \propto (\nu_{ei} N_e T_e / f_0)^{1/2}$, where $\nu_{ei} \propto N_e \propto f_0^2$, assuming that for $h_{ref} \ge$ 200 km damping of HF-induced plasma waves is mainly determined by electron-ion collisions.

[26] The SSA can be easily recognized in Figure 3, where the temporal evolution of the ionospherically reflected PW signal is represented by solid lines marked as PW. It manifests itself in a fast and strong decrease in the PW received intensity and can be characterized by the development time, τ_{SSA}, during which the received intensity decreases by a value of 8.6 dB relative to its undisturbed level, and by the fraction of absorbed energy in the turbulent plasma layer, k_p. The latter can be calculated using the relation $k_p = (E_0^2 - E_1^2)/E_0^2$, where E_0 and E_1 are the received PW signal strengths determined immediately after arrival of the PW and within a few milliseconds when the SSA has been developed, respectively. The method of determining τ_{SSA}, E_0, and E_1 is demonstrated in the lower right panel of Figure 3. It should be mentioned that for times exceeding 10 ms the development of quasi-periodical oscillations can be seen, and only later the anomalous absorption stage, which has been demonstrated in Figure 2a, will set in. The amplitude-time history of the ionospherically reflected PW signal has been analyzed in more detail by *Frolov et al.* [1997c].

[27] The dependence $\tau_{SSA}(\tilde{P}_{eff})$ for the data presented in Figure 3 is plotted in Figure 4a. This function has almost the same slope as the two $t_{\max}(\tilde{P}_{eff})$ curves, but the time τ_{SSA} is considerably shorter than $t_{\max}$. However, for the frequency offset $\Delta f^- \simeq 5$ kHz it has been found that $t_{\max} \simeq \tau_{SSA}$. This allows us to conclude that a broadening of the NC_p

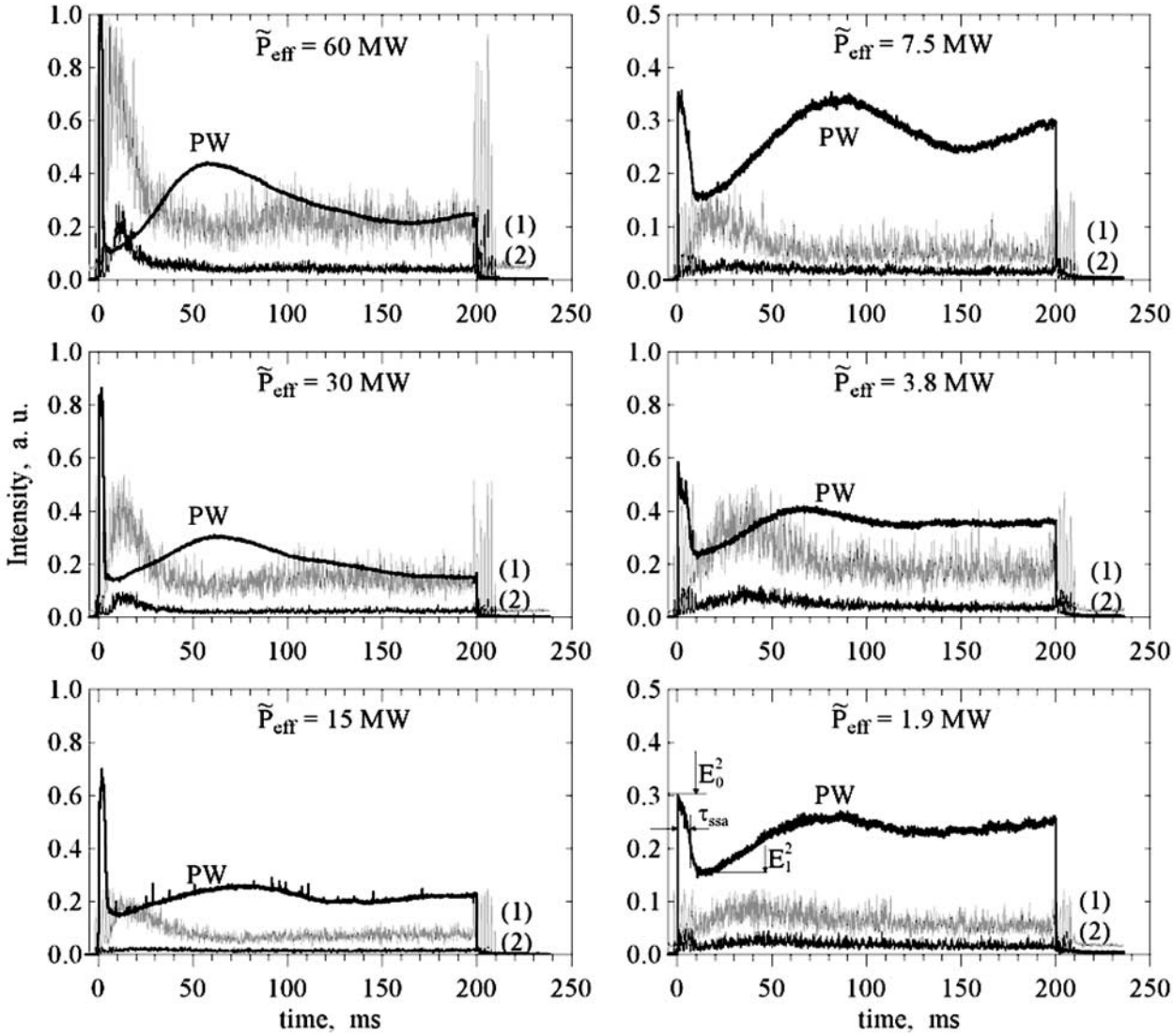

Figure 3. Examples of the NC_p temporal development at two frequency shifts, $\Delta f^- = 13$ kHz (curves 1) and 20 kHz (curves 2), for different pump powers varying in 3-dB steps from full power, $\tilde{P}_{eff} = 60$ MW ERP, down to $\tilde{P}_{eff} = 1.9$ MW ERP. The temporal evolution of the ionospherically reflected PW signal is represented here by lines marked as PW. An averaging of the SEE intensity over 22–30 pulse data sets with subsequent subtraction of the background noise has been done here in the data processing. The technique for determiningthe quantities τ_{SSA}, E_0, and E_1 is demonstrated in the lower right panel. The measurements were performed with pump frequency $f_0 = 4785$ kHz in 0.2 s on, 9.8 s off pumping mode on 17 June 1994, T = 1910–1940 LT.

spectrum occurs in the initial stage, i.e., during the first few tens of milliseconds of the PW-plasma interaction. As seen in Figure 4c, k_p shows only a weak dependence on P_{eff} and does not show any peculiarity at $\tilde{P}_{eff} \simeq 15$ MW ERP, as for the NC_p intensity displayed in Figure 4b. Such a weak dependence of k_p on P_{eff} can be understood as being due to the fact that for well-developed SSA, when $E_1^2 \ll E_0^2$, the PW energy is near totally absorbed in the disturbed volume, independent of the pump wave power [*Erukhimov et al.*, 1982]. On the other hand, the substantial enhancement of the NC_p intensity when $\tilde{P}_{eff} \geq 15$ MW ERP can be taken as an indication that the character of the interaction of the powerful electromagnetic wave with the plasma undergoes some changes. However, without additional experiments, it is presently not possible to identify the physical nature of these changes. One possibility could be that the Langmuir turbulence excited by the PDI goes through a change from being wave to caviton dominated.

[28] Completing the analysis of the data represented in Figure 3, it should be noted that the decrease in the NC_p intensity after its maximum level coincides in time with a growth of the intensity of the reflected PW signal. The latter is a result of the occurrence of quasi-periodic oscillations, QPO, in the PW reflected signal [*Frolov et al.*, 1997c]. Comparison of the PW and NC_p behavior clearly shows an anticorrelation between their temporal variations, which is

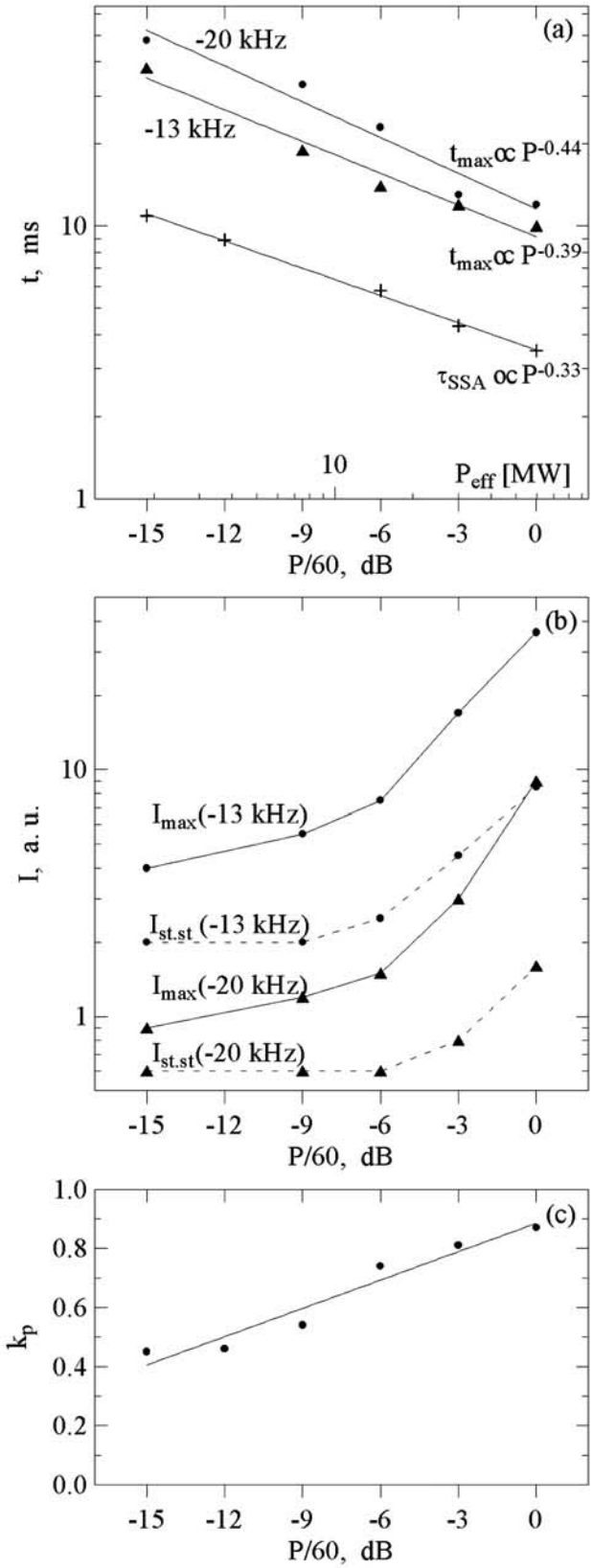

most distinctly seen at higher PW powers where even a repeat maximum of the NC_p intensity can be distinguished at about 100–150 ms after PW switch-on. These data indicate a relationship between the QPO and the Langmuir turbulence evolution. However, more experimental data are needed to draw definite conclusions on that relationship. It should be pointed out that up to now there exists no solid theoretical explanation of the QPO. Our experiments can shed light on the physical nature of the QPO.

[29] Further detailed studies of the NC_p temporal evolution at several chosen frequency shifts were conducted at the Sura facility on 31 March 1995 with a maximum PW power of $\tilde{P}_{eff}$ = 70 MW ERP and with four different PW schemes, namely [+15 ms; −985 ms], [+30 ms; −970 ms], [+100 ms; −4900 ms], and [+200 ms; −9800 ms] [*Sergeev et al.*, 1998]. For the pumping mode [+200 ms; −9800 ms], Figure 5a demonstrates the temporal behavior of both the NC_p at the frequency shift Δf^{-} = 13 kHz and the PW sky signal strength. In this figure, the PW intensity is normalized to its maximum value, occurring before the SSA development, and the received SEE signal is normalized to the spectral power density $S_{cal} = 3 \cdot 10^{-9}$ W/Hz. In these measurements, the maximum in the NC_p intensity occurs at $t_{max} \simeq 3$ ms, immediately after the beginning of the SSA development ($t_{max} \simeq \tau_{SSA}$), opposite to the results of earlier experiments (see Figure 4a) for which $t_{max} \simeq 4\tau_{SSA}$. Here we can also see the aforementioned prominent maximum in the NC_p intensity at 100–120 ms after PW switch-on, reflecting the anticorrelation between the temporal evolution of the PW and the NC_p in the QPO stage. Figure 5b will be discussed in section 4.5.

[30] For the pumping mode [+15 ms, −985 ms], the NC_p evolution at the four frequency shifts Δf^{-} = 8, 11, 18, and 22 kHz is presented in Figure 6 with a temporal resolution of $\delta t \simeq 300$ μs. Here the sharp periodic peaks after the PW switch-on/switch-off represent the receiver response to abrupt changes in the signal strength, due to interference between the ground wave and multiple hops of the ionospherically reflected PW sky signal. The data show that after the PW switch-on in the plasma the NC_p intensity increases rapidly, attaining a maximum at a time $t_{max} \simeq 2$–5 ms, where shorter times correspond to smaller frequency shifts. Following the maximum, the intensity decreases by 6–12 dB, stronger for smaller Δf^{-}. Such an emission behavior leads to a larger slope of the NC_p spectrum (∼4 dB/kHz) in the initial ($t \simeq 2$–5 ms) stage of pumping,

Figure 4. Pump power dependences of: (1) time of NC_p intensity maximum, t_{max}, for the two frequency shifts δf^{-} = 13 and 20 kHz, and typical time of the SSA development, τ_{SSA} (Figure 4a); (2) NC_p intensity maximum, I_{max}, at the two frequency shifts δf^{-} = 13 and 20 kHz in the stage of its maximum within $t \simeq 10$–50 ms after PW switch-on in the plasma (solid lines), and in the quasi-stationary state reached near the end of the 200 ms pulses of pumping, $I_{st.st}$ (dashed lines) (Figure 4b); (3) fraction of PW absorbed energy due to the striction self-action (SSA) effect, k_p (Figure 4c). The pump power is normalized here to $\tilde{P}_{eff}$ = 60 MW ERP. The measurements were performed with pump frequency f_0 = 4785 kHz in 0.2 s on, 9.8 s off pumping mode on 17 June 1994, T = 1910–1940 LT.

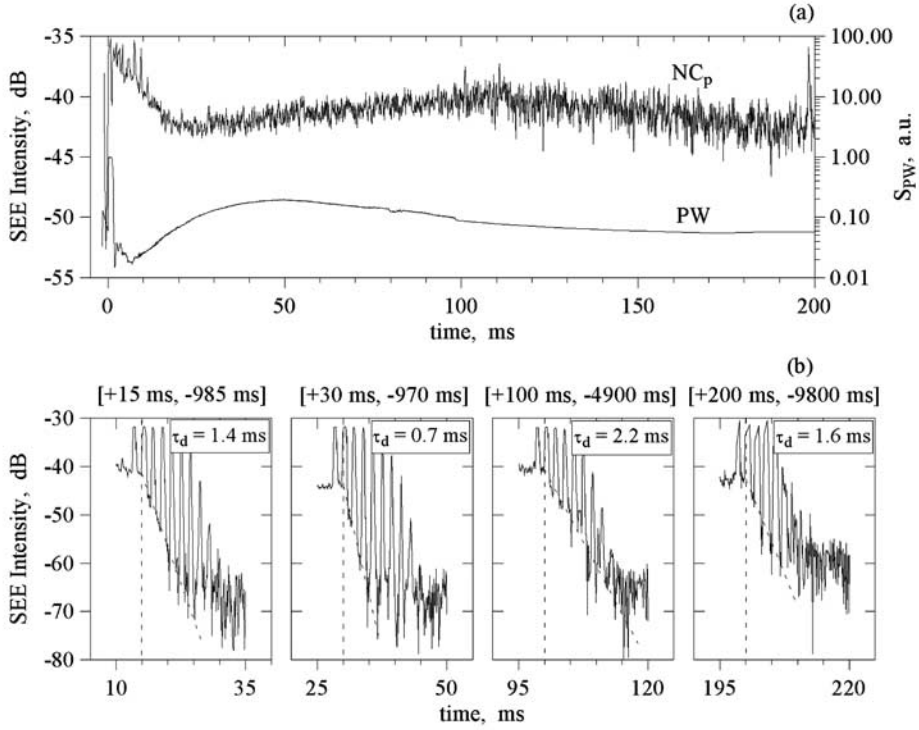

Figure 5. (a) Oscillograms of the NC$_p$ intensity at the frequency shift $\Delta f^- = 13$ kHz, marked as NC$_p$, and the PW sky signal strength, marked as PW. (b) Oscillograms of the emission at $\Delta f^- = 13$ kHz, obtained for different pumping modes: 15 ms on, 985 ms off; 30 ms on, 970 ms off; 100 ms on, 4900 ms off; and 200 ms on, 9800 ms off, showing the emission evolution after the PW switch-off in different stages of pumping. For the data presented in Figure 5b, an averaging of the SEE intensity over 40–100 pulse data sets with subsequent subtraction of the background noise has been done in the data processing. The measurements were performed on 31 March 1995, T = 1700–1720 LT, using PW radiation with pump frequency $f_0 = 4785$ kHz and ERP power $\tilde{P}_{eff} = 70$ MW.

which is reduced to about 1 dB/kHz toward the end of the PW pulse, corresponding to a broadening of the spectrum. Measurements with other PW pumping modes have allowed to conclude that the time to attain the minimum in the NC$_p$ intensity during heater-on, τ_{min}, is about 10–20 ms for $\Delta f^- \simeq$ 8–11 kHz, increasing to $\tau_{min} \simeq$ 30–40 ms for $\Delta f^- \simeq$ 20–30 kHz. Thus for a 15 ms pumping pulse, the time of PW switch-off in the plasma corresponds to different stages in the emission development at different frequency shifts. This aspect has to be taken into account when experimental data concerning the stage of SEE relaxation are considered and when new experiments are designed.

4.3. Pump Power Dependence

[31] It had been concluded from earlier measurements that the generation of the NC$_p$ occurs only when the PW power exceeds the SSA threshold, $\tilde{P}_{th\ SSA}$, suggesting that the PDI is the cause of the NC$_p$ [*Erukhimov et al.*, 1987b, 1988]. Later this finding was repeatedly confirmed by *Frolov et al.* [1997a] and *Sergeev et al.* [1994, 1998]. For $\tilde{P}_{eff} > \tilde{P}_{th\ SSA}$, the dependence of the NC$_p$ intensity on the PW power was studied for the stage of the NC$_p$ maximum development and for steady state under daytime (see Figure 1) and evening (see Figure 3) ionospheric conditions. Based on these data we can conclude the following: First, there is a complete similarity between the NC$_p$ spectra at the stage of maximum emission intensity ($t \simeq$ 30–70 ms) and in the quasi-stationary state ($t \simeq$ 0.3–0.5 s). Second, the NC$_p$ spectra are broadened with increasing power, from $\Delta F \simeq$ 1–2 kHz for $\tilde{P}_{eff}$ slightly above $\tilde{P}_{th\ SSA} \simeq$ 2 MW ERP to $\Delta F \simeq$ 8 kHz for $\tilde{P}_{eff} = 30$ MW ERP. The spectral width, ΔF, is defined here as the frequency difference between $\Delta f^- = 4$ kHz and that value of Δf^- for which the SEE intensity is decreased by 10 dB if the spectral slope, determined in the frequency range $\Delta f^- = 4$–8 kHz, is extrapolated to lower frequencies. According to the experimental data, the dependence $\Delta F(\tilde{P}_{eff})$ can be well represented by a power law with a power index of about 0.6–0.8. Third, the dependence of the NC$_p$ intensity on the PW power is somewhat enhanced for both stages of the NC$_p$ development when $\tilde{P}_{eff} \geq 20$ MW. This can be seen in Figure 4b where the dependence of the NC$_p$ intensity on the PW power is plotted at the two SEE frequency shifts $\Delta f^- = 13$ and 20 kHz, in both the stage of maximum intensity at $t \simeq$ 10–50 ms (solid lines) and the NC$_p$ quasi-stationary state reached at the end of the 200 ms pumping pulses (dashed lines). In the stage of the NC$_p$ maximum, the $I_{NCp}(\tilde{P}_{eff})$ dependence is rather weak for $\tilde{P}_{eff} \leq 15$ MW ERP and is noticeably increased for larger PW powers. This effect is somewhat stronger for larger negative frequency shifts, being connected with the broadening of the NC$_p$ spectrum.

Contrary to the daytime conditions (see Figure 1), the measurements performed in the evening have shown the absence of any significant dependence of $I_{NCp}(\tilde{P}_{eff})$ in the stationary state for $\tilde{P}_{eff} \leq 15$ MW ERP. This is a rather unexpected result which is most likely connected with the increase in the short-time overshoot of the NC_p intensity with increasing PW power. The same explanation may also be applicable to the more pronounced maximum of the NC_p intensity for larger pump powers occurring in the initial stage ($t \simeq 10-50$ ms) of pumping.

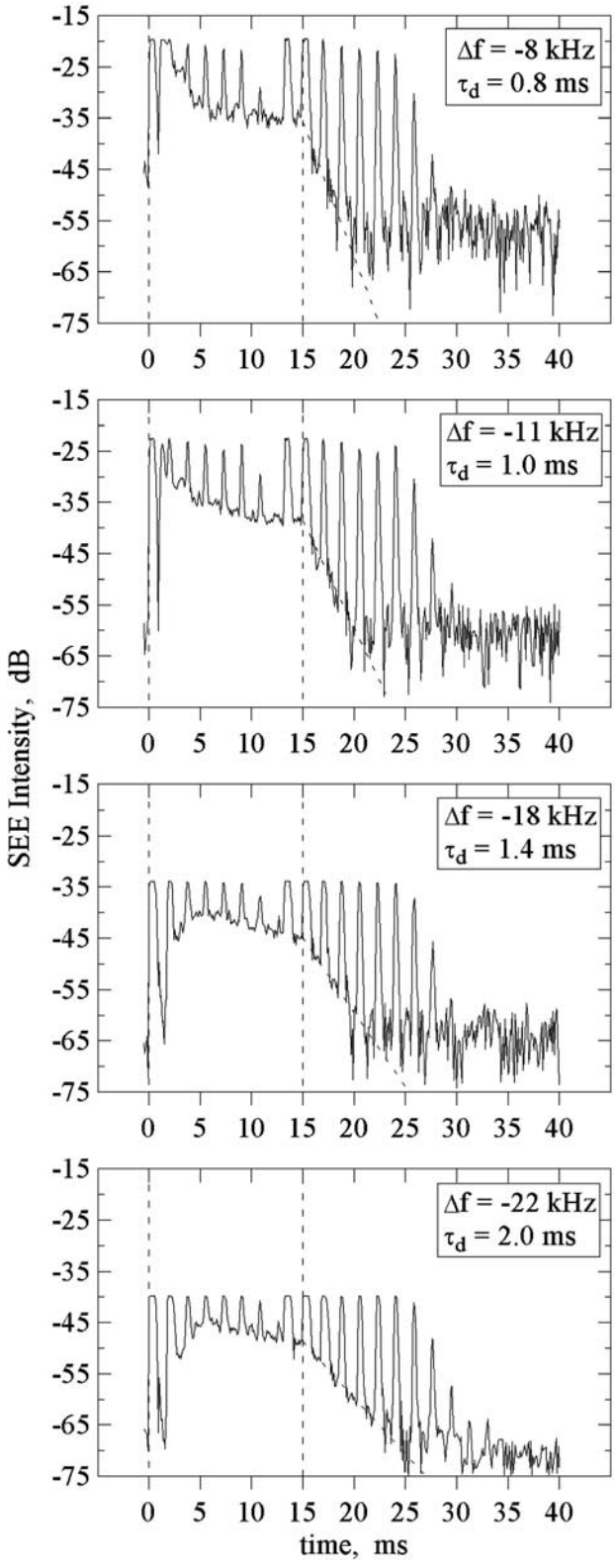

4.4. Pump Frequency Dependence

[32] Up to the present time we do not have a complete coverage of the dependence of the NC_p intensity on pump frequency for the whole frequency range (4.3–9.5 MHz) of the Sura heating facility. Here we can only point to an experiment by *Erukhimov et al.* [1987b], in which features of the NC_p were studied at the pump frequencies $f_0 \simeq 4.0$, 5.0, and 6.0 MHz with pump powers ($P_{eff} \leq 7$ MW ERP) only slightly above the PDI threshold. In these measurements it has been found that the dependence $I_{NCp}(f_0)$ is approximately $I_{NCp} \propto f_0^{-\beta}$, with $\beta \simeq 2-3$. This pump frequency dependence is in agreement with the dependence of the PDI threshold on f_0, thereby presenting one more proof of the close relationship between the NC_p generation and the PDI development.

4.5. Decay Features

[33] The first studies of the SEE relaxation characteristics for the NC_p were performed at the Sura facility in 1990–1991 [*Sergeev et al.*, 1994]. They showed that after PW switch-off in the plasma the emission intensity decreases exponentially with a typical e-folding decay time $\tau_d \simeq 1-5$ ms, depending on many factors. With the progress in our knowledge of the NC_p features a demand arose for studying in greater detail the characteristics of the emission relaxation at all stages of the NC_p development. Such measurements were begun in the June 1994 heating campaign and have been repeated many times in later experiments.

[34] Figure 6 shows the NC_p intensity versus time at four frequency shifts, $\Delta f^- = 8$, 11, 18, and 22 kHz, obtained in measurements on 3 April 1995 under evening conditions when the PW was radiated at $f_0 = 4785.6$ kHz with $\tilde{P}_{eff} \simeq 75$ MW ERP in the mode [+15 ms; −985 ms]. It is seen that after PW switch-off in the plasma ($t = 15$ ms) the emission intensity decreases exponentially, with typical e-folding decay times of $\tau_d \simeq 0.8-1.0$ and 1.8–2.0 ms, pertaining to the frequency ranges $\Delta f^- \simeq 8-11$ and 18–22 kHz, respectively. We see that the NC_p relaxation time increases with increasing Δf^-. The existence of such a $\tau_d(\Delta f^-)$ dependence has been confirmed later in many other measurements.

Figure 6. Examples of the NC_p temporal evolution at the four frequency shifts $\Delta f^- = 8$, 11, 18, and 22 kHz. Sharp periodic peaks after the PW switch-on/switch-off are the response of the receiver to abrupt changes in the signal strength due to interference between the ground wave and multiple hops of the ionospherically reflected PW sky signal. An averaging of the SEE intensity over 75 pulse data sets with subsequent subtraction of the background noise has been done here in the data processing. The measurements were performed on 3 April 1995, T = 1830–1900 LT, using PW radiation with pump frequency $f_0 = 4785$, 6 kHz and ERP power $\tilde{P}_{eff} = 75$ MW in the pumping mode 15 ms on, 985 ms off.

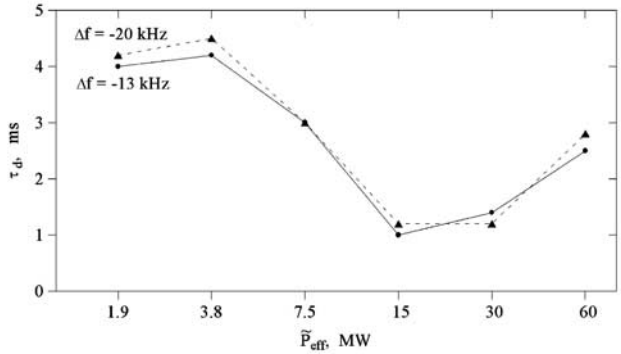

Figure 7. Dependence of the NC_p typical decay time, τ_d, on PW power, measured at the two emission frequency shifts $\Delta f^- = 13$ and 20 kHz. The measurements were performed on 17 June 1995, T = 1910–1940 LT, using PW radiation with pump frequency $f_0 = 4785$ kHz and maximum ERP power $\tilde{P}_{eff} = 60$ MW in the pumping mode 0.2 s on, 9.8 s off.

[35] The dependence of the NC_p relaxation features on the pulse length, i.e., on different stages of the NC_p development, is demonstrated in Figure 5b, displaying the temporal decrease of the emission intensity at $\Delta f^- = 13$ kHz after PW switch-off for the pumping modes [+15 ms; −985 ms], [+30 ms; −970 ms], [+100 ms; −4900 ms], and [+200 ms; −9800 ms]. From these data we can conclude that the smallest decay time, $\tau_d \simeq 0.7$ ms, occurs after 30 ms of pumping, corresponding to the minimum in the NC_p intensity after the short-time overshoot (see Figure 5a). Conversely, the largest decay time, $\tau_d \simeq 2.2$ ms, occurs here when the PW pulse duration is 100 ms, which is close to the second temporal maximum of the NC_p emission intensity.

[36] In measurements performed in June 1994 (see Figure 7) a strong dependence of the decay time on the pump power was found. In this experiment the ionospheric plasma was modified under evening conditions at the frequency $f_0 = 4785$ kHz with a maximum ERP of $\tilde{P}_{eff} \simeq 60$ MW and with the pulse scheme (200 ms; 9.8 s]. The results obtained in these measurements are thus related to the quasi-stationary stage of the NC_p development, studied here at two frequency shifts, $\Delta f^- = 13$ and 20 kHz. Several conclusions can be drawn from these observations: First, τ_d has a maximum value of about 4–4.5 ms for low pump powers, $\tilde{P}_{eff} \leq 3.8$ MW ERP, which is in good agreement with the damping time of Langmuir waves due to Coulomb collisions, $\tau_d \simeq \nu_{ei}^{-1}$, where $\nu_{ei} \simeq 220$ s^{-1}. Second, as the PW power is increased to $\tilde{P}_{eff} = 15$ MW ERP, the magnitude of τ_d decreases to ~1–1.3 ms, remains almost constant in the power range $\tilde{P}_{eff} \simeq 15$ – 30 MW ERP, and increases to ~2.5 ms for $\tilde{P}_{eff} = 60$ MW ERP. The latter may be a result of the preconditioning effect for $\langle \tilde{P}_{eff} \rangle = \tilde{P}_{eff}/Q \simeq 1.25$ MW ERP mentioned above. Third, it is seen that the $\tau_d(\tilde{P}_{eff})$ dependence is approximately the same for both frequency shifts.

[37] The study of the NC_p relaxation was continued in March and April 1995, when the dependence of τ_d on both PW power and HF pulse duration was investigated [*Sergeev et al.*, 1998]. Some results of these observations were considered in subsection 4.2 (see Figure 5). In Figure 8 the dependence of τ_d on PW power, normalized to its maximum value ($\tilde{P}_{eff\ max} = 75$ MW ERP), is displayed. These data were obtained under evening conditions in the frequency range $\Delta f^- \simeq 11$–13 kHz for the three pumping modes [+200 ms; −9800 ms] (marked as 1), [+30 ms; −970 ms] (marked as 2), and [+15 ms; −985 ms] (marked as 3).

[38] As for the data presented in Figure 7, the maximum decay time $\tau_d \simeq 4$–4.5 ms occurs here for low powers ($\tilde{P}_{eff} \leq \tilde{P}^*_{eff}$ with $\tilde{P}^*_{eff} = 4$, 12, and 20 MW ERP for curves 1, 2, and 3, respectively). From the data presented in Figure 8 it follows that the magnitude of $\tilde{P}^*_{eff}$ depends strongly on the HF pulse duration (τ_p), showing an increase from 4 to 18–40 MW ERP when τ_p decreases from 200 to 15 ms.

[39] The above measurements relate to evening conditions. During daytime, typical NC_p e-folding decay times are about 1–1.3 ms for pump pulse durations of 20–30 ms and low ERP ($\tilde{P}_{eff} \simeq 10$ MW). Such a diurnal variation of τ_d can be indicative of an influence of photoelectrons on the Langmuir wave energy dissipation by Landau damping. Taking this into account, it is reasonable to expect that similar to photoelectons, HF-accelerated electrons can exert an analogous influence on the emission evolution, in particular on the rate of the emission relaxation. If so, we would have to infer that accelerated electrons occur in the HF-pumped ionosphere a few tens of milliseconds after PW switch-on in the plasma but sometimes also at times not longer than a few milliseconds. As unambiguous evidence for the appearance of HF-produced suprathermal electrons already in the earliest stage of PW-plasma interaction, airglow measurements [*Gumerov et al.*, 1999] have shown that artificial 557.7 nm optical emissions, due to excitation of the $O(^1D)$ state by electron impact, are excited by 5-ms-long pump pulses in the *F* layer.

4.6. SEE Features Near Twice the PW Frequency

[40] It has long been known in solar physics that the excitation of high-frequency plasma turbulence leads to the generation of electromagnetic emissions at $\omega \approx 2\omega_p$, due

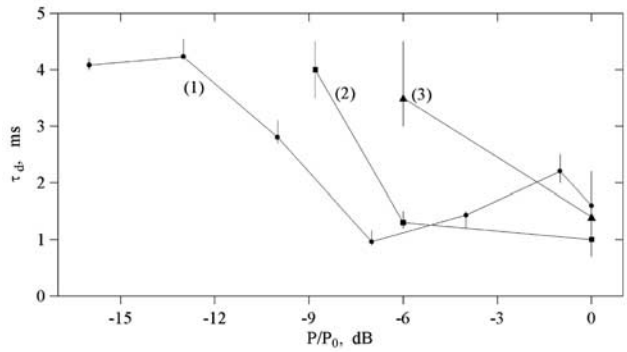

Figure 8. Dependence of the NC_p typical decay time, τ_d, on PW power, obtained for the three pumping modes [+200 ms; −9800 ms] (curve 1), [+30 ms; −970 ms] (curve 2), and [+15 ms; −985 ms] (curve 3). The measurements were performed at the emission frequency shift $\Delta f^- \simeq 11$–13 on 17 June 1995, T = 1910–2220 LT, using PW radiation with pump frequency $f_0 = 4785$ kHz and maximum ERP power $\tilde{P}_{eff} = 75$ MW.

to the coalescence of plasma waves [*Zheleznyakov*, 1995]. This type of processes was studied in experiments performed in April 1984 at the Zimenki heating facility (Nizhny Novgorod, former Gorky) [*Karashtin et al.*, 1986]. A brief description of these measurements will be given because they are relevant to the NC_p feature.

[41] In the experiments an O-mode pump with f_0 = 5750 kHz and $\tilde{P}_{eff} \simeq 15$ MW ERP was used. SEE signals at $f \simeq 2f_0$ = 11500 kHz were received using a horizontal phased antenna array with linear polarization and with a gain of $G \simeq 30$. In order to be able to detect signals at small (up to $|\Delta f| \simeq 1$ kHz) frequency shifts around the PW frequency, HF receivers with a frequency band of $\delta f \simeq 300$ Hz were used. Besides, to minimize the influence of the PW and of other powerful radio stations, a LC narrow-band pass filter with $2\Delta f \simeq 100$ kHz was used, tuned to $2f_0$ = 11500 kHz. To ensure truly "cold" start conditions, the ionosphere was modified every 2 min in the mode [+1 s; −4 s] during the first minute and switch-off during the second. The key findings were the following:

[42] 1. The emission near twice the PW frequency is strongly variable and is generated only by O-mode pumping when the SSA is observed for the PW.

[43] 2. The emission has a maximum intensity at early times ($\leq$100 ms) following the PW switch-on in the plasma. At longer times its intensity is decreased during the pumping. This is a result of the fast anomalous absorption. Continued heating in the mode [+1 s; −4 s] leads to a suppression of the emission generation in the form of a decrease of the emission intensity from pulse to pulse. This corresponds fully to the behavior of the SSA [*Erukhimov et al.*, 1982].

[44] 3. The relaxation time following the PW switch-off is about 6 ms, corresponding to a typical collisional damping time of HF plasma waves.

[45] 4. A maximum spectral emission power of $S \simeq 10^{-20}$ $mW^{-2}Hz^{-1}$ is observed at $f - 2f_0 \simeq -2$ kHz. For larger frequency shifts the slope of the emission spectrum is about 1 dB/kHz.

[46] 5. In the upper sideband of $2f_0$ no emission is detected, and thus its intensity does not exceed 10^{-21} $mW^{-2}Hz^{-1}$.

[47] The experimental data, as well as theoretical considerations [*Karashtin et al.*, 1986], allow to conclude that the emissions near twice the PW frequency are caused by the coalescence of Langmuir waves, HF-induced by the PDI. From the emission intensity, the power density of the Langmuir waves, W, can be evaluated as $W/N_eT_e \simeq 10^{-2}$, which is in good agreement with theoretical estimates. Because Langmuir waves produce both the NC_p and this emission, studies of the two features can supplement each other.

[48] It should be pointed out that emission near twice the PW frequency has recently been observed by *Blagoveshchenskaya and Kornienko* [1998] in experiments with the Troms heating facility and a receiver placed near St. Petersburg. In these measurements, the maximum of the spectral intensity was downshifted by 16–20 kHz, which is about twice the DM frequency shift. With the given experimental geometry, upper-hybrid waves can be considered as main candidates for the generation of this emission, as opposed to Langmuir waves in the case of the NC_p.

4.7. NC_p Gyroharmonic Features

[49] The first measurements focusing on the investigation of possible variations of NC_p characteristics when the PW frequency is close to a gyroharmonic frequency, $f_0 \simeq nf_{ce}$ (n is the harmonic mode number), were performed on 26 September 1998, T = 1450–1610 LT. In these measurements $f_{ce} \simeq 1.3$–1.35 MHz, depending on the PW reflection height, $h_{ref} \simeq 200$–300 km. Modification of the ionosphere with $\tilde{P}_{eff} \simeq 100$ MW ERP was conducted at the three pump frequencies 6808, 6778, and 6728 kHz. The first is about 40–50 kHz higher than $5f_{ce}$, the second is close to $5f_{ce}$, and the third is about 10–30 kHz below $5f_{ce}$. To study the NC_p gyrofeatures at different stages of the emission development, transmissions with the pulse lengths 10, 20, 50, 100, and 200 ms and with a 2 s interpulse period were sequentially used in the experiments. Notice that according to the experimental data obtained, the time of the NC_p culmination and of the establishment of its quasi-stationary state was, respectively, about 5–8 ms and 20 ms after PW switch-on in the plasma.

[50] The following conclusions can be derived from these experiments:

[51] 1. The SSA features do not show any peculiarities for pump frequencies close to the fifth cyclotron harmonic.

[52] 2. Likewise, no modification of the NC_p features has been found for times prior to the short-time overshoot.

[53] 3. In the quasi-stationary stage of the NC_p development (for $\tau_p \geq 20$ ms), a decrease has been observed of the typical decay time from $\tau_d \simeq 0.7$–0.9 ms when $f_0 > 5f_{ce}$ to $\simeq$0.5 ms when $f_0 \approx 5f_{ce}$, together with a narrowing of the NC_p spectrum from $\Delta F \simeq 10$ to about 6 kHz. This conclusion is related to the frequency range $\Delta f^- \simeq 10$–18 kHz.

[54] Further experiments, in more detail and for other gyroharmonics, are required and will be performed in the future.

4.8. Some Remarks on a SEE Component Observed at Small Positive Frequency Shifts

[55] Completing the analysis of the NC_p features, we will briefly present some characteristics of another emission component, denoted NC^+, which is observed at small positive frequency shifts, $\Delta f^+ \leq 20$–30 kHz (see Figure 1). The first observations made by *Boiko et al.* [1985] have shown (1) that its temporal evolution follows the evolution of the NC_p, (2) that it is mainly detected before the development of the anomalous absorption, and (3) that the NC^+ intensity is 10–20 dB lower than the emission intensity at the mirror frequency Δf^-. According to *Frolov* [1995], the NC^+ and NC_p intensities have approximately the same dependence on PW power. However, the variations of the NC^+ intensity from cycle to cycle of pumping are stronger than for the NC_p for which strong intensity variations are observed at low PW powers only. There is reason to assume that the NC^+, like the NC_p, is produced by excitation of the PDI. However, this emission component has not been studied yet in detail, and new experiments are needed to work out an empirical model.

[56] It should be noted that the weak lobe structure in the frequency range +(20–40) kHz in the SEE spectra

presented in Figures 1a–1e is usually related to transmitter noise of the Sura facility and has to be considered with great caution. Special test measurements are always needed to clarify its real nature.

5. SEE Evolution Under the Influence of Additional Heating

5.1. Additional O-Mode Heating

[57] In this subsection we present results obtained in modification experiments with two powerful O-mode waves. One of them is the pump wave (PW), serving as additional heating and causing artificial ionospheric perturbations. Its influence on plasma processes and wave-plasma interactions is monitored through variations in the turbulence characteristics induced by the second wave (DW), which has a diagnostic function. The DW has a comparatively low power to induce an unsaturated turbulence level, thereby being able to respond to the PW-created perturbations. In the measurements performed on 25 April 1991 (t = 1507–1619 LT) [*Sergeev et al.*, 1998], results of which are shown in Figures 9 and 10, the PW was radiated during 30 s (t = 0–30 s in Figure 9) in a quasi-continuous mode [+180 ms; −20 ms] at f_0 = 5752 kHz with $\tilde{P}_{eff} \simeq 40$ MW ERP. Thereafter the radiation schedule was changed over to a diagnostic mode [+20 ms; −980 ms] for the remaining 150 s of the 3-min heating cycle (t = 30–180 s in Figure 9). The DW was radiated during all heating cycles in the diagnostic mode [+20 ms; −980 ms] at f_{DW} = 5456 kHz with $\tilde{P}_{eff} \simeq 10$ MW ERP. The difference between f_0 and f_{DW} was chosen at about 300 kHz so that the resonance regions for the PW and DW would not overlap each other. Very stable ionospheric conditions during the experiment allowed to overlay and average the data from 23 consecutive pumping cycles (69 min of observations) to produce the final results represented in Figures 9 and 10.

[58] Figure 9a demonstrates the temporal behavior of the ionospherically reflected PW signal (marked here as PW), the intensity of which has been measured during the first two milliseconds for each of the 180-ms pulses in the quasi-continuous mode or for each of the 20-ms pulses in the diagnostic sounding mode. Also shown in Figure 9a is the absorption index k_p defined in subsection 4.2. It can be clearly seen that once the quasi-continuous pumping is switched on, at first the fast stage of the anomalous absorption and, a few seconds later, its slow stage is developed. The total decrease in the PW intensity amounts to about 17 dB. Together with the anomalous absorption development, a significant suppression of the SSA occurs, which is reflected in a decrease in the k_p value. These phenomena are closely related to the generation of striations at the upper hybrid resonance level due to the TPI, resulting in a large decrease in the PW amplitude and a suppression of the PDI. After the PW switch-off, together with the decay of the striations, both the intensity of the reflected PW signal and k_p are restored to their unperturbed values within about 10–15 s.

[59] The SEE evolution at a frequency 11 kHz downshifted from the PW frequency f_0 = 5752 kHz and at a frequency 12 kHz downshifted from the DW frequency f_{DW} = 5456 kHz is presented in Figures 9b and 9c, respectively. In the stage of diagnostic sounding during about 1.5 min before the quasi-continuous PW is switched on, the generation of the NC_p is observed for both PW and DW pulse pumping ($t \simeq 90$–180 s in the figure). To record this short pulse emission in a continuous signal form and exclude the influence of signal jumps connected with the interference of the ground wave and multiple reflections of the powerful wave from the ionosphere, we used a peak detector which determines the signal strength in a time interval of a few milliseconds just before the end of the pump pulse, keeping the signal level constant within the interpulse period (for more details of the diagnostic SEE, DSEE, scheme of measurements, see *Erukhimov et al.* [1988] and *Frolov et al.* [1994]). Once the quasi-continuous pumping has been switched on at t = 0, the NC_p is rapidly suppressed, and the growth of emission components of thermal origin (DM at $\Delta f^- = 11$ and 12 kHz in our case) is beginning to be observed. This emission evolution shows up more clearly for the DW (Figure 9c), where the delay in the development of the thermal stage has a much longer time compared with SEE components near the PW. This is the result of a finite time for the spread of the HF-induced turbulence along the geomagnetic field. Besides, due to the small average DW power, a longer time (of about 30 s here) is needed for the DM to reach its steady state. After switching to the diagnostic mode at t = 30 s, the average PW power decreases abruptly and, as a result, quenching of the TPI occurs. Under these conditions, the DSEE behavior represents, first of all, the evolution of the HF-induced striations in the disturbed volume [*Erukhimov et al.*, 1988; *Frolov et al.*, 1994; *Grach et al.*, 1998]. During the first phase after the PW switch-off, of about 1 s duration, the DSEE intensity increases and reaches its culmination. Here the growth of the DSEE intensity is a result of the decay of meter-scale striations, which are responsible for the fast anomalous absorption of the PW, as well as for the absorption of the emissions in the disturbed volume. In this phase the intensity of the ionospherically reflected PW wave increases abruptly. During the second phase of a few seconds duration, the DSEE intensity, after its culmination, decreases to a minimum at $t \simeq 40$–45 s, concurrently with a restoration of the intensity of the reflected signal back to its unperturbed value. Here the decrease of the DSEE intensity is determined by the decay of dekameter-scale striations, which on the one hand are responsible for the slow stage of the anomalous absorption development for the PW, and on the other hand sustain the DSEE generation. Notice that during the second phase the magnitude of the PW striction self-action, k_p, is also restored almost completely. A distinct feature of the DSEE behavior is the longer time, approximately 1 min for the restoration of the NC_p intensity after the end of the quasi-continuous pumping, compared with the time of the anomalous absorption relaxation and the SSA recovery. Such a long-time aftereffect is a typical SEE feature which was often observed in earlier experiments [*Boiko et al.*, 1985; *Frolov*, 1995; *Wagner et al.*, 1999], but its physical nature is unknown yet. The value of about 1 min for the decay time of the aftereffect suggests that large-scale artificial irregularities with scale lengths $l_\perp \simeq 500$–2000 m could play a role. These can exert a strong influence on wave-plasma interactions [*Duncan and Behnke*, 1978; *Morales et al.*, 1982; *Frolov*, 1995]. However, other experimental facts

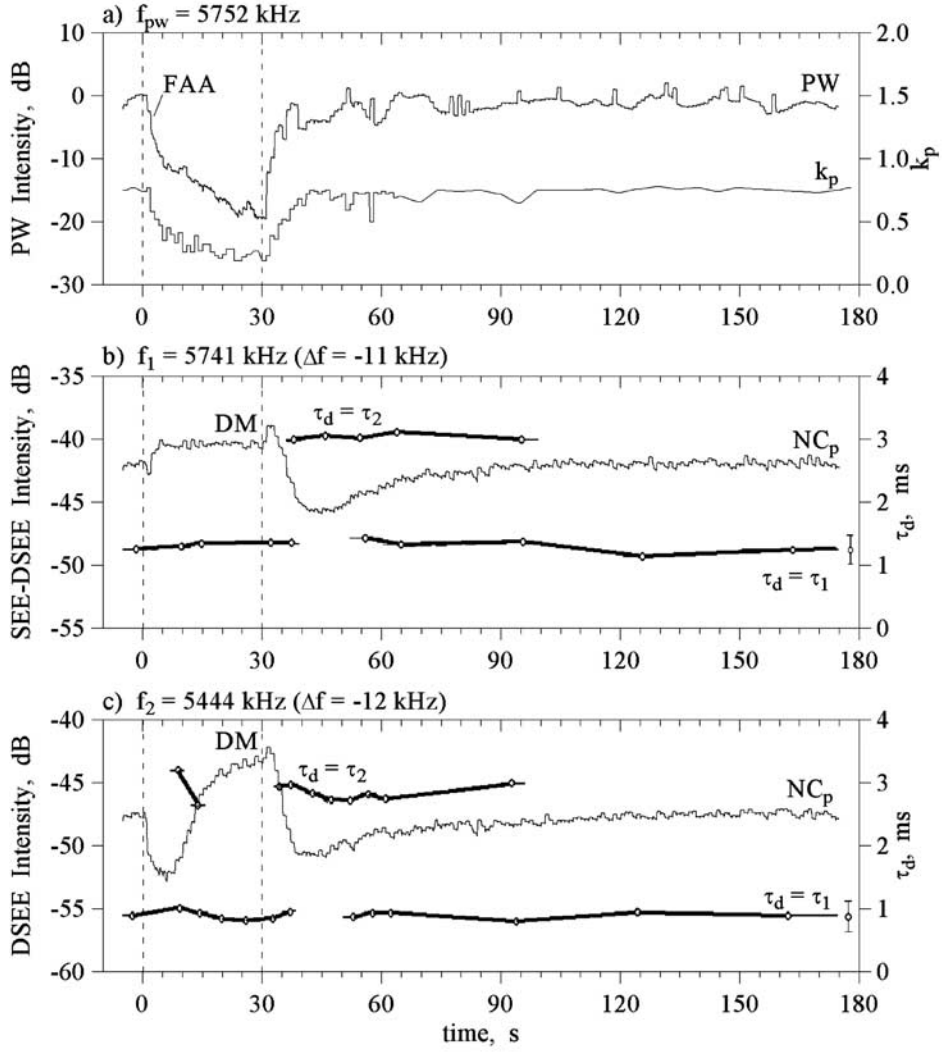

Figure 9. (a) Temporal evolution of the ionospherically reflected PW signal at the PW frequency 5752 kHz, $\tilde{P}_{eff}$ = 40 MW ERP (marked as PW), measured during the first two milliseconds of each 180-ms pulse in the stage of quasi-continuous pumping (t = 0–30 s) or for each 20-ms pulse during the diagnostic sounding mode (t = 30–180 s), and variations of the absorbed PW energy through the pumping cycle due to the striction self-action (SSA) effect (marked as k_p). (b) SEE evolution at the frequency shift $\Delta f^- = 11$, downshifted from the PW frequency f_0 = 5752 kHz, marked as DM, in the stage of the quasi-continuous pumping (t = 0–30 s), and as NC_p during the diagnostic sounding mode. (c) SEE evolution at the frequency shift $\Delta f^- = 12$, downshifted from the DW frequency f_0 = 5456 kHz (the ERP for the DW was here $\tilde{P}_{eff}$ = 10 MW), marked as DM in the stage of the quasi-continuous pumping (t = 0–30 s), and as NC_p during the diagnostic sounding mode. The solid lines in Figures 9b and 9c (marked as τ_d) show the magnitudes of the emission decay times for two relaxation stages through the pumping cycle. The measurements were performed on 25 April 1991, T = 1500–1620 LT.

(see, for example, the data presented in the following subsection 5.2) indicate that other factors have to be considered, too. A clarification of the physical nature of the long-time aftereffect requires further specially designed experiments.

[60] In order to study in detail the variations in the SEE evolution within the different phases of the heating cycle, as presented in Figure 9, we display in Figure 10 plots of the DSEE intensities at $\Delta f^- = 12$ kHz, induced by the pulse diagnostic wave at the frequency f_{DW} = 5456 kHz. To obtain smoothed curves, data from several consequent DW pulses for the respective time intervals have been overlaid and averaged. The magnitudes of the e-folding decay time τ_d, derived from these data, are presented in Figure 9c. The analogous procedure performed for the emissions at the frequency shift $\Delta f^- = 11$ kHz from the PW frequency leads to the τ_d values shown in Figure 9b. On the basis of these data it is found that the relaxation of the NC_p in steady state (t = 120–180 s) as well as for the stationary DM (t = 15–30 s) proceeds in one step, with

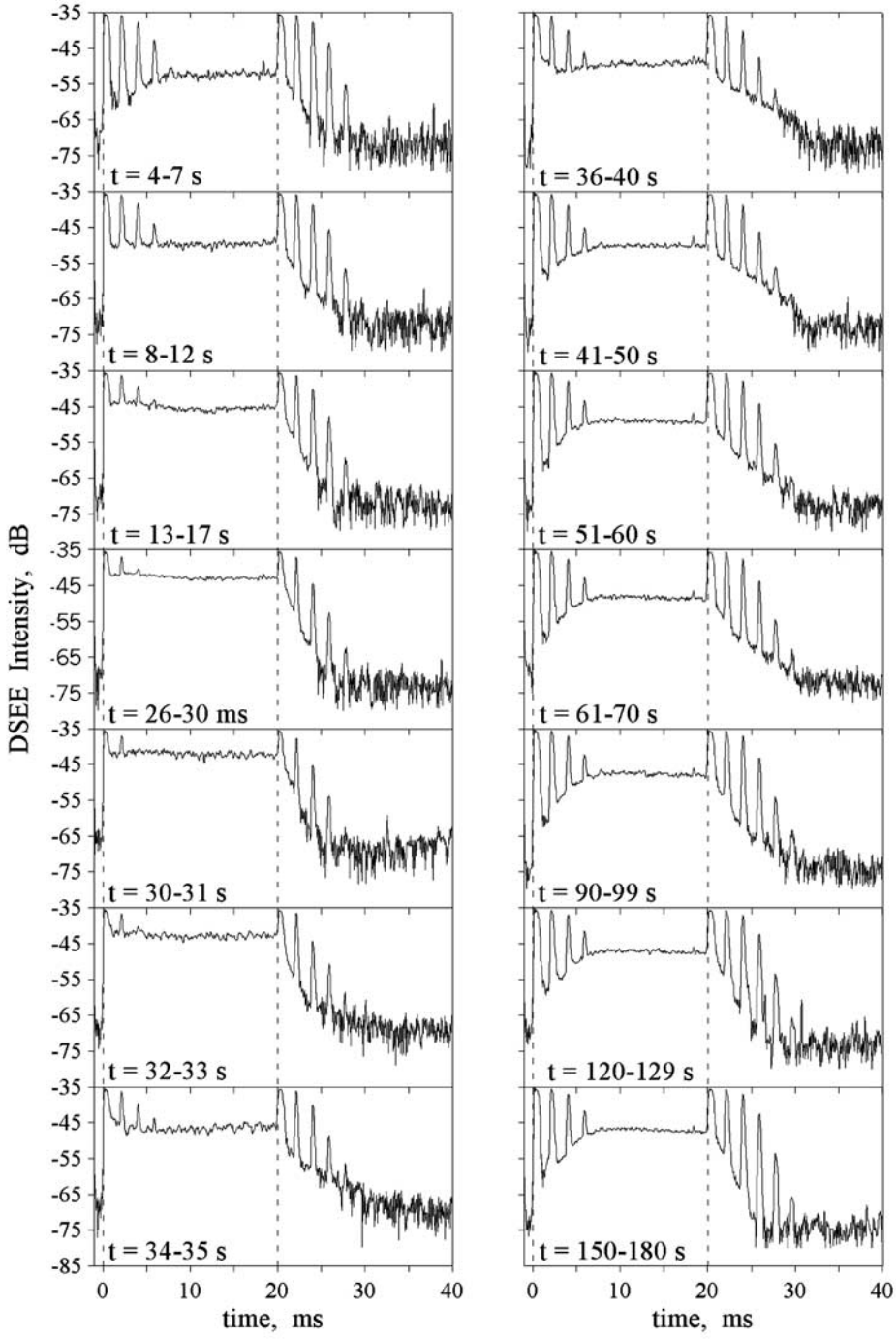

Figure 10. Examples of the SEE evolution at the frequency shift $\Delta f^{-} = 12$ kHz, downshifted from the DW frequency $f_{DW} = 5456$ kHz, obtained in different stages of PW radiation. The measurements were performed on 25 April, T = 1500–1620 LT (see Figure 9).

the decay time $\tau_d = \tau_1 \simeq 0.8$–$0.9$ ms. Under conditions of strong variations in the DM and NC_p intensities (t = 4–12 s and 30–100 s), the relaxation occurs as a two-stage process, containing both a fast stage with $\tau_d \simeq \tau_1$ and a slower stage with $\tau_d = \tau_2 \simeq 2.8$ ms, with the exception of the phase of minimum DSEE intensity (t = 40–50 s) where the fast stage is absent and the relaxation proceeds in one step with $\tau_d = \tau_2$. In the phase of NC_p growth (t = 50–120 s), a gradual transition from the slower relaxation stage with $\tau_d = \tau_2$ to the fast stage with $\tau_d = \tau_1$, via a two stage relaxation process, is observed, with a progressively increasing contribution of the fast stage.

[61] The following conclusions can be drawn from this experiment: (1) When either Langmuir or upper hybrid turbulence is saturated, as manifest in the attainment of the steady-state NC_p or DM level, approximately equal

maximum damping rates of these plasma waves with $\gamma = \tau_1^{-1} \simeq 1000\ s^{-1}$ are observed. (2) In contrast, the minimum damping rates with $\gamma = \tau_2^{-1} \simeq 330\ s^{-1}$ occur in the SEE intensity minimum when the DM is already decreased but the NC_p is only beginning to develop. This clearly demonstrates once again, as for the measurements of the $\tau_d(P_{eff})$-dependence discussed in subsection 4.5 (see Figures 7 and 8), the strong influence of the AIT level on the relaxation process. Another feature worthy of being noted is the simultaneous occurrence of the two-stage relaxation feature and the NC_p restoration. The latter has a longer time constant than the SSA (see Figure 9). This demonstrates unambiguously that small-scale striations must not be involved, at least not as a crucial element, in the explanation of both the two-stage emission relaxation and the longer time restoration of the NC_p. It is likely that longer-living aftereffects have to be taken into consideration here. The question of why the emission relaxation has two prominent stages with two well-defined decay times but no stage with the decay rate gradually changing jointly with the AIT relaxation and thermalization of the superthermal electrons still remains to be answered, representing a key problem left to be solved for a better understanding the of AIT features.

5.2. Additional Heating by a Powerful X-Mode Wave

[62] In the case of X-mode pumping the lack of resonant interactions between the X-mode wave and the plasma significantly limits possible mechanisms of AIT generation. Among these, we can note plasma heating caused by collisional absorption of PW energy and the generation of large-scale irregularities due to the the self-focusing instability of an electromagnetic wave beam [*Gurevich*, 1978].

[63] However, recent experiments carried out at the Sura heating facility [*Frolov et al.*, 1999b] have shown that phenomena induced in the ionosphere modified by powerful X-mode waves are not confined to these effects but are of a more complicated nature. In these experiments one transmitter radiated an O-mode wave to induce the SEE which was used as a diagnostic tool for AIT sounding. The other two transmitters radiated an X-mode wave which was used to create additional ionospheric perturbations whose influence on the AIT was investigated through variations in SEE intensity and the temporal evolution of the emissions.

[64] The basic findings can be summarized as follows:

[65] The switch-on of the additional X-heating leads to a decrease in the O-wave-induced HF turbulence level of both ponderomotive and thermal origin in the form of a suppression of the NC_p and DM generation.

[66] The SEE suppression, which may be as large as 4 dB, is most pronounced when the reflection altitudes of the O-mode and X-mode waves coincide. Test measurements have shown that such a suppression is neither caused by additional absorption of O-mode energy in the lower ionosphere nor by remnant O-mode radiation. Further, it cannot be caused by the wave defocusing at the artificial ionospheric lens. The influence of the additional X-wave heating is limited to relatively high PW_X powers, $P_X \geq 20$ MW ERP. The typical time constant for X-heating-induced effects on the NC_p is about 1–2 s. The duration of the X-heating aftereffect on the SEE features may be as much as 30–60 s. It is unlikely that the aftereffect is determined by HF-induced large-scale irregularities because of their small magnitudes under conditions of short-time pumping.

[67] Summing up the above listed properties of the additional X-mode heating, we may conclude with certainty that the X-mode wave effect manifests itself as a plasma modification in the vicinity of the PW_X reflection level. However, any conclusive explanation of the phenomena observed is still lacking, and further detailed experiments will be necessary.

6. Empirical Model of the NC_p

[68] From the experimental results presented in this paper, we can formulate the following empirical model for the NC_p.

[69] 1. The generation of the NC_p occurs in the plasma resonance layer near the PW reflection altitude due to the PDI. A significant enhancement of the NC_p generation is observed when the pump power is above about $\tilde{P}_{eff} \simeq 10$–15 MW ERP. The merging of Langmuir waves, responsible for the NC_p generation, causes emissions near twice the PW frequency. The latter gives an opportunity to evaluate the power density of the HF induced Langmuir waves as $W/NT \simeq 10^{-2}$ at $\tilde{P}_{eff} \simeq 15$ MW ERP, which is in good agreement with theoretical estimates. Excitation of the TPI and of small-scale striations of thermal origin leads to a suppression of the NC_p as a result of anomalous absorption of HF energy a few km below the PW reflection height.

[70] 2. After the PW switch-on in the plasma and the development of the striction self action a few milliseconds later, the NC_p intensity increases rapidly, having a maximum in the time interval 2–20 ms, depending strongly on the pump power and on the ionospheric conditions: A faster development of the NC_p is observed in the nighttime ionosphere at higher pump powers. One of the properties of the NC_p is an intensity drop, after attaining its maximum, to a lower quasi-steady-state level within a few tens of milliseconds after the PW switch-on, when the TPI is not observed yet. This is considered as an indication that the generation of small-scale striations, causing anomalous absorption, has set in. Consequently, this short-time overshoot reflects directly the evolution of HF-induced Langmuir waves in the resonance region. Notice that the overshoot value increases with growing PW power and is larger for smaller frequency shifts Δf^-.

[71] 3. In the initial stage of the NC_p development its maximum spectral intensity at $\Delta f^- \simeq 4$ kHz for $\tilde{P}_{eff} \geq 30$ MW ERP is more than 10 dB higher than the maximum spectral intensity of the DM, which is the most prominent emission component in the stationary SEE spectrum. In the quasi-steady state of the NC_p development its spectrum often has a nearly exponential form with a constant slope of about 1 dB/kHz in the frequency shift range $\Delta f^- \leq 20$–30 kHz, with a smaller slope for larger Δf^-. A stronger dependence of the NC_p intensity on Δf^- ($\sim$3 dB/kHz) is observed in the stage of maximum intensity after about 5–50 ms of pumping. The spectral width of the NC_p increases with growing PW power. It should be noted that for pump powers slightly above the threshold power for the NC_p

generation ($P_{thr} \simeq 2$ MW ERP at $f_0 \simeq 5$–6 MHz) the NC_p spectral intensity decreases strongly with increasing PW frequency f_0.

[72] 4. The magnitude of the e-folding decay time, τ_d, for the NC_p varies over a wide range from ~0.7 ms to 4–5 ms, depending on PW power, frequency shift, pumping scheme, stage, and level of the AIT development, and showing strong diurnal variations. The maximum value, $\tau_d \simeq 5$ ms, which is in good agreement with the damping time of Langmuir waves by Coulomb collisions, is observed under nighttime conditions when a rather low power, $\tilde{P}_{eff} \leq$ 10 MW ERP, is used for the pumping. On the basis of the experimental data obtained, it is reasonable to expect that both photo and HF-accelerated electrons are the reason for the more rapid decay of the Langmuir waves by collisionless Landau damping. The relaxation process also shows a strong dependence on the phase of the AIT evolution, when shorter (longer) decay times occur at times of smaller (larger) NC_p intensity. An explanation of this phenomenon is still lacking.

[73] 5. Experiments performed near the fifth electron cyclotron harmonic have shown that the plasma waves involved in the NC_p generation do not possess any significant gyro features (with the possible exception of the quasi-stationary stage in which some decrease of the decay time has been found when $f_0 \simeq 5f_{ce}$), in distinction to the thermal SEE components, DM and BC, which show a crucial dependence of their properties on the PW frequency when the latter is close to a gyroharmonic frequency [*Leyser et al.*, 1993, 1994; *Sergeev et al.*, 1997; *Stubbe et al.*, 1994; *Frolov et al.*, 2001]. This result can be considered as additional evidence that the NC_p is generated slightly below the PW reflection level where Langmuir waves propagate almost along geomagnetic field lines and thus do not depend strongly on the geomagnetic field.

[74] 6. The restoration of the NC_p intensity after long-time pumping has a typical time of about 1 min, which is longer than the time of the anomalous absorption relaxation and the recovery of the striction self action for the PW. These measurements, as well as experiments with X-mode additional heating, have unambiguously demonstrated that the small-scale striations are not the only reason for the suppression of the NC_p. Similarly, this aftereffect cannot be fully related to large-scale irregularities either. Taken together, these experiments have shown that more than one agent has to be invoked in the explanation of the aftereffect. It appears to us that further measurements employing the additional heating scheme are most promising for obtaining clues on the physical nature of the phenomena observed.

[75] According to *Stubbe et al.* [1984], the generation of the continuum (NC_p and NC^+ in our case) may be interpreted in terms of the strongest products of the PDI through the following processes:

[76] 1. Scattering of the monochromatic electromagnetic O-mode pump wave (symbolically written as EM) into primary Langmuir waves (symbolically written as L_0) from ion-acoustic waves (symbolically written as IA) due to the electromagnetic PDI, schematically written as

$$EM(f_0) \longrightarrow L_0(f_0 \pm f_{ia}) + IA(f_{ia}). \quad (1)$$

[77] 2. Decay of the primary Langmuir waves into secondary Langmuir waves through the cascading process in an electrostatic PDI which is responsible for the formation of the Langmuir turbulence spectrum

$$L_0(f_0 \pm f_{ia}) \longrightarrow L_1(f_0 \pm f_{ia} - 2f_{ia}) + IA(2f_{ia}), \quad (2)$$

and further

$$L_m(f_0 \pm f_{ia} - 2mf_{ia}) \longrightarrow L_{m+1}(f_0 \pm f_{ia} - 2(m+1)f_{ia}) + IA(2f_{ia}). \quad (3)$$

[78] 3. Reconversion of the secondary Langmuir waves into electromagnetic waves (SEE) escaping the disturbed volume

$$L(f) + IA(f_{ia}) \longrightarrow EM(f \pm f_{ia}). \quad (4)$$

[79] As shown by *Stubbe et al.* [1984], this generation scheme for the continuum explains the appearance of two emission components. The first component is symmetrical around f_0 in a frequency band of a few kHz, and its upshifted part can be related to the NC^+. The second component only contributes to the downshifted portion of the SEE spectrum and has a frequency band of a few tens of kHz, depending essentially on pump power and ionospheric conditions. This emission component can be related to the NC_p. A quantitative analysis of the NC_p generation has not been performed yet, and a comparison between the experimental results presented in the paper and theoretical studies can therefore not be made directly.

7. Closing Remarks

[80] The temporal development of the ponderomotive part of the narrow continuum (NC_p) spectrum, as well as the dependence of the NC_p properties on pump power, pump frequency, pump pulse duration, and ionospheric conditions, has been studied using the Sura heating facility located near Nizhny Novgorod, Russia. Features of the NC_p were investigated also for different additional heating schemes using both O-mode and X-mode pumping.

[81] The experiments performed have demonstrated once again the physical richness of the SEE technique as a tool for studying plasma turbulence in general and Langmuir turbulence in particular. The latter was previously investigated only by means of the incoherent scatter radar (ISR) technique in measurements of the HF-enhanced plasma line (HFPL) (see, for example, *Sulzer and Fejer* [1994], *Isham et al.* [1996], *Stubbe and Hagfors* [1997], and numerous references given therein), as well as recent observations published by *Isham et al.* [1999], *Rietveld et al.* [2000], and *Cheung et al.* [2001]. Considering the results obtained in SEE and ISR measurements, one must realize that these methods are distinctly different and thereby supplementary. The SEE technique provides an integrated picture of the physical phenomena in the sense that all secondary electromagnetic emissions from a wide spatial range, and hence from a wide plasma wave vector spectrum, contribute to the emission intensity observed at a given frequency. This is in contrast to the ISR technique by means of which Langmuir

waves satisfying simultaneously the Bragg scatter condition and the Langmuir dispersion relation in the ambient plasma can be detected only. In monostatic operation these waves have the wave vector $|\mathbf{k}| = 2\omega/c$ (i.e., twice the wave number of the ISR, where ω is the radar frequency) and are either parallel or antiparallel to the radar line of sight. It should be mentioned that recent developments in the ISR technique have made available measurements with a high-altitude discrimination of about of 150 m and a time resolution of about of 0.5 ms [e.g., *Sulzer and Fejer*, 1994; *Cheung et al.*, 2001]. One of the important advantages of the SEE technique is that the SEE equipment is comparatively simple and can be easily implemented at any ionospheric modification facility. Another advantage is the usefulness of the SEE technique for the study of upper hybrid turbulence excited by the TPI [*Sergeev et al.*, 1998] and of striations [*Boiko et al.*, 1985; *Leyser et al.*, 1993, 1994; *Frolov et al.*, 1994, 1997c; *Sergeev et al.*, 1999] which are not accessible to the available ISRs. Furthermore, the SEE measurements usually have a higher time resolution ($\sim$0.3 ms), which is of considerable importance in defining the decay features of the high-frequency plasma turbulence.

[82] The first comparative experimental study of SEE and HFPL has been performed by *Thidè et al.* [1995] in Arecibo by modification of the ionosphere at f_0 = 3.1745 MHz. These experiments have demonstrated that in the earlier stage of pumping, during a few tens of milliseconds, the two sets of spectra possess strong similarities, having the same total width and exhibiting a similar overshoot. The NC_p spectra discussed here are very close in form to the SEE spectra obtained in Arecibo, demonstrating the universal nature of the NC generation process, consisting of wave plasma interactions leading to the development of the PDI. It should be mentioned that in our SEE spectral measurements, carried out with 3-ms temporal resolution, we have not found any signs of strong parametric effects similar to the SEE "strong type spectra" predicted and reported by *Cheung et al.* [1997].

[83] The SEE technique has opened wide opportunities to study in detail the temporal evolution of high-frequency plasma turbulence [*Sergeev et al.*, 1997, 1998]. In the present paper it has been shown once again that the short-time overshoot (or miniovershoot introduced by *Showen and Kim* [1978] and studied later by *Duncan and Sheerin* [1985], *Djuth et al.* [1986], and *Sulzer and Fejer* [1994]) is fundamental to the evolution of HF-induced Langmuir waves in the resonance region.

[84] Theoretical aspects of the miniovershoot have been investigated by *Kuo et al.* [1987], *Muldrew* [1988], and *Kuo et al.* [1990]. They have considered the influence of anomalous damping due to electron scattering by the excited plasma waves, evolution of Langmuir waves in magnetic field-aligned ducts and the heating of the bulk plasma by HF-excited plasma waves. Nevertheless, the physical nature of the miniovershoot is not completely understood yet.

[85] Another possible cause of the short-time overshoot is the generation of small-scale striations during the stage of the ponderomotive instability development. In experiments conducted by *Boiko et al.* [1990] and *Frolov et al.* [1997c] it has been found that during the first 100–300 ms of pumping the generation of meter-scale striations in the vicinity of the PW reflection level is observed before the subsequent development of the anomalous absorption due to TPI growth. There are strong reasons to believe that these striations are of ponderomotive nature. We have denoted this type of striations as "striction striations." It is important that the striction striations can be excited by very short PW pulses of $\sim$10–50 ms duration only [*Zyuzin et al.*, 1987]. It should be mentioned that the artificial field-aligned irregularities studied by *Noble and Djuth* [1990] very likely are of ponderomotive nature too.

[86] Theoretical aspects of the generation of small-scale striations in the initial stage of ionosphere pumping, before the thermal structuring of the plasma, are discussed in many papers (see, for example, *Perkins and Valeo* [1974], *Lee and Fejer* [1978], *Rypdal and Cragin* [1979], *Vas'kov et al.* [1981], *Kuo et al.* [1983], and *Gurevich and Karashtin* [1994]). It has been stated that these striations are generated by a self-focusing mechanism of Langmuir waves and that they might result in ducted Langmuir wave modes modifying their saturated spectrum. It is well possible that the short-time overshoot in the NC_p intensity (as well as in the HFPL intensity) within 30–100 ms after PW switch-on is due to some properties of Langmuir waves trapped in these striations. The striction striations may also greatly influence the early time development of irregularities of thermal origin by acting as "seed" irregularities, amplifying the growth of the TPI at the upper hybrid resonance level and giving rise to the fast anomalous absorption as a result of that [*Frolov et al.*, 1997c]. They can also explain in a natural way the appearance of the "initial ducts" in the early stage of PW-plasma interaction incorporated by *Muldrew* [1988, 1992] in his duct model.

[87] At the present time it cannot be unambiguously stated what kind of HF-induced perturbations mentioned above plays a dominant role in the short-time overshoot. It cannot be excluded also that several factors have to be taken into account jointly for its explanation. Further theoretical and experimental work is needed to gain an improved understanding of this phenomenon.

[88] An important advantage of the experiments considered in this paper is the detailed insight into the dependence of the NC_p damping (or Langmuir turbulence damping) on various factors and on the pump power first of all. It has been found that only when the measurements are conducted under nighttime conditions at rather low pump powers, the decay of the NC_p after PW switch-off is determined by Langmuir wave damping due to Coulomb collisions, whereas for $\tilde{P}_{eff}$ higher than a few megawatts a considerably faster relaxation of these waves is observed. We have reasons to assume that HF accelerated electrons play an important role for such collisionless damping and thus the SEE measurements can be successfully employed for the study of electron acceleration mechanisms in the HF-perturbed ionosphere. However, on the basis of the present SEE results it is difficult to decide on the nature of these superthermal electrons, bearing in mind that they can be produced by either weak (wave determined) or strong (caviton determined) Langmuir turbulence. In order to decide this problem, simultaneous SEE and ISR measurements would be desirable in the future to provide a more complete diagnostic of the Langmuir turbulence HF-induced in the ionospheric plasma.

[89] It should be mentioned that some HFPL decay measurements have been carried out using the ISR technique. Based on experimental data obtained by *Wong et al.* [1983] and *Sulzer and Fejer* [1994], it may be concluded that plasma waves of different origins decay with different damping rates. It is conceivable that in this way the results of our measurements with O-mode additional heating (see subsection 5.1) can be understood, when in the nonstationary stage after long-time pumping, i.e., in the stage of transition from the thermal to the ponderomotive nonlinearity, a two-stage relaxation process is observed, depicting the simultaneous existence of two types of high-frequency plasma turbulence.

[90] Another interesting result of our measurements is the exhibition of aftereffects in the SEE behavior. In these measurements [see also *Boiko et al.*, 1985; *Frolov et al.*, 1999b; *Wagner et al.*, 1999] it was found that typically used approaches, taking into account only electron temperature enhancement and plasma density profile modification, as well as small-scale and large-scale irregularities in the perturbed ionospheric volume, cannot adequately explain the experimental data, and new mechanisms will have to be considered. At present, investigations in this field represent a major point of interest in our work, and important new experimental results pertaining to aftereffect features were recently obtained. A detailed presentation of these results will be the subject of a separate publication.

[91] **Acknowledgments.** We gratefully acknowledge the technical support from the staff of the SURA heating facility. We are very thankful for the financial support from the Max-Planck-Institut für Aeronomie. This work has been supported by INTAS grant 03-51-5583 and the grants from the Russian Basic Research Foundation 02-02-17475 and 04-02-17544.

[92] Michel Blanc thanks the referees for their assistance in evaluating this paper.

References

Alber, Y. I., Z. N. Krotova, N. A. Mityakov, V. O. Rapoport, and V. Y. Trakhtengerts (1974), Stimulated scattering effects on incidence of an electromagnetic pulse on a plasma layer, *Zh. Eksp. Teor. Fiz.*, *66*, 574.

Armstrong, W. T., R. Massey, P. Argo, R. Carlos, D. Riggin, P. Y. Cheung, M. McCarrick, J. Stanley, and A. Y. Wong (1990), Continuous measurement of stimulated electromagnetic emission spectra from HF excited ionospheric turbulence, *Radio Sci.*, *25*, 1283–1289.

Belikovich, V. V., E. A. Benediktov, S. M. Grach, and G. I. Terina (1981), Double transformation of waves by scattering from artificial ionospheric irregularities (in Russian), *XIIIth All Soviet Union Conf. of Radiowave Prop. Abstracts*, *1*, 107.

Blagoveshchenskaya, N. F., and V. A. Kornienko (1998), Remote observations of second harmonic stimulated emission in Tromsø heating experiment, paper presented at the Vth Suzdal URSI Symposium on the Modification of the Ionosphere (ISSMI'98), Union Radio Sci. Int., Suzdal, Russia.

Boiko, G. N., L. M. Erukhimov, V. A. Zyuzin, G. P. Komrakov, S. A. Metelev, N. A. Mityakov, V. A. Nikonov, V. A. Ryzhov, Y. V. Tokarev, and V. L. Frolov (1985), Dynamic characteristics of stimulated electromagnetic emission from ionospheric plasma, *Radiophys. Quantum Electron.*, *28*, 259–268.

Boiko, G. N., L. M. Erukhimov, and V. L. Frolov (1990), Excitation of small-scale irregularities near the excitation wave reflection level, *Geomagn. Aeron.*, *30*, 843–846.

Cheung, P. Y., E. Mjølhus, D. F. DuBois, J. Pau, H. Zwi, and A. Y. Wong (1997), Stimulated radiation from strong Langmuir turbulence in ionospheric modification, *Phys. Rev. Lett.*, *79*, 1273–1276.

Cheung, P. Y., M. P. Sulzer, D. F. DuBois, and D. A. Russell (2001), High-power high-frequency-induced Langmuir turbulence in the smooth ionosphere at Arecibo. II. Low duty cycle, altitude-resolved, observations, *Phys. Plasmas*, *8*, 802–812.

Das, A. S., and J. A. Fejer (1979), Resonance instability of small-scale field-aligned irregularities, *J. Geophys. Res.*, *84*, 6701–6704.

Djuth, F. T., C. A. Gonzales, and H. M. Ierkic (1986), Temporal evolutionn of the HF-enhanced plasma line in the Arecibo F region, *J. Geophys. Res.*, *91*, 12,089–12,107.

Duncan, L. M., and R. A. Behnke (1978), Observations of self-focusing electromagnetic waves in the ionosphere, *Phys. Rev. Lett.*, *41*, 998–1001.

Duncan, L. M., and J. P. Sheerin (1985), High-resolution studies of the HF ionospheric modification interaction region, *J. Geophys. Res.*, *90*, 28,371–28,376.

Erukhimov, L. M., S. A. Metelev, N. A. Mityakov, and V. L. Frolov (1982), Experimental studies of the striction parametric instability in the ionosphere, *Radiophys. Quant. Electron.*, Engl. Transl., *25*, 348–351.

Erukhimov, L. M., S. A. Metelev, E. N. Myasnikov, N. A. Mityakov, and V. L. Frolov (1987a), Artificial ionospheric turbulence (review), *Radiophys. Quant. Electron.,* Engl. Transl., *30*, 156–171.

Erukhimov, L. M., V. Y. Kovalev, E. N. Kurakin, S. F. Marchenko, L. N. Rubtsov, E. N. Sergeev, and V. L. Frolov (1987b), Study of the interaction of strong radio emission with the ionospheric plasma at middle latitudes, *Geomagn. Aeron.*, *27*, 659–663.

Erukhimov, L. M., S. A. Metelev, and D. V. Razumov (1988), Diagnostics of ionospheric inhomogeneities with the artificial radio emission, *Radiophys. Quant. Electron.*, Engl. Transl., *31*, 926–934.

Fejer, J. A., and H. Kopka (1981), The effect of plasma instabilities on the ionospherically reflected wave from a high-power transmitter, *J. Geophys. Res.*, *86*, 5746–5750.

Fejer, J. A., and Y. Y. Kuo (1973), Structure in the nonlinear saturation spectrum of parametric instabilities, *Phys. Fluids*, *16*, 1490–1496.

Frolov, V. L. (1991), Some remarks on the dynamics of artificial ionospheric radio emission, paper presented at the IIIrd Suzdal URSI Symposium on Modification of the Ionosphere by Powerful Radio Waves (ISIM-3), Union Radio Sci. Int., Moscow, Russia.

Frolov, V. L. (1995), Artificial plasma turbulence induced in the ionospheric F region by powerful HF waves: Results of experimental investigations (in Russian), Sc.D. dissertation, Radiophys. Res. Inst., Nizhniy Novgorod, Russia.

Frolov, V. L., G. N. Boiko, S. A. Metelev, and E. N. Sergeev (1994), On the study of artificial ionospheric turbulence by means of stimulated electromagnetic emission, *Radiophys. Quant. Electron.*, Engl. Transl., *37*, 593–603.

Frolov, V. L., S. M. Grach, L. M. Erukhimov, G. P. Komrakov, E. N. Sergeev, B. Thidé, and T. Carozzi (1996), Investigation of the temporal evolution of the broad upshifted maximum (BUM), *Radiophys. Quant. Electron.*, Engl. Transl., *39*, 241–254.

Frolov, V. L., G. P. Komrakov, E. N. Sergeev, B. Thidé, M. Waldenvik, and E. Veszelei (1997a), Experimental results of investigation of narrow continuum features in stimulated electromagnetic emission spectra, *Radiophys. Quant. Electron.*, Engl. Transl., *40*, 731–744.

Frolov, V. L., L. M. Erukhimov, E. N. Ermakova, G. P. Komrakov, E. N. Sergeev, and P. Stubbe (1997b), A new upshifted spectral stimulated electromagnetic emission structure, observed between electron cyclotron harmonics, *Geophys. Res. Lett.*, *24*, 1647–1650.

Frolov, V. L., L. M. Erukhimov, S. A. Metelev, and E. N. Sergeev (1997c), Temporal behavior of artificial small-scale irregularities: Review of experimental results, *J. Atmos. Sol. Terr. Phys.*, *59*, 2317–2333.

Frolov, V. L., L. M. Erukhimov, L. M. Kagan, G. P. Komrakov, E. N. Sergeev, and P. Stubbe (1998), Two-component nature of the broad upshifted maximum in stimulated electromagnetic emission (SEE) spectra, *Phys. Rev. Lett.*, *81*, 1630–1633.

Frolov, V. L., L. M. Kagan, and E. N. Sergeev (1999a), Review of features of stimulated electromagnetic emission (SEE): Recent results obtained at the "Sura" heating facility, *Radiophys. Quant. Electron.*, Engl. Transl., *42*, 557–561.

Frolov, V. L., L. M. Kagan, E. N. Sergeev, G. P. Komrakov, P. A. Bernhardt, J. A. Goldstein, L. S. Wagner, C. A. Selcher, and P. Stubbe (1999b), Ionospheric observations of F region artificial plasma turbulence, modified by powerful X-mode radio waves, *J. Geophys. Res.*, *104*, 12,695–12,704.

Frolov, V. L., E. N. Ermakova, L. M. Kagan, G. P. Komrakov, E. N. Sergeev, and P. Stubbe (2000), Features of the broad upshifted structure (BUS) in stimulated electromagnetic emission spectra, *J. Geophys. Res.*, *105*, 20,919–20,933.

Frolov, V. L., E. N. Sergeev, E. N. Ermakova, G. P. Komrakov, and P. Stubbe (2001), Spectral features of stimulated electromagnetic emissions, measured in the 4.3–9.5 MHz pump wave frequency range, *Geophys. Res. Lett.*, *28*, 3103–3106.

Grach, S. M. (1985), Electromagnetic radiation of artificial ionospheric plasma turbulence, *Radiophys. Quant. Electron.*, Engl. Transl., *28*, 470–477.

Grach, S. M., A. N. Karashtin, N. A. Mityakov, V. O. Rapoport, and V. Y. Trakhtengertz (1977), Parametric interaction between electromagnetic

radiation and the ionospheric plasma, *Radiophys. Quant. Electron.*, Engl. Transl., *20*, 1254–1258.

Grach, S. M., M. M. Shvarts, E. N. Sergeev, and V. L. Frolov (1998), Broad continuum feature of stimulated electromagnetic emission, *J. Atmos. Sol. Terr. Phys.*, *60*, 1233–1246.

Gumerov, R. I., V. B. Kapkov, G. P. Komrakov, and A. M. Nasyrov (1999), Artificial luminescence of the ionosphere caused by the short-term influence of powerful RF radiation, *Radiophys. Quant. Electron.*, Engl. Transl., *42*, 524–527.

Gurevich, A. V. (1978), *Nonlinear Phenomena in the Ionosphere*, Springer-Verlag, New York.

Gurevich, A. V., and A. N. Karashtin (1994), Self-focusing instability of plasma waves excited by powerful HF radiation, *Phys. Lett. A*, *195*, 362–368.

Gurevich, A. V., H. Carlson, A. V. Lukyanov, and K. P. Zybin (1997), Parametric decay of upper hybrid plasma waves trappid inside density irregularities in the ionosphere, *Phys. Lett. A*, *231*, 97–108.

Isham, B., C. La. Hoz, H. Kohl, T. Hagfors, T. B. Leyser, and M. T. Rietveld (1996), Recent EISCAT heating results using chirped ISR, *J. Atmos. Terr. Phys.*, *58*, 369–383.

Isham, B., C. La. Hoz, M. T. Rietveld, T. Hagfors, and T. B. Leyser (1999), Cavitating Langmuir turbulence observed during high-latitude ionospheric wave interaction experiments, *Phys. Rev. Lett.*, *83*, 2576–2579.

Kagan, L. M., and V. L. Frolov (1996), Significance of field-aligned currents for F region perturbations, *J. Atmos. Terr. Phys.*, *58*, 1465–1474.

Karashtin, A. N., Y. S. Korobkov, V. L. Frolov, and M. S. Tsimring (1986), Stimulated radio emission of the ionospheric plasma at the second harmonic of the pump wave frequency, *Radiophys. Quant. Electron.*, Engl. Transl., *29*, 22–25.

Kuo, S. P., B. R. Cheo, and M. C. Lee (1983), The role of parametric decay instabilities in generating ionospheric irregularities, *J. Geophys. Res.*, *88*, 417–423.

Kuo, S. P., M. C. Lee, and F. T. Djuth (1987), A new interpretation of plasma-line overshoot phenomena, *Geophys. Res. Lett.*, *14*, 961–964.

Kuo, S. P., A. Y. Ho, and M. C. Lee (1990), Temporal evolution of HF-enhanced plasma lines, *Geophys. Res. Lett.*, *17*, 2209–2212.

Lee, M. C., and J. A. Fejer (1978), Theory of short-scale field-aligned dencity striations due to ionospheric heating, *Radio Sci.*, *13*, 893–899.

Leyser T. B. (2001), Stimulated electromagnetic emissions by high-frequency electromagnetic pumping of the ionospheric plasma, *Space Sci. Rev.*, *98*, 223–328.

Leyser, T. B., B. Thidé, H. Derblom, Å. Hedberg, B. Lundborg, P. Stubbe, and H. Kopka (1990), Dependence of stimulated electromagnetic emission on the ionosphere and pump wave, *J. Geophys. Res.*, *95*, 17,233–17,244.

Leyser, T. B., B. Thidé, M. Waldenvik, S. Goodman, V. L. Frolov, S. M. Grach, A. N. Karashtin, G. P. Komrakov, and D. S. Kotik (1993), Spectral structure of stimulated electromagnetic emission between electron cyclotron harmonics, *J. Geophys. Res.*, *98*, 17,597–17,606.

Leyser, T. B., B. Thidé, M. Waldenvik, E. Veszelei, V. L. Frolov, S. M. Grach, and G. P. Komrakov (1994), Downshifted maximum features in stimulated electromagnetic emission spectra, *J. Geophys. Res.*, *99*, 19,555–19,568.

Mjølhus, E. (1998), Theoretical model for long time stimulated electromagnetic emission generation in ionospheric radio modification experiments, *J. Geophys. Res.*, *103*, 14,711–14,728.

Morales, G. J., A. Y. Wong, J. Santoru, L. Wang, and L. M. Duncun (1982), Dependence of plasma line enhancement on HF pulse length and ionospheric preconditioning, *Radio Sci.*, *17*, 1313–1320.

Muldrew, D. B. (1988), Duct model explanation of the plasma line overshoot observed at Arecibo, *J. Geophys. Res.*, *A93*, 7598–7604.

Muldrew, D. B. (1992), Initial duct growth determined from cold-start plasma-line data recorded at Arecibo, *Geophys. Res. Lett.*, *19*, 65–68.

Noble, S. T., and F. T. Djuth (1990), Simultaneous measurements of HF-enhanced plasma waves and artificial field-aligned irregularities at Arecibo, *J. Geophys. Res.*, *95*, 15,195–15,207.

Perkins, F. W., and E. J. Valeo (1974), Thermal self-focusing of electromagnetic waves in plasmas, *Phys. Rel. Lett.*, *32*, 1234–1237.

Perkins, F. W., C. Oberman, and E. J. Valeo (1974), Parametric instabilities and ionospheric modification, *J. Geophys. Res.*, *79*, 1478–1496.

Rietveld, M. T., B. Isham, H. Kohl, C. LaHoz, and T. Hagfors (2000), Measurements of HF-enhanced plasma and ion lines at EISCAT with high altitude resolution, *J. Geophys. Res.*, *105*, 7429–7439.

Rypdal, K., and B. L. Cragin (1979), HF-induced parametric decay in presence of field-aligned irregularities, *J. Geophys. Res.*, *84*, 6407–6416.

Sergeev, E. N., G. N. Boiko, and V. L. Frolov (1994), Investigation of the dynamics of HF plasma turbulence by means of artificial ionospheric radioemission, *Radiophys. Quant. Electron.*, Engl. Transl., *37*, 495–506.

Sergeev, E. N., V. L. Frolov, G. P. Komrakov, B. Thidé, and T. Carozzi (1997), Temporal evolution of HF-exited plasma waves, measured at different pump frequencies by stimulated electromagnetic emission, *J. Atmos. Sol. Terr. Phys.*, *59*, 2383–2400.

Sergeev, E. N., S. M. Grach, G. P. Komrakov, V. L. Frolov, and G. N. Boiko (1998), Results of the investigation of Langmuir and upper hybrid plasma turbulence evolution by means of the stimulated electromagnetic emission, *Radiophys. Quant. Electron.*, Engl. Transl., *41*, 313–347.

Sergeev, E. N., V. L. Frolov, G. N. Boiko, G. P. Komrakov, P. Stubbe, B. Thidé, T. B. Leyser, and T. Carozzi (1999), Influence of small-scale irregularities on characteristics of the overshoot-effect in the temporal evolution of stimulated electromagnetic emission. part I. Development stage, *Radiophys. Quant. Electron.*, Engl. Transl., *42*, 619–634.

Showen, R. L., and D. M. Kim (1978), Time variations of HF-induced plasma waves, *J. Geophys. Res.*, *83*, 623–628.

Stubbe, P., and T. Hagfors (1997), The Earth's ionosphere: A wall-less plasma laboratory, *Surv. Geophys.*, *18*, 57–127.

Stubbe, P., et al. (1982), Ionospheric modification experiments in northern Scandinavia, *J. Atmos. Terr. Phys.*, *44*, 1025–1041.

Stubbe, P., H. Kopka, B. Thidé, and H. Derblom (1984), Stimulated electromagnetic emission: A new technique to study the parametric decay instability in the ionosphere, *J. Geophys. Res.*, *89*, 7523–7536.

Stubbe, P., A. J. Stocker, F. Honary, T. R. Robinson, and T. B. Jones (1994), Stimulated electromagnetic emission and anomalous HF wave absorption near electron gyroharmonics, *J. Geophys. Res.*, *99*, 6233–6246.

Sulzer, M. P., and J. A. Fejer (1994), Radar spectral observations of HF-induced ionospheric Langmuir turbulence with improved range and time resolution, *J. Geophys. Res.*, *99*, 15,035–15,050.

Thidé, B., H. Kopka, and P. Stubbe (1982), Observations of stimulated scattering of a strong high-frequency radio wave in the ionosphere, *Phys. Rev. Lett.*, *49*, 1561–1564.

Thidé, B., A. Hedberg, J. A. Fejer, and M. P. Sulzer (1989), First observations of stimulated electromagnetic emission at Arecibo, *Geophys. Res. Lett.*, *16*, 369–372.

Thidé, B., F. T. Djuth, T. B. Leyser, and H. M. Ierkic (1995), Evolution of Langmuir turbulence and stimulated electromagnetic emission excited with a 3-MHz pump wave at Arecibo, *J. Geophys. Res.*, *100*, 23,887–23,889.

Vas'kov, V. V., and A. V. Gurevich (1973), Parametrical exitation of the Langmuir waves in the ionosphere by HF powerful waves, *Izv. Vyssh. Uchebn. Zaved., Radiofizika*, *16*, 188.

Vas'kov, V. V., and A. V. Gurevich (1975), Nonlinear resonant instability of a plasma in the field of the ordinary electromagnetic wave, *J. Exp. Theor. Phys.*, *42*, 91–97.

Vas'kov, V. V., A. V. Gurevich, and A. N. Karashtin (1981), Thermal self-focusing instability of plasma waves near resonance, *Geomagn. Aeron.*, *21*, 724–728.

Wagner, L. S., P. A. Bernhardt, J. A. Goldstein, C. A. Selcher, V. L. Frolov, and E. N. Sergeev (1999), Effect of ionospheric self-conditioning and preconditioning on the broad upshifted maximum component of stimulated electromagnetic emission, *J. Geophys. Res.*, *104*, 2573–2590.

Waldenvik, M., B. Thidé, T. B. Leyser, E. Veszelei, V. L. Frolov, S. M. Grach, and G. P. Komrakov (1993), Studies of the temporal evolution of SEE at the Sura ionospheric modification facility, paper presented at XXIVth General Assembly, Int. Union of Radio Sci., Kyoto, Japan.

Waldenvik, M. (1994), The dinamics of electromagnetic radiation from a HF perturbed space plasma, *IRF Sci. Rep. 216*, Swedish Institute of Space Physics, Uppsala.

Wong, A. Y., J. Santoru, C. Darrow, L. Wang, and J. G. Roederer (1983), Ionospheric caviton and related nonlinear phenomena, *Radio Sci.*, *18*, 815–830.

Zheleznyakov, V. V. (1995), *Radiation in Astrophysical Plasmas*, Kluwer Acad., Norwell, Mass.

Zyuzin, V. A., G. P. Komrakov, A. M. Nasyrov, V. A. Ryzhov, and V. A. Strekalov (1987), On development of small-scale irregularities excited in the ionosphere under its short-time modification by powerful radio waves (in Russian), *Geomagn. Aeron.*, *27*, 942–947.

V. L. Frolov, G. P. Komrakov, and E. N. Sergeev, Radiophysical Research Institute, B. Pecherskaya Str. 25, 603950, Nizhny Novgorod, Russia. (vf@nirfi.sci-nnov.ru; evg@nirfi.sci-nnov.ru)

T. B. Leyser, B. Thidé, E. Veszelei, and M. Waldenvik, Swedish Institute of Space Physics, SE-75221 Uppsala, Sweden. (tbl@itfu.se; bt@irfu.se; ev@irfu.se; mw@irfu.se)

P. Stubbe, Max-Planck-Institut für Aeronomie, 371916 Katlenburg-Lindau, Germany. (stubbe@linmpi.mpg.de)

PROPERTIES OF THE THERMAL NARROW-CONTINUUM COMPONENT IN THE SPECTRUM OF STIMULATED IONOSPHERIC EMISSION

V. L. Frolov,[1] * D. I. Nedzvetsky,[1] E. N. Sergeev,[1] E. A. Shorokhov,[1] and P. Stubbe [2]

UDC 533.951+537.868

We present the results of experimental studies of the properties of the thermal narrow-continuum component $NC_{\rm th}$ of stimulated electromagnetic emission (SEE) of the ionosphere observed in a narrow region between the pump frequency and the downshifted maximum (DM). Spectral and dynamic characteristics of the $NC_{\rm th}$ component are considered and the dependence of its properties on the frequency and power of the pumping wave as well as on the zenith angle of a high-power radio-wave beam in the geomagnetic-meridian plane is analyzed. It is proved that the $NC_{\rm th}$ generation is determined by the thermal (resonant) parametric instability near the level of the upper-hybrid resonance for a high-power radio wave. New experimental data on the properties of the main DM thermal component in the spectrum of stimulated electromagnetic emission, which we used as the reference component in most measurements, are presented.

1. INTRODUCTION

Stimulated electromagnetic emission excited by high-power O-mode waves near the level of their reflection in the ionospheric F region has intensely been studied for over 30 years since it was discovered [1, 2]. This radiation appears as a result of different processes of interaction between electromagnetic waves and high-frequency plasma oscillations with low-frequency plasma turbulence, among which artificial small-scale plasma-density irregularities with sizes $l_\perp \leq 30{-}50$ m in the direction orthogonal to the geomagnetic field lines play a crucial role. Interrelation and mutual influence of different plasma processes during SEE generation in a magnetoactive plasma stipulate its wide diagnostic capabilities for a study of properties of both artificial and natural plasma turbulence. Naturally, this requires knowledge of the mechanisms of generation of the radiation components used for diagnostics and the dependence of these mechanisms on a broad range of ionospheric parameters.

According to the studies performed in the middle [3–9] and polar [1, 10–14] latitudes, the SEE in its stationary state, which is usually reached a few seconds (or a few tens of seconds) after the interaction begins, is a composition of more than ten separate spectral structures (radiation components), which is evidence for the variety of the plasma processes occurring simultaneously in the perturbed region (PR) of the ionosphere. An overview of the results obtained in these experiments is given in, e.g., [15–17]. The initial classification of the main components of SEE was given in [1, 3, 10]. Later, other discovered components were added. A complete list of SEE components, in which their main properties are considered, is given in [16]. The main SEE components that are most frequently mentioned in various studies comprise (i) the

* vf@nirfi.sci-nnov.ru

[1] Research Radiophysical Institute, Nizhny Novgorod, Russia; [2] Max-Plank Institut für Aeronomie, Katlenburg-Lindau, Germany. Translated from Izvestiya Vysshikh Uchebnykh Zavedenii, Radiofizika, Vol. 12, No. 48, pp. 1013–1032, December 2005. Original article submitted July 30, 2004; accepted June 23, 2005.

0033-8443/05/1248-0901

main spectral maximum of radiation, or downshifted maximum (DM), whose frequency f_{DM} is shifted down from the pumping-wave (PW) frequency by $\Delta f^- \approx 9{-}18$ kHz [1, 3, 5, 10, 16]; (ii) broadband radiation in the negative-detuning region, or broad continuum (BC), which is detected at frequencies below f_{DM} in the range of detunings of up to $\Delta f^- \approx 60{-}120$ kHz [3, 4, 16]; (iii) the maximum in the region of positive detunings $\Delta f^+ \approx 7{-}12$ kHz, or upshifted maximum (UM), which is about symmetric to DM with respect to the pumping-wave frequency in the SEE spectrum [10, 16]; (iv) broadband radiation in the region of positive detunings $\Delta f^+ \approx 15{-}150$ kHz, or broad upshifted maximum (BUM), which is generated when the pumping-wave frequency f_{PW} is close to or is slightly above the gyroresonant-harmonic frequency in the region of interaction between a high-power radio wave and a plasma (under conditions of the measurements performed using the "Sura" facility, the electron gyrofrequency $f_{\mathrm{ce}} \approx 1.3{-}1.35$ MHz) [4, 7, 10, 16–18]; (v) striction narrow-band radiation component, or ponderomotive narrow continuum $\mathrm{NC_p}$, which is observed for detunings of up to $\Delta f^- \approx 30{-}50$ kHz at the stage of striction parametric instability development [8, 9, 16]; (vi) broadband radiation, which is similar to BUM and is detected in frequency ranges between the gyroharmonics, or broad upshifted structure (BUS) [19]. By tradition and to avoid therminological mess, we will use the above-mentioned English-language names of the radiation components. Generation of different components in the SEE spectrum significantly depends on the frequency and power of the PW as well as ionospheric conditions. In particular, the performed studies [4, 5, 7, 11, 13, 15–18] showed that the form of the SEE spectrum is changed radically in a narrow range of PW frequencies if $f_{\mathrm{PW}} \approx n f_{\mathrm{ce}}$, where n is the gyroharmonic number. One of the most important gyroharmonic properties of the SEE, which is often used in various experiments is suppression of the DM generation in a very narrow frequency range of a few kilohertz or less if $f_{\mathrm{PW}} \approx n f_{\mathrm{ce}}$. This property of DM permits one to determine quickly and with high accuracy the gyroharmonic resonance frequency directly during measurements. In recent years, dynamic and spectral characteristics of the main components of SEE (DM, BC, BUM, $\mathrm{NC_p}$, UM, and BUS) have been studied in detail and their empiric models [4–8, 15–19] have been developed. Theoretical models of generation are proposed for some radiation components. An overview of such models is given in [16].

In the first papers devoted to the SEE properties [1, 10], a component called Continuum was introduced. This component is radiation without distinct structures, which is observed mainly at frequencies below the PW frequency and whose intensity, as a rule, exponentially decays with increase in the detuning Δf^-. Later on, after a more detailed study of its spectral and evolution characteristics [3, 4, 12, 13], this component was divided into three components: $\mathrm{NC_p}$ (fast narrow continuum, following the classification adopted in [16]), whose properties were studied in detail in [8, 9, 20], $\mathrm{NC_{th}}$ (thermal narrow continuum, or, following [16], slow narrow continuum), and BC, whose properties were considered in detail in [3, 4, 16, 17]. In what follows we consider the properties of the least explored thermal narrow-band component $\mathrm{NC_{th}}$, whose generaion is observed in a narrow region of detunings $\Delta f^- \leq 7$ kHz between the frequencies f_{DM} and f_{PW}. Since the detuning from the PW frequency is small, measurement of characteristics of $\mathrm{NC_{th}}$ encounters certain difficulties because the high-power radio-wave signal and the stimulated electromagnetic emission, received simultaneously, whose intensity ratio is $70{-}110$ dB, significantly influences the receiving apparatus. Since on the basis of the already performed experiments [8] it is quite reasonable to assume that $\mathrm{NC_{th}}$ refers to the class of thermal components of SEE, during the whole work the obtained characteristics of $\mathrm{NC_{th}}$ are compared with the properties of DM as the thermal component which is most completely studied at present and whose generation is certainly determined by the development of thermal (resonant) parametric instability [21–24]. It is also important that theoretical models are better developed for the DM component compared with other SEE components. All this is significant when DM is used as the base (reference) radiaion component which is convenient for comparing the properties of other SEE components. It should be mentioned that in this paper considerable attention is paid to the data which we obtained in the last experiments on the properties of DM, enabling one to refine the empiric model of this component. The possible mechanism of $\mathrm{NC_{th}}$ generation is discussed in the closing part of this paper.

2. RESULTS OF EXPERIMENTAL STUDIES OF THE PROPERTIES OF THE THERMAL NARROW-BAND COMPONENT OF SEE

2.1. Main characteristics of NC_{th}

In stationary SEE spectra (see Fig. 1 showing the intensity I of stimulated electromagnetic emission in decibels relative to 1 mW), the NC_{th} component is located in a narrow frequency range between f_{PW} and the high-frequency edge of DM, i.e., in the band $\Delta f^- \leq 7$ kHz, as radiation with intensity rapidly decreasing with increase in Δf^-. Dependence of the radiation intensity on Δf^- is often exponential, with decrease rate 2−4 dB/kHz. Under quiet geomagnetic conditions, the threshold power of the pumping-wave radiation at which this component begins to be generated (with allowance for the linear absorption of a high-power radio wave in the lower ionosphere) $P_{eff} \approx 0.1-0.3$ MW, which, as we mentioned as early as in [10], can even be somewhat smaller than the PW power at which the DM component begins to be manifested in the SEE spectrum. According to the results presented in [3], these two components are generated even in the absence of a visible anomalous attenuation of the high-power radio-wave signal reflected from the ionosphere. Numerous studies of the dependence of the spectral intensity of DM (for the peak frequency) and NC_{th} (for $\Delta f^- \approx 4$ kHz) on the PW power, performed using the "Sura" facility, show that these dependences can be represented in power-law form with the average exponent $\langle\alpha\rangle \approx 0.5-0.7$ for DM and 0.4−0.6 for NC_{th}. As for DM (see [3, 5]), the dependence of the intensity of the NC_{th} component on the PW power is of hysteresis nature if after the ionosphere is affected by a high-power wave the radiation on the decreasing PW-power branch appears to be more intense than that on the increasing PW-power branch. Hereafter, for control of NC_{th} we choose the spectral intensity of radiation for the detuning $\Delta f^- \approx 4$ kHz, which is about the middle of the frequency range of possible detection of the mentioned component. For such detunings, we manage to avoid, on the one hand, strong influence of the intense PW and, on the other hand, strong influence of the contribution of the DM component on the measurement results.

Figure 2 shows the averaged stationary intensities of DM and NC_{th} components, as functions of the PW frequency, which usually are settled a few tens of seconds after the interaction begins. The dependences were plotted on the basis of the measurements performed in 1996–1999 under conditions of a quiet evening ionosphere when the PW frequency was fairly close to the critical frequency of the ionospheric F_2 layer and was outside the gyroharmonic-resonance regions. All the results of the SEE intensity measurements presented here are given for the reception band 300 Hz and are expressed in decibels with respect to 1 mW (dBm). It is well seen in Fig. 2 that the maximum intensity of both components is observed in the frequency range $f_{PW} \approx 5-7$ MHz. For the higher PW frequencies, the intensity of DM and NC_{th} components decreases

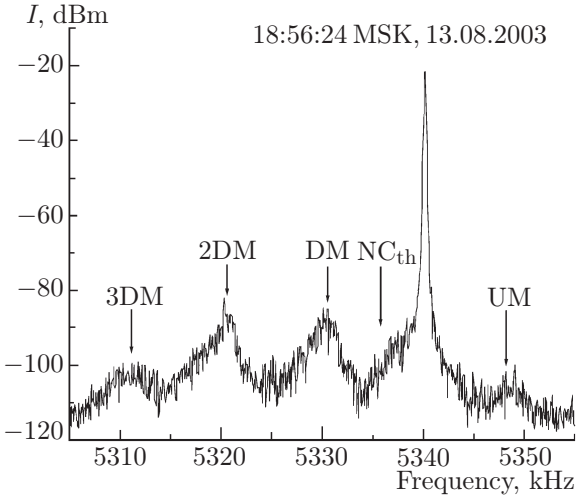

Fig. 1.

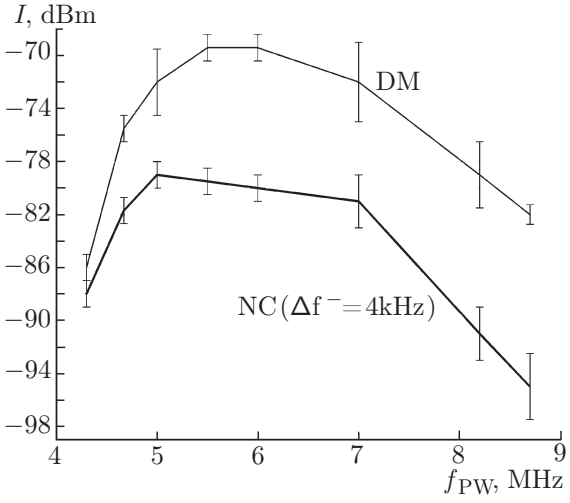

Fig. 2.

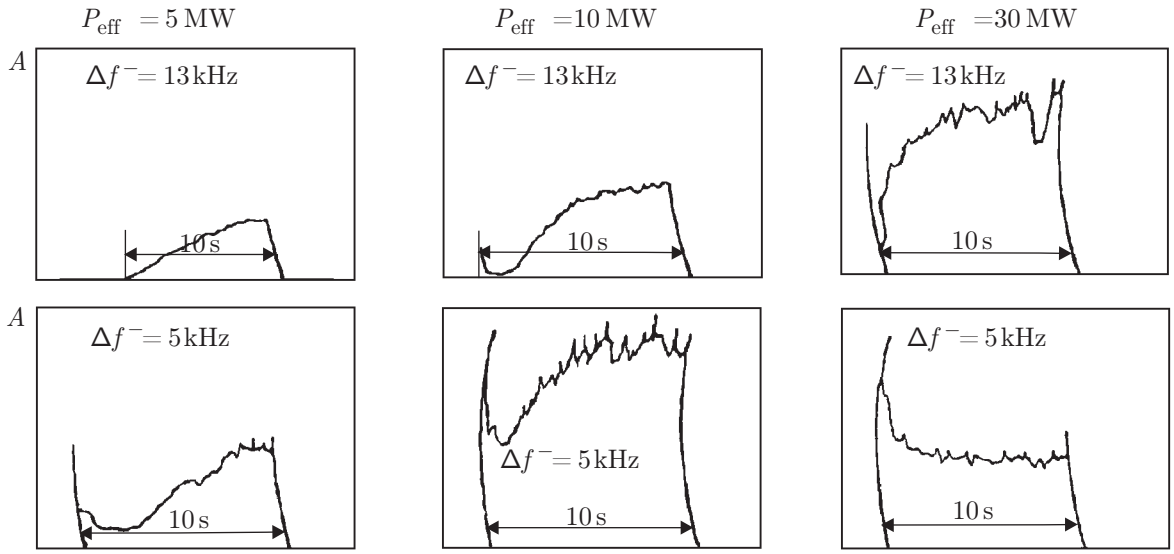

Fig. 3.

with increase in f_{PW} at a rate of about 1 dB per 100 kHz. The intensity of these components decreases still more abruptly (at a rate of 2−3 dB per 100 kHz) when f_{PW} decreases in the range $f_{\text{PW}} \leq 5$ MHz. The intensity of the DM component decreases more rapidly, so that even for $f_{\text{PW}} \approx 4.3$ MHz, the stationary intensities of DM and NC_{th} components become almost equal. Such a behavior of the intensities leads to the fact that for $f_{\text{PW}} \leq 4$ MHz at the stationary stage of SEE development, the DM component can often be not detected against the background of NC_{th}, as was mentioned in, e.g., [10, 12]. Note that a rapid decrease in the stationary level of DM in the range $f_{\text{PW}} \leq 5.5$ MHz is to a considerable degree determined by the more and more increasing rate of decrease in the radiation intensity during transition from the stage of the maximum development of the DM component to the stationary state (overshoot effect). It is assumed that this process is controlled by the influence of small-scale artificial ionospheric irregularities on the generation of radiation and its attenuation during leaving the perturbed region due to the anomalous-attenuation effect [25, 26]. The overshoot effect is not detected for the DM component at $f_{\text{PW}} \geq 6$ MHz. It amounts to 1−2 dB in the frequency range $f_{\text{PW}} \approx 5.6$−5.8 MHz, 5−8 dB for $f_{\text{PW}} \approx 4.7$−4.8 MHz and 9−13 dB for $f_{\text{PW}} \approx 4.3$−4.5 MHz. Unfortunately, such data are absent for NC_{th} since, as is shown below, at the initial stage of development this component of radiation is usually masked by the striction narrow-band component NC_{p}. At the same time, the results of measurements of the radiation development and relaxation dynamics in the diagnostic SEE regime [25, 26] (the diagnostic SEE method is discussed in, e.g., [27]) show that the spectral characteristics of small-scale artificial ionospheric irregularities also exert a strong influence on the stationary intensity of the NC_{th} component.

Figure 3 shows examples of records of the radiation amplitude for two detunings, namely, $\Delta f^- =$ 13 kHz (the DM region) and $\Delta f^- = 5$ kHz (the NC_{th} region), during effect on the ionospheric plasma at the frequency $f_{\text{PW}} \approx 5828$ kHz for 10 s followed by a 50-s pause. Oscillograms are presented for three levels of effective radiation power of the pumping wave $P_{\text{eff}} = 5$, 10, and 30 MW, which is given here with allowance for the linear absorption of radio waves in the lower ionosphere. Note that the radiation was recorded for $\Delta f^- = 5$ kHz and $P_{\text{eff}} = 30$ MW in this measurement cycle with the additional 6-dB attenuation included in the reception circuit. From the data presented in Fig. 3 it is clearly seen that for low levels of power ($P_{\text{eff}} = 5$ and 10 MW), the dynamics of the radiation intensity in the DM and NC_{th} regions is almost the same except for the first intensity peak which appears immediately after the interaction begins and is related to the manifestation of NC_{p} [7, 8, 20]. For a higher power of the pumping-wave radiation $P_{\text{eff}} = 30$ MW, the significantly enhanced NC_{p} component masks the initial stage of NC_{th} development. In this case, the transition to the stationary level of radiaion intensity occurs via suppression of the striction narrow-

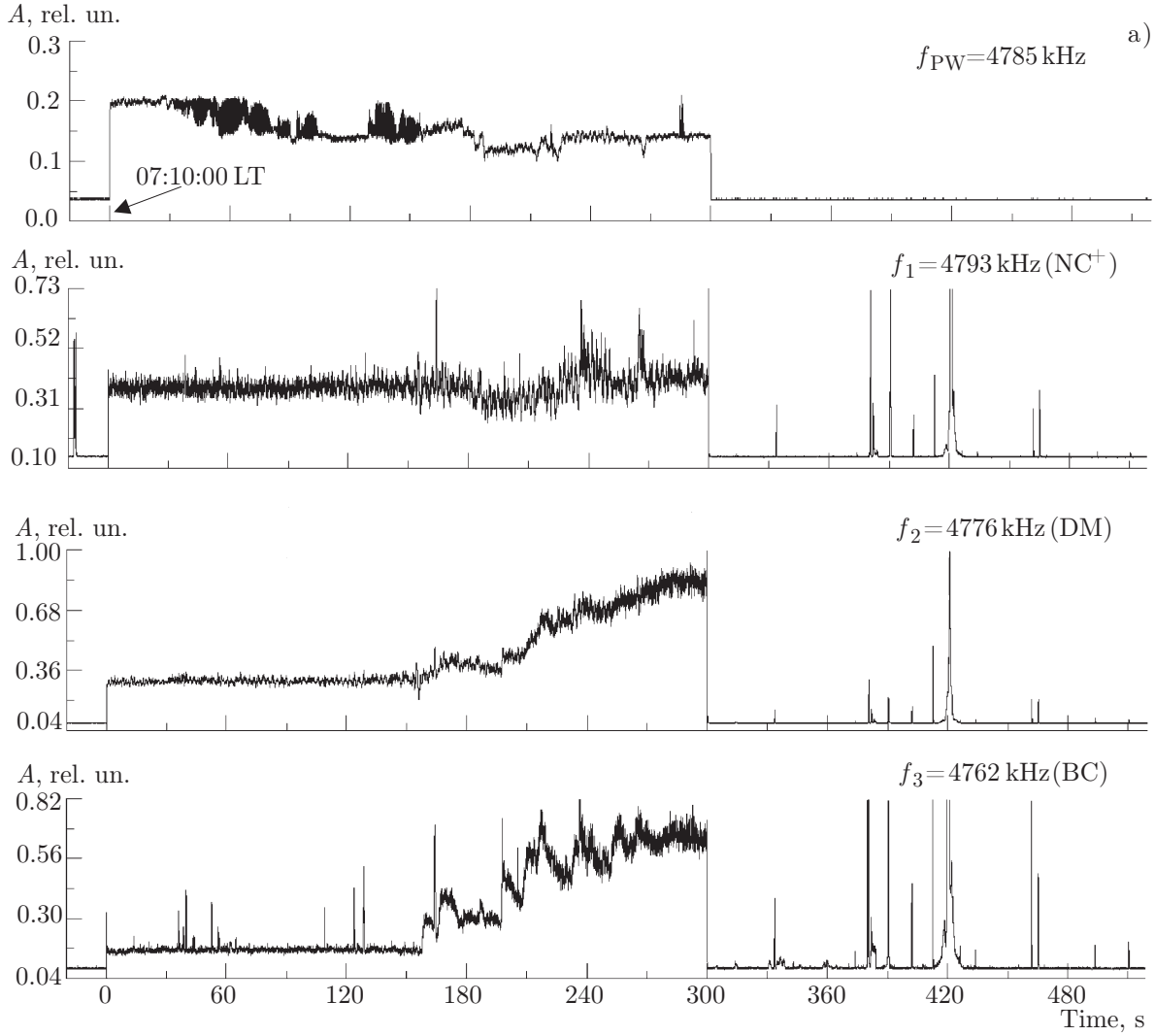

band component during development of the thermal (resonant) parametric instability. Such a dynamics of radiation development was studied in detail in, e.g., [25, 26, 28].

Important information on the properties of the SEE can be obtained by studying its characteristics as functions of the ratio between the pumping-wave frequency f_{PW} and the critical frequency f_{0F_2} of the ionospheric F_2 layer. Such experiments are most easy at sunrise or at sunset when the critical frequency is gradually varied in a natural way. According to [12, 29] and many other measurements, the DM component appears even in the case where f_{PW} exceeds the critical frequency of the ionospheric F_2 layer by 100−200 kHz. This, in particular, gave grounds to state [5] that the DM is generated near the level of the upper-hybrid resonance for the O-mode pumping wave, which is usually located several kilometers below the height of reflection of this wave in the ionosphere. Figure 4 presents the results of SEE measurements performed in August 20, 1998 when the critical frequency gradually increased, but remained below the

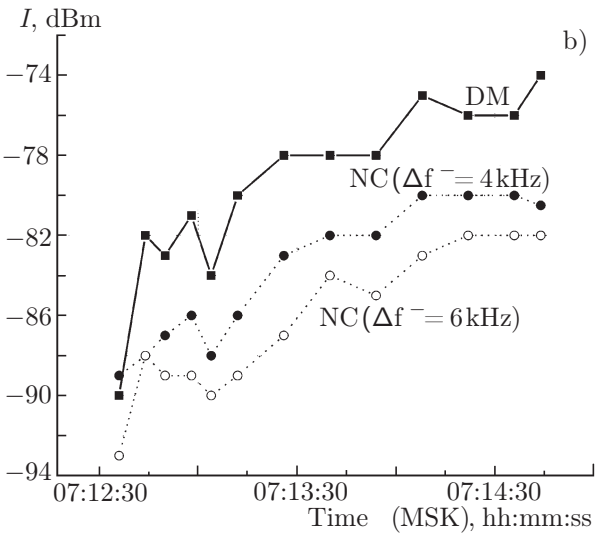

Fig. 4.

pumping-wave frequency. Figure 4*a* shows oscillograms of the pumping-wave amplitude ($f_{\rm PW} = 4785$ kHz, upper track) and stimulated ionospheric radio emission at frequencies 4793 kHz (the region of small positive detunings), 4776 kHz (DM region), and 4762 kHz (BC region). Unfortunately, the radiation in the $\rm NC_{th}$ region was not recorded, and the data on the radiation intensity for DM and the detunings $\Delta f^- = 4$ and 6 kHz, presented in Fig. 4*b*, were taken from spectral measurements performed simultaneously. It is seen in Fig. 4*a* that, although the PW was switched on at 07:10:00 LT, the DM and BC components appeared only since 07:12:40 LT. In this case, according to ionospheric data and based on the fact that both the PW amplitude fluctuations and the radiation are absent in the region of small positive detunings $\Delta f^+ \approx 4{-}8$ kHz, the PW frequency remained slightly higher than f_{0F_2} throughout the entire heating cycle. The data presented in Fig. 4*b* show that the radiation in the DM and $\rm NC_{th}$ regions appears simultaneously and, which is very important, the behavior of the intensities of these components is repeated in detail in their temporal variations. This can indicate that the mechanisms responsible for generation of these components in the same ionospheric region are of similar nature. Similar results were obtained by us in other measurements of the features of the SEE behavior when the relationship between $f_{\rm PW}$ and f_{0F_2} was changed at sunrise or at sunset.

The properties of the SEE as functions of the inclination angle of the radiation of a high-power radio wave in the geomagnetic-meridian plane from 12° to the North to 12° to the South with a 4° step were studied from August 9 to 16, 2003 using the "Sura" facility. The results of these experiments for the stationary intensities of the DM and $\rm NC_{th}$ components are presented in Fig. 5 for two measurement cycles where the PW frequency was approximately 20−40 kHz higher (the index +) or lower (−) than the fourth-harmonic frequency $4f_{\rm ce}$. It can easily be seen that the dependences of the studied radiation components are very similar in both cases.

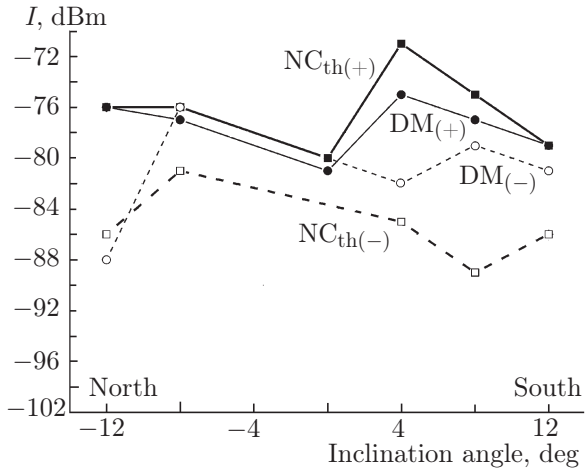

Fig. 5.

Summarizing the above-considered properties of $\rm NC_{th}$, we can conclude that by threshold generation powers, the form of frequency dependences of the stationary radiation intensity, the dynamics of development upon PW switch-on, the behavior of the radiation intensity during passage through the critical frequency of the ionospheric F_2 layer, and, finally, the dependence on the inclination angle of the radiation of a high-power radio wave in the geomagnetic-meridian plane, the narrow-band component $\rm NC_{th}$ and the component DM have almost identical characteristics. This gives strong grounds to state that both $\rm NC_{th}$ and DM are generated as a result of development of the thermal (resonant) parametric instability in the upper-hybrid resonance region for the pumping wave.

2.2. On properties of $\rm NC_{th}$ in the gyroharmonic-resonance region

One of the main properties of the SEE is abrupt and significant variation in its characteristics in a narrow frequency band where the gyroharmonic-resonance condition $f_{\rm PW} \approx nf_{\rm ce}$, where n is the gyroharmonic number, is fulfilled in the region of interaction between the PW and the plasma. Critical frequencies permitting, the "Sura" facility allows experiments to be performed for $n = 4{-}7$. The results of such experiments are given in [17] and the references cited therein. Recall that one of the most important results obtained here is that we detected suppression of the thermal (resonant) parametric instability development and, as a consequence, suppression of the DM generation in a very narrow frequency range, whose width amounts to about several kilohertz for $n = 4$ and decreases to fractions of a kilohertz for $n = 7$ [5, 16]. Since, as was mentioned above, there is good reason to assume that both $\rm NC_{th}$ and DM are generated in the upper-hybrid resonance region as a result of the development of thermal (resonant) parametric instability,

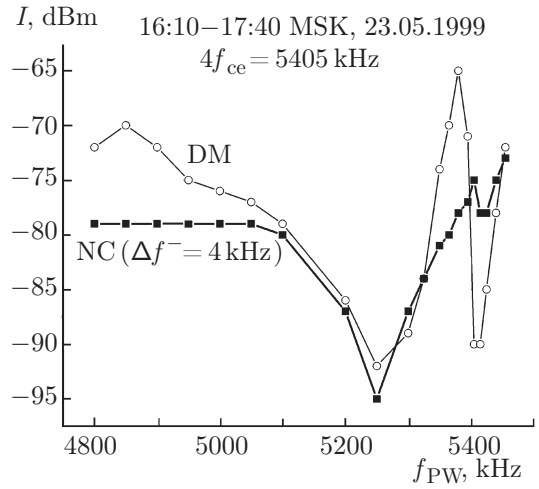

Fig. 6.

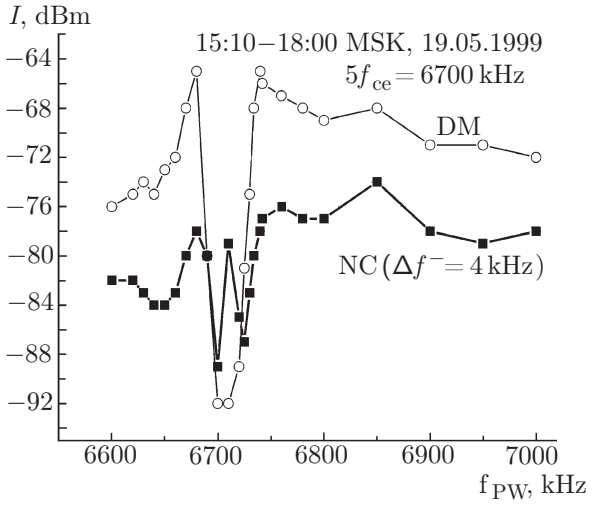

Fig. 7.

it seems important to study the gyroharmonic properties of this SEE component.

Figures 6, 7, and 8 present the results of May 1999 measurements of spectral characteristics of the SEE near the fourth, fifth, and sixth harmonics of electron gyrofrequency, respectively. In these measurements, the frequency step was 50 kHz far from the gyroresonances and 5−10 kHz for $f_{\rm PW} \approx nf_{\rm ce}$. Figures 6–8 show the intensities of DM and $\rm NC_{th}$ as functions of the PW frequency for $\Delta f^- \approx 4$ kHz. By measurements in the vicinity of the three gyroharmonics, the intensity of the DM component in the gyroharmonic-resonance region decreased by about 20−25 dB with respect to the intensity of this SEE component outside these regions. ¿From the presented data it can easily be seen that, although outside the narrow resonant regions of strong suppression of DM the behavior of the DM and $\rm NC_{th}$ intensities is about the same, for measurements near the fourth and fifth gyroharmonics, a decrease in the intensity of $\rm NC_{th}$ for $f_{\rm PW} \approx nf_{\rm ce}$ did not exceed 15 and 10 dB, respectively. According to the data presented in Fig. 8 for $f_{\rm PW} = 6f_{\rm ce}$, a well pronounced minimum with a depth of about 20 dB was also observed for the radiation in the $\rm NC_{th}$ region, but it could be not as deep in other measurements.

The second important feature of the gyroharmonic properties of the DM and $\rm NC_{th}$ components is that the frequencies of their intensity minima for $f_{\rm PW} \approx nf_{\rm ce}$ do not coincide. Namely, for $\rm NC_{th}$, this minimum is observed, as a rule, at a frequency about 10 kHz higher than that for DM. This is clearly seen in, e.g., Fig. 8. Note that according to [30] and our other measurements, during transition through $nf_{\rm ce}$ the UM intensity minimum, whose frequency is 8−10 kHz higher than the PW frequency, is downshifted in terms of the PW frequency by 10−20 kHz compared with the DM suppression frequency. It is clear that such a shift of the suppression frequencies with respect to each other for three thermal SEE components considered here cannot be occasional and should carry certain information on their generation mechanisms. In what follows we will return to this issue during discussion of the results obtained in this paper.

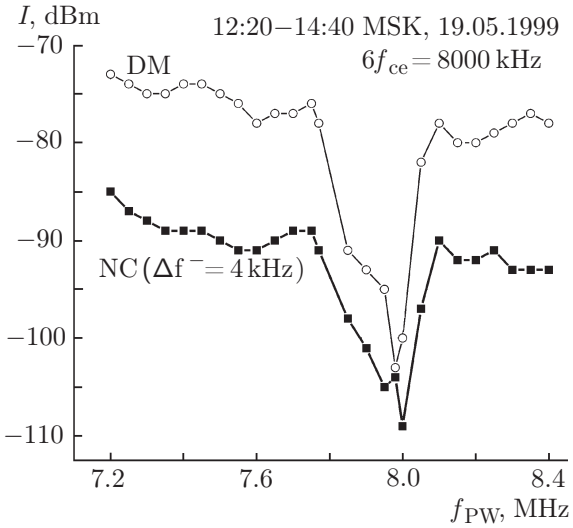

Fig. 8.

The performed experiments also show that for $f_{\rm PW} \approx nf_{\rm ce}$, along with the attenuation of the intensity of $\rm NC_{th}$, the spectrum of this component becomes slightly narrower. In this case, a plateau or even a

weak maximum, which is similar by its characteristics to the earlier observed spectral maximum of the striction narrow-band component NC_p, can often be seen in the radiation spectrum for the detunings $\Delta f^- \approx 3-4$ kHz. Such variations in the spectral characteristics of the SEE for small negative detunings from the PW frequency were analyzed earlier in detail in [20, 31]. Taking all said above into account, it is reasonable to assume that in the case where the PW frequency is close to the gyroharmonic frequency and suppression of the thermal (resonant) parametric instability development and generation of small-scale artificial ionospheric irregularities is observed, the energy of a high-power radio wave, not undergoing a strong anomalous attenuation due to transformation of the pumping wave to upper-hybrid plasma oscillations, is transported to the level of PW reflection in the ionosphere at which strong excitation of the striction parametric instability becomes possible even in the regime of continuous radiation of a high-power radio wave and, as a consequence, NC_p can be generated. It is important to emphasize that in the region of negative detunings, NC_p is generated in the same frequency band as NC_{th} and these components of radiation have similar spectral characteristics [9, 20]. This explains why the attenuation of the radiation intensity in the region of the narrow-band SEE component is considerably smaller than that for DM since, instead of the suppressed component NC_{th}, the component NC_p, which is very similar to it, begins to be recorded. As the PW frequency increases (with the transition to the higher-order gyroharmonics), threshold powers of the striction parametric instability also increase notably [32]. This leads to the attenuation of the NC_p generation and, therefore, an increase in the recorded attenuation of radiation in the NC_{th} region.

Detailed studies of the SEE properties in the last decade show that in a narrow range of PW frequencies $f_{PW} \approx nf_{ce} - 30$ kHz ($n = 5-7$), where local amplification of the DM-component intensity takes place, a high-power broadband component BC is also observed in the region of negative detunings [3, 4, 17]. Besides the mentioned range, generation of the intense broadband component BC is also detected in the range $f_{PW} \approx 5.5-6.0$ MHz between the fourth and fifth gyroharmonics [17], where the most intense DM and NC_{th} components are also recorded (see Fig. 2). All this is important evidence that similar processes of PW – plasma interaction should lie at the base of generation of these three thermal components of SEE. It should be mentioned that the development of a high-power BC component also leads, in some cases, to flattening of the radiation spectrum in the NC_{th} region at about the level of the intensity of the BC component for the detunings $\Delta f^- \approx 20$ kHz. Based on these data, it can be assumed that in this case BC occupies the entire frequency band in the negative-detuning region beginning with the pumping-wave frequency, as is assumed in the theoretical model of generation of this SEE component [33]. However, in other experiments discussed in, e.g., [16], the maximum spectral intensity of the BC component can be even higher than the radiation intensity in the gap between the DM and the PW frequency. Nevertheless, along with the BC, the NC_{th} component is also well extracted in the radiation spectrum. An interesting experimental fact is that for $n = 4$, generation of the high-power BC component is not observed in the DM amplification region at frequencies 20−40 kHz below nf_{ce} and that only the NC_{th} and the multiple DM maxima [7, 17] are recorded in the negative-detuning region (see, e.g., Fig. 1). The entire set of experimental data obtained to date favor the fact that BC and NC_{th} are different thermal SEE components, whose generation mechanisms have own specific features. According to [17], the structure of the SEE spectrum with multiple DM maxima and well-pronounced NC_{th} component is also characteristic of pumping-wave frequencies slightly exceeding nf_{ce}, but for $f_{PW} \geq 7$ MHz. Here, the BC component has a fairly low intensity (significantly smaller than that of the DM component) and extends no further than to the detunings $\Delta f^- \approx 40-60$ kHz.

Finalyzing consideration of the experimental data related to gyroharmonic properties of the thermal SEE components, we note that the observed minimum of the radiation intensity of the DM and NC_{th} components at the frequencies $f \approx 5.2-5.3$ MHz (see Fig. 6) is to a considerable degree determined by the local impairement of the performance of the receiving antenna in this frequency range. This requires additional special test measurements for determining the true frequency dependences of the intensity of the studied radiation components.

2.3. On one feature of spectral characteristics of the DM and NC_{th}components

It was noted as early as in [10] that the spectra in the NC_{th} region and at the low-frequency edge of DM are often of exponential form with close indices. This can be seen in Fig. 1 showing an example of an SEE spectrum with DM and two well-developed multiple maxima 2DM and 3DM. It is seen from this example that the inclinations of the spectra for NC_{th} and DM almost coincide for slightly smaller inclinations for 2DM and 3DM. According to different measurement data, the inclination of spectra is varied in a wide range from 1.5 to 4.5 dB/kHz, reflecting the variation in generation conditions for these radiation components. It is also important that inclinations of the spectra for DM and NC_{th} can be varied in a consistent way with the variation in measurement conditions. This fact is a weighty argument that the mechanisms of radiation formation in these parts of the SEE spectra are of the same type, which is due, e.g., to the induced scattering of intense plasma oscillations into lower-frequency oscillations by background-plasma ions [34]. We will return to this question in Sec. 3, in which we discuss the obtained results and the model of generation of the NC_{th} component.

2.4. On the essence of the "DM splitting" effect during heating of the ionospheric plasma at the frequencies $f_{PW} \approx nf_{ce}$

One of the features of DM, which have not been studied to a sufficient degree at present, is that the DM spectrum comprises two closely located narrow-band maxima if the ionosphere is affected at frequencies almost coincident with the gyroresonance harmonic frequency. For the first time, this phenomenon, called the "DM splitting," was discovered in the experiments at the heating facility in Tromsø(Norway) [12, 13]. Later, this phenomenon was also observed in the measurements of SEE characteristics at the "Sura" facility. In what follows, based on the experiments performed in September 1997, we consider the dynamics of spectral characteristics of DM with the variation in f_{PW} with a 2−5-kHz step and passage through the fourth harmonic of the electron gyrofrequency.

Figure 9 shows a family of SEE spectra for the case where the PW frequency decreased from 5410 to 5385 kHz ($4f_{ce} \approx 5400$ kHz according to the data on the intensity-minumum frequency of the DM component). From the presented data it is well seen that in the frequency range $|f_{PW} - 4f_{ce}| \leq 5$ kHz there are two narrow-band maxima in the DM region for the detunings $\Delta f^- \approx 10$ and 8 kHz with approximately the same intensity. In this case, the maximum with a smaller detuning ($\Delta f^- \approx 8$ kHz), whose broad low-frequency edge covers the maximum-generation region with a larger detuning, prevails in the region $4f_{ce} - f_{PW} > 5$ kHz. Hence, it is difficult to judge how the intensity of this maximum is varied with decreasing PW frequency. Above the gyroresonance (for $f_{PW} - 4f_{ce} > 5$ kHz), on the contrary, the low-frequency maximum is more intense. Since the low-frequency edge of this maximum has a more abrupt drop compared with the low-frequency edge, one can distinctly determine the attenuation of the low-frequency maximum of DM. Detailed analysis of the dependence of the intensity of both maxima of DM on the frequency of a high-power radio wave in the range $f_{PW} = 5385-5410$ kHz shows that as the PW frequency increases, the intensity of the lower-frequency maximum increases by about 10 dB, while the intensity of the high-frequency maximum decreases by 20−25 dB. Thus, the considered dynamics of the radiation spectrum in the DM region clearly demonstrates that the "DM splitting" phenomenon is actually a result of the manifestation of two separate narrow-band spectral maxima, biased with respect to each other, whose intensity is determined by the magnitude and sign of detuning of the PW frequency relative to the frequency of the gyroresonant harmonic. It can be assumed that the generation of two maxima is a consequence of the features of the dispersion characteristics of the upper-hybrid and Bernstein plasma oscillations, which determine the gyroharmonic properties of the interaction between a high-power O-mode radio wave and a magnetoactive plasma and are considered in detail for the case of the upper ionosphere in [35].

We note that in Fig. 9 one can see the appearance of the radiation intensity maximum for the detunings $\Delta f^- = 3-4$ kHz when $|f_{PW} - 4f_{ce}| \leq 5$ kHz.

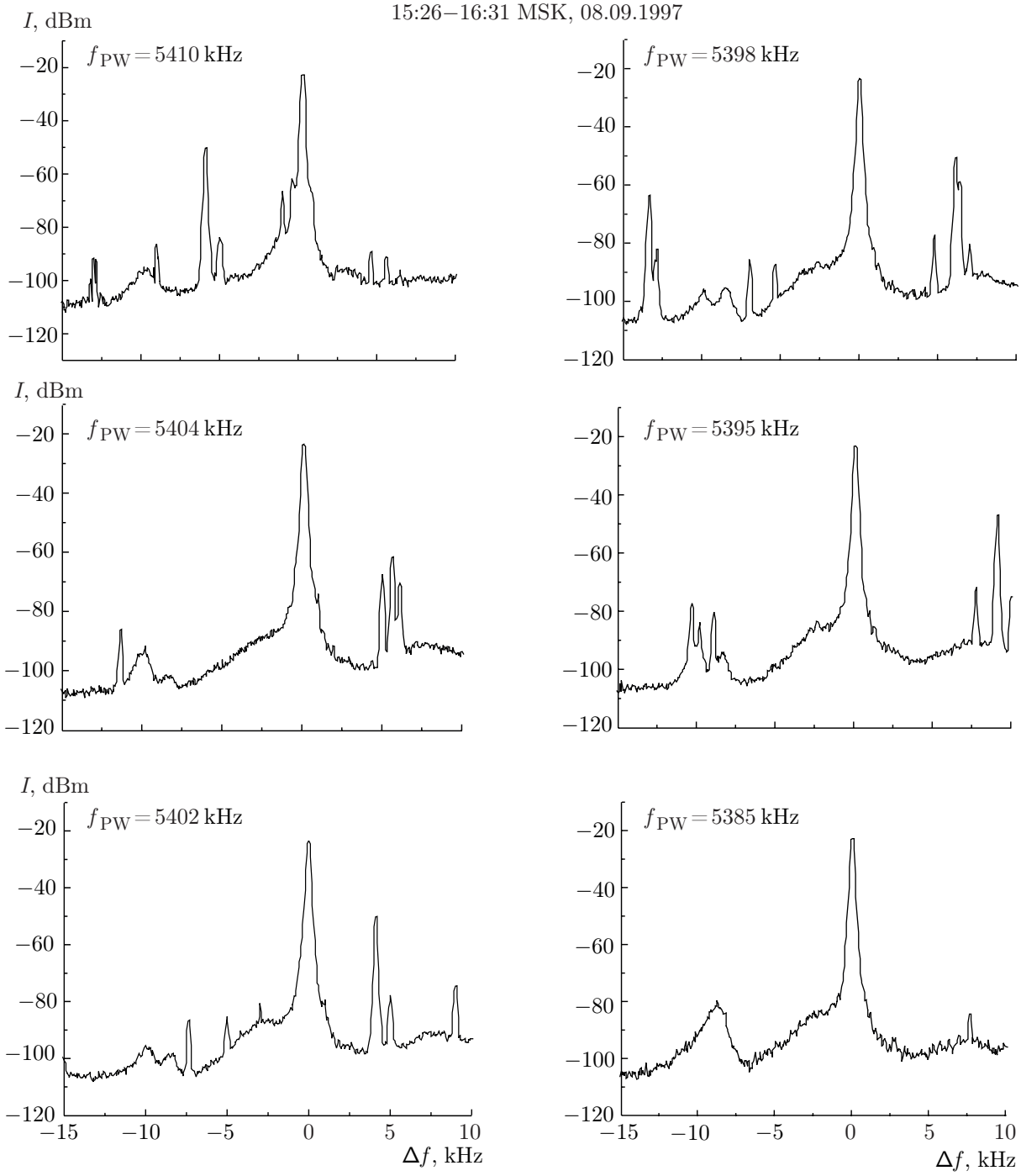

Fig. 9.

2.5. Features of the dynamics of the thermal components of radiation in experiments with additional heating of ionospheric plasma

Finalizing consideration of experimental results, we briefly dwell on studies of the SEE properties in measurements with the use of the scheme of additional heating of ionospheric plasma (a detailed description of the scheme of such experiments and features of the measurements performed with its help is given in [36]). In the course of such experiments performed in August 30, 2002, the radiation of two transmitters of the facility with the effective power $P_{\text{eff}} \approx 180$ MW at a frequency of 6250 kHz was used for the creation of intense artificial ionospheric turbulence. The ionosphere was affected for three minutes in the 3-s heating —

12-s pause regime. The next two minutes the PW was not emitted to let the appeared perturbations relax. For the radiation of the diagnostic wave, we used the third transmitter which continuously generated radiation at a frequency of 5730 kHz with a sufficiently low power ($P_{\text{eff}} \approx 5$ MW). In the ionosphere, the diagnostic wave excited SEE not saturated in intensity. By response of this radiation to switching the PW radiators on and off, one can judge the nature of the influence of different components of artificial ionospheric turbulence on the SEE generation. Analysis of ionograms for the considered experiment shows that the distance between the reflection heights h_{ref} of the diagnostic wave and the pumping wave amounted to $\Delta h \approx 23$ km ($h_{\text{ref}} \approx 255$ and 278 km for the diagnostic and pumping waves, respectively). In this case, the PW was reflected near the maximum of the F_2 layer.

Figure 10*a* shows the evolution of the intensity of the pumping wave reflected from the ionosphere. Figures 10*b–f* show fragments of SEE signals at frequencies 5722, 5720, 5718, 5716, and 5714 kHz, respectively, which included the time interval of the PW radiation. Figure 10*g* presents the SEE spectrum for the diagnostic wave, from which it is seen that only three middle frequencies of signal recording correspond to the DM generation region (its maximum and side slopes), the top frequency enters the region of the valley between DM and NC_{th}, and the bottom frequency is already in the BC region. It should be mentioned that the oscillograms presented in Fig. 10 were obtained by averaging the intensity of the recorded signals by 8 sequential PW pulses of one 3-min interaction cycle which conformed to the settled nature of the SEE intensity variations for the pulsed regime of additional heating.

Consider first the behavior of the intensity of the pumping wave reflected from the ionosphere (Fig. 10*a*). Here, in the first 0.2 s of heating, one can clearly see the development of fast anomalous attenuation, after which the second, slower stage of growth of anomalous attenuation begins. As was found earlier (see, e.g., [37]), anomalous attenuation and fast anomalous attenuation are determined by the development of plasma-density inhomogeneities with $l_\perp \geq 10$ m and $l_\perp \leq 3{-}5$ m, respectively, where $l_\perp$ is the size of inhomogeneities in the direction orthogonal to the geomagnetic field. The fairly short time of fast anomalous attenuation, observed in the considered session, is due to the features of the cyclic heating regime of ionospheric plasma when the aftereffects lead to an increase in the rate of development of plasma perturbations. Also taking into account the results of the earlier measurements with longer PW pulses, it can be assumed that in the considered case, anomalous attenuation is almost over by the end of a 3-s PW pulse. It should also be mentioned that fast anomalous attenuation is preceded by the PW striction self-action effect when the amplitude of a high-power radio wave reflected from the ionosphere decreases by a factor of 1.5−2 already in the first milliseconds of action [38]. Thus, the behavior of the intensity of a high-power radio wave reflected from the ionosphere makes it possible to obtain certain information on the dynamics of small-scale artificial ionospheric irregularities in the perturbed region of the ionosphere, which, as was mentioned several times, exerts a determining influence on generation and evolution of the thermal components of SEE [24, 35]. It is clear that the PW-induced appearance or amplification of small-scale irregularities at the level of interaction between the diagnostic wave and the plasma can radically change the condition of generation of the SEE excited by the diagnostic wave.

We now analyze the evolution of the SEE induced by a diagnostic wave (see Fig. 10*b–f*). We will call this radiation the diagnostic radiation (or DSEE). It is well seen that the PW as a source of additional plasma turbulence leads at first to an amplification of the DSEE at all recorded frequencies. However, attention should be drawn to the fact that the dynamics of the radiation-intensity variation is different. The slowest development of the PW-induced radiation with $\tau_{\text{dev}} \approx 2$ s, which is only slightly smaller than the development time of anomalous attenuation, and the longest relaxation of this radiation after the PW switch-off, with $\tau_{\text{rel}} \approx 2$ s, takes place for the highest recorded radiation frequency $f = 5722$ kHz (or for the minimum detuning from the PW frequency) which enters the valley between DM and NC_{th}. Similar dynamics is also recorded for the radiation on the high-frequency slope of the spectrum of the DM component ($f = 5720$ kHz). However, in this case, the increase in the radiation intensity with $\tau_{\text{dev}} \approx 1$ s is somewhat faster and the overshoot effect (decrease in the DSEE intensity) appears already during the PW radiation. With decrease in the frequency of the recorded radiation, the rise time of the DSEE intensity decreases after

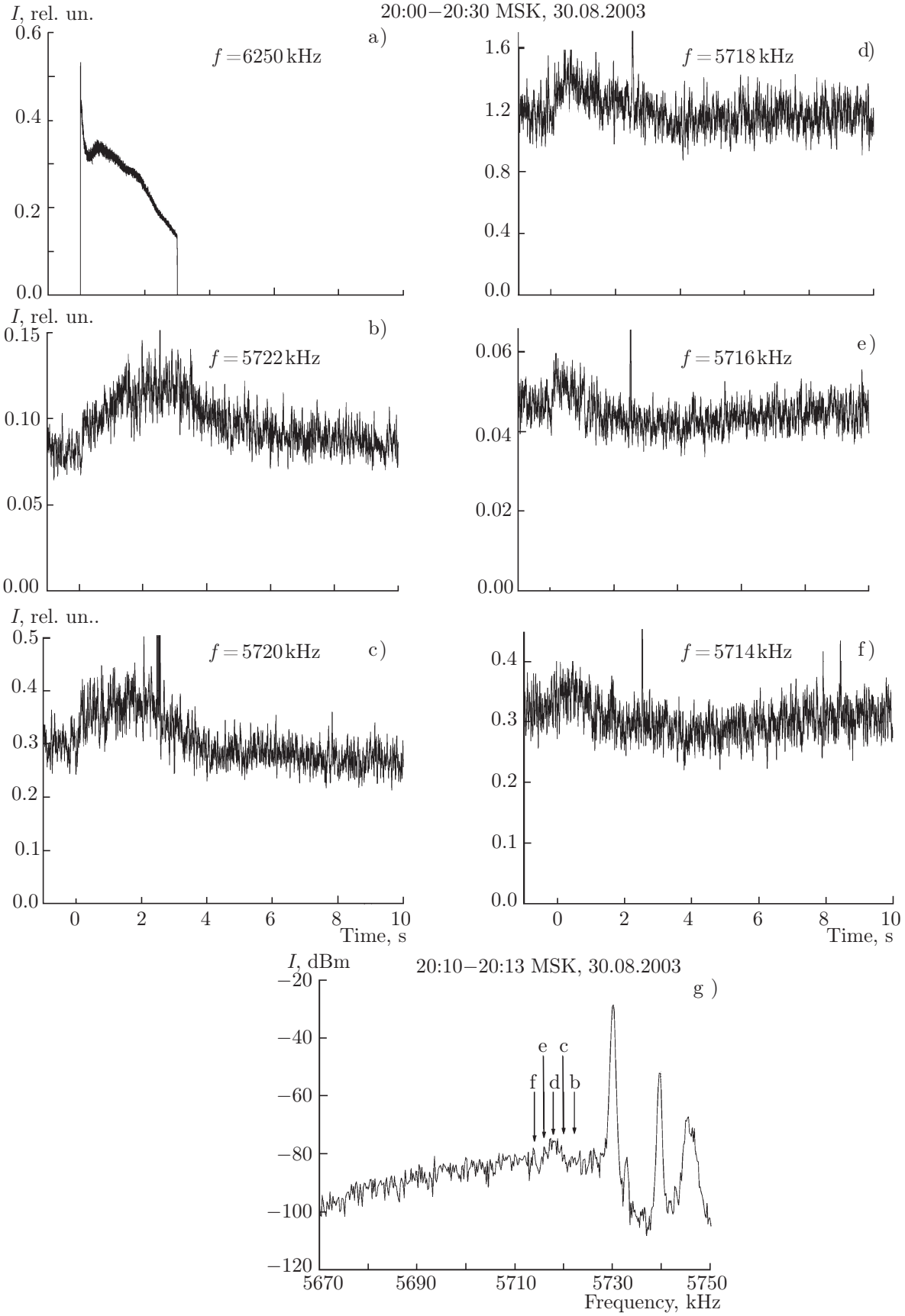
20:00−20:30 MSK, 30.08.2003
I, rel. un.
a)
f = 6250 kHz
d)
f = 5718 kHz
b)
f = 5722 kHz
e)
f = 5716 kHz
I, rel. un..
c)
f = 5720 kHz
f)
f = 5714 kHz
Time, s
Time, s
I, dBm
20:10−20:13 MSK, 30.08.2003
g)
e c
f d b
Frequency, kHz

Fig. 10.

the beginning of the pumping-wave radiation and, simultaneously, attenuation of the radiation intensity due to the overshoot effect increases. As a result, even for $f = 5716$ and 5714 kHz, very fast amplification of the DSEE for a characteristic time of fast anomalous attenuation, followed by a decrease in the radiation intensity for a time of the order of 1.5 s, takes place. This decrease can be so large that by the end of a PW pulse and immediately after its end the radiation intensity appears to be even smaller than the DSEE level unperturbed by the pumping wave and whose recovery proceeds for approximately 4 s. Generally speaking, the fast component of DSEE at the beginning of the pumping-wave radiation with the development time of fast anomalous attenuation can also be extracted for the higher-frequency components of this radiation. In this case, as for $f = 5716$ and 5714 kHz, a local maximum of the radiation intensity, although a fairly small one, is observed for the frequency $f = 5722$ kHz at times $0.1-0.8$ s. On the whole, such dynamics of the DSEE clearly demonstrates that additional heating exerts a multifactor influence, leading, at the first stage, to an amplification of the intensity of the recorded radiation which can be changed for its attenuation (the second stage). After the PW pulse is over, the stage of recovery of the DSEE intensity to the unperturned state (the third stage) is observed. Such a sequence of stages in the manifestation of the additional heating is a characteristic feature of such experiments. Their detailed description is given in [36].

The basis for interpretation of data similar to those obtained in the above-considered experiment is often the model according to which variations in the spectral characteristics and intensity of small-scale ionospheric irregularities determine the DSEE dynamics [25, 26, 33]. In this case, the choice of particular scales of irregularities is determined from comparison of temporal characteristics of the DSEE with characteristic times of development and relaxation [37]. Then, taking into account the results obtained here, it should be concluded that meter irregularities, whose intensity is maximum during the development of fast anomalous attenuation and decreases together with the development of anomalous attenuation and increase in the intensity of decameter irregularities [37], lead to an amplification of the radiation in the entire range from the valley between DM and $\mathrm{NC_{th}}$ to BC. This amplification increases with increase in the detuning Δf^-. At the same time, the SEE amplification stipulated by the influence of larger-scale irregularities with $l_\perp \geq 6-10$ m is mainly manifested for the radiation frequencies responsible for the high-frequency edge of the spectrum of the DM component and the region of the valley (i.e., for the radiation with small detunings $\Delta f^- \leq 8$ kHz), while for the lower frequencies (larger negative detunings with respect to the PW frequency), these irregularities must cause a decrease in the intensity of the received radiation due, as is often assumed, the stronger anomalous attentuation during output of the radiation from the perturbed region. Such dual influence of small-scale artificial ionospheric irregularities on the SEE dynamics was mentioned many times in the earlier publications (see, e.g., [3, 7, 18, 25, 26, 33, 36]). However, remaining within the framework of such a scheme of DSEE dynamics interpretation, we at once encounter certain contradictions during analysis of the obtained results. Firstly, all experiments on studying the properties of small-scale artificial ionospheric irregularities show that meter irregularities occupy a fairly narrow altitude interval of the order of several kilometers [37]. Hence, in our case, for $\Delta h \approx 23$ km, it is not reasonable to assume that these irregularities can exert direct influence on the DSEE generation processes. Secondly, it is diffucult to explain the strongly varied influence of small-scale artificial ionospheric irregularities on the DSEE dynamics in such a narrow (less than 10 kHz) range of generation frequencies. In this case, as was shown above, variations in the DSEE dynamics are determined by the detuning Δf^- to a greater degree than by the belonging to the particular component of radiation. Thirdly, by the delay time of the beginning of the DSEE intensity variation relative to the beginning of the PW pulse and by the distance between the reflection levels of the pumping and diagnostic waves, one can determine the propagation velocity of the perturbations, which cause the initial growth of the DSEE intensity, along the geomagnetic field lines, as was done in [36]. In our case, this delay time amounted to about 0.1 s for the distance $\Delta h \approx 23$ km. Thus, the transfer velocity of the perturbations leading to a variation in the DSEE level after the beginning of the PW radiation amounted to about $2 \cdot 10^7$ cm/s, which corresponds to the thermal velocity of electrons. This excludes the possibility to explain the rapid response of the DSEE to a PW pulse by the fact that plasma-density inhomogeneities, induced by a high-power radio wave near the level of its reflection, appear

at the level of reflection of the diagnostic wave due to "penetration" of these inhomogeneities as a result of ambipolar diffusion whose velocity along the geomagnetic-field lines is determined by the ion thermal velocity V_{T_i} (under our measurement conditions, $V_{T_i} \approx 10^5$ cm/s). Here, as was assumed in [36], allowance for the unipolar diffusion processes, as well as for the flows of thermal and suprathermal electrons, induced as a result of heating by the ionospheric plasma, and the related closure currents by the background plasma must be of crucial significance during the formation of the secondary turbulence at the DSEE generation level. However, it should be mentioned that the mechanisms of generation of the PW-induced secondary turbulence (which, in general, determines the DSEE dynamics) in the region of interaction between the diagnostic wave and the plasma are not fully clarified for now. This remains the main difficulty for interpretation of a broad range of obtained experimental data similar to those considered above.

Recently, a large amount of experimental work on studying the properties of the secondary turbulence has been performed at the "Sura" facility. The results of studies of the structure of the perturbed ionospheric region by the satellite tomography method [39] are of particular significance. According to these results, large-scale artificial perturbations of the plasma density are detected in almost the entire bulk of the ionosphere above the heating facility, and they occupy an area greatly exceedng the zone determined by the radiation pattern of the PW. This is direct evidence that intense resonant interaction between the PW and the plasma, which takes place in the central part of the perturbed region, induces the development of the secondary ionospheric turbulence far beyond this ionospheric region. In recent years, wide experimental experience has also been accumulated regarding the action by short PW pulses in which the influence of fast processes on the DSEE dynamics is most obvious. However, a detailed analysis of the results obtained in measurements using both additional heating of the ionospheric plasma and the satellite tomography is far beyond the scope of this paper and will be done in separate publications. In the present paper, we only draw attention to the fact that in the experiments with additional heating, only part of the features of the dynamic behavior of the DM (and, therefore, other thermal components of radiation) can be related to the influence of small-scale artificial ionospheric irregularities.

3. DISCUSSION OF THE RESULTS. EMPIRICAL MODEL OF THE NC_{TH} GENERATION

Multiple and versatile experiments on studying the properties of the stimulated ionospheric radio emission clearly demonstrated its complex multicomponent structure as a manifestation of the simultaneous development of different processes of interaction between a high-power radio wave and the ionospheric F-region plasma. Knowledge of the features of these processes and mechanisms of generation of separate components of the SEE ensures the possibility of its wide use for diagnostics of ionospheric turbulence of not only artificial, but also natural origin. However, for now there is no full understanding of the processes leading to the formation of even DM and BC, which are the most powerful and regularly observed thermal components of radiation and are most often used for diagnostics of artificial ionospheric turbulence [16]. The properties of the third thermal component, NC_{th}, which is recorded at the stage of stationary development of artificial ionospheric turbuence in a narrow band of negative detunings with respect to the pumping-wave frequency $\Delta f^- \leq 7$ kHz, have been studied to a still lesser degree.

In the present paper, based on various experiments and comparative studies of the DM and NC_{th} properties, we analyzed in detail the characteristics of the narrow-band radiation component. It is proved that NC_{th}, as well as DM and BC, is related to the class of thermal components of SEE whose generation is determined by the development of thermal (resonant) parametric instability near the upper-hybrid resonance level for the pumping wave. It is important that the DM and NC_{th} components have almost identical characteristics for their main key parameters. Moreover, the integral intensity of NC_{th}, which is one of the most powerful radiation components, is quite comparable with the intensities of the DM and BC components. Based on the said above, it is reasonable to assume that the NC_{th} component, as well as DM, must be a result of the most intense processes of interaction between the PW and the ionospheric plasma. It should be emphasized that the spectral characteristics of NC_{th} and the low-frequency edges of the spectra of the DM components, as well as of the multiple maxima of 2DM and 3DM, are similar, which is demonstrated

in Fig. 1. This can be evidence that the processes leading to generation of radiation in these parts of the SEE spectrum are identical. We also considered new experimental data concerning some features of DM generation, which contribute to the further development of the empirical model of this component. In particular, the data concerning the "DM splitting" were analyzed. It is found that this effect is determined by the presence of two narrow-band maxima in the DM generation band in the case where the PW frequency almost coincides with the electron gyrofrequency harmonic in the interaction region.

The performed studies made it possible to determine the relationship between the properties of the NC_p and NC_{th} components observed in the SEE spectra in the region of the same negative detunings with respect to the pumping-wave frequency, but at different stages of interaction between the PW and the ionospheric plasma and to specify conditions under which this or that radiation component is observed. This is important for interpretation of a number of experimental data, in particular, measurements near the electron gyrofrequency harmonics, amd for development of the SEE-based methods for diagnostics of the ionospheric plasma turbulence.

In this analysis of experimental data we did not dwell upon problems related to the properties of SEE for small positive detunings. This concerns both the characteristics of the narrow-band component NC^+ [8] and the UM component [10, 16, 30]. The data obtained here are the subject of separate consideration by virtue of their specificity.

The theoretical models of the DM component generation were considered in detail in [16] (see also the references cited therein) for both the case where the PW frequency is far the gyroresonance harmonic and where $f_{PW} \approx nf_{ce}$. The basis of all these models is interaction between an electromagnetic wave and upper-hybrid (as well as Bernstein near the gyroresonance) and lower-hybrid plasma oscillations in the presence of small-scale plasma-density irregularities extended along the geomagnetic field. In [40], the authors analyzed different proposed schemes of the DM component generation based on three-wave interaction in the weak-turbulence approximation and on scattering of waves by small-scale artificial ionospheric irregularities. They showed that the most preferable scheme includes (i) generation of the "parent" upper-hybrid wave due to scattering of a high-power radio wave by small-scale artificial ionospheric irregularities; (ii) decay of the "parent" upper-hybrid wave into a "daughter" upper-hybrid wave and a lower-hybrid wave (with a possible repeated cascade decay); (iii) scattering of "daughter" and cascade upper-hybrid waves into electromagnetic waves by small-scale ionospheric irregularities, which determines the formation of the DM component and multiple 2DM and 3DM maxima in the SEE spectra. This model explains a number of main properties of the DM component, but does not explain the dependences of the frequency and width of the spectral maximum on the PW frequency [5]. However, interpretation of namely these dependences is of decisive significance for choosing the correct mechanism of the DM component generation. Remaining within the framework of this model, it can be assumed that besides the above-considered decay process, the "parent" upper-hybrid waves can also form their spectrum due to the induced scattering by thermal ions with the subsequent scattering of secondary upper-hybrid waves by small-scale artificial ionospheric irregularities into electromagnetic radiation which is recorded as NC_{th}. Such a process is known as the double transformation mechanism, which was proposed for explaining the BC component generation [2, 33]. It is clear that within the framework of the above-presented model of the DM component generation, the spectrum of secondary upper-hybrid waves will also contribute to the low-frequency edge of the DM spectrum (and, correspondingly, the 2DM and 3DM spectra), which will result in close inclinations of the spectra of these radiation components, as was observed in the experiment.

Along with the above-mentioned models of generation of thermal radiation components, there has recently been intense development of the model of decay instability of upper-hybrid oscillations trapped in inhomogeneities with decreased density [41–44]. Such inhomogeneities play the role of cavities for plasma oscillations trapped in them. Actually, this model considers, in the approximation of strong turbulence, the interaction between a high-power radio wave and a plasma and the formation of small-scale plasma-density irregularities extended along the geomagnetic field. The numerical calculations of SEE generation [42, 43], even performed in approximations rather far from the realistic ones, show acceptable agreement with the

experimental data. This makes it possible to explain the generation of the DM component and multiple maxima of 2DM and 3DM in the case where for a sufficiently high excess over the threshold, the frequency of the DM maximum is shifted to greater negative detunings than the lower-hybrid oscillation frequency. Note that within the framework of such a model, the DM component is a result of the decay instability of trapped upper-hybrid oscillations, while the BC component, which has a broad weakly decaying spectrum and, as follows from the experiments, is a separate SEE component rather than NC_{th} amplified for some reasons, is related to the cavitation processes in individual inhomogeneities. Such a model is confirmed by the experimental data [16, 17], according to which the generation frequency ranges of the intense BC component coincide with the ranges of enhanced generation of the DM component (except for the PW-frequency range slightly below the fourth harmonic of the electron gyrofrequency where the intense BC component is not observed). Since in this paper we did not aim at a detailed analysis of the properties of BC, we confine ourselves to making comments relative to the possible generation model for this component.

The problem of studying the gyroharmonic properties of DM and NC_{th} holds a particular place in our research. Based on the obtained results, it can be concluded that the frequencies of the intensity minima of these components during passage of the PW frequency through the electron gyrofrequency harmonic do not coincide. For NC_{th}, the minimum is observed for the PW frequency about 10 kHz higher than the frequency of the intensity minimum of the DM component. It should be emphasized that the double resonance condition $f_{PW} = f_{UHR} = nf_{ce}$, where f_{UHR} is the frequency of the upper-hybrid resonance, for each harmonic of the electron gyrofrequency for a given altitude profile of the plasma density can be fulfilled for the single PW frequency and at a certain altitude. This excludes the possibility of interpreting the presented results by satisfying the double resonance condition for different radiation components and at different altitudes of the perturbed region. The situation becomes still more complicated if the results of [30] are taken into account. It was found there that the intensity minimum of the UM component, which is the most high-frequency thermal component among those considered in that paper, takes place for a PW frequency about 20 kHz lower than the PW frequency at which the intensity minimum of the DM component is reached. The above-presented results indicate the ambiguity of the choice of criteria for determining the condition of coincidence of the PW frequency and the gyroharmonic frequency in the region of interaction between the PW and the ionospheric plasma. Solution of this problem is an important step in choosing the correct models of generation of thermal radiation components.

In this paper, we briefly analyzed the results of experiments with additional heating of ionospheric plasma. It is shown that the DSEE intensity variations observed during switching the PW radiator on and off in the region of detunings $\Delta f^- = 8-16$ kHz are determined by the detuning of the frequency of the received radiation rather than its belonging to a particular thermal component of SEE. The obtained data also clearly demonstrate that although small-scale artificial ionospheric irregularities certainly play a crucial role in the mechanisms of generation of thermal radiation components, other components of artificial ionospheric turbulence, which strongly affect the dynamics of interaction between a high-power radio wave and a plasma and the development of secondary turbulence outside the central part of the perturbed ionospheric region, also exist. The properties of the mechanisms of such an influence cannot be considered fully studied, and it is necessary to continue experimental and theoretical studies in this field.

This work was supported in part by the Russian Foundation for Basic Research (project Nos. 02–02–17475 and 05–02–16493), the program "Universities of Russia" (project UR. 01.01.025), the CRDF (project No. RPO–1334), and INTAS (project No. 03–51–5583).

REFERENCES

1. B. Thidé, H. Kopka, and P. Stubbe, *Phys. Rev. Lett.*, **49**, 1561 (1982).
2. V. V. Belikovich, E. A. Benediktov, S. M. Grach, and G. I. Terina, in: *Proc. XIIIth All-Union Conf. Propagation of Radiowaves, Part 1* [in Russian], Nauka, Moscow (1981), p. 107.
3. G. N. Boiko, L. M. Erukhimov, V. A. Zyuzin, et al., *Radiophys. Quantum Electron.*, **28**, 259 (1985).

4. T. B. Leyser, B. Thidé, M. Waldenvik, et al., *J. Geophys. Res.*, **98**, 17597 (1993).
5. T. B. Leyser, B. Thidé, M. Waldenvik, et al., *J. Geophys. Res.*, **99**, 19555 (1994).
6. V. L. Frolov, L. M. Kagan, and E. N. Sergeev, *Radiophys. Quantum Electron.*, **42**, 557 (1999).
7. V. L. Frolov, S. M. Grach, L. M. Erukimov, et al., *Radiophys. Quantum Electron.*, **39**, 241 (1996).
8. V. L. Frolov, G. P. Komrakov, E. N. Sergeev, et al., *Radiophys. Quantum Electron.*, **40**, 731 (1997).
9. V. L. Frolov, E. N. Sergeev, G. P. Komrakov, et al., *J. Geophys. Res. A*, **109**, 07304 (2004), DOI:10.1029/2001JA005063.
10. P. Stubbe, H. Kopka, B. Thidé, H. Derblom, et al., *J. Geophys. Res.*, **89**, 7523 (1984).
11. T. B. Leyser, B. Thidé, H. Derblom, et al., *Phys. Rev. Lett.*, **63**, 1145 (1989).
12. T. B. Leyser, B. Thidé, H. Derblom, et al., *J. Geophys. Res.*, **95**, 17233 (1990).
13. P. Stubbe, A. J. Stocker, F. Honary, et al., *J. Geophys. Res.*, **99**, 6233 (1994).
14. P. Y. Cheung, A. Y. Wong, J. Pau, and E. Mjølhus, *Phys. Rev. Lett.*, **80**, 4891 (1998).
15. P. Stubbe and T. Hagfors, *Surveys Geophys.*, **18**, 57 (1997).
16. T. B. Leyser, *Space Sci. Rev.*, **98**, 223 (2001).
17. V. L. Frolov, E. N. Sergeev, E. N. Ermakova, et al., *Geophys. Res. Lett.*, **28**, 3103 (2001).
18. V. L. Frolov, L. M. Erukhimov, L. M. Kagan, et al., *Phys. Rev. Lett.*, **81**, 1630 (1998).
19. V. L. Frolov, E. N. Ermakova, L. M. Kagan, et al., *J. Geophys. Res.*, **105**, 20919 (2000).
20. E. N. Sergeev, S. M. Grach, G. P. Komrakov, et al., *Radiophys. Quantum Electron.*, **45**, 193 (2002).
21. V. V. Vas'kov and A. V. Gurevich, *Zh. Éksp. Teor. Fiz.*, **69**, 176 (1975).
22. S. M. Grach, A. N. Karashtin, N. A. Mitykov, et al., *Fiz. Plazmy*, **4**, 1321 (1978).
23. S. M. Grach, A. N. Karashtin, N. A. Mityakov, et al., *Fiz. Plazmy*, **4**, 1330 (1978).
24. A. C. Das and J. A. Fejer, *J. Geophys. Res.*, **84**, 6701 (1979).
25. E. N. Sergeev, S. M. Grach, G. P. Komrakov, et al., *Radiophys. Quantum Electron.*, **42**, 544 (1999).
26. E. N. Sergeev, S. M. Grach, G. P. Komrakov, et al., *Radiophys. Quantum Electron.*, **42**, 715 (1999).
27. V. L. Frolov, G. N. Boiko, S. A. Metelev, and E. N. Sergeev, *Radiophys. Quantum Electron.*, **37**, 593 (1994).
28. E. N. Sergeev, V. L. Frolov, G. N. Boiko, and G. P. Komrakov, *Radiophys. Quantum Electron.*, **41**, 206 (1998).
29. V. L. Frolov, V. V. Chugurin, G. P. Komrakov, et al., *Radiophys. Quantum Electron.*, **43**, 446 (2000).
30. E. N. Sergeev, V. L. Frolov, G. P. Komrakov, et al., *Proc. XXth Russian Conf. on Propagation of Radio Waves, Nizhny Novgorod, 2002* [in Russian], p. 315.
31. B. Thidé, F. T. Djuth, T. B. Leyser, and H. M. Ierkic, *J. Geophys. Res.*, **100**, 23887 (1995).
32. L. M. Erukhimov, V. Ya. Kovalev, E. P. Kurakin, et al., *Geomagn. Aéron.*, **27**, 758 (1987).
33. S. M. Grach, M. M. Shvarts, E. N. Sergeev, and V. L. Frolov, *J. Atmos. Sol.-Terr. Phys.*, **60**, 1233 (1998).
34. N. A. Mityakov, V. O. Rapoport, and V. Yu. Trakhtengerts, *Geomagn. Aéron.*, **14**, 36 (1974).
35. S. M. Grach, B. Thidé, and T. Leyser, *Radiophys. Quantum Electron.*, **37**, 392 (1994).
36. V. L. Frolov, E. N. Sergeev, and P. Stubbe, *Radiophys. Quantum Electron.*, **45**, 109 (2002).
37. V. L. Frolov, L. M. Erukhimov, S. A. Metelev, and E. N. Sergeev *J. Atmos. Sol.-Terr. Phys.*, **59**, 2317 (1997).

38. L. M. Erukhimov, S. A. Metelev, N. A. Mityakov, and V. L. Frolov, *Radiophys. Quantum Electron.*, **25**, 348 (1982).
39. E. D. Tereshchenko, B. Z. Khudukon, A. V. Gurevich, et al., *Phys. Lett. A*, **325**, 381 (2004).
40. M. M. Shvarts and S. M. Grach, *J. Atmos. Sol.-Terr. Phys.*, **59**, 2421 (1997).
41. V. V. Vas'kov and A. V. Gurevich, *Geomagn. Aéron.*, **23**, 544 (1983).
42. E. Mjølhus, *J. Geophys. Res.*, **103**, 14711 (1998).
43. A. V. Gurevich, H. Carlson, A. V. Lukyanov, et al., *Phys. Rev. Lett.*, **23**, 97 (1997).
44. Ya. N. Istomin and T. B. Leyser, *Phys. Plasmas*, **5**, 921 (1998).

Radiophysics and Quantum Electronics, Vol. 48, No. 9, 2005

FEATURES OF EXCITATION OF STIMULATED ELECTROMAGNETIC EMISSION OF THE IONOSPHERE MODIFIED BY AN OBLIQUE HIGH-POWER RADIO WAVE

V. L. Frolov, * **D. I. Nedzvetsky, and G. P. Komrakov**

UDC 533.951+537.868

We present the results of measuring the characteristics of the stimulated electromagnetic emission (SEE) of the ionosphere with variation in the zenith angle of a pump beam of high-power O-mode radio waves in the geomagnetic-meridian plane. The experiments were performed at the mid-latitude heating facility "Sura." It is established that the maximum intensity of the DM and BC components of SEE is observed for southward inclination angles $\theta \approx 8^\circ - -12^\circ$ of the antenna beam, for which the most intense generation of artificial small-scale ionospheric irregularities also takes place. Based on the results of measurements near the fourth and fifth harmonics of the electron gyrofrequency, it is found that the first component of the BUM (BUM-1) is generated only when the pump wave reaches the plasma-resonance region. This allows one to assume that, unlike the second component of the BUM (BUM-2), whose generation is determined by development of instability in the upper-hybrid resonance region, the BUM-1 generation mechanism should be related to processes of interaction between a high-power radio wave and the plasma in the plasma-resonance region.

1. INTRODUCTION

The numerous experiments performed at the auroral and middle latitudes with variation in the beam orientation of the transmitting antenna of a high-power heating facility show that artificial ionospheric turbulence (plasma heating and plasma-density variations, low- and high-frequency plasma oscillations, flows of plasma and accelerated electrons, etc.) is excited most intensely when a high-power O-mode electromagnetic wave (pump wave) is launched at angles close to the direction of the geomagnetic-field lines. In the previous years, such measurements were related, first of all, to studying specific features of excitation of artificial small-scale ionospheric irregularities of plasma density (ASIIs). Such irregularities determine the anomalous attenuation of both the pump wave and the probing waves used for sounding the perturbed region of the ionosphere [1], as well as the intensity of aspect scattering of HF and VHF radiation [2, 3]. Later, it was found that the generation of large-scale plasma-density irregularities is also more efficient at small angles between the wave vector of a high-power radio wave and the geomagnetic field [4, 5]. Under conditions of "superrefraction" of high-power radio waves in the perturbed ionospheric region near their reflection altitude where the rays bend in such a way that the region of their reflection is confined in a narrow tube of the geomagnetic-field lines, very strong heating of a plasma and considerable variation in the plasma density are possible [6]. Finally, in the last experiments at the heating facility in Tromsø(Norway) [7], which were performed with the use of different methods of diagnosing artificial ionospheric turbulence (AIT) in one measurement cycle, it was convincingly shown that the strongest artificial ionospheric perturbations,

* vf@nirfi.sci-nnov.ru

Radiophysical Research Institute, Nizhny Novgorod, Russia. Translated from Izvestiya Vysshikh Uchebnykh Zavedenii, Radiofizika, Vol. 48, No. 9, pp. 743–756, September 2005. Original article submitted November 4, 2003; accepted April 28, 2005.

0033-8443/05/4809-0661

including a rise in the electron temperature in a plasma, an increase in the intensity of small-scale plasma-density irregularities, and an enhancement of airglow from the perturbed ionospheric region, are observed when the antenna beam of the facility is aligned with the geomagnetic field. Considerable enhancement of the airglow intensity from the perturbed ionospheric region in the atomic-oxygen line with the wavelength $\lambda = 5577$ Å was also observed in the experiments at the HAARP facility (Alaska, USA) in which the antenna beam of the facility was aligned with the geomagnetic field [8].

At present, for explaining most of the above-mentioned effects, a theory of nonlinear resonant parametric instability and generation of large-scale plasma irregularities in the presence of developed ASIIs is proposed [9]. This theory allows for the nonlinear self-focusing of a high-power radio wave propagating along the geomagnetic-field lines in the local regions with developed anisotropic small-scale plasma-density fluctuations, which results in significant enhancement of the plasma heating and the AIT generation. The results of the experiments [6] are explained within the framework of the nonlinear-refraction theory [10] which takes into account the plasma-density variation in the field of a high-power radio wave.

In the present paper, we consider the results of experiments performed at the "Sura" facility (of the Radiophysical Research Institute, Nizhny Novgorod, Russia) and aimed at studying specific features of the stimulated electromagnetic emission (SEE) of the ionosphere as a function of the zenith angle at which a high-power radio wave is launched by scanning the antenna beam in the geomagnetic-meridian plane within $\pm 16^\circ$ from the vertical.

Study of the SEE features, which permits diagnostics of high- and low-frequency plasma processes in the perturbed ionospheric region without using additional technical means of sounding in the passive-radar mode, has been the objective in a large number of papers (see, e.g., [11–14] and references therein). At present, empirical characteristics of separate components of the SEE spectrum are studied well enough and theoretical models explaining their most important properties are proposed for the main SEE components, namely, the down-shifted maximum (DM), the broad continuum (BC), the narrow continuum (NC), and the broad up-shifted maximum (BUM). A discussion of these models can be found in, e.g., [13]. Recently, various methods of diagnosing high- and low-frequency AIT components have intensely been developed and have widely been used on the basis of the SEE. This required a more complete study of the SEE characteristics, in particular, study of the dependence of the SEE-intensity distribution over the perturbed ionospheric region. If a fairly narrow beam of high-power radio waves is used, then such data can most easily be obtained in experiments with variation in the radiation angle with respect to the vertical or the direction of the geomagnetic-field lines. Moreover, it follows from the obtained results that the same experiments make it possible to obtain some important additional information on the SEE generation mechanisms.

Studies of the dependence of the characterisitcs of the DM, BC, and NC components of SEE on the inclination angle of the transmitting-antenna beam in the geomagnetic-meridian plane were started at the "Sura" facility as long ago as 1986. The obtained results were published in part in [15]. In view of the recent increase in interest in the studies of interaction between high-power radio waves and ionospheric plasma for pump waves propagating at angles close to the direction of geomagnetic-field lines, new experiments for different angles at which a high-power radio wave was launched were performed in 2002–2003 at the "Sura" facility. Additional data on the gyroharmonic characterisitcs of SEE, obtained in recent years, were also taken into account in these experiments. Detailed analysis of the results of the above-mentioned measurements is exactly the subject matter of the present paper. In Sec. 2, we analyze the results of the experiments performed in 1986 when the ionosphere was modified at the frequency $f_{\mathrm{PW}} = 4785$ kHz lying outside the gyroharmonic-resonance regions. In Secs. 3 and 4, we present the measurement data for pump-wave frequencies close to the fifth (measured in 2002) and the fourth (measured in 2003) harmonics of the electron gyrofrequency $f_{\mathrm{ce}} = 1.3 - -1.35$ MHz. In these sections, we mainly consider the characteristics of the BUM component, although some results obtained in the experiments also concern the properties of the DM, NC, and UM (up-shifted maximum) components. The obtained results are summarized in Sec. 6 and concluding remarks are presented in Sec. 6.

2. RESULTS OF MEASUREMENTS PERFORMED IN 1986

The first experiments on studying the SEE features with the transmitting-antenna beam scanned in the geomagnetic-meridian plane were performed at the "Sura" facility in March–May 1986 under diurnal conditions in a quiet ionosphere. The beam scanning was performed with a step of 4° in the range between 16° to the north and 16° to the south (the dip angle of the geomagnetic field above the facility amounts to $\chi \approx 19°$). A high-power radio wave was radiated at the frequency $f_{\rm PW} = 4785$ kHz, lying about in the middle of the frequency range between the third and fourth harmonics of the electron gyrofrequency, outside the regions with strong gyroharmonic effects observed for $|f_{\rm PW} - nf_{\rm ce}| \leq 100{-}{-}200$ kHz. Here, n is the gyroharmonic number [12–14]. In these measurements, the synchronous regime of radiation from three transmitting modules of the facility was used to ensure the formation of a narrow, pencil-beam antenna pattern with beamwidth about 10°. The reduced effective radiated power with allowance for regular absorption of radio waves in the lower layers of the ionosphere amounted to about 20 MW. The pump wave was radiated for 0.5 min, and then a pause for 4.5 min followed. The SEE dynamics was measured for three detunings from the pump-wave frequency, namely, at −11 kHz (the DM region) and at −24 and −46 kHz (the BC region).

The results of the measurements performed in these experiments are presented in Fig. 1. Here, the solid faint lines show the dependences of the SEE intensity on the inclination angle of the antenna beam for the stage of the maximum SEE level observed within 1−−3 s after the pump-on, and the dotted lines, for the stationary stage which takes place after the overshoot effect develops (i.e., when a decrease in the SEE intensity occurs after the stationary level of SEE is reached) [11]. All the dependences are normalized to the maximum SEE intensity observed in this measurement cycle at $\Delta f = -11$ kHz for the southward zenith inclination angle $\theta = 4°$ of the antenna beam. The bold line in Fig. 1 shows the normalized dependence, taken from [2], of the stationary intensity of a signal of aspect scattering from irregularities with the typical transverse scale $l_\perp \approx 3$ m. This line displays the features of the dependence of the ASII intensity on the antenna-beam orientation. Note that the presented results of measurements of SEE and aspect-scattering signals were obtained under similar ionospheric conditions, but in different observation times. The differences concern the duration of the pump-wave radiation. Namely, in the experiments on studying the characteristics of scattering from ASIIs, the heating-pulse duration amounted to 2 min with the same 5-min repetition period.

Consider at first the dependences of the intensities of the DM and BC components of SEE at the stage of their maximum development (solid faint lines in Fig. 1). The three detunings feature the presence of the SEE-intensity maximum, which occurs in the case of southward deflection of the beam by an angle of 4° for the DM component ($\Delta f = -11$ kHz) and by an angle of 8° for the BC component ($\Delta f = -24$ and −46 kHz). The SEE intensity decreases fairly gradually as the beam approaches the zenith and then for $\theta < 0$ (northward deflection of the beam) and decreases more abruptly for a larger southward deflection of the beam ($\theta > 0$). The difference between SEE intensities for the southward inclinations, at which the most intense SEE is observed, and the northward inclinations corresponding to them is 4−−6 dB and, on the whole, conforms to the angular dependence of the ASII intensity presented in Fig. 1.

The angular dependence is somewhat different in the case of stationary SEE intensity which is reached at the end of the pump-wave radiation pulse (dotted lines in Fig. 1). An almost constant SEE intensity is observed for the three detunings over the entire region of northward inclinations of the antenna beam up to the zenith for the DM component or even up to $\theta = 4°$ for the BC component. For $\theta \approx 8°{-}{-}12°$, a pronounced maximum of the SEE intensity with a contrast of 5−−8 dB (with the higher contrast for the larger negative detunings) is observed for the three detunings. Since the stationary levels of intensity of the DM and BC components for such pump-wave powers undergo saturation and, therefore, depend only weakly on the pump-wave power and the ionospheric parameters [11], such a notable maximum of the SEE intensity at the stationary stage of AIT development can be indicative of a fairly strong variation in the SEE generation conditions and, therefore, in the properties of the excited ionospheric turbulence. Similar results concerning the relationship between SEE intensities in the sectors of northward and southward inclinations

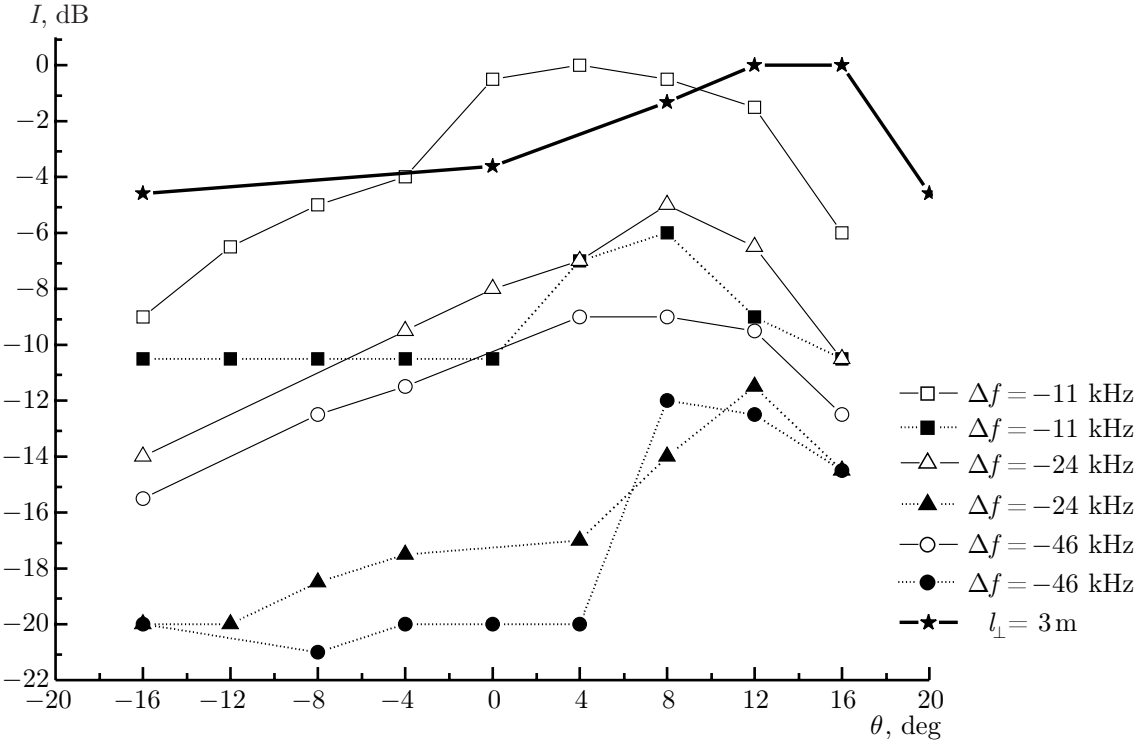

Fig. 1.

(for $\theta = \pm 8°$) were obtained later in the experiment described in [16]. We should also mention the recently initiated measurements based at the HAARP facility (Alaska, USA) [17], which show the maximum intensity of the DM and BC components for the pump wave launched along the geomagnetic-field lines ($\chi \approx 15°$).

It should be emphasized that correlation between the generation of the thermal SEE components (DM and BC) and the development of ASII was mentioned in a number of earlier papers (see, e.g., [11, 13, 18]). The obtained fairly good coincidence between the angular dependences of the intensities of the DM and BC components and the corresponding angular dependence of the ASII intensity can be considered another important proof that the generation mechanisms of the above-mentioned SEE components can be closely related to generation of small-scale irregularities.

The presented results lead to the conclusion that when using broad vertical beams (with a width of about 20°) of high-power radio waves, at least for the DM and BC components, the southern boundary of the perturbed region gives a notably larger contribution to the total SEE intensity recorded in the measurements, both at the maximum and stationary phases. This must be taken into account when interpreting the measurement results in which the SEE is used as the basis for the methods of diagnosing artificial ionospheric turbulence.

3. RESULTS OF MEASUREMENTS PERFORMED IN 2002

Based on the known experimental and theoretical results, a new cycle of studies of the dependence of the AIT characteristics on the zenith angle of radiation of a high-power radio wave was performed in August 2002 at the "Sura" facility. The measurements were carried out using the antenna-beam scanning in the geomagnetic-meridian plane with a 2° step in the angular range $\theta = 6°{-}{-}14°$, for which, as was shown in Sec. 2, the most intense generation of SEE and ASII is observed. A distinctive feature of these experiments is that they were performed at a pump-wave frequency close to the fifth harmonic of the electron gyrofrequency ($f_{\rm PW} \approx 5 f_{\rm ce} \approx 6.6{-}{-}6.7$ MHz). In this case, strong variations in the characteristics of the excited turbulence are observed, even for small variations in the frequency $f_{\rm PW}$, which leads to drastic changes in the SEE features. For example, this is manifested as disappearance of the DM component for

$f_{PW} \approx 5f_{ce}$, enhancement of the DM and BC components for a pump-wave frequency slightly lower (by 30−−40 kHz) than $5f_{ce}$, generation of the BUM component in the pump-wave frequency region $f_{PW} - 5f_{ce} \approx (-10)--200$ kHz, etc. [12–14]. It is important to note that, according to [14], the BUM component is a composition of two components. For $|f_{PW} - nf_{ce}| \leq 20$ kHz, the first component (BUM-1) prevails. A distinctive feature of this component is that it is observed under conditions of quenching of generation of the thermal (resonant) parameteric instability and has weak dependence of the frequency of the spectral-intensity maximum on f_{PW}. In [19], the BUM-1 corresponds to the "fast" component of the BUM. Generation of the BUM-2 component is observed for $f_{PW} - nf_{ce} > 0$ and is related to development of turbulence in the upper-hybrid resonance region, while the frequency of the spectral-intensity maximum of the BUM-2 linearly increases with increasing f_{PW}.

In the considered cycle of studies, the measurements were performed with the use of only two modules of the facility. The effective radiated power amounted to about 100 MW for a beamwidth of about $7^\circ \times 11^\circ$ (the beam is wider in the geomagnetic-meridian plane). The experiments were carried out in the evening time under unperturbed conditions when the linear absorption of the pump wave in the lower layers of the ionosphere on the upward-propagation path did not exceed several decibels, so that the effective radiated power with allowance for such an absorption amounted to 50−−80 MW.

The measurement layout was as follows. The pump wave was radiated by pulses with a duration of 20−−60 s and a repetition period of 5 min. The pulse duration was chosen such that the SEE stationary level be settled. The SEE spectral intensity was recorded using an HP-3585A spectrum analyzer with an accuracy of 1−−2 dB in one measurement session. Variations in the SEE intensity in different days, even under similar ionospheric conditions, can reach 3−−5 dB owing to somewhat different values of the linear absorption, critical frequencies, and plasma-density profiles in the ionospheric F region near the reflection point of the pump wave. The pulse duration 4−−4.5 min was sufficient for relaxation of the created artificial perturbations. Hence, each new switch-on of the pump wave was accompished in a regime close to "cold start." For each inclination angle of the antenna beam, the gyroharmonic frequency was first determined from the frequency of disappearance of the DM component in the SEE spectrum [12–14]. Checking of the gyroharmonic frequency was occasionally repeated to make it possible to follow variations in the reflection altitude of the pump wave and allow for these variations and the related variations in the SEE characteristics when processing experimental data. The pump-frequency range from $f_{PW} \approx 5f_{ce}$ to $f_{PW} \approx 5f_{ce} + 100$ kHz was passed with a 10- to 20-kHz step (with a smaller step near the frequency $5f_{ce}$), using one or two heating cycles at each frequency, until the BUM component was reliably distinguished in the SEE spectrum. This permitted us to determine the variation in the SEE characteristics almost in the entire region of the BUM-component generation. The duration of a measurement cycle for each inclination angle θ amounted to about 1.5−−2 h. After a cycle was over, the inclination angle was changed, and the measurements were repeated, which, most often, was done already in the next day, but under about the same ionospheric conditions. The latter were monitored during the experiments by an automated ionospheric station "Bazis" operated in a 5- or 15-min regime of obtaining ionograms. Because of a fairly long measurement cycle and the limited financial resources for "Sura"-based experiments, we managed only one passage over the assumed range of beam inclination angles of a high-power radio wave in each heating campaign. However, the obvious drawbacks of one-time measurements, as is clear from what follows, are to a remarkable degree compensated by the fact that our analysis of experimental data is based on comparison of the obtained angular dependences of intensities for the DM and both BUM components rather than of the absolute intensities of the received radiation.

Figure 2 shows examples of the results of measuring the peak values of spectral intensities of the DM and BUM components expressed in decibels relative to 1 mW (dBm) for the beam inclination angles $\theta = 6^\circ$ (Fig. 2*a*) and $\theta = 10^\circ$ (Fig. 2*b*). Here, by the effect of DM-component quenching, one clearly sees the gyroharmonic-resonance regions for $5f_{ce} = 6670$ kHz (Fig. 2*a*, the pump-wave reflection altitude $h \approx 216$ km) and $5f_{ce} \approx 6610$ kHz (Fig. 2*b*, the pump-wave reflection altitude $h \approx 237$ km). These dependences show the presence of a much more powerful BUM component for small differences between the pump-wave frequency

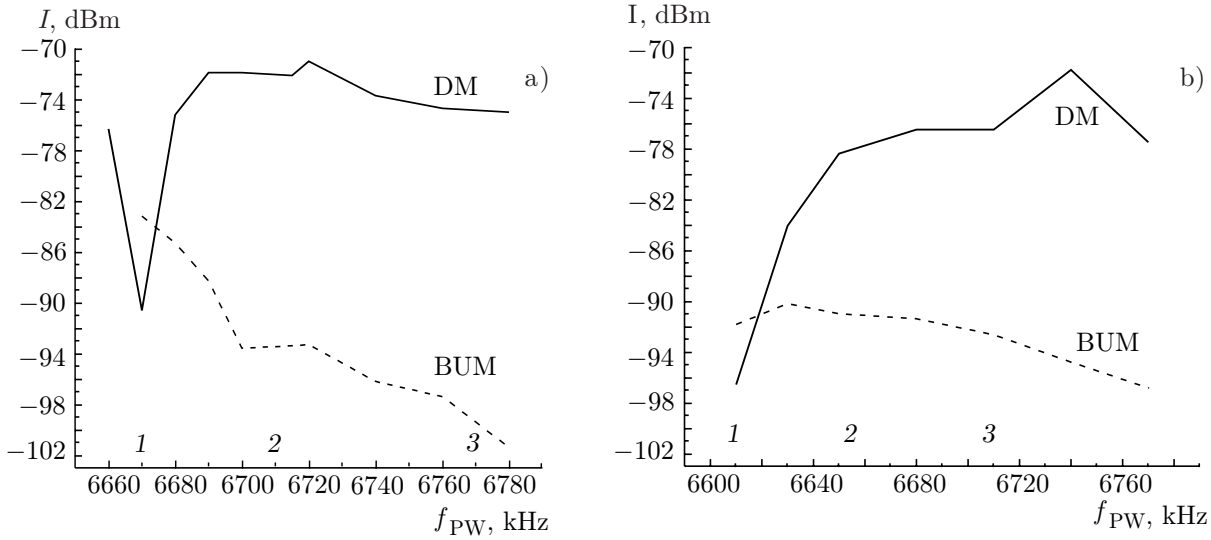

Fig. 2.

and the gyroresonance frequency $f_{PW} - 5f_{ce} \approx 0 - -20$ kHz). compared with the larger frequency differences for the inclination angle $\theta = 6°$, and the absence of such a drastic variation in the dependences for $\theta = 10°$.

Detailed analysis of experimental data obtained for different inclination angles of the antenna beam was performed for the peak values of the spectral density of the DM and BUM intensities in three ranges of the pump-wave frequency with respect to $5f_{ce}$.

1. If the pump-wave frequency coincides with the fifth gyroresonance harmonic, then quenching of the DM generation is observed in the SEE spectrum, and the BUM component for radiation angles θ close to the zenith corresponds to the BUM-1 component, whose generation in stationary SEE spectra is detected only in a narrow frequency region near the gyroharmonic resonance [14].

2. If the pump-wave frequency is higher than $5f_{ce}$ by approximately 40 kHz, then the already recovered DM component and the intense BUM component corresponding to the BUM-2 component, whose generation takes place only for $f_{PW} > nf_{ce}$ [14], are observed in the SEE spectrum.

3. If the pump-wave frequency is higher than $5f_{ce}$ by approximately 100 kHz, then the DM component predominates in the SEE spectrum, but the weak BUM-2 component is also observed.

Regions *1, 2* and *3* are marked in the frequency axis in Fig. 2. Figure 3 shows the dependences of the peak values of the spectral densities of the DM, BUM-1, and BUM-2 intensities as functions of the zenith inclination angle of the antenna beam.

Analysis of the obtained data permitted us to state that the dependences of the BUM intensity on the angle θ for regions *2* and *3* almost coincide. This indicates that the same BUM component, namely, BUM-2, is recorded here. Hence, the dependence of the BUM-2 intensity on the angle θ only for region *2* is presented in Fig. 3. It is seen in this figure that as θ increases from 6° to 12°, the intensity of the BUM-2 component decreases with increase in the inclination angle only weakly on the average (by about 2−−3 dB, which, generally speaking, is within the measurement error). Note that the intensity of the DM component in region *2* also decreases by a close value. The angular dependence of the BUM-1 intensity determined from measurements for $f_{PW} \approx 5f_{ce}$ shows completely different behavior compared with the BUM-2. Namely, the maximum intensity of the BUM-1 component is observed for $\theta \leq 8°$, while it sharply decreases by approximately 16 dB as the angle θ increases from 8° to 12°. Such a strong difference in the behavior of the BUM-1 and BUM-2 intensities, which occurs with the variation in the inclination angle of the antenna beam, is clear evidence that different components of SEE are observed in this case. This can be regarded as a new confirmation of the two-component structure of the BUM, which was established earlier in [14, 19]. It should be mentioned that in this measurement cycle, the gyroharmonic frequencies for inclination angles 8° and 10°, for which exactly an abrupt change in the BUM-1 intensity is observed,

amounted to 6630 and 6610 kHz, respectively. Therefore, measurements for these inclination angles of the beam were conducted at almost the same altitudes. This excludes correlation between the observed sharp decrease in the BUM-1 intensity and the variation in the generation altitude of this component.

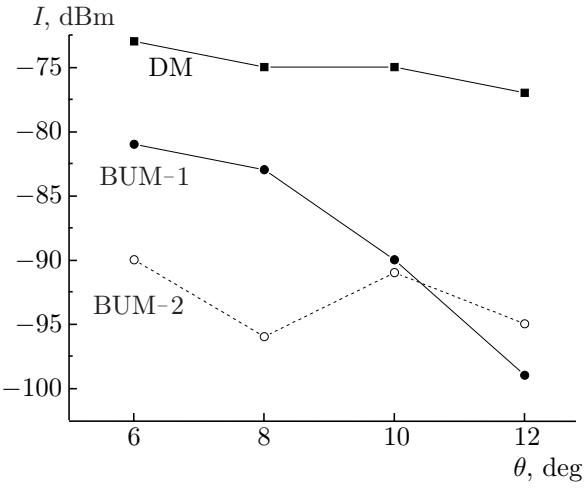

Fig. 3.

Using model calculations with allowance for the threshold generation power $P_{\rm thr} \approx 5$ MW [19] of the BUM component and the beamwidth of the transmitting antenna (which is approximately 11°), it can easily be shown that the angle $\theta \approx 10°$, which determines the boundary of the BUM-1 generation region, is in good agreement with the critical angle $\theta_{\rm cr} = \arcsin[f_{\rm ce}^{1/2}\,(f_{\rm ce}+f_{\rm PW})^{-1/2}\sin\chi] \approx 6°$ for the conditions of our experiments ($\chi \approx 19°$ is the dip angle of the geomagnetic field above the "Sura" facility). In this case, according to [20], the O-mode waves are reflected at the same altitude in the plasma resonance region only for $\theta \le \theta_{\rm cr}$. Then, based on the obtained results, it is expedient to assume that generation of the BUM-1 component must be related somehow to processes developing near the pump-wave reflection altitude. It should be mentioned that no mechanism of BUM-1 generation has been proposed up to now in the literature. It is believed that the BUM-2 component is generated in the upper-hybrid resonance region, which is usually located several kilometers lower than the pump-wave reflection altitude. In this case, excitation of the BUM-2 component is related to generation of the upper-hybrid and Bernstein plasma modes. A discussion of theoretical models proposed by now for describing generation of this SEE component can be found in, e.g., [13, 14, 19].

4. RESULTS OF MEASUREMENTS PERFORMED IN 2003

To confirm the conclusion that the BUM-1 and BUM-2 components have different dependences on the zenith angle at which the pump wave is launched and that the generation of the BUM-1 is determined by the condition under which the plasma-resonance region is reached, one more cycle of measurements of SEE characterisitcs was performed at the "Sura" facility from August 11 to 16, 2003. In this cycle, the inclination angle of the transmitting-antenna beam in the geomagnetic-meridian plane was varied in the interval $-12° < \theta < 12°$. The state of the ionosphere in that period featured low indices of magnetic activity. The program of measurement cycles and the algorithm of data processing were the same as in 2002, with the only difference that, by virtue of the lower critical frequencies, the measurements were performed near the fourth harmonic of the electron gyrofrequency. Also, to reduce the measurement time, the stepping with respect to angle θ was not 2° (as in the measurement cycle of 2002), but 4°. For inclination angles $\theta = -12°$, $-8°$, 0, 4°, 8°, and 12°, the gyroharmonic frequency in this measurement cycle amounted to 5320, 5400, 5360, 5380, 5370, and 5380 kHz, respectively. Thus, for any inclination angle, except for $\theta = -12°$, the measurements were performed at close altitudes of pump-wave reflection $h \approx 190{-}{-}210$ km. It was found during data processing that the experiments for $\theta = -4°$ were unsuccessful because of the strong variations in the ionospheric conditions at the time of this measurement cycle, and these results are omitted. For this range of pump-wave frequencies, when two modules of the facility were used for heating the ionosphere, the antenna beamwidth was approximately $8° \times 13°$ (the larger size is in the geomagnetic-meridian plane).

Figure 4 shows the results of measuring the stationary values of the peak intensity of the BUM-1 component for the frequency region $f_{\rm PW} \approx 4f_{\rm ce}$ as well as of the peak intensities of the DM and BUM-2 components for $f_{\rm PW} \approx 4f_{\rm ce} + 40$ kHz as functions of the zenith angle at which a high-power radio wave was launched. Here, as for the measurements presented in Fig. 1, the intensity maximum of the DM component is observed for inclination angles $\theta = 8°$ with an insignificant decrease in the intensity in the case of

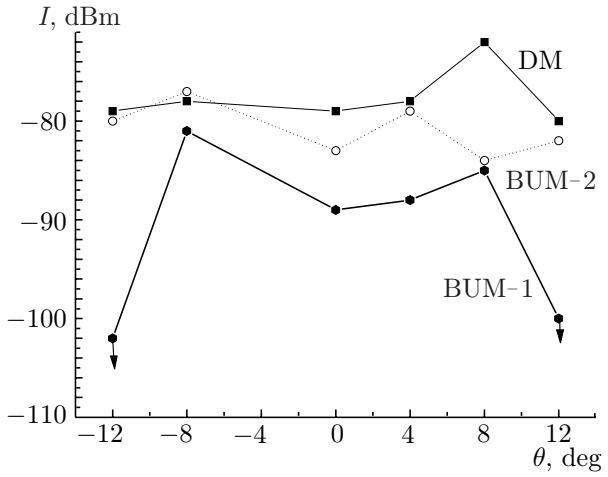

Fig. 4.

northward deflection of the antenna beam (solid faint line), while the intensity of the BUM-2 component is approximately constant over the entire range of angles θ (dotted line). Conversely, the intensity of the BUM-1 component (solid bold line), as in the measurement cycle of 2002, has strong angular dependence. This SEE component was recorded only in the angular interval $-8^\circ < \theta < 8^\circ$, and its intensity outside this interval was lower than the detection threshold $-(102--105)$ dBm, i.e., this component was attenuated by more than 17−−20 dB in the transition from zenith angles $\theta = \pm 8^\circ$ to angles $\theta = \pm 12^\circ$. In this case, the obtained dependence is fairly symmetric with respect to the angle $\theta = 0^\circ$ (with respect to the vertical radiation of the pump wave), despite the fairly large (20−−35 km) difference of the pump-wave reflection altitude for $\theta = -12^\circ$ compared with other inclination angles of the antenna beam. This shows once again that for the studied range of altitudes of pump-wave reflecion (190−−225 km), the altitude dependence of the characteristics of the BUM-1 component is not the reason for an abrupt change in its intensity with the variation in the inclination angle at which a high-power radio wave is launched. Thus, the measurement cycle of 2003 confirms the conclusion, drawn in the previous section, that the BUM-1 component is generated only in the case where the pump wave reaches the plasma-resonance region.

Comparison of the experimental data obtained in 2002 and 2003 leads to the following conclusion. Although, judging from measurements near the fifth (in 2002) and fourth (in 2003) gyroharmonics, the behavior of the angular dependences of the BUM-1 and BUM-2 intensities for the southward inclinations almost coincides, the intensity ratio of the components is considerably different. From the data presented in Figs. 3 and 4, it can easily be concluded that in the transition from the fourth to the fifth gyroharmonic, the maximum spectral intensity of the BUM-1 component increases by 4−−7 dB, while that of the BUM-2 component decreases by 10−−13 dB. In this case, the BUM-2 component turns out to be more intense compared with the BUM-1 for $f_{\rm PW} \approx 4f_{\rm ce}$. For $f_{\rm PW} \approx 5f_{\rm ce}$, the ratio of the component intensities reverses. This result can be considered an additional confirmation of the two-component structure of the BUM, as well as an indication of the existence of certain dependence of the characteristics of the BUM components on the gyroharmonic number, which was also mentioned in [12, 19].

Among other results of measurements for different inclination angles of the antenna beam, obtained in this measurement cycle, we note that the angular dependences for the DM, NC, and UM components have similar behavior. From this, in particular, we can infer that the processes underlying generation of all these SEE components should be of the same or similar nature. As concerns these SEE components, we here restrict ourselves to only this brief comment since a detailed analysis of the obtained results is outside the scope of the present paper and will be made in a separate publication.

5. DISCUSSION OF MEASUREMENT RESULTS

Studies of the SEE characteristics, which were performed at the mid-latitude "Sura" facility for different zenith angles of a pump beam of high-power O-mode radio waves in the geomagnetic-meridian plane with heating duration about 1 min, showed that the maximum intensity of the DM and BC components, whose generation is associated with the development of themal (resonant) parametric instability, takes place for southward inclination angles $\theta \approx 8^\circ--12^\circ$. In this case, a gradual decrease in the intensity of these components is observed when passing from the zenith to the northward inclinations, and a more abrupt decrease takes place in the transition to the greater southward inclinations. The angular dependence

obtained for the DM and BC intensities is similar to that for the ASII intensity. This is indicative of the fact that generation of these SEE components is closely related to generation of small-scale irregularities in the perturbed region of the ionosphere. Since the observed SEE signal is determined by the total SEE intensity of the perturbed region, for fairly large (greater than $15^\circ - -20^\circ$) beamwidths of the transmitting and receiving antennas with vertically oriented beams, which is often used in the heating experiments, the southern boundary of the perturbed region gives the main contribution to the total signal intensity. This must be taken into account when interpretating experimental data in the case where the SEE is used for diagnostics of artificial ionospheric turbulence.

Similar to ASIIs [3], the obtained angular dependence of the DM and BC intensities can be explained by the properties of propagation of the ordinary wave in a magnetoplasma [20] and by the enhancement of the AIT generation when the propagation direction of the pump wave in the region of its interaction with the plasma coincides with the direction of the geomagnetic-field lines [9]. According to calculations for the unmodified ionosphere in the case of the mid-latitude "Sura" facility, the zenith angles $\theta \approx 10^\circ$ are optimal for $f_{\rm PW} \approx 5$ MHz, provided the wave vector of a high-power radio wave in the upper-hybrid resonance region is parallel to the geomagnetic-field lines. These angles slightly decrease with increasing pump-wave frequency. For $\theta \geq 20^\circ - -30^\circ$, a high-power O-mode radio wave is reflected below the upper-hybrid resonance region, and, therefore, instability and generation of ASIIs and SEE are quenched (see also [3]). This stipulates an abrupt decrease in the SEE intensity for large southward inclinations with zenith angles $\theta \geq 16^\circ$. For the Tromsø(Norway) and HAARP (Alaska, USA) facilities located at the northern higher latitudes and having smaller dip angles χ of the geomagnetic field, excitation of thermal (resonant) parametric instability is possible if the pump wave is launched along the geomagnetic-field lines where exactly strong artificial ionospheric turbulence develops [7, 8, 21]. In conclusion, we note that according to [22], even in the case of vertical radiation of the pump wave and antenna beamwidths $20^\circ - -30^\circ$ the center of the region of the most intense aspect scattering (and, therefore, the region of most intense ASIIs) is gradually shifted, within several minutes after the switch-on of high-power radio emission, from the geographical zenith to the south, namely, to the direction determined by the geomagnetic-field dip angle, and even goes slightly beyond the limits of the transmitting-antenna beam. The last fact can evidence that the spatial structure of the perturbed ionospheric region varies with time (and, therefore, is a function of the duration of pumping of the ionospheric plasma) due to the increasingly intense development of plasma-density irregularities, provided that a pump wave is launched at angles close to the geomagnetic-field dip angles because of, e.g., the nonlinear structuring of the ionospheric-plasma density [21]. This, in particular, can be used to explain the difference between the angles for which the maximum intensity of ASIIs and SEE is observed for different durations of pumping (see Fig. 1), as well as the appearance of regions with low plasma density at angles close to the direction of the geomagnetic-field lines, far beyond the pump beam of a high-power radio wave [23].

The performed studies gave a new important confirmation of the two-component structure of the BUM, which was detected earlier in [14], and demonstrated that the intensity of the BUM-1 and BUM-2 components have essentially different angular dependences. It was found that the intensity of the BUM-2 component does not have pronounced angular dependence over the entire region $-12^\circ \leq \theta \leq 12^\circ$, while the BUM-1 component is only observed for radiation angles of a high-power radio wave equal to $-(8^\circ - -10^\circ) \leq \theta^* \leq (8^\circ - -10^\circ)$. The model calculations showed that with allowance for the threshold generation power of the BUM component [19] and the beam half-width of the transmitting antenna, which amounts to $5^\circ - -6^\circ$ in our measurements, this value of θ^* well agrees with the critical angle $\theta_{\rm cr} \approx 6^\circ$ determining the condition under which the pump wave reaches the plasma-resonance region [20]. Then it follows from the obtained experimental data that the BUM-1 component is generated only in the case where a high-power radio wave reaches the plasma-resonance region. Taking this into account, it is reasonable to assume that the generation mechanism of the BUM-1 component must be related to interaction between a high-power radio wave and the ionospheric plasma in the plasma-resonance region, as well. It is important that this conclusion is mainly based on comparison of the behavior of the obtained angular dependences for both BUM components, rather

than on measurement of their absolute values. In this case, although the measurements were performed in different days under similar, but not identical ionospheric conditions for each inclination angle of the beam of a high-power pump wave, the conclusion on fundamental difference between the angular dependences of the BUM-1 and BUM-2 intensities raises no doubt.

It is important to note that the above conclusion on correlation between the BUM-1 generation mechanisms and the plasma processes developing near the pump-wave reflection altitude in the plasma-resonance region is fully confirmed by a number of its features studied before. For example, according to the results given in [14], the BUM-1 component is generated if pump-wave frequencies almost coincide with the gyroharmonic frequency when the thermal (resonant) parametric instability and the ASII generation are quenched. This leads to isolation of the upper-hybrid resonance region from the intense interaction between a high-power O-mode wave and the plasma. In this case, blanketing of the upper ionospheric layers, which is related to the AIT development at the upper-hybrid resonance altitude and almost total absorption of the pump-wave energy, disapperas, which results in enhancement of the plasma modification at the plasma-resonance altitude. This also conforms to the results given in [19], where it is shown that the BUM-1 component (or, following the classification adopted in [19], the fast component of the BUM) has shorter onset times than the BUM-2 (slow component of the BUM) and, moreover, is attenuated as the BUM-2 intensity rises. On the whole, these experimental data make it possible to conclude that generation of the BUM-1 component is determined by processes which are faster than the BUM-2 generation and can evidently be referred to the plasma-resonance region.

As a plausible mechanism of the BUM-1 generation, we should mention the model proposed in [24], which is based on the cyclotron instability of accelerated electrons. Within the framework of this model, plasma waves with frequencies higher than the pump-wave frequency are excited when a beam of accelerated electrons passes through the double-resonance region in which the gyroharmonic frequency coincides with the upper-hybrid frequency. It should be assumed that, unlike [24], where acceleration of electrons in the upper-hybrid resonance region is considered, the electrons are accelerated in the plasma-resonance region. Such a scheme of BUM-1 generation can be checked by experiments on a study of the characteristics of the BUM component during its excitation at low altitudes (less than 200 km) of pump-wave reflection, at which the high collision rate significantly attenuates the electron-acceleration efficiency and the electron-flow intensity in the upper-hybrid resonance region.

Among other results concerning the characterisitcs of the BUM component, we mention the regular features of variation in the BUM-1 and BUM-2 intensities in the transition from the fourth to the fifth gyroharmonic, which were ascertained by measurements with varied zenith angle at which a high-power radio wave was launched. In particular, it was found that the BUM-1 component turns out to be more intense compared with the BUM-2 component for $f_{\mathrm{PW}} \approx 5f_{\mathrm{ce}}$, while the BUM-2 component is more intense for $f_{\mathrm{PW}} \approx 4f_{\mathrm{ce}}$. Certain differences between the SEE features near these gyroharmonics were mentioned earlier in [12, 19]. In our case, it can be assumed that an increase in the pump-wave frequency leads to an increase in the threshold generation power of ponderomotive parametric instability [25]. The latter determines the AIT development in the plasma-resonance region, which, in turn, can result in impairment of the BUM-1 generation conditions. For obtaining more detailed dependences on the pump-wave frequency, in the further analysis it seems interesting to conduct similar measurements of the BUM-1 and BUM-2 intensities near the higher-order harmonics of the electron gyrofrequency.

6. CONCLUSIONS AND FINAL REMARKS

Based on the performed measurements of SEE characteristics for different inclination angles of a beam of high-power radio waves in the geomagnetic-meridian plane, the following is established.

1. The maximum intensity of such thermal components of SEE as the DM and the BC in the case of plasma heating well away from the gyroharmonic-resonance regions takes place for inclination angles $8^\circ - -12^\circ$ to the south of the vertical where the most intense ASII generation also takes place.

2. The BUM-1 generation takes place only under conditions where a high-power radio wave reaches

the plasma-resonance region. This enables us to assume that, unlike the BUM-2 component, whose generation is determined by development of instabilities in the upper-hybrid resonance region, the BUM-1 generation mechanism is related to processes of interaction between a high-power radio wave and the plasma in the plasma-resonance region.

In Secs. 3 and 4, we mainly considered the features of the BUM component. When the discussed experiments were conducted at pump-wave frequencies lying near the gyroharmonics, measurements of the DM characteristics were mainly auxiliary (e.g., for determination of the gyroharmonic frequency) or were used as reference measurements with which variations in the characteristics of other SEE components were compared. However, the studies for different inclination angles of a beam of high-power radio waves also yielded important information on the characteristics of the DM, BC, NC, and UM components. The obtained new experimental data make it possible to refine the empirical models of generation of these SEE components as well as the degree of their interaction during the formation of the SEE spectrum. Detailed analysis of these data is outside the scope of the present paper and will be made in a separate publication [26].

The authors are thankful to the staff of the "Sura" facility, as well as to G. N. Boiko and E. N. Sergeev for help with the measurements and S. M. Grach for discussing the results of the studies and valuable comments on the text of the paper. This work was supported in part by the Russian Foundation for Basic Research (project Nos. 02–02–17475 and 05–02–16493), the program "Universities of Russia" of the Ministry of Education and Science of the Russian Federation (project No. UR.01.01.025), the Civilian Research and Development Foundation (project No. RPO–1334), and the INTAS (project No. 03–51–5583).

REFERENCES

1. T. M. Allen, J. D. Thom, and P. B. Rao, *Radio Sci.*, **9**, No. 11, 905 (1974).
2. V. A. Zyuzin, G. P. Komrakov, A. M. Nasyrov, and V. A. Strekalov, *Izv. Vyssh. Uchebn. Zaved., Radiofiz.*, **31**, 622 (1988).
3. N. I. Bud'ko, V. V. Vas'kov, G. P. Komrakov, et al., *Geomagn. Aéron.*, **29**, 973 (1989).
4. J. H. Pope and R. B. Fritz, *J. Geophys. Res.*, **79**, 1065 (1974).
5. E. N. Myasnikov, V. L. Frolov, N. V. Muravieva, et al., in: *VIth Int. Suzdal URSI Symp. "Effects of Artificial Action on the Earth Ionosphere by Powerful Radio Waves,"* Moscow, October 19–21, 2004, p. 21.
6. L. M. Duncan, J. P. Sheerin, and R. A. Behnke, *Phys. Rev. Lett.*, **61**, 239 (1988).
7. M. T. Rietveld, M. J. Kosch, N. F. Blagoveshchenskaya, et al., *J. Geophys. Res.*, **108**, No. A4, 1141 (2003).
8. T. R. Pedersen, M. McCarrick, E. Gerken, et al., *Geophys Res. Lett.*, **30**, No. 4, 1169 (2003), doi:10.1029/2002GL016096.
9. A. V. Gurevich, K. P. Zybin, H. Carlson, et al., *Phys. Lett. A*, **305**, 264 (2002).
10. J. D. Hansen, G. J. Morales, L. M. Duncan, et al., *Phys. Rev. Lett.*, **65**, No. 26, 3285 (1990).
11. G. N. Boiko, L. M. Erukhimov, V. A. Zyuzin, et al., *Radiophys. Quantum Electron.*, **28**, No. 4, 259 (1985).
12. V. L. Frolov, E. N. Sergeev, E. N. Ermakova, et al., *Geophys. Res. Lett.*, **28**, No. 16, 3103 (2001).
13. T. B. Leyser, *Space Sci. Rev.*, **98**, Nos. 3–4, 223 (2001).
14. V. L. Frolov, L. M. Erukhimov, L. M. Kagan, et al., *Phys. Rev. Lett.*, **81**, No. 8, 1630 (1998).
15. E. N. Sergeev and V. L. Frolov, "The structure of the stimulated electromagnetic emission of the ionospheric plasma at frequencies below the pump-wave frequency," Preprint No. 324 [in Russian], Radiophys. Res. Inst., Nizhny Novgorod (1991).

16. G. P. Komrakov, I. V. Berezin, S. M. Grach, et al., in: *Proc. IIIrd Suzdal URSI Symp. on Modification of the Ionosphere by Powerful Radio Waves, Moscow, September 9–13, 1991*, p. 152.
17. J. Pau, A. Wong, E. Gerken, et al., in: *"RF Ionospheric Interactions Workshop," Santa Fe, New Mexico, USA, 2002*, p. 574.
18. E. N. Sergeev, S. M. Grach, G. P. Komrakov, et al., *Radiophys. Quantum Electron.*, **42**, No. 7, 619 (1999).
19. V. L. Frolov, S. N. Grach, L. M. Erukhimov, et al., *Radiophys. Quantum Electron.*, **39**, 241 (1996).
20. V. L. Ginzburg, *The Propagation of Electromagnetic Waves in Plasmas*, Pergamon Press, Oxford (1970).
21. A. V. Gurevich, H. Carlson, M. Kelley, et al.. *Phys. Lett. A*, **251**, 311 (1999).
22. A. F. Belenov, V. A. Bubnov, L. M. Erukhimov, et al., *Radiophys. Quantum Electron.*, **20**, No. 12, 1240 (1977).
23. E. D. Tereshchenko, B. Z. Khudukon, A. V. Gurevich, et al., *Phys. Lett. A*, **325**, 381 (2004).
24. S. M. Grach, *Radiophys. Quantum Electron.*, **42**, No. 7, 571 (1999).
25. L. M. Erukhimov, V. A. Kovalev, E. P. Kurakin, et al., *Geomagn. Aéron.*, **27**, 758 (1987).
26. V. L. Frolov, D. I. Nedzvetsky, E. N. Sergeev, et al., *Radiophys. Quantum Electron.*, **48**, No. 12 (2005), in press.

Optical and RF diagnostics of the ionosphere over the Sura facility. Review of Results.

L.M. Kagan
University of Western Ontario, London, ON, Canada

M.J. Nicolls, M.C. Kelley
Cornell University, Ithaca NY, U.S.A.

V.L. Frolov, V.V. Belikovich, N.V. Bakhmet'eva, G.P. Komrakov, D.I. Nedzvetski, V.P. Uryadov,
Radiophysical Research Institute, Nizhniy Novgorod, Russia

Yu. M. Yampolski, A.V. Koloskov, A.V. Zalizovski, V.L. Galushko, S.B. Kasheev
Institute of Radio Astronomy, NAS Ukraine

N.F. Blagoveshenskaya, V.A. Kornienko, T.D. Borisova,
Arctic and Antarctic Research Institute, St. Petersburg, Russia

A.V. Gurevich
Lebedev's Institute of Physics, Moscow, Russia

G.G. Vertogradov, V.G. Vertogradov
Rostov-on-Don State University, Rostov-on-Don, Russia

T.S. Trondsen, and E. Donovan
University of Calgary, Calgary, AB, Canada

Abstract. We give an overview of the design and results of the optical-backscatter-heating campaign which we conducted at the Sura facility near Nizhniy Novgorod, Russia on August 10-20, 2004. This campaign was the first to combine optical observations with simultaneous plasma diagnostics by the method of artificial periodic irregularities and with multi-position backscatter measurements and is an example of the clustering of instruments for the purpose of enhancing research results. Some of the results of the campaign have been published in a special issue of Radiophysics and Quantum Electronics and in Physical Review Letters and will only be summarized here. New results include offset of the optical emissions by 1-2 degrees from magnetic zenith; broadening of the backscatter spectrum for heating at the fourth harmonic of the electron gyro frequency; observation of self-scattered signals at the second harmonic of the heater frequency; first observations of vector plasma drift/electric field measurements using field-aligned irregularities as tracers; verifying the refractive index mechanism for the Doppler shift of self-scattered signals and first observations of synchronized variations in self-scattered and backscattered signals. The electric field observations confirm that the ionosphere over a mid-latitude site such as SURA can be affected by high latitude processes.

1. Introduction.

The optical-backscatter-heating campaign took place at the Sura facility (geographical coordinates 56.13°N, 46.10 °E; the magnetic dip angle is 71°, declination angle 10 degrees) on August 10-20, 2004. The goal of the campaign was to accomplish as completely as possible 3D diagnostics of natural and induced processes in the ionosphere and neutral atmosphere using multi-instrument remote sensing of the HF-illuminated volume. This campaign was the first to combine optical observations with simultaneous plasma diagnostics by the method of artificial periodic irregularities and with multi-position backscatter measurements. We complimented our diagnostics by making use of the recently discovered self-scattering effect (*Zalizovski et al.,* 2004), based on the distant receiving of fundamental and second harmonics of the transmitted signal (including an approximately 16,000-km long-distance reception along the path Sura – Antarctica) (*Yampolski et al,* 2005). We also recorded geomagnetic field variations in the immediate proximity of the transmitter site to compare dynamic effects in the heated volume with geomagnetic field data.

The first part of the experiments (August 10-15, 2004) were devoted to studying low-altitude ionospheric processes by inducing sporadic E-associated airglow (*Djuth et al,* 1999; *Kagan et al.,* 2000) with simultaneous diagnostics by the method of artificial periodic irregularities (*Kagan et al.,* 2002; *Belikovich et al,* 2002). The second part of the observations (August 16-20, 2004) were planned to study F-region processes. Multi-position backscatter observations of the heated volume were carried out throughout both parts of the campaign. The first part defined the special planning of the campaign we had made by carefully choosing the time for the experiment to have an optimal combination of maximum occurrence of sporadic ionization, maximum dark time for optical observations, and a high enough F-region critical frequency to reflect the transmitted radiowaves. Measurements of this type were expected to allow reconstruction of sporadic ionization structure and the 3D neutral wind velocity vector in the E region proposed in (*Kagan et al.,* 2000; *Kagan et al.,* 2002) and the 3D drift velocity and estimates of electric and magnetic fields in the F region (*Blagoveshchenskaya and Troshichev*, 1996; *Yampolski et al*., 1997; *Ponomarenko et al*., 2000).

The advantage of Sura over other operating powerful radiowave facilities which are all located at high latitudes (the only other midlatitude heating facility in Arecibo, Puerto Rico was destroyed by a hurricane in 1999), is that as a midlatitude facility it lacks a great number of sources of energy present at high latitudes. Sura's disadvantage is the lack of its own optical instrumentation, preventing optical observations on a routine basis and requiring special efforts.

Some of the results of the campaign have been already published (*Kagan et al.,* 2005) and some are in press in the special issue of Radiophysics and Quantum Electronics devoted to the VI URSI Suzdal Symposium in October 2004, which held a special workshop on our Sura campaign in August 2004 (*Bakhmet'eva et al.,* 2005a). In this paper we give an overview of all results from our campaign with only a brief description of previously published effects.

The paper is organized as follows. We describe all instruments and techniques in Section 2. We give short introductions to previous work in each of Sections 3-7. We start with a brief overview of the results obtained with the use of the artificial periodic irregularities (API) technique in Section 3 (more details can be found in *Bakhmet'eva et al.,* 2005a and *Kagan et al.,* 2005). In Section 4 we report the main results from the optical observations including a brief description of our discovery of the hydroxyl red artificial aurora (*Kagan et al,* 2005). In Sections 5-7 we show results from multi-position bi-static HF Doppler radio-scatter observations of the radiowave-modified ionosphere volume above the Sura facility. Section 5 discusses the spectral characteristics of signals scattered by artificial ionosphere turbulence when the pump frequency was close to the 4^{th} electron gyro harmonic. Sections 6 and 7 present multi-position bi-static HF Doppler radio-scatter observations of artificial field-aligned irregularities and recently discovered self-scattering phenomena (*Zalizovski et al.,* 2004). We give summary and conclusions in Section 9.

2. Instruments and Techniques.

The Sura facility belongs to and is operated by the Radiophysical Research Institute (NIRFI). The powerful radiowave transmitter is composed of three 250 kW transmitters; each transmitter, if necessary, can be operated independently. The transmitter frequency can be varied from 4.3 to 9.5 MHz and may be changed step by step. This capability allows complicated programs to be run, such as, for example, stepping through the electron gyro harmonics. Phasing of the transmitters permits steering of the antenna beam ±40° from the zenith in the geomagnetic north-south direction. The full antenna beam is frequency dependent and is 12°× 12° at 4.3 MHz, 10.7°×10.7° at 4.7 MHz and 9°×9° at 5.8 MHz for vertical pumping. Antenna gain is also frequency dependent and is 80 dB at 4.3 MHz, 120 dB at 4.8 MHz and 150 dB at 5.8 MHz.

To monitor ionospheric conditions we ran the ionosonde (vertical sounding) about every 10 minutes. The ionosonde located at the Sura site, was sensitive to plasma frequencies above 1.75-2 MHz (corresponding to plasma densities at the reflection level in the range 3.8×10^4 to 4.9×10^4 cm^{-3}) and up to 9 MHz (corresponding to a plasma density at the reflection level of about 10^6 cm^{-3}). A ground-based magnetometer located 30 km to the south-west from the Sura facility provided data on the geomagnetic field.

The campaign was equipped with an all-sky charge-coupled-device (CCD) camera (made by Keo Scientific Ltd.) from the NORSTAR project at the University of Calgary. The CCD camera used three interference filters: 557.7 nm with a filter bandwidth of 2 nm, 630.0 nm with a filter bandwidth of 2 nm, and a background (BGND) filter with a wavelength of 541 nm and a bandwidth of 2 nm. The software developed at Cornell University and used for operating the CCD imager allowed us to manually set any desirable sequence of filters and adjust the exposure time as needed.

In Fig. 1 we give a map showing the geometry of the observations. Four coherent scatter receiving sites (located near Kharkov, near Rostov, near Odessa and near St.-Petersburg) were used to measure signals scattered by the perturbed ionospheric volume above the radiowave source. For backscatter measurements we used what is now called a

passive radar technique (for details see *Yampolsky*, 1989 and *Blagoveshenskaya et al.,*1992). To this end we chose broadcasting stations near Moscow, Serpukhov and Krasnodar whose CW signals (scattered by field-aligned irregularities induced by high-power radiowaves above the Sura facility) satisfied the Bragg resonant condition to be registered at the four abovementioned radar sites, allowing reconstruction of 3D Doppler velocities inside the Sura-illuminated ionospheric volume.

For the first time in this type of experiment, we supported optical observations with simultaneous plasma diagnostics using the so-called artificial periodic irregularities (API) technique (*Belikovich et al.,* 2002).

In the second part of the campaign devoted to the F-region diagnostics we used a spectrum analyzer to observe stimulated electromagnetic emission (SEE) from the radiowave-modified ionosphere to determine such plasma parameters as, for example, the frequency of electron gyro harmonics. The real-time observations allowed prompt adjustments of the pump frequency in accordance with ionospheric conditions if necessary.

3. Artificial periodic irregularities.

Artificial periodic irregularities (API) are generated in antinodes of the standing electromagnetic wave formed due to interference of the HF radio waves transmitted vertically and reflected from the ionosphere. The API are horizontally aligned with a vertical scale of one-half of the wavelength λ of the transmitted wave. When probed with radiowaves of the same wavelength, this weak API grid (imposed on the existing natural ionospheric structure) returns an enhanced signal from the altitudes occupied by natural plasma inhomogeneities, thus giving information about ionospheric structure up to the pump wave reflection level. The receiver and transmitter are located at the same site. There are two ways to satisfy the Bragg resonant backscatter condition: (1) using the same frequency and polarization for the pump and probe waves and (2) using different frequencies and polarization giving the same wavelength for pumping and probing.

As a rule, the API method uses X-mode polarization to avoid inducing plasma instabilities. However, to combine optical observations with the API diagnostics, we had to use O-mode polarization for both pumping and probing in order to have maximum possible power for inducing optical emissions.

Among other advantages, the API method is capable of detecting sporadic ionization with plasma densities as low as about 1000 cm^{-3}, and is thus more than an order of magnitude more sensitive than ionosondes. In the upper panel of Fig.2 we show E-region sporadic ionization (Es) seen by the API technique on August 15-16, 2004 (during the daytime, no optics) as an enhanced backscattered signal and plotted as a function of local time and altitude (more details on producing altitude-time-intensity plot using API technique may be found in *Bakhmet'eva et al.,* 2005b). In brief the standing wave pattern from F layer reflection creates Bragg scattering targets which are more effective in the sporadic E layers. In the lower panel we show three ionograms taken at

times 18:28:05 LT (yellow line), 18:45:41 LT (orange line) and 20:29:44 LT (red line). Here we created API using an X-mode polarization radiowave at a frequency of 4.7003 MHz, which we then probed with X-mode waves at 4.7 MHz. From Fig. 2 it is clear that the ionosonde was capable of detecting a reflected signal only when the amplitude of the API signal was near 50 dB or higher (the upper part of the double Es near 100 km altitude). For example, it didn't register the signal backscattered from the low-altitude ionization near 80 km detected by the API technique.

The backscatter from the abovementioned weak layer of ionization near 80 km registered on August 15-16, 2004 with the API method (but undetectable by the ionosonde) looks like mesosphere summer echoes (MSE) that have been registered at Sura using the API method on many occasions, including simultaneous observations at 3 and 9 MHz (*Belikovich et al.,* 2003). These low-altitude ionization clouds caused radiowave focusing therefore providing enough energy to vibrationally excite hydroxyl molecules (*Kagan et al.,* 2005). We give more details on induced optical emissions in the next section.

Note that to effectively induce optical emissions scientists use high-power radiowaves of O-polarization and a continuous heating scheme. To match this requirement and to be able to do simultaneous atmospheric diagnostics by the API technique, we developed a special pumping/probing scheme, shown in Fig. 3. We use the O-mode polarization for pumping (5 min on / 5 min off) and O-mode polarization of the same wavelength for probing during the heater-off periods. For 2 s after every 13 s of continuous heating during each 5-min heater-on period, we transmitted 30-μs pulses (at a repetition frequency of 50 Hz) probing the induced API structure. We use the usual probing scheme during the heater-off periods. Despite the fact that we cannot run the complete API diagnostics using O-mode heating because of distortions caused by induced ionospheric instabilities, it is very important that O-mode heating is effective in detecting even relatively weak sporadic ionization. For example, it showed weak patchy-type Es pulsating near 80 km altitude during the night of August 15-16, 2005, the night when we observed radiowave-induced hydroxyl airglow (for details see *Kagan et al.,* 2005).

Along with plasma and atmospheric diagnostics, the API observations were aimed at studying the effects of the ionosphere modification on E-region sporadic ionization. Obviously, to make it efficient the Es critical frequency should exceed the pump frequency. These ionospheric conditions were at the end of the daytime API observations on August 15, 2004 (see Fig. 2). The respective ionograms show the strong overdense sporadic ionization near 100 km and the API method additionally recorded the weaker sporadic E just below it near 90 km. *Bakhmet'eva et al.* (2005a) found that while the amplitude of the probing signal coming from 90 km didn't change, the amplitude of the signal from 100 km was decreasing with heating (the heating did not noticeably affect the API relaxation time). The reasons for such a difference are not yet understood. A possible explanation may be related to the difference in the magnitude of the electric field of the radiowaves at the two altitudes and the influence of heating on ionospheric irregularities, as for example the triggering of different instability mechanisms at different altitudes. *Frolov et al.* (2002) showed that for a patchy type of Es the intensity of the backscattered signal increased with heating and induced signal fluctuations

appeared. Clearly, high-power radiowaves can modify sporadic ionization, but to understand how and why this modification takes place requires further experimental and theoretical investigation.

4. Optical observations.

Artificial airglow occurs when, due to the interaction of a powerful electromagnetic wave with the ionospheric plasma, electrons acquire enough energy for collisional excitation of neutral species. The most frequently observed artificial emissions occur when excited atomic oxygen in the $O(^1D)$ state relaxes to the ground state, emitting a photon with a wavelength of 630.03 nm (the excitation energy is 1.97 eV). This emission comes from altitudes 250±50 km and may be accompanied by significantly less intense F-region green-line emission of atomic oxygen (because of a higher excitation energy, 4.19 eV, compared to that of the 630.0-nm airglow), which occurs when atomic oxygen in the $O(^1S)$ state relaxes and emits a photon with a wavelength of 557.7 nm.

All three preceding campaigns at the Sura facility involving optics (1990, 1993 and 1995) were aimed at measuring the F-region airglow in 630.0-nm emission from $O(^1D)$ state from atomic oxygen and at using these measurements for determining plasma drifts, neutral winds, diffusion coefficients, and collisional quenching times (*Bernhardt et al.,* 1991, 2000). Bernhardt and coauthors didn't observe green line emission of atomic oxygen at 557.7-nm. Concerning F-region 557.7-nm radiowave-induced airglow, most probably Bernhardt and co-authors didn't observe it because there were not enough accelerated electrons with high enough energy to excite a detectable airglow. Neither one of these three campaigns was aimed at measuring E-region airglow, since it had not yet been discovered, and therefore the experiments were carried out when there was no E-region sporadic ionization.

In the F-region studies-oriented part of our August 2004 campaign, we investigated 630.0-nm optical signatures of the radiowave pumping into the geomagnetic zenith which for the Sura location was predicted to be the most effective for transmissions at the 12° geomagnetic south (*Gurevich et al.,* 2002, 2005). Because the weather was not cooperative for optical observations, we weren't able to accomplish the planned program. However, we observed on two days, August 13 (vertical heating) and August 20 (pumping into the magnetic zenith by heating at the 12° angle), when the ionospheric conditions were very similar (the F-maximum critical frequency in both cases was 5.8 MHz) as well as the effective radiative power of about 120 MW and the heating schedule 5 min on / 5 min off in both cases. The heating frequency was 4.7 MHz on August 13, 2004 and 4.7853 MHz on August 20, 2004. The angular dimensions of the heater beam for these two days were also very close: 10.7° E-W by 10.7° N-S for the vertical heating and 10.7° E-W by 11.1° N-S for the heating at the 12°-south angle in the geomagnetic coordinates. According to the ionosonde observations the pump wave was reflected from the virtual height of about 330 km in both cases.

In Fig. 4 we show two images of the F-region 630-nm induced airglow unwarped at 300 km altitude (a) for vertical radiowave transmission (22:33:47 LT on August 13, 2004, the heater was on for 167 s) and (b) for transmission at an angle of 12-degrees to

the geomagnetic south in order to direct the electromagnetic power into the magnetic zenith (22:13:57 LT on August 20, 2004; the heater was on for 177 s). The exposure time for both images was 30 s. We also took 30 s background exposures (off-band) to background correct the 630.0-nm images after applying a star removal algorithm to both background and red line images. We mark the center of the heater beam with the dot. We impose a geomagnetic meridian and show the location of magnetic zenith by the cross to make it easier to identify the location of the 630.0-nm artificial airglow for heating at the 12° angle. One can clearly see that on August 20 the center of the induced airglow cloud lies on the geomagnetic meridian to the geomagnetic south from the center of the heater beam, indicating that the radiowave energy was going into about 1-2° off the magnetic zenith (recall that the Sura dip angle is 71°).

The width of the airglow spot in this case was about one half of that for vertical heating observed on August 13, 2004. We are planning to study these data in more detail, although preliminary analysis of sequential images shows that (i) for well-developed airglow the maximum of relative intensity was more than twice as high while heating at the 12° angle than vertically, and (ii) the center of the airglow cloud for the oblique heating seems to appear more distant from the geomagnetic zenith and then to move closer to it with heating going on.

E-region radiowave-induced airglow was discovered recently, and the two types observed are 557.7-nm emission from atomic oxygen (*Djuth et al.,* 1999; *Kagan et al.*, 2000) and red hydroxyl aurora (this campaign, *Kagan et al.,* 2005). Both types are associated with sporadic ionization. While O(^{1}S) 557.7-nm airglow was a footprint of the overdense E-region sporadic ionization (E_s) (the pump frequency was less than the Es critical frequency) (*Kagan et al.,* 2000), the red hydroxyl aurora was a result of radiowave focusing by low-altitude ionization clouds near 80 km altitude (the pump frequency was more than the Es critical frequency) (*Kagan et al.,* 2005). The schematic illustration of the two mechanisms may be found in (*Kagan,* 2005). As we have already mentioned in Section 3 the density of these low-altitude ionization clouds was not high enough to be detectable by the Sura ionosonde but was registered with the method of artificial periodic irregularities (API) (*Belikovich et.,* 2002) using a diagnostic scheme of simultaneous optical and API observations suggested in (*Kagan et al.,* 2002). The key in these observations is that the light detected in a 2 nm wide filter centered on 630 nm was seen quite quickly (1-2 s) after launching the radiowaves. This short response time rules out 630 nm emission from atomic oxygen since it has a rise time of near 30 seconds (*Mantas and Carlson,* 1996).

We successfully induced 557.7-nm airglow from the O(^{1}S) state of atomic oxygen. However it was much weaker than we observed in Arecibo (*Kagan et al*., 2000) and didn't exceed 10 Rayleighs on all occasions. The sporadic ionization in all these cases had a critical frequency exceeding the pump frequency and was located near 110 km altitude. Similarly to atmosphere clouds the ionization clouds sometimes could be of a quite unusual shape. In Fig. 6 in *Bakhmet'eva et al.* (2005a) we present a 557.7-nm image of patchy sporadic ionization of a V-shape pointing to the west with a size of the shoulders of 10 by 3 km and 9 by 1-1.5 km (Es critical and blanketing frequencies were 5.4 and 2.7 MHz respectively) observed at 23:04 LT on 19 August, 2004.

5. Spectral characteristics of backscatter from artificial ionosphere turbulence when the pump frequency is close to the 4th electron gyro harmonic.

The second part of the campaign was predominantly aimed at studying radiowave-induced processes in the upper atmosphere (the ionosphere F region), artificial ionosphere turbulence (AIT) in particular, using simultaneous diagnostics of the heated ionospheric volume by multi-position backscatter measurements and by the method of stimulated electromagnetic emission (SEE). Multi-position backscatter observations give information on the dynamics of artificial small-scale irregularities (field-aligned irregularities with a field-perpendicular scale less than about 50 m) and drifts in the heated volume (*Blagoveshchenskaya and Troshichev*, 1996; *Yampolski et al*., 1997; *Ponomarenko et al*., 2000) while the SEE measurements allow us to experimentally find the frequency of the electron gyro harmonics (*Leyser et al.,* 1994). The latter are seen as a complete depression of the down-shifted maximum component in the SEE spectrum when the pump frequency is close to the frequency of the electron gyro harmonics.

Recent SEE experiments have shown the AIT properties in the perturbed ionospheric volume change significantly when the pump frequency lies in the 100-200 kHz vicinity of the frequency of the electron gyro harmonics (*Leyser et al.,* 1993; *Leyser*, 2001; *Stubbe et al.,* 1994; *Frolov et al.*, 1998; 2001).

Backscatter spectra were found to broaden from fractions of Hz during AIT development and relaxation to several Hz at the stage of well-developed turbulence (*Hysell et al,* 1996). *Koloskov et al.* (2002) showed that the splitting of the Doppler spectra of backscattered signals into a series of well-defined harmonics was caused by induced plasma heating by radial drifts inside the heated volume. Alternatively the splitting may be due to a radial electric field causing rotation about the heated volume (Hysell et al., 1996). Indeed *Peria and Kelley* (2001) have reported quasi-dc electric fields created inside a heated volume. Yampolski and coauthors (*Yampolski,* 1989; *Ponomorenko et al.,* 2000) discovered 20-150-s quasi-periodicity in Doppler shifts of backscattered signals and its correspondence to Pc 3-4 magnetic pulsations. *Ponomarenko et al.* (1999) and *Honary et al.* (1999) observed that, when the pump frequency was close to the 4th gyro harmonic, along with depression of the downshifted maximum and broad continuum components in the SEE spectra, there was a minimum of backscatter intensity accompanied by SEE spectra broadening for the pump frequency slightly exceeding the 4th gyro harmonic compared to the case when the pump frequency was slightly less than the 4th gyro harmonic. The magnitude of spectral broadening depended on pump power. The transition from broad to narrow spectra after pump turn-off took not more than 50-70 ms and it took 10 to 20 s for these narrow spectra to relax.

To understand the abovementioned broadening of Doppler spectra near the 4th gyro harmonic on August 19, 2004 (15:00-17:00 UT), we observed backscatter from the radiowave-modified ionospheric volume over the Sura heating facility using a so-called "passive radar" technique. Three radio systems (including the UTR-2 radio telescope) located near Kharkov, St-Petersburg, and Rostov were registering exact time signals of the Moscow broadcasting station operating at 9.996 and 14.996 MHz that according to

the Bragg resonance conditions, were backscattered by radiowave-induced field-aligned irregularities with field-perpendicular scales of 16 and 11 m respectively.

The Sura facility allows pumping at frequencies close to the frequencies of the 4th to 7th electron gyro harmonics. The electron gyro frequency above Sura is $f_{ce} \approx 1.3 - 1.35$ MHz. We vertically transmitted O-mode polarized waves with an effective radiative power ERP≈150 MW. The frequency of the electron gyro harmonics (the 4th one in this case) was determined by the depression of the downshifted maximum (*Leyser et al.*, 1994; *Grach et al.*, 1994) and the properties of the broad upshifted maximum (*Frolov et al.,* 1998) in the SEE spectra at the double resonance when the pump frequency $f_{pump} \cong f_{uh} \cong 4f_{ce}$ (f_{uh} is the upper hybrid frequency and $4f_{ce}$ is the frequency of the 4th electron gyro harmonic at the level of the upper hybrid resonance). The SEE method was capable of detecting $4f_{ce}$ with an accuracy of better than 5 kHz.

We started each observational cycle by finding $4f_{ce}$. Based on the ionospheric conditions we then chose a frequency range of about 80-100 kHz enveloping $4f_{ce}$ for radiowave transmissions and step-by-step changed the transmitter frequency with a step of 20 kHz. The transmission timing at each sequential pump frequency was 105 s on, 15 s off. The pause time of 15 s gave us enough time to switch to the next pump frequency during the pump-off periods. Such a diagnostic scheme gave us information on the temporal evolution of the scattered signal intensity with optimal resolution in the backscatter spectral measurements.

During each cycle of the abovementioned frequency scanning we kept diagnosing ionospheric conditions with the SEE observations to follow variations in the electron gyro frequency caused by changes in natural ionospheric conditions. This allowed us to promptly correct the magnitude of $4f_{ce}$ and to define the frequency range for the next scanning cycle. The duration of one observational cycle was about 10-12 minutes. From 15:00 to 17:00 UT we ran in total 8 cycles in the $4f_{ce}$ frequency range.

The day of August 19, 2004 was geomagnetically quiet with $K_p \approx 1$.

We present examples of dynamical spectra of signals scattered by 11- and 16-m irregularities recorded near Kharkov at 14.996 and 9.996 MHz from 15:59 to 16:09 UT ($4f_{ce} \approx 5.36$ MHz, scanning range was 5.34-5.44 MHz) in Fig. 5. In Fig. 6 we show backscatter spectra observed at 14.996 MHz (11-m irregularities) at two stations, near Kharkov and near Rostov, simultaneously from 16:28 to 16:39 UT ($4f_{ce} \approx 5.34$ MHz, scanning range was 5.32-5.40 MHz). It is clear that, compared to frequencies below $4f_{ce}$, a noticeable spectral broadening occurred when the pump frequency was close to or above $4f_{ce}$.

Backscatter from 11- and 16-m artificial field-aligned irregularities is seen as having two components (narrow and wideband) distinguished by their relaxation times and dependence on pump frequency. The effect of backscatter spectral broadening is clearly seen in both narrow and wideband backscatter components near $f_{pump} \cong 4 f_{ce}$ (the region of radiowave interaction with ionospheric plasma) reaching its maximum at a frequency

offset $f_{\text{pump}} - 4 f_{\text{ce}} = 20 - 40$ kHz which corresponds to the most effective generation of the second component in the broad upshifted maximum in the SEE spectra and to the most effective excitation of the electron Bernstein modes (*Frolov et al.,* 1998). The spectrum broadening decreases with a further increase of $f_{\text{pump}} - 4 f_{\text{ce}}$. The narrowband backscatter component carries the major part of the backscatter power, which is about an order of magnitude higher than the wideband one.

We estimate the growth time t_1 of the broad-band component after the pump switch-on and its relaxation time t_2 after the pump switch-off as t_1 = 0.5-1 s and $t_2 \leq 1$ s. This relaxation time is significantly less than the relaxation time of the 11-16-m irregularities generated by radiowaves with frequencies far from the electron gyro harmonics, which is about 10-15 s (*Hysell*, 1996; *Frolov,* 1997). Therefore the broadening of backscatter spectra at pump frequencies close to the 4$^{\text{th}}$ electron gyro harmonics seems to be caused by radiowave-induced random motions of scatterers inside the perturbed ionosphere volume rather than irregularity drift, which would shift the whole backscatter spectrum. The speed of these random motions may reach 100 m/s and does not depend on scatterer scales. *Ponomarenko et al.* (1999) explained these motions by excitation of the electron Berstein modes. The alternative explanation may be in excitation of irregularities associated with motions that are not as strongly elongated along the magnetic field as is usually the case. Then the diffusion coefficient will be larger, the lifetime less and the Doppler spread, which is inversely proportional to the lifetime, will be greater. Rocket observations in the presence of a pump wave detected irregularities with short parallel wavelengths at heights where the local plasma frequency equaled an electron gyro harmonic suggesting generation of electron Bernstein modes and possibly lower hybrid waves which have a finite field-aligned wave number (*Gelinas et al.*, 2003). Note though that the pump in this rocket experiment was not matched to an electron gyro harmonic but irregularities nonetheless formed at heights which not related to reflection.

6. Multi-position bi-static HF Doppler radio-scatter observations of artificial field-aligned irregularities.

To study dynamics in the HF-illuminated volume we used as a diagnostic the signals from three broadcasting stations located in Moscow (55.80° N, 38.30° E; distance to Sura is 490 km; operating frequencies were 14.996 MHz, 9.996 MHz and 12.070 MHz), Serpukhov (55.00° N, 37.50° E; distance to Sura is 550 km; operating frequency was 11.630 MHz) and Krasnodar (45.00°N, 39.50° E; distance to Sura is 1320 km; operating frequency was 15.455 MHz). The broadcasting HF signals were scattered by 10–15-m irregularities generated by high-power radiowaves above the Sura facility and were received at three locations: near St-Petersburg, near Kharkov and near Rostov (see the map in Fig. 1). Reception of HF diagnostic waves by means of the Doppler spectrum method was used for analyzing the fine structure of scattered signals. Viewing line-of-sight Doppler velocities from different angles allowed reconstruction of the temporal behaviour of the 2D velocity of the scatterers in the radiowave-illuminated volume.

We observed diagnostic signals scattered from artificial field-aligned irregularities (AFAIs) during most of the high-power radiowave transmission sessions. The intense scattered signals were simultaneously registered at three receiving locations on August 13, 15, 17, 18, 19, and 20. As an example we present in Fig. 7 the dynamic Doppler spectra (sonograms) on the Armavir-Sura-St. Petersburg (f=15.455 MHz; top panel), Serpukhov-Sura-Kharkov (f=11.630 MHz, east-west and north-south beams of UTR-2; upper and lower middle panel respectively), Serpukhov-Sura-Rostov (f=11.630 MHz; bottom panel) and Moscow-Sura-Rostov (f=14.996 MHz; bottom panel) paths on August 20, 2005 from 18:20 to 19:30 UT. A signature of HF-induced field-aligned irregularities is seen as additional tracks shifted from zero Doppler frequency corresponding to the direct signal propagating from the transmitter to the receiver along the great-circle path. From Fig. 7 one can see that scattered signals were observed during all heater-on periods shown with bars along the UT axis.

From multi-position bi-static Doppler scatter observations it is possible to estimate the magnitude and direction of plasma velocities in the HF-induced ionospheric patch. Calculations performed by using the model described in (*Borisova et al.,* 2002) showed that from 18:20 to 19:30 UT on August 20, 2004, AFAIs were moving in the south-west direction (azimuthal sector of 210-250 degrees counted clockwise from the direction to the north). From Doppler measurements we found the magnitude of AFAI velocity to be varying from about 50 to 150 m/s. Note that the day of August 20, 2004 was geomagnetically perturbed with $K_p = 3 - 4$. A similar reconstruction for the previous day, August 19, 2004, that was geomagnetically quiet ($K_p \approx 1$), gives a north-eastward motion (azimuths from 30 to 60 degrees) of the AFAIs with much more modest velocities of 30-70 m/s. These results are in excellent agreement with current ideas about the penetration of magnetospheric processes to middle latitudes. For example, *Gonzales et al.,* (1978) found that at very low Kp the zonal drifts at Millstone Hill Observatory were small and eastward while at modest Kp they are westward. This could be due to penetration of the convection electric field or to a disturbance dynamo due to winds blowing out of the polar cap/auroral oval.

The most prominent feature in the observed line-of-sight velocities (Doppler frequencies f_d) of the artificial field-aligned irregularities is their wavelike behavior presenting a wide spectrum of wave processes. The oscillations in Doppler-shifted frequencies showed two types of wave processes. The first is a relatively slow process with periods between 10 and 45 minutes that is close to the periodicity of medium-scale traveling ionospheric disturbances caused by atmospheric gravity waves. The amplitude of these oscillations was on the order of about 2 to 5 Hz. These relatively slow f_d variations were often modulated by shorter-period wave processes with periods of 30 to 60 s and amplitudes of 0.5-1 Hz. These shorter periodicities correspond to the Pc3-4 magnetic pulsations.

The pulsations with periods 20-80 s in the intensity of signals scattered by artificial irregularities above the Sura radio transmitter have been routinely observed in such types of experiments (*Blagoveshchenskaya and Troshichev*,1996; *Yampolski et al*., 1997; *Blagoveshchenskaya et al.,* 1998; *Sinitsin et al*., 1999). During the second part of the campaign we modulated the power of one of the Sura transmitters using the scheme 15 s

on / 15 s off to artificially induce Pc3 magnetic pulsations. Some of our transmissions were successful and we observed quasi periodical variations in Doppler shifts from the transmitted frequency with the same period of 15 s and amplitude up to 0.5 Hz. We are going to discuss these results in more detail in the near future.

The other feature of the signals scattered by radiowave-induced irregularities is the splitting of the scattered signal into two (or sometimes three) components already mentioned in Section 5 above (see for example cycles 18:21-18:26 and 19:16-19:26 UT in Fig. 7). This effect has been observed in both midlatitude [*Koloskov et al.,* 2002] and highlatitude ionosphere [*Blagoveshchenskaya et al.,* 2005]. *Koloskov et al* [2002] saw a possible explanation of the phenomenon in the radial drift of artificial irregularities from the center of the heated volume.

Based on rocket measurements during the heating experiment in Arecibo [*Kelley et al.,* 1995] that showed the presence of several altitude-separated regions of artificial small-scale irregularities, *Franz et al.* [1999] supposed that a temperature-gradient-driven instability such as the drift wave could be responsible for the patches of heater-induced striations at different heights. The question is still open and to answer it we need more observations.

Finally we would like to note that (i) during some of HF transmitting sessions when the Sura ionosonde observed intense sporadic ionization in the E region and no F-spread (as for example from 17 to 18 UT on August 18 and from 19 to 20 UT on August 19) the signals scattered by artificial field-aligned irregularities in the F2 layer exhibited strong spectral broadening in the Doppler sonogram; and (ii) we successfully excited Alfven waves using ±15 s modulation and pumping into the geomagnetic zenith (transmitting at 12° to the south) on August 19, 2005.

7. Multi-position observations of the self-scattering effect.

The effect of self-scattering was discovered during the 2002 campaign when the high-power radio signal radiated by the Tromsø heating facility was scattered by the irregularities it had induced in the heated volume (*Zalizovsky et al,* 2004). The distinct feature of self-scattering compared to backscattering is its wide angular indicatrix allowing observations of the scattered radio signal from different locations corresponding to propagation paths of different length and orientation. Coherent reception and spectral analysis of the self-scattered signals were performed simultaneously near St-Petersburg (Russia), Kharkov (Ukraine) and at the Ukrainian Antarctic station "Academician Vernadsky". Along with regular narrow-band signals at the pump frequency (associated with radiation from side lobes of the heater beam) we observed wide-band components that were well correlated in intensity and Doppler frequency shifts (as a rule several Hertz in magnitude) at all the receiving sites. Such a similar behavior allowed us to suppose that the Doppler variations are produced by the processes inside the heated volume. Since this is the only common volume for all radio paths, natural processes generated by electric fields, neutral winds, atmospheric gravity waves, magneto-hydrodynamic waves, *etc.* inside the heated volume may cause changes in the radiowave-induced irregularities, thus resulting in a similar modulation of the scattered signals.

The exciting discovery of the self-scattering effect (*Zalizovsky et al*, 2004) triggered several questions which we made an effort to clarify during our Sura campaign in August 2004. The primary issues were (i) the mechanism of radio signal scattering over a large range of azimuthal angles that assumed a horizontal isotropy of the scattering irregularities; (ii) the nature of the motions causing synchronous variations in Doppler frequency shifts and in the intensity of the scattered signals at very distant receiving sites; and (iii) the relation between variations in the self-scattered signal and signals scattered by small-scale radiowave-generated irregularities.

In addition to the observations of scattered signals at the pump frequency f_{pump} (as in the Tromsø campaign), we were monitoring simultaneously scattered spectra at the second harmonic of the pump frequency, 2 f_{pump}. Synchronized registration of the three components of geomagnetic field variations near the Sura heating facility allowed us to correctly identify the nature of motions inside the heated volume. As usual we routinely monitor the critical frequency of the ionosphere from ionosonde measurements.

Shown in Fig. 8 is an example of dynamic spectra of the self-scattered signals at the first harmonic of the pump frequency observed near St-Petersburg (the radio path is 963-km long) and Kharkov (the radio path is 994-km long) (see panels b and a, respectively), at the second harmonic of the pump frequency observed near St-Petersburg (panel d) and synchronous variations of one component of the Earth's magnetic field (panel c). A cross-correlation analysis of the Doppler frequency shifts in the self-scattered signals showed their high correlation with geomagnetic variations, giving a maximum of the cross-correlation coefficient of about 0.65. This allows us to suggest: 1) that the signals from both radio paths were indeed scattered over the Sura heating facility and 2) the motion of the ionospheric plasma was due to crossed electric and magnetic fields associated with MHD processes and therefore the velocity of the stimulated irregularities was modulated by geomagnetic field variations.

Concerning the nature of variations in the Doppler shifts of the self-scattered signals, we see two possible explanations. The first explanation is true physical motions of the scattering irregularities. In this case

$$f_{\text{d}} = V_s \, f_s / c \,, \qquad (1)$$

where V_s is the projection of the scatterer's velocity on the scattering direction, f_s is the carrier frequency of the scattered signal (in our case f_s was f_{pump} and 2 f_{pump}) and c is the speed of light. The second possibility is variations in the refraction index n(*l)* along the radio propagation path:

$$f_{\text{d}} = \frac{f_{\text{s}}}{c} \frac{\partial}{\partial t} \int_L n(l) dl \,. \qquad (2)$$

The two mechanisms have different frequency dependences. The f_d variations are proportional to f_s in the first case and are inversely proportional to f_s in the second case. Either of the two mechanisms could work. However, our analysis of simultaneous observations of the self-scattering effect at the first (Fig. 8b) and the second Fig. 8d)

harmonics of the pump frequency shows that the refractive mechanism dominates. Indeed, the maximum variation of f_d of self-scattered signals at 2 f_{pump} was about one half of that at f_{pump}.

This suggests that the upgoing trajectory segment from the heater to the scattering volume, which is common to all the radio paths, is the major contributor to the Doppler shift variations. Therefore the magneto-hydro-dynamical (MHD) process modulates not only the position of irregularities inside the scattering volume but also the electron density above the high-power radio source.

In Fig. 9 we show an example of data in which the modulation of the scattered signals was caused by MHD processes. One can clearly see that the Doppler frequency shifts f_d of the self-scattered signals (in m/s) recorded simultaneously near St-Petersburg (blue line) and Kharkov (green line) are well correlated with each other and with the geomagnetic variations (black line). The aspect-scattered signal observed near Kharkov and the intensity of the aspect-scattered signal recorded near St-Petersburg are shown by grey line and red lines, respectively.

Understanding the formation of a self-scattered signal in the perturbed ionospheric volume requires reconstruction of the 3D structure of the high-power radio wave near its reflection level. The task is extremely difficult. Obviously there are two factors that should be taken into account: the regular structure of artificial periodic irregularities below the reflection level produced by the incident and reflected waves (section 3) and stochastic irregularities associated with the plasma turbulence inside the heated volume. We will present the corresponding model calculations in our future publications. Comparison of the model with observations would allow us to use the effect of self-scattering for diagnostics of the spatial structure of the high-power radiowave and 3D spectra of the irregularities induced by this radiowave. We expect to obtain further insight into the self-scattering effect from its comparative analysis with API observations in which we used the diagnostic scheme (shown in Fig. 3) specifically developed for O-mode continuous heating in order to induce optical emissions. For understanding the generation mechanism of the self-scattering at the second harmonic of the pump frequency, further expressly designed experimental studies are needed.

8. Summary and Conclusions.

In this paper we aimed to give an overview of the optical-backscatter-heating campaign which we have conducted on August 10-20, 2004 rather than presenting several detail case studies that are the subject of separate publications. We believe that our campaign was so successful because of two major factors: (i) carefully chosen time of campaign to have the best possible combination of sporadic E occurrence and dark time required for optical observations at the highest possible maximum plasma density of the ionosphere, and (ii) simultaneous observations by different instruments and methods. For example, in order to make use of several diagnostic methods (as for example optical and API) we developed the scheme of the API diagnostics shown in Fig. 3, based on O-mode probing during O-mode continuous heating. Despite the fact that such a scheme is significantly less effective than the classical one (*Belikovich et al.,* 2002) it served its

purpose of observing weak sporadic ionization undetectable by the ionosonde. We also expect that this regime of the API method, as well as processing the self-scattered signals recorded at the Ukrainian Station "Academician Vernadsky" in Antarctica, will give a further insight in the self-scattering effect.

Below we briefly summarize the main results from our optical-backscatter-heating campaign at the Sura facility on August 10-20 2004.

- Optics and API
    - *Discovery of radiowave-induced red OH(9-3) Meinel band emission* caused by ray focusing due to weak (underdense) sporadic ionization near 80-85 km altitude (*Kagan et al,* 2005);
    - *Es-associated 557.7-nm radio-induced airglow from O(^{1}S)* (*Bakhmet'eva et al.,* 2005)*;*
    - *Pumping the radiowave energy into the geomagnetic zenith by transmitting at a 12°- to-the-south angle from the vertical* observed in 630.0-nm emissions from O(^{1}D) and *offset of these optical emissions by 1-2 degrees from magnetic zenith*;
    - *Natural bore wave observed in red OH(9-3) and 557 .7-nm from O(^{1}S)* (to be submitted as a separate paper).
- Backscatter
    - *Reconstruction of the temporal behavior of the 2D velocity vector of the radio wave-induced irregularities in the heated volume (Blagoveshenskaya et al.,* 2005b);
    - *Alfven Wave generation* using ±15 s modulation and pumping into the geomagnetic zenith (transmitting at 12° to the south);
    - *Long "independent" life of the backscatter signal after the pump turn-off* most probably associated with sporadic ionization (Aug 13, 2004 (18:00-18:20 UT);
    - *Splitting in the Doppler spectra of the scattered signal into two (or sometimes three) components (Blagoveshenskaya et al.,* 2005);
    - *Two well-distinguished components (narrow and wide) in the Doppler spectra of the scattered signal* with the narrow component being more intensive than the broad one by a factor of 10 (*Frolov et al.,* 2005; *Blagoveshenskaya et al.,* 2005b).
    - *Broadening of the frequency spectrum of the artificial ionosphere turbulence* when the pump frequency was close to the 4th electron gyro

harmonic with a maximum spectral width at the frequency offset of about 20-40 kHz (*Frolov et al.,* 2005). We have proved that the effect of spectral broadening was not caused by the irregularity drift in the heated volume.

- The effect of the self-scattering (*Yampolski et al.,* 2005)
    - *Observation* (for the first time) *of self-scattering signals at the second harmonic of the pump frequency* that allowed
    - p*inning down the refractive mechanism of Doppler variations;*
    - *Observations* (for the first time) *of synchronic variations in backscattered and self-scattered radio signals*;
    - *Correlation of the self-scattered signal with the magnetic field fluctuations.*

We are going to give more detail presentations of case studies with simultaneous use of several instruments and techniques in separate publications to follow.

Acknowledgments. This work has been supported by Grant ATM-0000196 from the Atmospheric Science Section of the National Science Foundation. LMK's work has been supported via a contract with Cornell University and by the Canadian Natural Sciences and Engineering Research Council. ED and TST acknowledge the Canadian Space Agency for their support of NORSTAR through the Canadian GeoSpace Monitoring Program. The work has been in part supported by Russian Foundation of Basic Research grants 04-05-64140, 05-05-64304, 05-02-16493 and 04-05-64160, 02-05-65281, the INTAS grant 03-51-5583 and the CRDF grant 1334-NO-2. The authors thank D.S. Kotik and S.V. Polyakov for the magnetometer data.

References

Bakhmet'eva, N.V., V.V. Belikovich, L.M. Kagan, A.A. Ponyatov, A.V. Tolmacheva, M.C. Kelley and M.J. Nicolls, New results of the lower ionosphere studies by the method of resonant backscatter of radiowaves from artificial ionospheric irregularities, *Radiophysics and Quantum Electronics, 48(9)*, 2005a.

Bakhmet'eva, N.V., V.V. Belikovich, L.M. Kagan, and A.A. Ponyatov, Sunset-to-sunrise characteristics of sporadic layers of ionization in the lower ionosphere observed by the method of resonance scattering of radio waves from artificial periodic inghomogeneities of the ionospheric plasma, *Radiophysics and Quantum Electronics*, *48(1)*, 14-28, 2005b.

Belikovich, V. V. , E. A. Benediktov, A. V. Tolmacheva, and N. V. Bakhmet'eva, *Ionospheric Research by Means of Artificial Periodic Irregularities,* Copernicus GmbH, Katlenburg-Lindau, Germany, 2002.

Belikovich, V. V. ,A.N. Karashtin, G.P. Komrakov, Yu.V. Shliugaev, Simultaneous radiowave sounding of the midlatitude mesosphere at MF- and HF- frequency ranges, *Geomagnetism & Aeronomy,43(1)*, 1-6, 2003.

Bernhardt, P. A., W. A. Scales, S. M. Grach, A. N. Keroshtin, D. S. Kotik, S. V. Polyakov, Excitation of artificial airglow by high power radio waves from the ‘‘SURA’’ ionospheric heating facility, *Geophys. Res. Lett., 18(8)*, 1477-1480, 10.1029/91GL01847, 1991.

Bernhardt, P. A., M. Wong, J. D. Huba, B. G. Fejer, L. S. Wagner, J. A. Goldstein, C. A. Selcher, V. L. Frolov, E. N. Sergeev, Optical remote sensing of the thermosphere with HF pumped artificial airglow, *J. Geophys. Res., 105(A5)*, 10657-10672, 10.1029/1999JA000366, 2000.

Blagoveshchenskaya, N.F., V.A. Bubnov, and V.A. Shelukhin, Experimental studies of scattered HF diagnostic signals during ionospheric modification by powerful HF radio waves, *Radiophysics and Quantum Electronics, 35(1)*, 24-30, 1992.

Blagoveshchenskaya, N.F., and O.A. Troshichev, Ionospheric phenomena produced by modification experiments, *J. Atmos. Terr. Phys.*, *58*, 397–406, 1996.

Blagoveshchenskaya, N.F., M.Yu. Chernyshev, and V.A. Kornienko, Excitation of of small-scale waves in the F region of the ionosphere by powerful HF radio waves, *J. Atmos. Terr. Phys., 60*, 1225-1232, 1998.

Blagoveshchenskaya, N. F., T. D. Borisova, V. A. Kornienko, T. B. Leyser, M. T. Rietveld, and B. Thidé. Artificial field-aligned irregularities in the nightside auroral ionosphere, *Adv. Space Res,* 2005. (in press).

Blagoveshchenskaya, N. F., T.D. Borisova, V.A. Kornienko, M.T. Rietveld, L.M. Kagan, Y.M. Yampolsky, V.L.Frolov, V.G.Galushko, A.V. Koloskov, S.B. Kascheev, A.V. Zalizovky, and G.V. Vertogradov, M.C. Kelley, Probing of medium-scale traveling ionospheric disturbances using HF-induced scatter targets, *Ann. Geophys*, 2005b (submitted).

Borisova, T. D., N. F. Blagoveshchenskaya, I. V. Moskvin, M. T. Rietveld, M. J. Kosch, and B. Thidé. Doppler shift simulation of scattered HF signals during the Tromsø HF pumping experiment on 16 February, 1996, *Ann. Geophys*., *20*, 1479-1486, 2002.

Gelinas L. J., M. C. Kelley, M. P. Sulzer, E. Mishin, M. J. Starks, In situ observations during an HF heating experiment at Arecibo: Evidence for Z-mode and electron cyclotron harmonic effects, *J. Geophys. Res., 108 (A10)*, 1382, doi:10.1029/2003JA009922, 2003.

Gonzales, C. A., Kelley, M. C., Carpenter, L. A. and Holzworth, L. H., Evidence for a magnetospheric effect on mid-latitude electric fields, *J. Geophys. Res., 83(A9),* 4397-4399, 1978.

Grach S. M., B. Thide, and T.B. Leyser, Plasma waves near the double resonance layer in the ionosphere, *Radiophys. Quantum Electron., 37*, 392-402, 1994.

Gurevich, A.V., K.P. Zybin, H.C. Carlson, T. Pedersen, Magnetic zenith effect in ionospheric modifications, *Physics Letters A 305*, 264–274, 2002.

Gurevich, A.V., K.P. Zybin, H.C. Carlson, Magnetic Zenith Effect, *Radiophysics and Quantum Electronics, 48(9)*, 2005.

Djuth, F.T., P.A. Bernhardt, C.A. Tepley, J.A. Gardner, M.C. Kelley, A.L. Broadfoot, L.M. Kagan, M.P. Sulzer, J.H. Elder, C. Selcher, B. Isham, C. Brown, and H.C. Carlson, Large Airglow Enhancements Produced via Wave-Plasma Interactions in Sporadic E, *Geophys. Res. Lett., **26***, 1557-1560, 1999.

Franz, T. L., M. C. Kelley, and A. V. Gurevich, Radar backscattering from artificial field-aligned irregularities, *Radio Sci*., *34*, 465-475, 1999.

Frolov V.L., L.M. Erukhimov, S.A. Metelev, and E.N. Sergeev, Temporal behaviour of artificial small-scale ionospheric irregularities: Review of experimental results, *J. Atmos. Sol.-Terr. Phys., 59*, 2317-1333, 1997.

Frolov V.L., L.M. Erukhimov, L.M. Kagan, G.P. Komrakov, and E.N. Sergeev, Two-component nature of the broad up-shifted maximum in stimulated electromagnetic emission spectra, *Phys. Rev. Lett.*, *81*, 1630-1633, 1998.

Frolov V.L., E.N. Sergeev, E.N. Ermakova, G.P. Komrakov, and P.Stubbe, Spectral features of stimulated electromagnetic emission, measured in the 4.3 – 9.5 MHz pump wave frequency range, *Geophys. Res. Lett*., 28, 3103-3106, 2001.

Frolov, V.L., L.M. Kagan, G.P. Komrakov, E.N. Sergeev, E.A. Shorokhova, Results of modification of the ionosphere sporadic-E layer by HF power radio emission, *Radiophys. Quantum Elecron., **45***(12), 917-928, 2002.

Frolov, V.L., D.I. Nedzvedski,Yu.M. Yampolski, A.V. Kolockov, A.V. Zalizovski, V.L. Galushko, S.B. Kascheev, G.G. Vertogradov, V.G. Vertogradov, N.F. Blagoveschenskaya, V.A. Kornienko, L.M. Kagan, M.C. Kelley, Spectral characteristics of signals scattered by artificial small-scale irregularities for the pump frequency close to a frequency of electron gyro harmonics, *Proceedings of XX1 Russian National conference on Radiowave Propagation*, Ioshkarala, Russia, 2005 (in Russian).

Honary F., T.R. Robinson, D.M. Wright, A.J. Stocker, M.T. Rietveld, and I. McCrea, First direct observations of the reduced striations at pump frequencies close to the electron gyro harmonics, *Ann. Geophysicae, 17,* 1235-1238, 1999.

Hysell D.L., M.C. Kelley, Y.M. Yampolski, V.S. Beley, A.V. Koloskov, P.V. Ponomarenko, and O.F. Tyrnov. HF radar observations of decaying artificial field – aligned irregularities, *J. Geophys. Res., 101*, NO A12, 26,981-26,993, 1996.

Kagan, L.M., M.C. Kelley, F. Garcia, P.A. Bernhardt, F.T. Djuth, M.P. Sulzer, C.A. Tepley, The Structure of Electromagnetic Wave-Induced 557.7 nm Emission Associated With a Sporadic-E Event over Arecibo, *Phys. Rev. Lett., **85***, 218, 2000.

Kagan, L.M., N.V. Bakhmet'eva, V.V. Belikovich, A.V. Tolmacheva, and M.C. Kelley, Structure and dynamics of sporadic E layers in the ionospheric E region, *Radio Sci.,* **37**(6), 1106, 2002.

Kagan, L.M., M.J. Nicolls, M.C. Kelley, H.C. Carlson, V.V. Belikovich, N.V. Bakhmet'eva, G.P. Komrakov, T.S. Trondsen, and E. Donovan, Observation of Radiowave-Induced Red Hydroxyl Emission at Low Altitude in the Ionosphere, *Phys. Rev. Lett.*, *94(9),* 095004, 2005.

Kagan, L.M., Aurora-associated phenomena and the e-POP mission, *Advances in Geosciences 2005.*

Kelley M.C., T.L.Arce, J.Salowey, M.Sulzer, T.Armstrong, M.Carter, and L.Duncan, Density depletion at the ten meter scale induced by Arecibo heater, *J. Geophys. Res.*, *100*, 17367, 1995.

Koloskov, A.V., T.B. Leyser, Yu.M. Yampolski, and V.S. Beley. HF pump-induced large scale radial drift of small scale magnetic field-aligned density striations, *J. Geophys. Res*., *107*(A7), doi: 10. 1029/2001 JA000154, 2002.

Leyser T.B., B. Thide, M. Waldenvik, E. Veszelei, V.L. Frolov, S.M. Grach, and G.P. Komrakov, Downshifted maximum features in stimulated electromagnetic emission spectra, *J. Geophys. Res., 99A*, 19555-19568, 1994.

Leyser T.B., B. Thide, M. Waldenvik, S. Goodman, V.L. Frolov, S.M. Grach, A.N. Karashtin, G.P. Komrakov, and D.S. Kotik, Spectral structure of stimulated electromagnetic emissions between electron cyclotron harmonic, J. Geophys. Res., 98A, 17597-17606, 1993.

Leyser T.B., Stimulated electromagnetic emissions by high frequency electromagnetic pumping of the ionospheric plasma, Space Sci. Rev., 98, 223-328, 2001.

Mantas, G. P., and H. C. Carlson, Reinterpretation of the 6300-Å airglow enhancements observed in ionosphere heating experiments based on analysis of Platteville, Colorado, data, *J. Geophys. Res., 101,* 195, 1996.

Peria, W. J., and M.C. Kelley, Convection electric field observations near the Arecibo HF heater beam, *J. Geophys. Res.*, *106(A9)*, 18517-18524, 10.1029/2000JA000279, 2001.

Ponomarenko P.V., T.B. Leyser, and B. Thide. New electron gyroharmonic effects in HF scatter from pump-excited magnetic field-aligned ionospheric irregularities, *J. of Geophys. Res*.,. *104A,* 10081-10087, 1999.

Ponomarenko, P.V., A.V. Zalizovski, Yu.M. Yampolski D.L. and, Hysell, Interaction between artificial ionospheric irregularities and natural MHD waves, *J. Geophys. Res., 105*(A1), 171-181, 2000.

Sinitsin, V.G., M.C. Kelley, Yu. M. Yampolski, D.L. Hysell, A.V. Zalizovski, and P.V. Ponomarenko. Ionospheric conductivities according to Doppler radar observations of stimulated turbulence, *J. Atmos. Terr. Phys*., *61*, 903-912, 1999.

Stubbe P., A.J. Stocker, F. Honary, T.R. Robinson, and T.B. Jones, Stimulated electromagnetic emissions and anomalous HF wave absorption near electron gyroharmonics, *J. Geophys. Res*., 99A, 6233-6246, 1994.

Zalizovski, A. V., S. B. Kashcheyev, Yu. M. Yampolski, V. G. Galushko, V. S. Beley, B. Isham, M. T. Rietveld, C. La Hoz, A. Brekke, N. F. Blagoveschenskaya, and V. A. Kornienko, Spectral Features of HF Signals from the EISCAT Heating Facility in Europe and in Antarctica, *Radio Physics and Radio Astronomy, 9(3)*, 261-273, 2004.

Yampolski, Yu.M., Echo-scattering of HF signals on the Artificial Ionospheric turbulence, *Radiophys. Quantum Elecron.*, *32(6),* 457-461, 1989.

Yampolski, Y.M., V.S. Beley, S.B. Kascheev, A.V. Koloskov, V.G. Somov, D.L. Hysell, B.Isham, and M.C. Kelley, Bistatic HF radar diagnostics induced field – aligned irregularities, *J. Geophys. Res., 102(A4)*, 7461 – 7467, 1997.

Yampolski, Yu. M., A. V. Zalizovski, V. G. Galushko, A. V. Koloskov, and S. B. Kascheev. *Self-scattering effect of powerful HF radiation as observed in Europe and Antarctica*. RF Ionospheric Interactions Workshop, Santa Fe, New Mexico, 17-20 April, 2005.

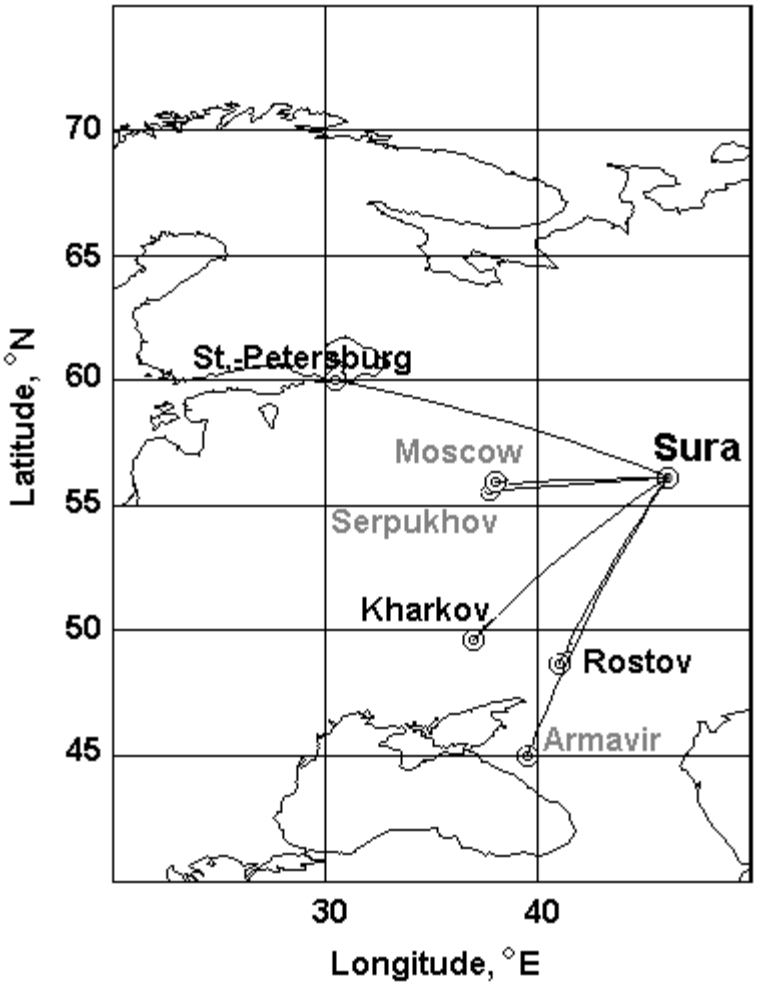

Fig. 1. The geometry of the Sura experiment on August 10-20, 2004. Locations of broadcasting stations and receiving sites are shown in grey and black, respectively.

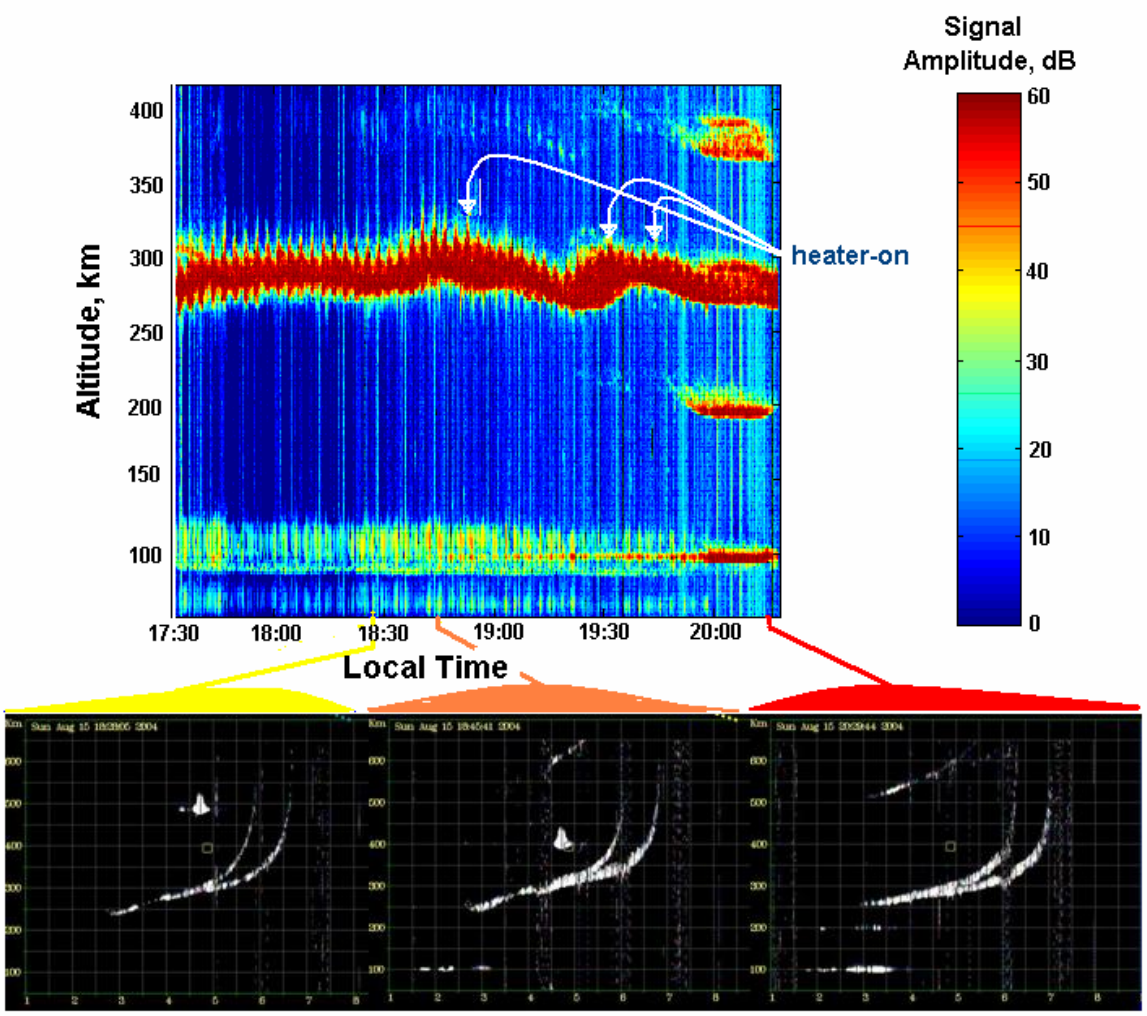

Fig. 2. Altitude-time-intensity plot (upper panel) reconstructed using the API data from 17:30 till 20:30 LT on August 13, 2004. The O-mode heating was at 4.3 MHz with the pumping scheme 1 min on / 2 min off. API formation and probing was by X-mode radiowaves at 4.7 MHz. In the lower panel we show the ionograms from the Sura ionosonde taken from left to right at 18:28:05 LT (yellow line), 18:45:41 LT (orange line) and 20:29:44 LT (red line).

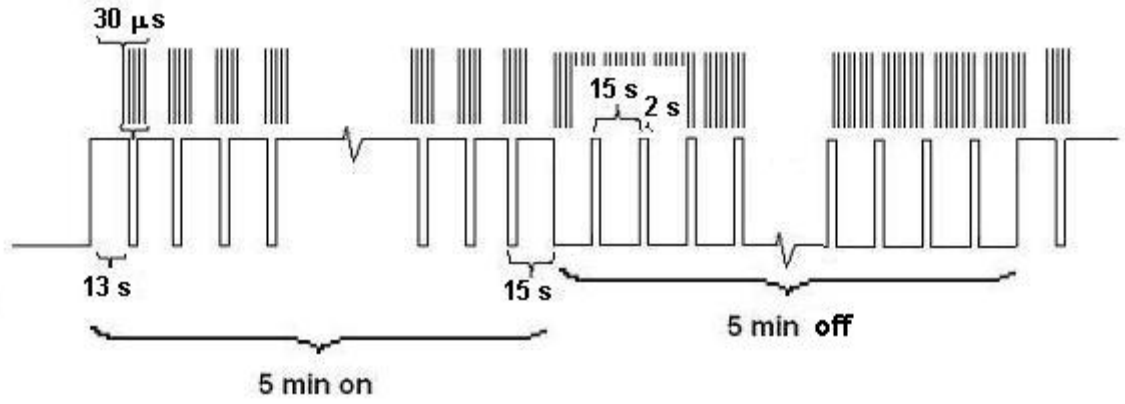

Fig. 3. The scheme of API diagnostics used during dark time of the day to combine it with optical observations.

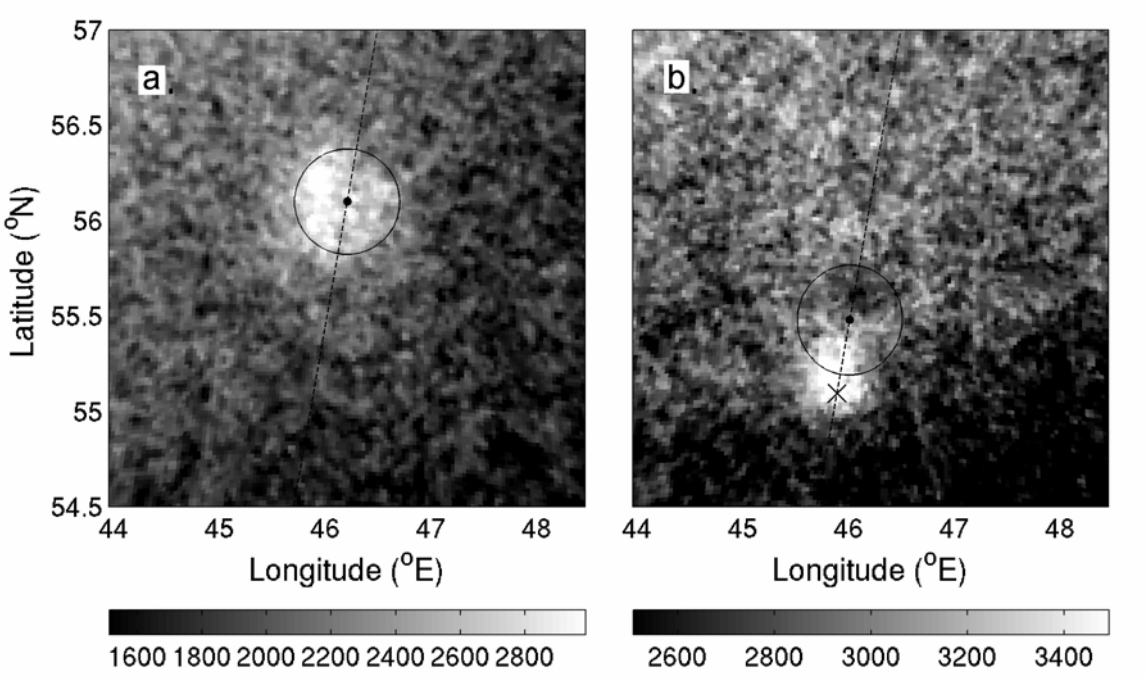

Fig. 4. The part of all-sky images of the F-region 630-nm induced airglow unwarped at 300 km altitude (a) for vertical radiowave transmission (22:33:47 LT on August 13, 2004, the heater was on for 167 s) and (b) for transmission at a the angle 12-degree to geomagnetic south (22:13:57 LT on August 20, 2004; the heater was on for 177 s). The images are 30 s exposures at 630.0 nm. 30 s background exposures (off-band) were also taken, and the 630.0-nm images have been background corrected after a star removal algorithm was applied to both background and red line images. After background correction, the images were projected onto a flat surface at 300 km and this geographic projection was translated to geographic latitude and longitude. Post-

processing also included the application of a 2x2 median filter to smooth the image. The x and y axes represent approximately the same distance from zenith so that the structures in the images are not distorted. The intensities given are counts and are proportional to Rayleighs. The dot marks the center of the heater beam, the cross in Fig. 4b shows the geomagnetic zenith.

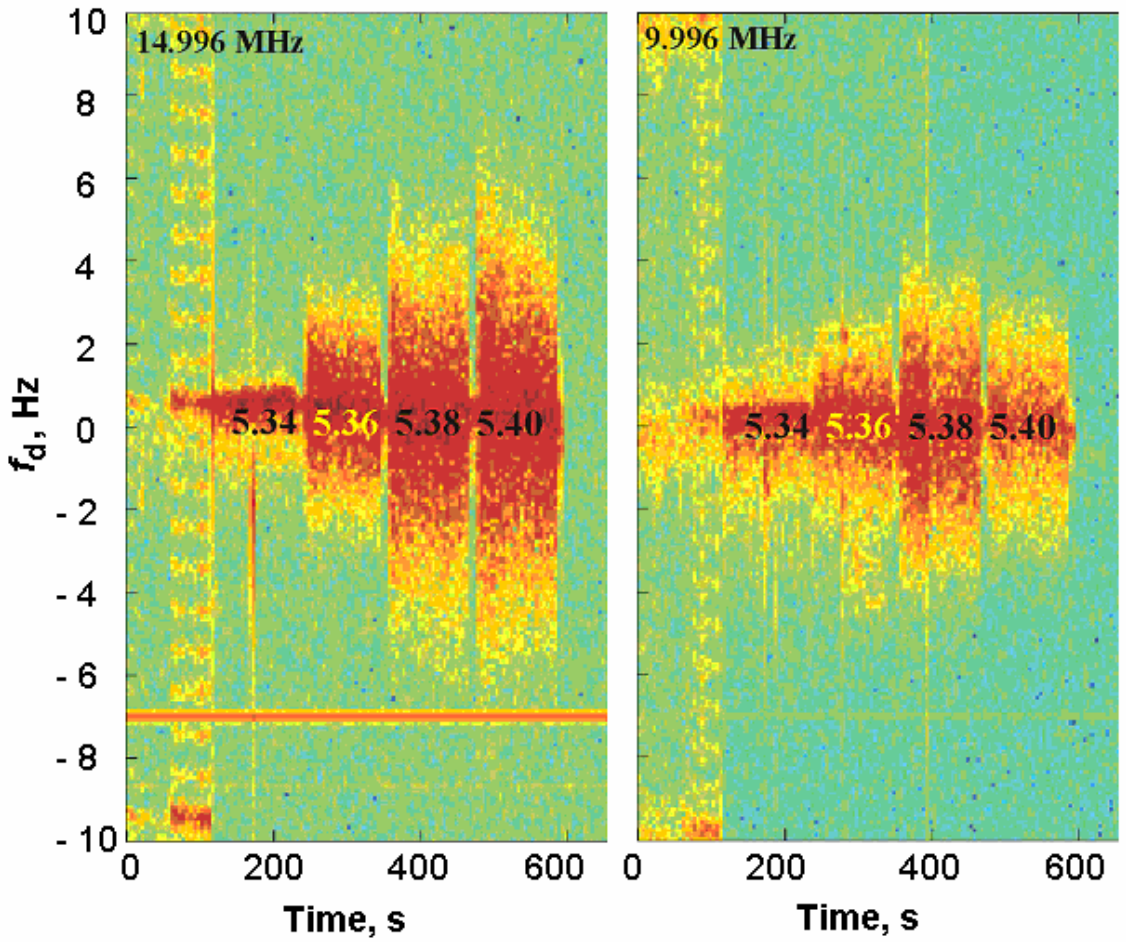

Fig. 5. Doppler spectra of the scattered signals recorded by the N-S array of UTR-2 in Kharkov at 14.996 and 9.996 MHz (corresponding to field-aligned irregularities with field-perpendicular scales 11 and 16 m) from 16:00 to 16:11 UT (UT=LT + 4 h) on August 19, 2004. We step-by-step changed the transmitter frequency from 5.34 to 5.40 MHz with a step of 20 kHz. The transmission timing at each sequential pump frequency was 105 s on, 15 s off. The 4th gyro harmonic frequency was about 5.36 MHz.

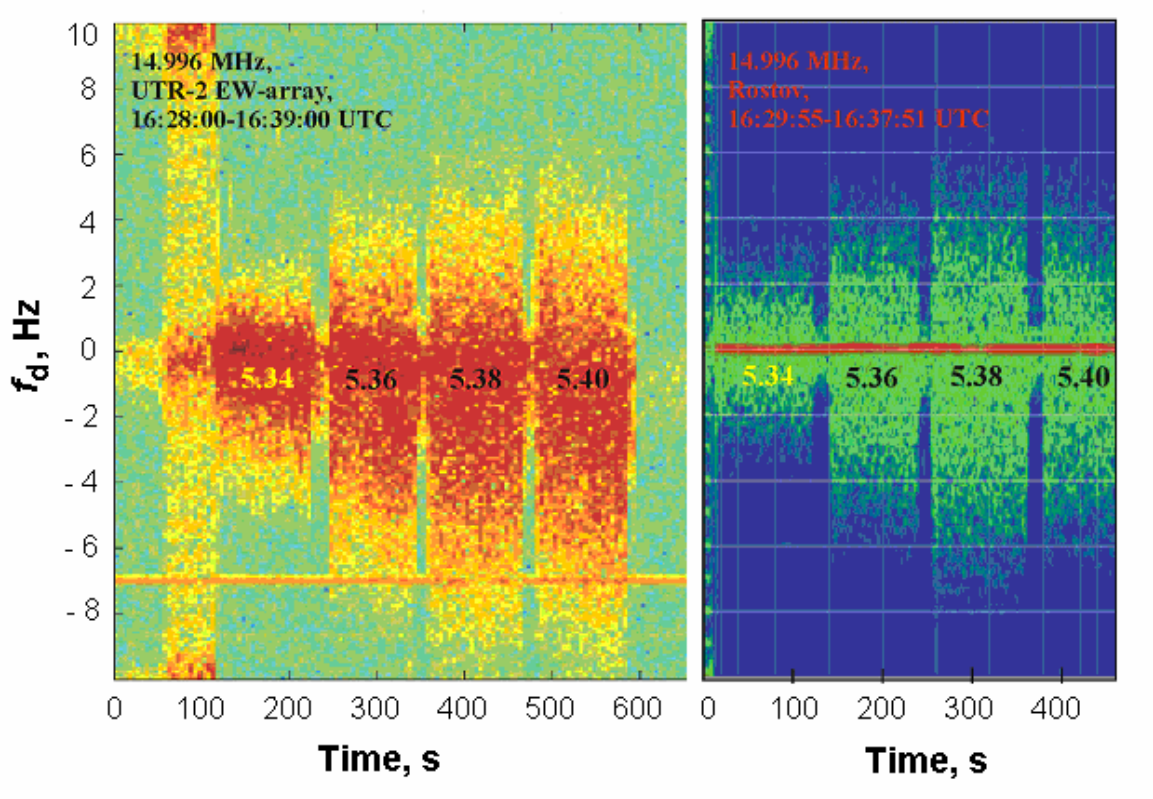

Fig. 6. Doppler spectra of the scattered signals recorded by the N-S array of UTR-2 in Kharkov (left panel) and by the receiving site near Rostov (right panel) at 14.996 MHz (corresponding to field-aligned irregularities with field-perpendicular scales 11 m) on August 19, 2004. We step-by-step changed the transmitter frequency from 5.34 to 5.40 MHz with a step of 20 kHz. The transmission timing at each sequential pump frequency was 105 s on, 15 s off. The 4th gyro harmonic frequency was about 5.34 MHz

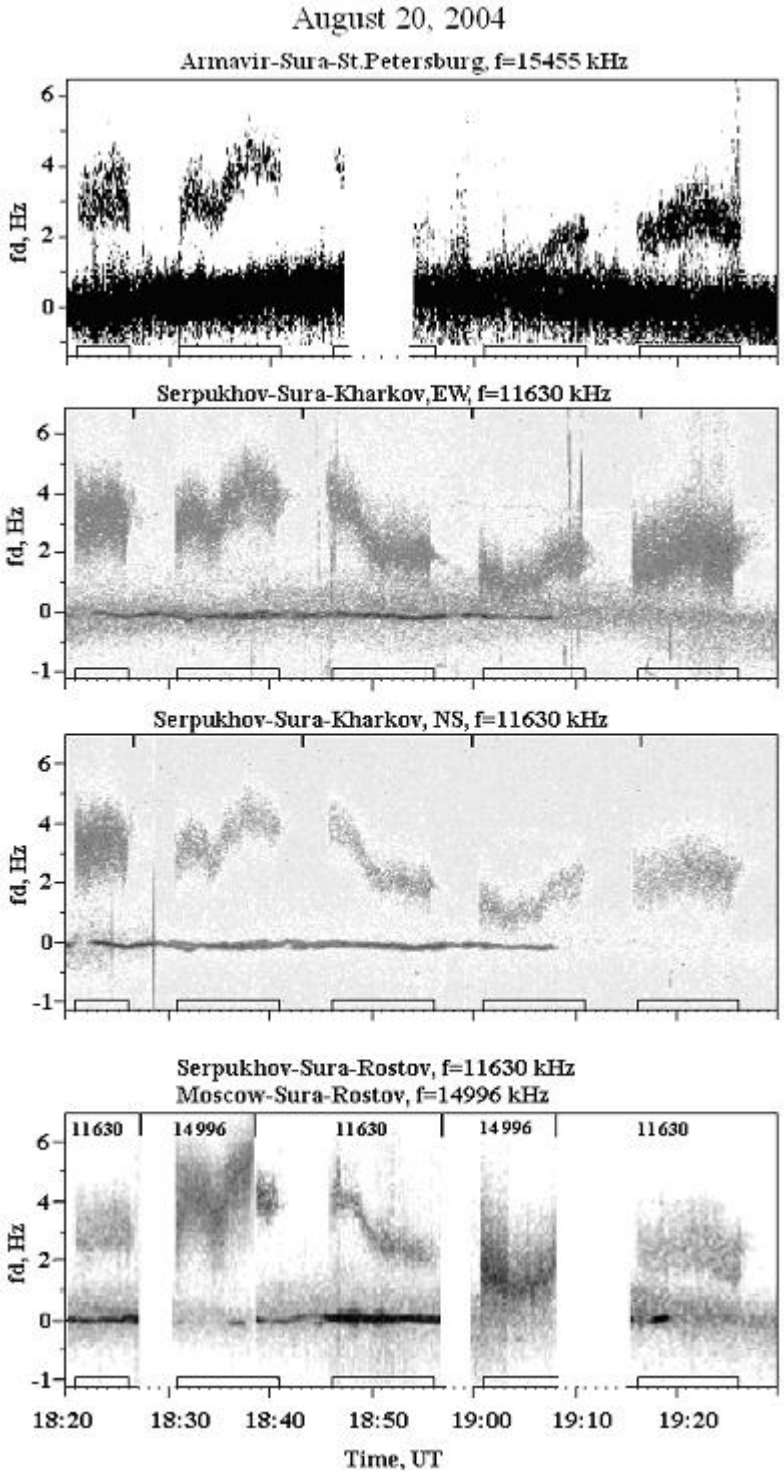

Fig. 7. Dynamic Doppler spectra of HF broadcasting signals from 18:20 to 19:30 UT on August 20, 2004, observed along the Armavir-Sura-St. Petersburg path at 15.455 MHz (top panel); along the Serpukhov-Sura-Kharkov path at 11.630 MHz with EW (upper middle panel) and NS (lower middle panel) beams of the UTR-2; and along the Serpukhov (Moscow)-Sura-

Rostov path at 11.630 and 14.996 MHz (bottom panel). For each path the direct signal propagating from the transmitter to the receiver along a great circle corresponds to a zero Doppler shift. The intervals of high-power radio transmissions are marked by bars on the time axis.

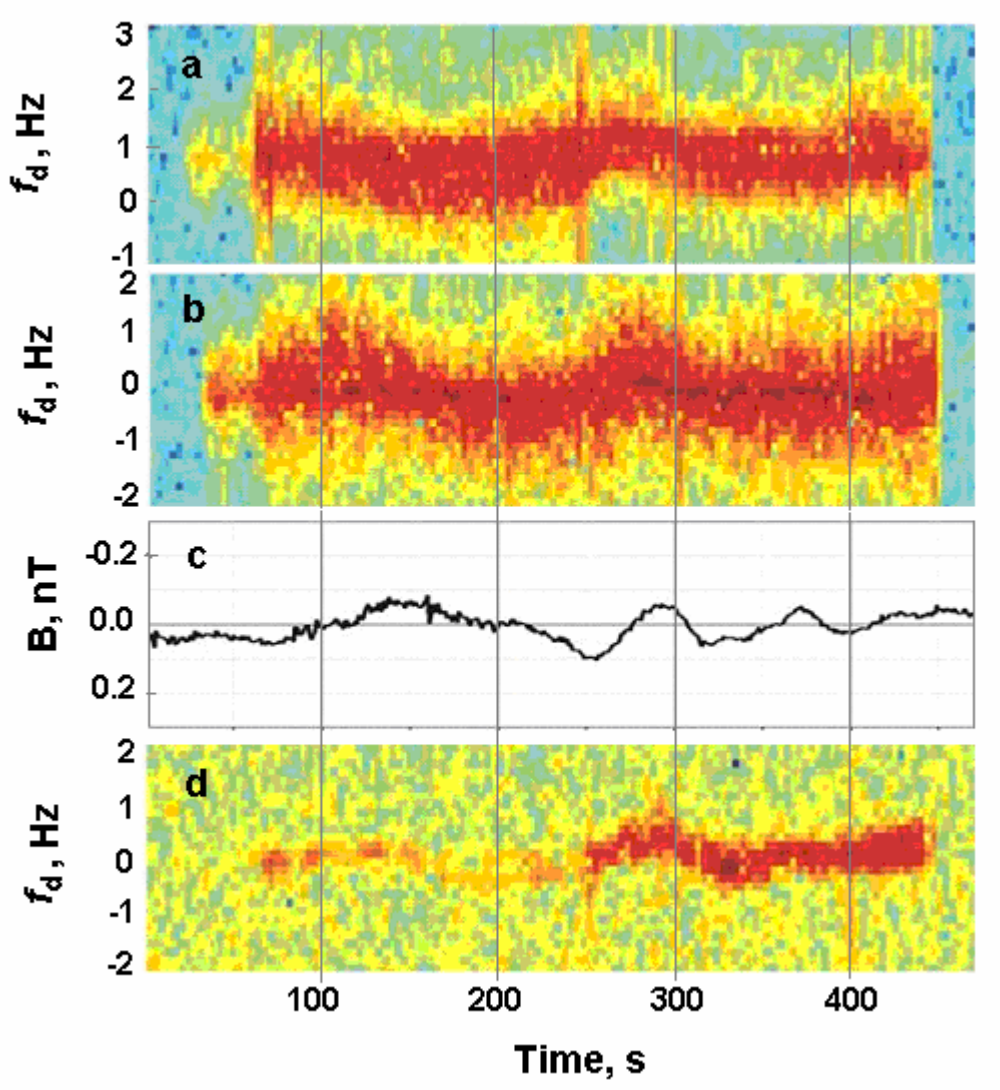

Fig. 8. Spectrograms of "self scattered" signals and geomagnetic field variations. "Sura" campaign, from 04:34 to 04:37 UT, 15 August, 2004.a) 1st harmonic at RAO, b) 1st harmonic at AARI, c) H_y component of geomagnetic field close to the "Sura", d) 2nd harmonic at AARI.

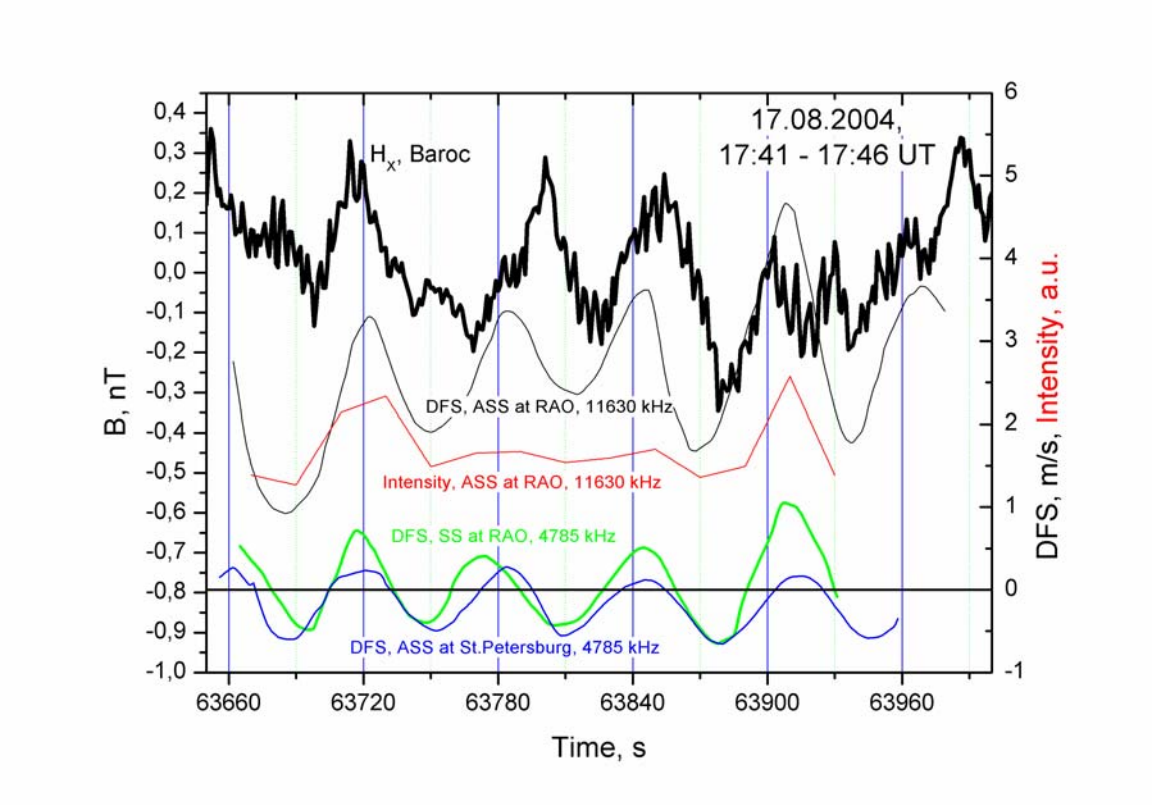

Fig.9. Doppler frequency shifts of self scatter signals, back-scattered signals and variations of the H_x magnetic field component close to the "Sura" heater during the heater-on period. (DFS of SS at AARI – blue line; DFS for SS at RAO – green line; ASS at RAO – grey line; H_x - black line, intensity of ASS at AARI intensity -red line)

Available online at www.sciencedirect.com
SCIENCE DIRECT®
Physics Letters A 325 (2004) 381–388
PHYSICS LETTERS A
www.elsevier.com/locate/pla

Radio tomography and scintillation studies of ionospheric electron density modification caused by a powerful HF-wave and magnetic zenith effect at mid-latitudes

E.D. Tereshchenko [a], B.Z. Khudukon [a], A.V. Gurevich [b], K.P. Zybin [b,*], V.L. Frolov [c], E.N. Myasnikov [c], N.V. Muravieva [c], H.C. Carlson [d]

[a] *Polar Geophysical Institute of the Kola Scientific Center, Russian Academy of Sciences, 183010 Murmansk, Russia*
[b] *P.N. Lebedev Institute of Physics, Russian Academy of Sciences, 117924 Moscow, Russia*
[c] *Radiophysical Research Institute, 603950 Nizhniy Novgorod, Russia*
[d] *Northwest Research Associates (NWRA), Washington, DC, USA*

Received 25 February 2004; accepted 5 March 2004

Communicated by V.M. Agranovich

Abstract

Observations of the ionospheric electron density modified by a powerful wave of the Sura HF heating facility were carried out in Russia at middle latitudes in August 2002. Amplitude scintillations and variations of the phase of VHF signals from Russian orbiting satellites passing over the heated region along the chain of three satellite receivers have been recorded. The experimental data were converted to electron density maps using a stochastic inversion. Tomographic measurements conducted during a low magnetic activity revealed that HF powerful waves can produce significant electron density disturbances up to heights significantly exceeding altitudes of the F layer peak. Both large-scale plasma enhancements and small-scale density irregularities can be generated by the HF radiation. Wavy density structures were also observed within a sector which is much wider than the area covered by the main lobe of the heating antenna. Small-scale density irregularities are mostly field-aligned although large-scale structures can be detected within a much larger area. A distinctive peculiarity of electron density changes occurred during heating is producing a zone of low density inside the area illuminated by the antenna beam. The results indicate that satellite radio tomography and scintillation measurements are effective diagnostic techniques giving a valuable information to studies of effects induced by HF modification. The complete system of plasma density disturbances describing by the theory of "the magnetic zenith effect" has been for the first time studied in this Letter. A good agreement between the theory and experimental data has been obtained.

1. Introduction

Satellite radio tomography is an effective, modern and inexpensive method producing maps of electron density (vertical cross-sections of the density distribution) which can cover a wide region of the ionosphere

* Corresponding author.
E-mail address: zybin@lpi.ru (K.P. Zybin).

0375-9601/$ – see front matter
doi:10.1016/j.physleta.2004.03.055

within a relatively short time [1]. There is a growing interest in these studies and new networks and instruments are being constructed as well as new measurements suitable for tomographic measurements are being performed. In a tomographic experiment, radio signals from orbiting satellites are observed simultaneously at several ground-based receivers carrying out difference Doppler measurements which are arranged in a chain close along the satellite movement. This method makes use of the phase difference of two coherent radio waves, which is proportional to the integral of electron density along the ray from the satellite to the receiver. During the passage of the satellite, these integrals can be measured along a great number of rays crossing each other in the ionosphere, and thus two-dimensional profiles of the electron density in the vertical plane above the receiver chain can be reconstructed by means of tomographic inversion.

Modification of the ionosphere by HF radio waves is an efficient method for studying physical processes in the ionosphere. When the ionosphere is affected by a powerful radiation, fast heating of the plasma causes drastic changes in the energy distribution. The resulting instabilities can provide appropriate conditions for generation of artificial ionospheric irregularities.

Investigations using satellite radio probing have shown that if the line-of-sight between a receiver and a satellite is close to the direction of the magnetic line then significant changes of the satellite signal phase, i.e., changes in the electron content along the ray, as well as amplitude scintillations can be observed [2–5]. Studies showed that heating the ionosphere can produce electron density irregularities with scale sizes from tens of meters up to tens of kilometers [2,4] and investigating the spatial location and dynamics of the heated plasma clouds helps in deeper understanding the physical processes controlling the ionospheric conditions. The generation, structure and the evolution of the artificial irregularities are strongly dependent on the natural conditions in the ionosphere. When investigating the heated ionosphere, it is therefore of great importance to know the state of electron density within a larger region both before and during heating periods. Unlike other methods, ionospheric radio tomography is capable of mapping the electron density within a large region at a temporal resolution of about 1–2 hours within a large spatial region.

The ray (phase) tomography applied in ionospheric modification experiments can produce maps of large electron density structures with scales from several km to about a hundred of km. Since the tomographic receivers can also record the amplitude scintillations of the satellite signals then, in common with large-scale irregularities, also small-scale inhomogeneities (less than a kilometre in size) can be studied using a rather new method developed at the Polar Geophysical Institute (PGI) in Murmansk, Russia [6,7] which is based on the amplitude scintillation analysis of satellite radio signals therefore allowing to analyze a relation between small-scale irregularities and large-scale plasma structures. In August 2002 an experiment on the ionospheric modification by powerful HF waves was carried out at mid-latitudes of Russia. This work reports results of this experiment.

The complete system of electron density disturbances is examined and the experimental evidence *of the magnetic zenith effect occurred during the HF modification of the mid-latitude ionosphere* has been established in this Letter. The magnetic zenith effect predicted by the theory is a result of a set of non-linear processes accompanying the propagation of powerful radio waves in the ionosphere [8]. The *resonance instability* developing in the upper hybrid plasma resonance leads to formation of a large number of small-scale density depletions—*striations* which align the Earth's magnetic field. Two main features of the striations are: the strong enhancement of electron temperature inside striations $T_e > (2\text{–}4)T_{e0}$ and a permanent small deficit of plasma density $N_1 = N_e - N_0 > (0.02\text{–}0.1)N_0$ because the average electron density is reduced during the excitation of a large number of striations. This fact results in a new non-linear process—*self-focusing on striations* of the pump wave E_0 [9]. In turn the enhancement of the field E_0 in the focusing region leads to an increase of the striations. Therefore, there exists a close non-linear relation between striation generating and focusing a pump wave which results in a formation of *non-linear structures* in the disturbed ionospheric region [9]. A significant peculiarity of self-focusing on striations is related to the fact that this process *is strongly anisotropic* because the focusing effect takes place in the plane perpendicular to the magnetic field only. Thus, the direction parallel to the Earth's magnetic field is singled out and all non-linear structures are self-organized due to self-focusing on

striations which are aligned by the magnetic field. One of such structures is a soliton which is a solution describing the striation of so-called "bunch" structures. The soliton-like pump wave field distribution was described in [9]. It was shown that in the high-latitude or mid-latitude ionosphere self-focusing leads to the formation of the large non-linear structures aligning the magnetic field and consisting of a number of closely packed solitons or bunches of striations [10]. A pump wave which is trapped and focused inside this structure propagates along the magnetic field lines toward the magnetic zenith. This process is called as the magnetic zenith effect. It is accompanying by strong ohmic heating of plasma electrons in the focused region. The density depletion inside striations and bunches formation were established in the low latitude ionosphere during in situ rocket experiments at Arecibo [11]. The ohmic heating optic emission and the indication of a large-scale plasma structure existence in the magnetic zenith direction of the high-latitude ionosphere were described in [12–14]. For the first time, the complete system of plasma density disturbances of the mid-latitude ionosphere both of large and bunch scales has been studied in the present Letter by using the radio tomography and scintillation methods.

2. Experimental setup

The heating campaign was arranged from 19 to 30 August, 2002 by means of the Sura HF heating facility located not far from Nizhniy Novgorod. The facility has 3 transmitters, each has 250 KW of the radiated power in the continuous wave mode (CW) and it can generate up to $P_0 = 15$–30 MW of CW at 4.785–9.310 MHz. The antenna system has 3 antenna arrays 300 by 100 m, each consisting of 4×12 wide-band cross-dipoles. During the reported sessions the facility was operated in CW mode at either 4.30 or 4.310 MHz for about 14–20 min when satellites passed heating regions. The facility transmitted radiation either vertically or the antenna beam was tilted by 12° to the south close to the geomagnetic line direction which is about 19°. Three tomographic receivers were installed under the heating region on a chain lying approximately along a satellite pass moving from the north, thereby making it possible to study the temporal features and the spatial electron density distribution both

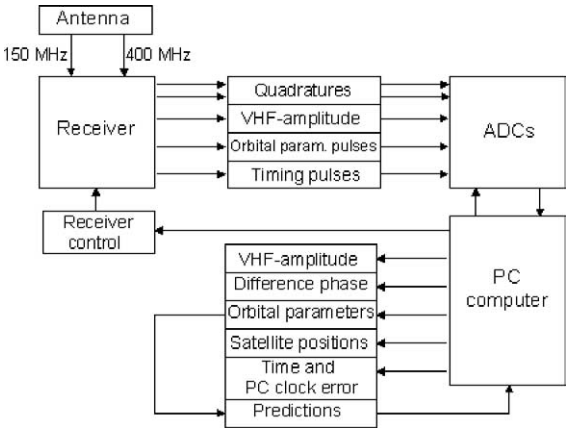

Fig. 1. Structure of the satellite receiving system.

in the F and E regions, within and outside the heating cone. The central site Sura (56.13° N, 46.1° E), the southern site Sechenovo (55.23° N, 45.87° E) and the northern station Arya (57.5° N, 46.0° E) were spaced by about 100 km (Sechenovo–Sura) and 150 km between Sura and Arya. In total 20 records from about 10 Russian satellites have been made at each site during the heating experiment.

The receivers measured radio signals from Russian navigational satellites flying at about 1000 km, the inclination of their orbits is 83° and the orbital period is 105 min. The receivers recorded the signals during 18 min for each satellite pass (±9 min from the time of closest approach). Only passes of satellites with such a high elevation that they could cross the ionospheric region illuminated by the main lobe of the heating facility were used in the tomographic analysis. Southward passes of such satellites lie close along to the receiver chain, which makes it possible to determine the electron density of the ionosphere in the vertical plane above the chain. PGI has constructed mobile automatic receiving systems capable to measure the relative phase between the VHF and UHF waves and the amplitude of the VHF signal. The block-diagram of the system is presented in Fig. 1. The receiving antenna is a combined system of two simple cross-dipole pairs fixed above a ground screen which provide circular polarizations matched to those on the satellite. The receiver has two channels, one for each frequency. The different coherent frequency pairs at around 150 and 400 MHz transmitted by different satellites, each with 3/8 frequency ratio between the two coherent

Table 1
The parameters of the satellite data and HF operation modes for the selected sessions

Heating session No.	Day and the satellite record start time (UT)	Coordinates of the satellite location closed to Sura (azimuth-elevation)		Heated time (UT)	Radiation modes	Heating antenna beam-width	Beam pointing
1	23.8.2002 22:19	197°	88°	22:10–22:33	CW, $3P_0$ 4.30 MHz	10.2°	−12°
2	26.08.2002 22:00	225°	87°	21:54–22:14	CW, $3P_0$ 4.30 MHz	10°	0°
3	29.08.2002 21:41	213°	85°	21:36–22:52	CW, $2P_0$ 4.31 MHz	13°	0°
4	30.8.2002 19:17	104°	82°	19:15–19:30	CW, $2P_0$ 4.31 MHz	13°	0°

carriers, are derived by an internal frequency synthesizer which is fed by a stable oscillator. The receiver performs signal searching and employs an analogue phase-locked loop to track the received UHF signal as its Doppler shift changes during the satellite path. The both signals are coherently mixed down to their intermediate images at about 2 MHz. These two RF signals come to a quadrature detector giving two final complex outputs containing both the dispersive phase and the VHF amplitude. The beacons employ carrier modulation containing the time, the satellite positions with the corresponding rates of their change, and the orbital parameters (OP) [15]. The receiver has a modulation decoding device which extracts the binary modulated words from the sub-carriers. The analogue outputs are sampled at a rate of 50 samples per second and stored on hard disks of an on-line PC computer. A signal processing program (SPP) automatically performs the following: (1) reading preprocessed prediction times and providing ON/OFF of data acquisition; (2) switching the receiver synthesizer to a defined frequency values corresponding to the beacon carriers; (3) controlling the ADCs and reading the outputs: the quadratures, the analogue VHF-amplitude from a separate amplitude detector, OP, satellite positions, their changes and time synchronization pulses; (4) decoding the binary modulation words and verifying their check-sums; (5) computing a shift between the satellite synchronization time and the PC's time value. (6) Finally, the SPP stores the sampled data to the PC's disk in a binary raw data file.

3. Experimental results

Four combined heating-tomographic sessions have been selected for reporting in this Letter and all the relevant experimental parameters for the sessions are given in Table 1. The period of these observations turned out to be favourable for investigating artificial irregularities, because the natural ionosphere was rather regular at that time. This is indicated by quiet geomagnetic conditions (the Kp index was usually close to 3). The raw satellite data were inverted into electron density plots using stochastic method [16]. The goal of this approach is to find the most probable values of the unknown electron density values by means of stochastic inversion once the measurement is known. This formalism provides including a priori information or additional measurements obtained by other instruments like an incoherent scatter radar or ionosonde. The bi-Gaussian regularization profiles have been usually applied as an initial ques in obtaining the electron density distributions. In the analysis an inversion grid is defined on the vertical plane above the receiving chain, and the inversion results are electron densities at the grid points. Due to the Earth curvature, the grid elements (pixels) have annular rather than rectangular shapes and their horizontal–vertical size in the F layer is usually about 30×20 km.

In the ray tomography the measured phase φ of the probing radio signal is proportional to the total electron content (TEC) along the ray from the satellite radio source to the ground-based receivers, i.e., $\varphi \propto \int Ne\,ds$, where Ne is the electron density and ds is the ray element. We assume that random electron density fluctuations δNe (artificial irregularities due to heating) can be separated from the effects of the average density $\langle Ne \rangle$ in the simple form $\delta Ne = Ne - \langle Ne \rangle$ and studied therefore separately. Fig. 2 show the tomographic reconstructions of Ne for the selected sessions. The positions of the receiving sites Sechenovo, Sura and Arya are indicated by the circles on the x-axis. The dashed lines define the beam-width

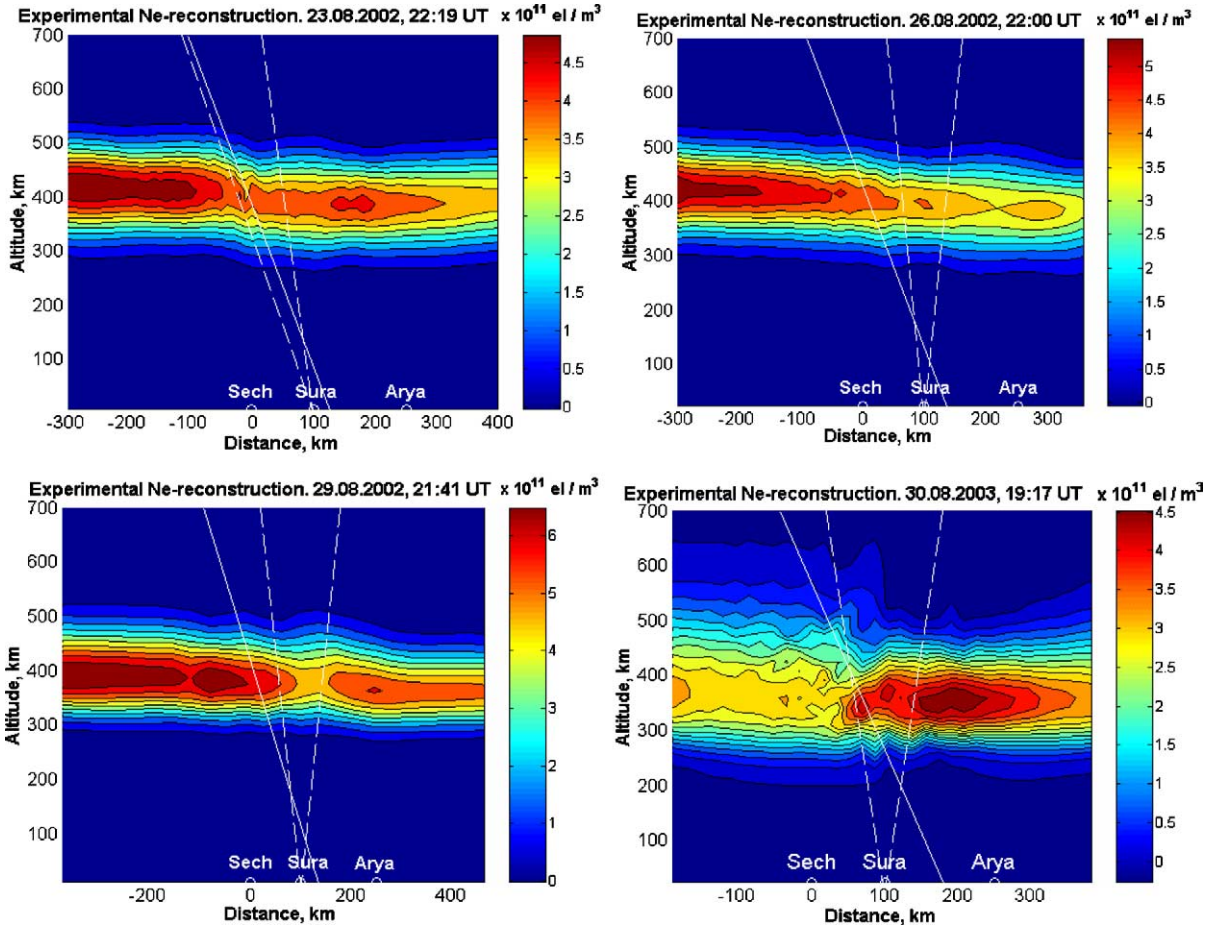

Fig. 2. The tomographic reconstructions of *Ne* for the selected sessions shown in Table 1.

of the heating antenna and the solid line indicate the direction of the geomagnetic field. It can be seen that HF heating considerably affects the ionosphere resulting noticeable changes in the electron density distribution practically throughout the ionospheric body up to heights much higher than the F layer peak altitudes. The figures show wavy density structures with fronts tilted southward (like propagating waves) occupying quite a large region which is much larger than the area covered by the antenna beam of the heating facility. A significant enhancement of large-scale irregularities along the magnetic zenith direction can be clearly seen in the top left panel of Fig. 2. Note, that the beam was tilted by 12° to the south at this case.

In contrast to the large-scale irregularities mostly contributing to phase fluctuations, the small-scale irregularities mainly affect the amplitude scintillation of radio signals and their parameters can be determined from the amplitude data using the statistical method [6]. Fig. 3 presents the difference electron density fluctuations for distinguishing changes between plasma enhancements of about 10–100 km in size as well as small-scaled ones. This fluctuation term has been obtained by subtracting the smoothed experimental reconstruction matrix inversed by employing the low-pass filtering (smoothing) to the experimental phases from the density matrix *Ne* made directly by using the measured phases. The upper imposed plot demonstrates the changes of the variance of the logarithmic relative amplitude fluctuations obtained from the amplitudes at the sites. From the composed figure we can estimate the variance values for a certain

ray by drawing a line from a receiver location on the bottom x-axis to the upper x-axis of the variance plot. The small-scale irregularities are assumed to lie between the satellite and the receiver confined by the region $z_u < z < z_d$. Here z_u, z_d are the lower and upper boundaries of the irregular layer. The signal strength observed on the ground is affected by irregularity scattering at or close to the z-axis. The variance of the logarithmic relative amplitude fluctuations σ_χ^2 is related to the spectral density of the electron density fluctuations Φ_N by the following form [1]:

$$\sigma_\chi^2 = \frac{\lambda^2 r_e^2}{4\pi^2} \int_{z_u}^{z_d} \int_{-\infty}^{\infty} \int \Phi_N(\vec{k}, z)\Big|_{\kappa_z=0} \times \sin^2 \frac{R_F^2(\kappa_x^2 + \kappa_y^2)}{4\pi}\, d\kappa_x\, d\kappa_y\, dz,$$

where $\chi = \ln(A/A_0)$ is the logarithmic relative amplitude, A is the field amplitude passed the irregular region, A_0 is the amplitude in the absence of irregularities, $R_F = [\lambda z(z_0 - z)/z_0]^{1/2}$ is the radius of the principal Fresnel zone, λ is the wave length, $r_e = 2.82 \times 10^{-15}$ m is the classical electron radius, κ_x, κ_y are the wave vector components perpendicular to the propagation direction, κ_z is the wave vector component parallel to the propagation direction, and z_0 is the distance between the satellite and receiver.

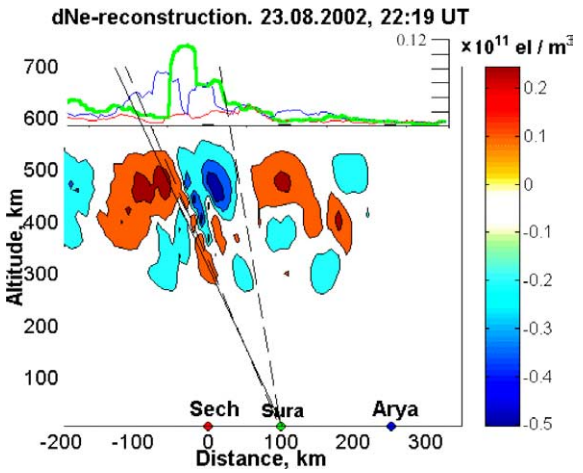

Fig. 3. The composed plot of the difference electron density fluctuations (the bottom figure) and corresponding changes of the logarithmic relative amplitude fluctuations (the upper curves).

Fig. 3 shows that the increase of the amplitude scintillations corresponds to the low density zone located inside of the area covered by the heating antenna beam. A low variance level in Sechenovo located southward from the heating region (which has a higher angle with the magnetic field direction) demonstrates that the spectral density Φ_N is anisotropic and the ir-

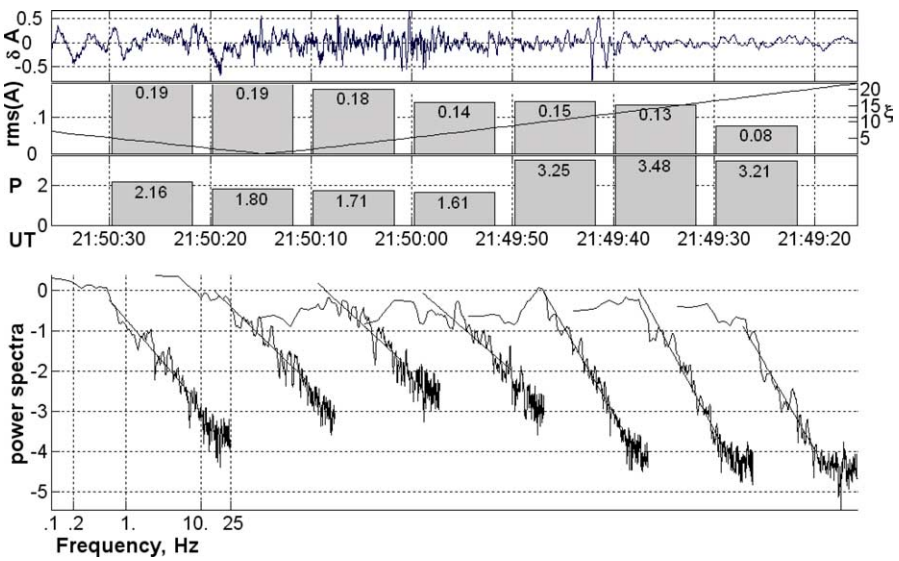

Fig. 4. A registration of satellite signals at 150 MHz and the spectral analysis of data obtained at the site Arya on August 29, 2002 at 21:49:15–21:50:35 UT.

regularities are field-aligned. The similar effect can be seen on plots of the other sessions.

A more detailed study of small-scale irregularities spectrum can be obtained from both amplitude and phase fluctuations. Fig. 4 demonstrates the results of a spectral analysis of 150 MHz amplitude fluctuations.

The top panel shows a fragment of time dependence of 150 MHz amplitude fluctuations $\delta A = (A - \langle A \rangle)/A$ after removing the trends. The direction of satellite movement during this session was from north to south. The patches in the second panel from the top show the root mean square (rms) of relative amplitude scintillations calculated for 20 s time intervals with 10 s overlapping. Time dependence of the ξ angle between the line-of-sight to the satellite and the magnetic zenith direction is shown in the same panel as a continuous line (ξ is in degrees). The third panel from the top displays the power indices of the amplitude scintillation power spectra at the frequency range of 1–10 Hz (equivalent to scales of approximately 0.2–2 km at the altitude 300 km) calculated at the same time intervals as the rms $\Delta A/\langle A \rangle$ indices. The bottom panel presents logarithmic plots of the amplitude scintillation power spectra and the straight lines illustrate the spectral indices approximation. The spectral frequency range between 0.1 and 25 Hz is indicated at the bottom of the left spectrum only and all the rest spectra occupy the same frequency range. The measurements are made near the minimal angle $\xi_{\min} = 0.27^\circ$. One can see from panel 3 that the spectral power index is sharply decreased to values $p = 1.6$–1.8 at the interval approximately corresponding to the region covered by the antenna beam. The power index grows with receding from the magnetic zenith and rapidly reaches up to $p = 3.2$–3.5. Therefore, these results demonstrate a noticeable rise of the number of bunch-scale irregularities located near the SURA magnetic zenith direction.

4. Summary

This Letter demonstrates high possibilities of the satellite radio tomography and scintillation measurements for detecting artificial electron density disturbances produced by Sura HF heating facility located at middle latitudes in Russia. The ionospheric HF modification results in generation of both irregularity families with sizes from about several tens of kilometres to about a hundred of km as well as small-scale ones (less than a kilometre). During quiet geomagnetic conditions when ionospheric disturbances might not be due to natural causes, it seems clear that heating-induced large-scale density variations can be observed by the tomographic method and the anisotropy parameters, especially the anisotropy perpendicular to the magnetic field, can be determined from amplitude scintillations. It is shown that the maximum of small-scale irregularity development happens in the direction parallel to the geomagnetic field lines. However large-scale density enhancements can arise within much larger region above the heating facility up to heights significantly exceeding altitudes of the F layer peak. It was revealed that artificial wavy electron density structures occupying a much larger region than the area covered by the antenna beam of the heating facility can be also generated by the HF heating. Of special interest is the zone of low density located inside the heating antenna beam which mainly contains small-scale anisotropic irregularities producing amplitude scintillations.

A comparison of the results obtained in the present work by using a prediction of the theory of magnetic zenith effect [8] shows the following. According to the considered here theory relating to a new nonlinear process—self-focusing on striations, a powerful pump wave is trapped in soliton like bunch structures and propagates along the Earth's magnetic field in the magnetic zenith direction. Strong ohmic heating of the ionospheric plasma by the trapped wave leads to the creation of large-scale irregularities as well.

The observations described here clearly demonstrate a simultaneous existence of large-scale irregularities and a high number of bunch-scale inhomogeneities located near the magnetic zenith direction. Therefore, the full system of plasma density disturbances determining the magnetic zenith effect has been observed in the heating experiment and a good agreement between the theory and observations has been for the first time established in this Letter.

Acknowledgements

The authors are grateful to R.Yu. Yuric and S.M. Chernyakov for their help in the tomographic campaign participation, to N.Yu. Romanova for making

the analysis of the amplitude data (all they work at PGI) as well as to G.P. Komrakov and E.N. Sergeev from NIRFI for their assistance in the campaign. This work was supported by the Russian Foundation of Fundamental Research grants 02-02-17475, 03-05-64636, 03-05-64637, CRDF-RPO-133, EOARD-ISTC 2236, INTAS 03-51-5583.

References

[1] V.E. Kunitsyn, E.D. Tereshchenko, Ionospheric Tomography, Springer-Verlag, Berlin, 2003.
[2] E.D. Tereshchenko, B.Z. Khudukon, M.T. Rietveld, A. Brekke, Ann. Geophys. 16 (1998) 812.
[3] A. Gurevich, E. Fremouw, J. Secan, K. Zybin, Phys. Lett. A 301 (2002) 307.
[4] E.S. Costa, S. Basu, R.C. Livingston, P. Stubbe, Radio Sci. 32 (1997) 191.
[5] E.N. Myasnikov, N.V. Muravieva , E.N. Sergeev, V.L. Frolov, A.M. Nasyrov, I.A. Nasyrov, V.S. Beley, A.V. Koloskov, Yu.M. Yampolsky, K.M. Groves, Radiophys. Quantum Electron. 44 (2001) 833.
[6] E.D. Tereshchenko, B.Z. Khudukon, M.O. Kozlova, T. Nygrén, Ann. Geophys. 17 (1999) 508.
[7] E.D. Tereshchenko, B.Z. Khudukon, M.O. Kozlova, O.V. Evstafiev, T. Nygrén, M.T. Rietveld, A. Brekke, Ann. Geophys. 18 (2000) 918.
[8] A.V. Gurevich, K.P. Zybin, H. Carlson, T. Pedersen, Phys. Lett. A 305 (2002) 264.
[9] A. Gurevich, T. Hagfors, H. Carlson, A. Karashtin, K. Zybin, Phys. Lett. A 239 (1998) 385.
[10] A. Gurevich, H. Carlson, M. Kelley, T. Hagfors, A. Karashtin, K. Zybin, Phys. Lett. A 251 (1999) 311.
[11] M.C. Kelley, T.L. Arce, J. Saloway, M. Sulzer, T. Armstrong, M. Carter, L. Duncan, J. Geophys. Res. 100 (1995) 367.
[12] T. Pedersen, M. McCarrick, E. Gerken, C. Selcher, D. Sentman, H. Carlson, A. Gurevich, Geophys. Res. Lett. 30 (4) (2003) 1169.
[13] B. Gustavson, T. Sergienko, M.T. Rietveld, F. Honary, A. Steen, B.U.E. Brandstrom, T.B. Leyser, A.L. Aruliah, T. Aso, M. Ejiri, S. Marple, J. Geophys. Res. 106 A 12 (2001) 29105.
[14] M. Rietveld, M.J. Kosch, N.F. Blagoveshchenskaya, V.A. Kornienko, T.B. Leyser, T.K. Yeoman, J. Geophys. Res. 108 (2003).
[15] C.D. Wood, G.E. Perry, Philos. Trans. R. Soc. London A 294 (1980) 307.
[16] T. Nygrén, M. Markannen, M. Lehtinen, E.D. Tereshchenko, B.Z. Khudukon, Radio Sci. 32 (1997) 2359.

On peculiarities of development of artificial ionospheric turbulence excited outside the regions of resonant interactions of HF radio wave with plasma in the Earth's upper ionosphere

V.L.Frolov
Radiophysical Research Instiute, Nizhny Novgorod, Russia
K.M.Groves
Air Force Research Laboratory, Massachusetts, USA

Experiments on ionospheric F-region modification by a beam of HF O-polarized radiation carried out at the Sura heating facility during 1993-2005 are discussed. Based on these experiments the analysis of peculiarities of development of the artificial ionospheric turbulence (AIT) excited outside the regions of the resonant interactions responsible for absorption of the main part of the wave energy is performed. The scheme of additional heating of plasma in the F-region by powerful HF radio wave and the diagnostics of the propagating plasma perturbations by the artificial radiation of the ionosphere (the so-called stimulated electromagnetic emission (SEE)) serves as a basis for the used method of measurements. The analysis of the observed forms of different components of the diagnostic SEE (d-SEE) in prolonged and in short-pulsed schemes of pumping is given. Special attention is focused on consideration of the effects revealed at short-pulsed pumping. In this scheme fast transport processes of perturbations with velocities achieving the thermal speed of electrons and sometimes exceeding it significantly registered by d-SEE manifest themselves in a most clear form. This points out on the importance of taking into account the fluxes of thermal and accelerated electrons in mechanisms of the SEE generation far from the regions of the resonant interaction of powerful wave with plasma. Peculiarities of such type of measurements are discussed and possible tasks for further investigations are determined.

1. Introduction

In the present paper we analyze the peculiarities of development of plasma turbulence induced by the interaction of powerful wave with plasma outside the regions of the resonant interaction where the main part of the wave energy is absorbed and transformed into plasma turbulence. The possibility to determine experimentally the velocities of different types of perturbations excited be powerful radio waves in plasma of the ionospheric F-region is discussed. Here the principal moment is that the interaction with plasma of powerful O-mode HF radio wave is accompanied by the generation of different types of the artificial ionospheric turbulence (AIT). Note, that the AIT is determined by development of a complex of nonlinear phenomena, such as high frequency turbulence (different types of plasma oscillations and waves) and low frequency plasma turbulence (first of all, temperature and plasma density irregularities of different sizes), modification of plasma density profile under the action of pondermotive and thermal pressure forces, acceleration of electrons up to suprathermal energies (which causes additional ionization of plasma and neutral gas emissions), generation of the secondary electromagnetic emissions (in particular, artificial radio emission of the ionosphere, known as the stimulated electromagnetic emission (SEE)), excitation of electric and magnetic fluctuating fields, *etc*. It is important that extensive theoretical and experimental investigations performed during the last thirty years (the main results of which are summarized in a complex of special issues of scientific journals [Radio Sci.. (1974), *9(12)*; J.Atm.Terr.Phys. (1982), *44(12)*; J.Atm.Terr.Phys. (1985), 47(12); Izv.VUZov Radiofizika, (1994), *37(5)*; Izv.VUZov Radiofizika, (1999), *42(7,8)*; Izv.VUZov Radiofizika. (2005), *48(9)*]) allowed us to work out a fairly complete picture of development of interaction of powerful radio waves with plasma and the generation of the AIT. It gives us an opportunity to embark on a next stage of investigations. The main goal of this stage is to develop new diagnostic methods based on AIT for different processes in magnetized plasma. In such case the ionosphere is considered as a natural plasma laboratory in which it is possible to investigate a variety of problems.

The investigations considered in the present paper were stimulated by some results, obtained earlier in heating experiments, which have not been completely explained up to now. For example, experiments utilizing the method of HF backscattering have shown that artificial irregularities with sizes $l_\perp \approx 50 - 200$ m transverse to the Earth's magnetic field can occupy the spatial region up to 100 km upward and downward from the level of reflection of the pump wave (PW), practically filling the whole width of the F-region of the ionosphere [Bahmetjeva et al., 1992; Hedberg et al., 1983]. The measurements [Yampolski et al., 1997] carried out with the help of unique radio telescope UTR-2 (Kharkov) with narrow diagram demonstrated that the region occupied by decameter irregularities can have a stratified structure with significant weakening of the irregularity intensity between layers. It is difficult to explain such scales and spacial structure of the ionospheric disturbed volume (IDV) within the mechanism of "spreading" of plasma density irregularities along the magnetic field lines upwards and downwards. Besides that, the measured in [Bahmetjeva et al., 1992] the effective longitudinal velocity of the expanding volume varied in wide limits 10^4 up to $2 \cdot 10^6$ cm s^{-1}, often exceeding the velocity of the longitudinal ambipolar diffusion for perturbations of plasma density. Here it is possible also to mention the results [Bernhard et al., 2001] of the experiments, dealing with the release of chemical reagents in the F_2-region of the ionosphere. Based on these results, it was established that the filling in of the formed "hole" in plasma density takes place with the speed much higher than it follows from the ambipolar diffusion theory. Finally, the measurements of the IDV spatial structure, recently fulfilled with the help of the radio tomography method, have demonstrated that the HF modification of the night ionosphere causes the perturbations of plasma density with sizes ~ 250 – 300 km noticed in wide height interval from the PW reflection level ~ 20 – 100 km up to, at least ~ 600 km [Tereshchenko et al., 2004]. In the same experiments it was established that in the horizontal plane these perturbations occupy the region up to ~ 200 km from the center of the powerful beam, covering the area much larger than the diagram of the HF radiation. It should be mentioned also the experimental results in laboratory plasma [Egorov et al., 1988], where it was shown by direct measurements that «*the process of thermodiffusion of plasma in a magnetic field is accompanied by the excitation of the solenoidal currents that flow in the disturbed and in the backgroumd plasma. The characteristic times of the changes of plasma density is determined by unipolar transport coefficients*». All results mentioned above have stimulated the formulation of the task of more detailed experimental investigation of a complex of problems connected with peculiarities of spreading of perturbations in magnetized plasma. These problems incorporate the following: interaction and mutual transformation of different types of perturbations, including generation and evolution of the secondary plasma turbulence initiated by the propagating in plasma initial perturbations, generated in the regions of intensive (resonant) interaction of powerful radio wave of O-polarization with plasma.

The progress in solution of the formulated task is connected in our experiments with the utilization of SEE for diagnostics of AIT. The performed investigations [Frolov, 1996; Frolov et al., 1996; Frolov et al., 1998; Frolov et al., 2001; Grach, 1985; Grach et al., 1998; Leyser et al., 1993; Leyser et al., 1994; Leyser, 2001; Thide et al., 1982; Sergeev et al., 1998; Sergeev et al., 1999a, Sergeev et al., 1999b; Stubbe et al., 1994; Stubbe and Hagfors, 1997] have shown that SEE is the result of reradiation of the electrostatic plasma oscillations into the electromagnetic waves and gives a print of the processes developing in the IDV. An important moment is that artificial small-scale (with $l_\perp \leq 30 - 50$ m) field-aligned ionospheric irregularities (ASSI), from one side, cause the determinative influence on generation of such thermal components as downshifted maximum (DM) and broad continuum (BC) and determine the properties of the source in mechanisms of their formation. From the other side, due to anomalous absorption (AA) of the electromagnetic waves outgoing from the IDV such irregularities cause the attenuation of these and other SEE components playing a role of a depressant. This property of SEE serves as a foundation for the development of methods for diagnostics of high frequency and low frequency

components of AIT [Erukhimov et al., 1988; Frolov et al., 1994; Frolov, 1996; Sergeev et al., 1998; Sergeev et al., 1999a, Sergeev et al., 1999b]. As DM and BC are the most powerful and usually observed components in SEE spectrum and mechanisms of their generation are explored in a most detailed form (see, for example [Grach, 1985; Grach et al., 1998; Gurevich et al., 1997; Leyser, 2001; Leyser et al., 1994; Stubbe and Hagfors, 1997] they are most often used in our measurements for diagnostics of AIT. Besides them, when the frequency of the pump wave is close to one of harmonics of electron gyrofrequency in the region of positive frequency shift from f_{PW} the generation of broad wide-range emission, known as broad upshifted maximum (BUM), is observed [Frolov et al., 1996; Frolov et al., 1998; Leyser et al., 1993; Leyser, 2001; Stubbe and Hagfors, 1997]. We also use this component for diagnostics of AIT.

In the present paper the generalization of the results of investigations fulfilled at the SURA heating facility during the period 1993 – 2005 is presented. Some experimental results partly have been published in [Frolov et al., 1996; Frolov, 1996; Frolov et al., 1997b; Frolov et al., 2002; Frolov et al., 2005b, Frolov et al., 2006]. Neverthelesss, some of them are also included in the present paper for more detailed and comprehensive consideration of the observed phenomena taking into account the whole amount of the obtained up to now experimental data, which influence in some cases the interpretation of the data.

The SURA heating facility is situated in the Nizhny Novgorod region near Vasilsursk. It includes three transmitters PKV-250, each of which is loaded on its own sub-antenna array, which consists of 4×12 broadband crossed dipoles. Each of such modules can work independently radiating waves of O- or X- polarization in a selected schedule in time for a given frequency and power of the pump wave. The effective radiated power of one module is 15 – 30 MW in the frequency range 4.3 – 9.5 MHz, increasing with the growth of the radiating frequency. Such configuration appeared to be convenient for fulfillment of measurements according to the so-called scheme of "additional heating", the peculiarities of which are considered in the second section of this work.

In the discussed measurements the registration tools was used that included professional HF radio receivers "Katran", the spectrum-analyser HP 3585A, and a computer (Pentium). To register the receiving signals in the experiments destined for exploration of the SEE dynamical properties fast analog/digital converter of the type AT-MIO-16E-2 (National Instruments) with specially worked out program software based on C^{++} and LabVIEW was utilized. The used spectrum-analyzer allows to measure SEE spectrum in the frequency band 100 – 400 kHz within ~ 1 – 10 s. Time resolution while receiving SEE signals at the fixed frequencies, no doubt, is much higher. It comprises ~ 0.3 ms, which allows us to fulfill detailed investigations of the development and the relaxation of high frequency plasma turbulence (see, e.g. [Sergeev et al., 1998]) and provides the required time resolution (~ 5 ms) in the measurements according to the scheme of additional heating.

Our paper has the following structure. In its second section the method of measurements including the scheme of additional heating of the ionosphere is discussed. In the third section the results of investigations concerning the influence of additional heating of the ionospheric plasma on characteristics of the diagnostic SEE for comparatively long periods of PW radiation are analyzed. Here also the influence of the diagnostic wave on interaction of the pump wave with plasma is briefly analyzed. Possible influence of the lower ionosphere (*D* and *E* regions) on the results of measurements is discussed in the fourth section. In the fifth section some peculiarities of the behavior of different SEE components at the additional heating of plasma are considered. It is important to take into account these peculiarities for correct interpretation of the observed phenomena. The sixth section is devoted to the analysis of the effects observed during

ionosphere short pulse pumping. In the last part we discuss the obtained results and make some conclusive comments.

2. Method of Measurements Utilizing the Scheme of «Additional Heating» of the Ionospheric Plasma

The method of «additional heating» of the ionospheric plasma with the help of the second powerful radio wave includes the following [Frolov, 1996; Frolov et al., 1997a]. In such measurements one pump wave of O-mode polarization fulfills the role of the diagnostic wave (DW). It is radiated continuously or in a quasicontinuous schedule and it is used for diagnostics of SEE. Its power is chosen from the measurements requirements in such a way that the artificial emissions initiated by this wave should be fairly stable. At the same time the emissions should not be saturated. The latter is required to reflect in a most adequate manner the variations in the conditions of interaction between powerful wave and plasma. The second wave (pump wave (PW)) is used to create additional perturbations in the ionosphere. Note, that its schedule of radiation in time, frequency, power, and polarization are selected taking into account the conditions for the solution of the formulated task. Changing these parameters of the PW we are able to create artificial perturbations of the selected type with certain and controlled properties at a given distance above or below the region of SEE generation by DW (or diagnostic SEE (d-SEE)). These perturbations spreading along the magnetic field lines enter the region of interaction of the DW with plasma where they change the development of the excited SEE. This should be reflected in the changes of the SEE characteristics. Such changes allow us to discuss the influence of different factors (e.g. ASSI, temperature T_e, accelerated electrons, *etc*.) on generation of different emission components of and, hence, the development of the corresponding plasma instabilities. This scheme of measurements also makes it possible to investigate the evolution and spreading of additional perturbations. Note, that in such experiment the power of the DW should be higher than the threshold for the development of instabilities, which cause SEE generation. Due to this the DW cannot be considered as a «diagnostic» wave in a usual sense because it itself causes appreciable perturbations in the ionospheric plasma. Hence, its influence should be taken into account at the stage of preparing the experiment and by interpretation of the results of the performed measurements. This is the peculiarity of the method of «additional heating ».

In experiments with additional heating of the ionosphere when there are no any special tasks the selected frequency difference between the DW and PW, as a rule, is no less than 200 – 300 kHz. This allows us to exclude the spatial overlapping of their resonance regions (the regions where parametric instabilities are excited and high frequency and low frequency plasma turbulence is generated [Erukhimov et al., 1987]. Also, it makes possible to reduce up to the minimum their mutual influence, for example, due to the development of the effect of anomalous absorption (AA). Because of this the scheme of additional heating differs from the scheme of two frequencies pumping, in which the difference in frequencies is, as a rule, ~ 0.1 – 100 kHz. In the latter case the regions of the resonant interaction with plasma overlap in space, which causes strong nonlinear interaction and mutual influence of the radiated waves [Frolov et al., 2005a].

Summarizing the result of the already performed experiments with utilization of the scheme of additional heating of plasma by powerful wave [Erukhimov et al., 1988; Frolov, 1996; Frolov et al., 1997a; Frolov et al., 2002], we are able to make a statement that the development of the observed phenomena depends on such factors as:

- Power of the diagnostic wave (DW) used for SEE generation;
- Power of the pump wave (PW) that induces additional plasma perturbations;
- The scheme of radiation of PW pulses in time;
- Relation between frequencies of the PW (f_{pw}) and DW (f_{DW});

- Ionospheric conditions and the prehistory of ionosphere modifications, *etc*.

Determination of the degree of influence of each of these factors on the results of measurements in each concrete case is a separate task. The totality of solution of this task determines to a significant extent the correctness of the following interpretation of the obtained data. This is the principal moment of utilization of this method for AIT diagnostics.

In conclusion it should be mentioned that while utilizing SEE for diagnostics of AIT it is important to control the DM component (which is well-singled out and practically always observed at frequencies shifts $\Delta f \approx -(9-15)$ kHz). Indeed, the DM evolution is directly determined by the development of ASSI. This can be used for separation in time of the developing in plasma processes. Also it can be used to single out among other factors the influence of ASSI with $l_\perp \leq 30$ m on generation of different SEE components and the development of the turbulence as a whole [Erukhimov et al., 1988; Frolov et al., 1994; Sergeev et al., 1998; Sergeev et al., 1999a].

3. Behavior of d-SEE for Prolonged Radiation of PW

In this section we consider the results of measurements carried out on 28 March 1996 (T=13:15 – 15:15 LT). The DW with the effective radiated power $P_{eff} \approx 2$ MW was radiated in the schedule: 3 min – on, 1 min – off at the frequency 4595 kHz (4580 kHz at the end of the measurements cycle). The PW frequency changed in the band from 5105 up to 4300 kHz with a step approximately equal to 100 kHz [Frolov et al., 2002]. The reflection height of DW was 200 – 220 km, slightly increasing during the measurements. Pause with duration of one minute made it possible to start the DW heating closely to the "cold start" conditions. In this case aftereffects caused by the previous switching on of DW radiation were weak enough. In the discussed measurements the PW with the power ~ 60 MW was switched on for 30 s after 30 s the DW started to radiate. Figure 1 on eight panels *a* – *h* presents the dynamics of the amplitude behavior of the reflected from the ionosphere DW signal (bottom oscillograms on each panel), and also amplitudes of the signal in the region of DM at the frequency shift $\Delta f = -10$ or -11 kHz (middle oscillograms) and in the region of BC at the frequency shift $\Delta f = -23$ or -29 kHz (top oscillograms). As the receiving point was close to the heating facility the signal at the frequency f_{DW} was the sum of the earth and the sky waves. Note, that amplitudes of these two waves for the measurements performed in daytime conditions are comparable. This causes strong interference beating of the amplitude of the registered signal that takes quasisinusoidal form while the phase variations of the wave reflected from the ionosphere are smooth enough. Note, that the attenuation of the signal at the input of the receiver was 6 db for all séances of measurements except those with $f_{PW} = 4595$ kHz (see, Figures 1*e*,*f*), where it was 12 db during the radiation of the PW, and that attenuation was absent only during the radiation of the DW.

First let us consider presented at the panel e the results of measurements for $f_{DW} = f_{PW} = 4595$ kHz and $P_{DW} \approx 2$ MW. Here d-SEE before the PW is switched on has very weak intensity. This witnesses that the selected power of the DW only slightly exceeds the threshold power for the emission generation. Spectral measurements have shown that at this stage of the development, the d-SEE spectrum for the negative frequency shifts corresponds to a component without emphasized structures, like DM and BC. Such a component is called the thermal narrow continuum (NC_{th}) [Frolov et al., 2005b]. The DM and BC structures appear on the background of the NC_{th} only after the additional heating is switched on and remain in the spectrum of the d-SEE after the PW is turned off. This points out on the sharp increase of the ASSI in the region where the thermal emission components are generated. As it is seen from the figure, in the dynamics of the d-SEE it is possible to single out at least five stages of emission evolution:

1) The observed strong burst of the emission intensity just after the additional heating is switched on. This burst is the result of the increase of the generated emissions due to the sharp growth

of the electromagnetic wave intensity in the region of its interaction with plasma in the presence of the ASSI induced by the diagnostic wave.

2) Fast (within the period ~ 2 – 3 s) decrease of the emission intensity during the PW pulse (the overshoot-effect). It is supposed that this effect is connected with the growth of the ASSI intensity in the region of PW interaction with plasma and with the influence of the ASSI on generation and intensity of the emissions outgoing from the IDV [Sergeev et al., 1999a];
3) Sharp decrease of the d-SEE intensity after the PW is turned off to the level much lower than the stationary level of emissions induced by the DW. This effect is determined by the decrease of the electromagnetic wave intensity in the region of its interaction with plasma for preserving at the beginning intensive ASSI and, hence, strong AA of the emissions out going from the IDV [[Sergeev, 1999b];
4) The restoration of the emission intensity up to the level determined by the power of the DW (here during the period ~ 10 – 15 s) connected with the decrease of the ASSI intensity during the transition to the lower power of pumping and, as a consequence, the decrease of the AA level;
5) Subsequent small and smooth decrease of the emission intensity between the PW pulses which is caused by two reasons: gradual change of the ASSI spectrum in the case when only the radiation of the DW is used for plasma modification and by the influence of aftereffects caused by the radiation of the PW.

As have shown our numerous measurements, for comparatively long and powerful pulses of the PW (for $\tau_p \geq 3$ s and $P_{PW} \geq 5 - 10$ MW) when the ASSI spectrum practically achieves its stationary state during the radiation of the PW, the observed smooth (for times $\geq 1 - 5$ s) changes of the DM and BC intensity are determined mainly by the changes of the ASSI intensity in the region of interaction of the powerful radio wave with plasma [Sergeev et al., 1999a, Sergeev et al., 1999b]. Significant distinction in the level of the SEE intensity for its DM and BC components before and after additional heating is the result of the hysteresis effect. This effect leads to higher level of the ASSI in the IDV and, as a consequence, more intensive generation of the DM and BC [Erukhimov et al., 1978; Hedberg et al., 1986]. From the temporal variations of the d-SEE intensity the characteristic times of the ASSI development can be estimated as 2 – 6 s, and their relaxation lasts for 10 – 15 s. Then, following [Frolov, 1996; Frolov et al., 1997b; Nasyrov, 1991] it is possible to conclude that the ASSI with $l_\perp \approx 10 - 20$ m should be responsible first of all for the observed variations of the emission intensity.

On the panel *f* the result of similar measurements but for lower power level of the DW $P_{DW} \approx 0.6$ MW is presented. Note, that in this cycle in contrast with other cycles the PW was radiating during 60 s. In comparison with the case for $P_{DW} \approx 2$ MW discussed above and presented at the panel *e*, dynamics of the d-SEE shows here the formation of the maximum in the signal intensity after ~ 8 s the PW was turned off (this effect is more pronounced for the DM). According to the increase of the amplitude beating of the receiving DW amplitude, this effect corresponds to the relaxation of the AA in the IDV (or the relaxation of the decametric ASSI [Frolov, 1996; Frolov et al., 1997b, Nasyrov, 2001]. This time is slightly shorter that the restoration time of d-SEE signal for $P_{DW} \approx 2$ MW. The latter is easily explained by stronger aftereffects and by support of the ASSI intensity after the PW with high power is turned off. Simultaneously the stationary intensity of the ASSI after the additional heating is turned off remains at the level sufficiently higher than that one before the PW was turned on. In the case of the lower level of the DW power ($P_{DW} \approx 0.6$ MW) the conditions for support of the turbulence at high level are not fulfilled and the d-SEE intensity gradually decreases practically to its level that was before the PW was turned on, but with the change of the emission spectrum. So, the performed measurement at different powers of the DW have shown quite clearly that at the power level $P_{DW} \approx 2$ MW, for which this cycle of measurements was carried out, there was definitely strong influence of the DW radiation on the d-SEE behavior after the PW was turned off.

After the comments mentioned above, let us start to discuss experiments in which $f_{PW} > f_{DW}$. The results of the measurements for f_{PW} = 5105 KHz ($\delta f = f_{PW} - f_{DW}$ = 510 kHz, the height distance between the reflection levels of the PW and the DW comprised $\Delta h \approx 50$ km) are presented in Figure 1*a*. Here with the delay $\Delta t \leq 0.5$ s after the PW was turned on, during ~ 3 – 4 s gradual decrease of the SEE amplitude was observed, but ~ 10 s after the additional heater began to operate, gradual growth of the emission intensity occurred. The emissions reached their saturation level practically at the end of the 30s PW pulse. Here the growth of the d-SEE intensity during the pulse of the PW (in this case of the DM and BC intensities) can be related (see, e.g. [Sergeev et al., 1999a]) to the ASSI amplification in the region where the emissions were generated. In this case the reasons that cause the decrease of the NC_{th} intensity during the first several seconds after the PW was turned on should be explained by other factors. Below in the sixth section while considering the effects observed during short-pulse pumping we'll return to this problem. It should be mentioned that after the PW was turned on, the fastest quasiperiodic oscillations of the DW appear. This is the evidence that the density profile of the ionospheric plasma changes under the action of the powerful radio wave [Berezin et al., 1991].

Let us consider now the peculiarities of variations of the d-SEE intensity after the PW is turned off. Here with the delay $\Delta t \leq 0.5$ s the growth of d-SEE intensity is observed. This intensity achieves its maximum value after ~ 13 s for the DM and ~ 25 s for the BC. Thereafter the emission intensity slowly decreases to some stationary level which is formed at the end of two-three minutes of the DW radiation. According to [Erukhimov et al., 1988; Frolov et al., 1994; Sergeev et al., 1999a, Sergeev et al., 1999b] the growth of the d-SEE intensity should be determined by the decrease of the AA for emissions outgoing from the IDV. This in turn is connected with the changes in intensity and spectral characteristics of the ASSI in the region of d-SEE generation in the transition stage from the state when the additional heating is turned on to the stage when only the DW is radiated. Aftereffects and changes of the ASSI spectral characteristics also cause small decrease of the d-SEE intensity during the transition to the stationary state. From the conclusions made above for the case $f_{PW} = f_{DW}$ = 4595 kHz, it is clear, that the action only of the DW radiation can cause strong influence. It should be mentioned that variations of the d-SEE intensity (hence the changes of the ASSI characteristics) are registered much quicker after the PW is turned on than after it is turned off. This can be caused by the fact that in the case of a more intensive turbulence the mechanism of influence of the perturbations created by the PW on ASSI generation is changed.

The results of measurements presented in Figure 1*a* allow us to estimate the vertical transport velocity for the perturbations induced by the PW (to be more correct, their transport velocity along the Earth's magnetic field due to the fact that plasma in the F-region of the ionosphere is strongly magnetized. The deviation of the magnetic field line from the vertical direction for the SURA heating facility is 19°). Time delay $\Delta t \leq 0.5$ s for the fastest response of the DW on the PW turning on and off (taking into account the difference of the reflection heights for the PW and the DW $\Delta h \approx 50$ km) it is easy to obtain that $V_{\parallel} \geq 10^7$ cm s^{-1}. This value appears to be close to the thermal velocity of electrons $V_{Te} \approx 2 \cdot 10^7$ cm s^{-1} for the conditions in which the experiment was carried out (especially if one takes into account finite time required fort the development of turbulence at reflection levels of the PW and the DW). Similarly, taking into account time delay for the beginning of the d-SEE amplification during additional heating ($\Delta t \approx 10$ s), it is easy to obtain that in this case the longitudinal velocity of the agent responsible for the ASSI amplification should be $V_{\parallel} \geq 5 \cdot 10^5$ cm s^{-1}. Taking into account the finite time required for the development of the turbulence induced by the PW and a time interval for the ASSI growth up to a necessary level in the region of the d-SEE generation for emission registration, we conclude that the discussed velocity can exceed the thermal velocity of ions $V_{Ti} \approx 10^5$ cm s^{-1} by one order of magnitude or more.

The results of measurements for f_{PW} = 5010 kHz, for which δf = 415 kHz and the height distance between the reflection heights of the PW and the DW comprised Δh ≈ 27 km are presented in Figure 2*b*. Here during additional heating the amplification of the d-SEE intensity appears significantly faster (after Δt ≈ 1 s) than in the previous case. From this it follows that there is a strongly nonlinear dependence of Δt on Δh at the distances 30 – 50 km. In comparison with the previous case (δf = 510 kHz) the d-SEE intensity after the PW is turned off achieves its higher stationary level. It points out on the presence of the stronger ASSI (see below). Here the new moment is the sharp decrease of the intensity of the BC (Δf = – 23 kHz) approximately at 2 dB practically immediately of the PW is turned off. Below, in the sixth section based on the experimental data obtained with high time resolution such effects are considered in detail. It should be mentioned also the appearance of the AA on the DW signal with characteristic time ~ 20 s. This time corresponds to the period required for the achievement of the stationary state of the SEE during additional heating of the ionosphere and it is connected with significant ASSI amplification in the region of interaction of the DW with plasma. Besides that, strong random fluctuations of the DW amplitude are observed. These fluctuations are determined by the generation of large-scale artificial ionospheric irregularities with $l_{\perp} \geq 1$ km. Relaxation of such irregularities is observed during the whole two minutes period after the PW is turned off. The absence of registration of such large-scale irregularities at Δh ≈ 50 km confirms that neither these irregularities nor the ASSI outgrow for such distances. The latter points out directly that the amplification of the ASSI at the level of the DW interaction with plasma is determined by plasma perturbations induced by the PW and hence should be considered as secondary perturbations HF-produced in the modified ionosphere.

All mentioned above confirms that at the decrease of Δh from 50 to 27 km sharp increase and qualitative change of the PW influence on the SEE features excited by the DW takes place. Time delay Δt ≈ 1 s between the beginning of registration of the DM and the BC amplification (connected with the growth of the ASSI intensity) and the turning on of the PW makes it possible to estimate the value of the longitudinal velocity with which the perturbations are transported from the region of their generation as $V_{\parallel} \geq 3 \cdot 10^6$ cm s^{-1}. This value certainly exceeds the value V_{Ti}.

The results of measurements for f_{PW} = 4900 kHz (δf = 305 kHz, Δh ≈ 17 km) and f_{PW} = 4785 kHz (δf = 190 KHz, Δh ≈ 5 km), presented at the panels *c* and *d,* show very similar dynamics of d-SEE. Here the development of emissions during additional heating of the ionospheric plasma is characterized by fast increase of their intensity with subsequent strong overshoot-effect (decrease of the emission intensity after it achieves its maximal level). As it is clearly seen from the presented oscillograms the DW is subjected to strong AA. The amplitude of oscillations of the registered signal quickly diminishes due to the decrease of the amplitude of the wave reflected from the ionosphere. The period of AA development corresponds to the time within which the d-SEE intensity achieves its maximal value. The time delay for the beginning of the growth of d-SEE intensity in these measurements by no means exceeds 0.5 s. This value is determined by the accuracy with which one can obtain the information by means of a chart recorder used. The magnitude of delay corresponds to the velocity $V_{\parallel} > 3 \cdot 10^6$ cm s^{-1}. After the PW is turned off the emission intensities in DM and BC regions grow up to the stationary level with the time of the AA relaxation. This level remains approximately the same for f_{PW} = 5010, 4900 and 4785 kHz. The last result confirms that in all these cases after the PW is turned off, almost the same level of AIT in the region of d-SEE generation is established. Taking into account strong correlation in the behavior of AA and d-SEE one may conclude that the development of ASSI initiated by the PW causes strong influence on features of SEE thermal components in the interaction region of the DW with plasma.

Spectral measurements fulfilled at all stages of d-SEE evolution have shown that before the PW is turned on, the emission occurred in the region of negative frequency shifts has a form of NC_{th}. Its spectrum is extended approximately 30 kHz down from f_{DW}. During the first several seconds after the PW is turned on, in the d-SEE spectrum one can detect the appearance of DM and BC. However, these components become significantly weaker and even disappear with the development of the overshoot-effect, and in the spectrum the NC_{th} remains mainly. The components DM and BC appear once again in the spectrum of d-SEE together with the AA relaxation and enhancement of the emission intensity after the PW is switched off. So, during additional heating of the ionospheric plasma the changes in d-SEE intensity is accompanied by the changes in the emission spectral structure. This should be taken into account in the analysis and interpretation of the results of such kind of measurements.

Up to now we have discussed the cases when the PW frequency exceeds the frequency of the DW and the region of strong perturbation in the ionospheric plasma is situated above the region of d-SEE generation. The results of measurements for $f_{PW} = 4580$ kHz and $f_{DW} = 4400$ kHz ($\delta f = -180$ kHz, PW was reflected approximately 6 km below than DW) are presented in Figure 1*g*. For such scheme of experiment the amplification of d-SEE is practically absent at the additional heating of the ionospheric plasma, because DW itself and the emissions outgoing from the IDV are strongly suppressed due to fast (within ~ 3 s) development of AA in the region of strong turbulence excited by the PW. After the PW is turned off, together with the disappearance of AA (within ~ 15 s) the growth of d-SEE intensity up to its maximal value is observed with slight subsequent weakening for DM ($\Delta f = -10$ kHz).

At last, for $f_{DW} = 4300$ kHz ($\delta f = -280$ kHz, see panel *h*), when the PW was reflected ~ 8 km below than the DW, AA for DW was sufficiently weaker in comparison with the previous case and the amplification of the d-SEE intensity can be noticed with the subsequent still sufficiently strong overshoot-effect. After the PW is turned off, with delay $\Delta t < 0.5$ s, which corresponds to $V_{\parallel} > 3 \cdot 10^6$ cm s^{-1}, the growth of the d-SEE intensity together with the AA relaxation (decrease of the ASSI intensity induced by the PW) is observed.

Based on the results of measurements of AA for different PW frequencies, one may conclude that decametric ASSI that determine the magnitude of AA for the stationary state of the powerful radiowave of O-mode polarization interacting with plasma in the F_2-region of the ionosphere [Frolov, 1996; Frolov et al., 1997b; Frolov, 1988], have longitudinal sizes ~ 10 – 20 km, which is in good accordance with the results of measurements [Fialer, 1974; Franz et al., 1999; Nasyrov, 1991].

In conclusion of our discussion of the experimental results presented in Figure 1 let us mention that in this cycle of measurements it was absent visible damping of the DW signal due to HF-induced cross-modulation absorption in the D and E regions of the ionosphere. Nevertheless, according to some other measurements such influence can show up, leading to decrease of the DW intensity, but no more than 1 – 2 dB [Utlatut and Violette, 1974].

The performed analysis of the experimental data has shown that in contrast with the case $f_{PW} \approx f_{DW}$, when the main peculiarities of d-SEE evolution at the additional heating of the ionospheric plasma can be explained by the changes of intensity and spectral characteristics of ASSI, the measurements with the heating sufficiently separated in height have demonstrated the presence of some other effects. These effects can not be connected with the spread of the region with irregularities due to ambipolar diffusion of small-scale ($l_{\perp} \leq 50$ m) plasma density irregularities induced by the PW. The experimental data considered above and also some other data have demonstrated that processes with fast ($V_{\parallel} \approx V_{Te}$) transport of perturbations after the PW is turned

on manifest themselves more clearly when the difference between the reflection heights of the PW and the DW does not exceed 20 – 30 km, that is smaller or of the order of the thermal conductivity characteristic length in the conditions of measurements [Gurevich, 1978]. For more detailed investigation of the observed fast transport processes below in the sixth section we consider in detail the results of experiments with the additional heating of the ionosphere by short-pulse pumping.

At the end of this section let us make some comments about the influence of the DW on the properties of AIT induced by the PW. It was shown above that the DW power determines the intensity and the evolution of d-SEE. However, it is clear that with the growth of the DW power and the increase of plasma perturbations induced by this wave, the conditions of the PW interaction with plasma are changed due to the presence, for example, of sufficiently high level of the initial (seed) turbulence. Besides, if the heights of heating produced by two waves are separated sufficiently in space, when $f_{DW} < f_{PW}$, the turbulence excited by DW can lead to significant attenuation of the PW propagating upward due to the effect of AA or due to the scattering from irregularities with $l_\perp \geq 100$ m [Zabotin et al., 2002]. In addition to these obvious consequencies, sufficiently high power of the DW can lead to the saturation of turbulence created by this wave. As a result, (see subsection 5.2) this effect causes the changes in the character of influence of the PW radiation on its characteristics. As this takes place, the observed effects connected with additional heating of the ionospheric plasma can either disappear completely or undergo qualitative changes. In this sense the most informative can be the case when the DW power only slightly exceeds the threshold power required for the SEE generation. However, to realize this condition in practice is rather complicated due to the following reasons. First, in the majority of cases significant variations in the ionospheric conditions during the cycle of measurements (the typical duration is of the order of 2 – 3 hours) are present. These variations can be the result of natural variations of ionospheric parameters as well as the changes in the level of ionospheric disturbance. Second, there exists significant distinction in threshold powers for generation of different SEE components used for the AIT diagnostics: from ~ 0.5 – 1 MW for DM and BC up to ~ 2 – 3 MW for BUM (here the power values are presented taking into account linear absorption in the lower ionosphere). Third, fluctuating character of SEE near the threshold of its generation [Frolov, 1996] can make the fulfilled measurements much more complicated. Fourth, some effects for short-pulse pumping, as it will be shown below, demonstrate themselves in a most clear form for sufficiently high powers of DW. Taking into account all mentioned above, one may conclude that the selection of the DW power during experiment should be determined by ionospheric conditions as well as the solving problems. It requires the fulfillment of certain test measurements. During these measurements the power level of the DW radiation should be chosen experimentally, otherwise or the measurements have to be carried out with different DW powers with subsequent selection of the obtained data at the stage of their processing and analysis.

4. Possible Influence of the Lower Ionosphere on the Observed Effects

It is important to be sure that in the performed measurements the observed effects are not the result of modification of the lower ionosphere. It is well known (see, e.g. [Gurevich, 1978]) that the propagating upward HF powerful wave is attenuated by the self-action effect due to the heating of electrons in the ionosphere D and E regions. Obviously, this effect causes an influence on the characteristics of the AIT excited in the upper ionosphere. The effect of self-action is easily observed in experiments (see, e.g. [Utlaut and Violette, 1974]) and completely corresponds to the theoretical views about its nature. In our experimental conditions for $P_{PW} \approx 40$ – 60 MW, the attenuation of the PW and DW powers due to the effects of self-action, as a rule, did not exceed 1 – 2 db in daytime conditions and was practically absent (was less than 0.1 db) during the measurements at nights. The performed test measurements have shown that such

small changes of the PW power transported into the upper ionosphere does not cause any significant influence on the d-SEE intensity**.** The following facts confirm that effects of self-action and cross-modulation do not cause any noticeable influence on d-SEE intensity. First, the important characteristic of the observed phenomena at the additional heating of the ionospheric plasma is the existence of the delay time from 5 – 10 ms and more [Frolov et al., 1997a; Frolov et al., 2002]. This period definitely exceeds the characteristic time of the absorption changing in the lower (D-region) ionosphere. Second, no regular changing in the characteristics of the observed phenomena were noticed before the sunset, when rather fast change in the electron concentration in the D and E regions takes place. Third, the investigated effects of additional heating are not observed at the heating of the ionospheric plasma with pump frequency exceeding the critical frequency of the F_2-layer $f_{PW} > f_{0F2}$ (to be more correct, when $(f_{PW}^2 - f_{ce}^2)^{1/2} > f_{0F2}$, where f_{ce} is the electron cyclotron frequency. This condition means that the Langmuir frequency that corresponds to the resonance between the PW and the upper hybrid resonance oscillations exceeds the critical frequency of the ionospheric F_2-layer) [Frolov et al., 2005b]. At last, the changing in the d-SEE intensity substantially depends on the ratio between the frequencies of the PW and the DW and also how close to one of the harmonics of the electron cyclotron frequency these frequencies are. Note, that the intensity of the d-SEE can change significantly from pulse to pulse of the PW.

The second moment, to which the attention should be attracted, is the formation in the ionospheric layer at the heights 120 – 150 km of the region with enhanced plasma concentration. The horizontal scale of this region is determined by the antenna beam of the heating facility. The region is formed due to the weakening of the recombination processes at the heating of the ionosphere by powerful wave. Such large-scale inhomogeneity of the electron density acts as a defocusing lens and causes strong attenuation of waves that propagate through it. This effect leads to the changing of the AIT excited by the PW. Features of such lens were investigated in detail in [Bojko et al., 1985]. In this paper it was shown that the creation of such lens is the most efficient in daytime ionosphere and it is required sufficiently high powers of the PW. Typical times of its appearance and disappearance comprise 15 – 20 s. In day-time conditions for the PW powers $P_{eff} \approx 50$ MW the attenuation of the intensity of the radio waves reflected from the ionosphere can achieve 5 – 10 dB. In our measurements control for the intensity of the DW reflected from the ionosphere did not show any significant changes even in the case when we used long pulses (≥ 30 s) of the PW for the ionosphere heating. Probably, it is connected with the fact that the measurements were performed mainly in the evenings when plasma density in the lower ionosphere became significantly smaller than in the daytime conditions. It is quite natural that it is difficult to expect any significant influence of the defocusing lens for short-pulse (≤ 1 s) pumping, whereas the effects of additional heating (in particular, those related to fast processes) were detected quite well. The mentioned comments allow us to conclude that the effects observed at the additional heating are not the result of defocusing of the radiowave. Nevertheless, possible influence of the defocusing should be taken into account and controlled if the measurements are carried out during the daytime.

While considering the mechanisms of influence of the lower ionosphere on the AIT characteristics excited in the F-region, let us point out on possible generation of large-scale plasma density irregularities in the E-region [Ignatjev, 1978]. These irregularities are able to focus the radiation of powerful wave propagating through them. Due to this the distribution of the electromagnetic wave intensity in the upper ionosphere in the regions of the resonant interaction of the PW with plasma changes. This influences the characteristics of the developing processes. It is possible that such irregularities manifest themselves by some aftereffects. It should be mentioned that our experiments on modification of semitransparent sporadic E-layer [Frolov and Sergeev, 2004a] have shown that irregularities with sizes $l_\perp \approx 1 - 3$ km appear in this layer after ~ 15 s of heating and relaxate within ~ 1 min after the end of heating. It is clear,

that the influence of generation of such irregularities on characteristics of the investigated at the additional heating effects can be easily avoided if one uses short pulses of the PW radiation.

5. Peculiarities in the Behavior of Different SEE Components at the Additional Heating of Ionospheric Plasma

5.1. On some peculiarities of dynamics of the thermal emission components in experiments with additional heating of ionospheric plasma. Above it was mentioned the importance to control the variations of the DW intensity in experiments with additional heating of the ionosphere. The detailed measurements of the dynamics of the thermal emission components including DM, BC and NC_{th} were carried out on August 30, 2002. In this experiment the radiation of two transmitters with the power $P_{eff} \approx 100$ MW at the frequency $f_{PW} = 6250$ kHz was used to create strong AIT. Ionosphere pumping was performed within three minutes according to the schedule 3 s – on, 12 s – off; next two minutes the PW was not radiated to give the created perturbations the opportunity to relaxate. For the DW radiation the third transmitter of the heating facility was used, which generated the radiation continuously at the frequency $f_{DW} = 5730$ kHz with the power $P_{eff} \approx 5$ MW. The analysis of ionograms has shown that in the discussed experiment the distance between the reflection heights of the PW and the DW comprised $\Delta h \approx 23$ km ($h \approx 255$ km and 278 km for PW and DW, respectively). The reflection height of the DW was close to the maximum of the F_2-layer of the ionosphere.

The evolution of the PW signal reflected from the ionosphere is presented in Figure 2a; at the panels *b-f* the fragments of the SEE signal with the frequencies 5722, 5720, 5718, 5716 and 5714 kHz are presented (including time interval within which the PW was radiating). On the panel *g* the SEE spectrum for the DW is shown. It is seen from the SEE spectrum that three middle frequencies of the registered signal correspond to the region of the DM generation (its maximum and the edges). The highest frequency corresponds to the range where the minimum of the emission intensity between DM and NC_{th} exists while the lowest frequency corresponds to the region where BC is situated. It should be mentioned that oscillograms presented in Figure 2 were obtained by averaging of the registered signal intensity. The averaging was fulfilled within 8 subsequent pulses of the PW in one three-minute cycle when d-SEE had steady state variations.

At the beginning let us discuss the behavior of the intensity of the PW signal reflected from the ionosphere (panel *a*). It is clearly seen the development of the fast anomalous absorption (FAA) within the first 0.2 s. After this the second, slower phase of the AA growth starts to develop. As was established in [Frolov, 1996; Frolov et al, 1997b; Frolov, 1988]), FAA is determined by the development of the meter-scale plasma irregularities with $l_\perp \approx 1 - 5$ m, while AA is determined by the development of the decametric irregularities with $l_\perp \geq 10$ m. Sufficiently short times of the FAA development observed in the discussed séance are connected with the peculiarities of the periodic heating of the ionospheric plasma with short pauses when aftereffects cause faster development of plasma irregularities. Taking into account the results of similar measurements with longer PW pulses performed in the same experiment, it is possible to confirm that the AA development practically finishes at the end of three-second pulse of the PW. Also it should be mentioned that before FAA develops, the effect of striction self-action of the PW takes place. This effect is characterized by the decrease in 1.5 – 2 times of the powerful wave signal reflected from the ionosphere within the first several milliseconds of pumping [Erukhimov et al., 1982; Vas'kov and Gurevich, 1973]. So, the behavior of the PW signal reflected from the ionosphere allows us to obtain certain information about the development of the ASSI with different scale lengths in the region of the resonant interaction of the PW with plasma. As it was mentioned many times before, these irregularities cause the determinative influence on the evolution of the SEE thermal components.

Let us come now to the analysis of the d-SEE evolution (see Figures 2*b-f*). It is clearly seen that the switching on of the PW as a source of additional plasma turbulence, causes first an increase of d-SEE for all registered frequencies, though with different temporal evolution of the emission intensity. The slowest development of emissions initiated by the PW takes place with the characteristic time $\tau_{dev} \approx 2$ s and the longest relaxation after the PW is turned off (with $\tau_{rel} \approx 2$ s) takes place for the highest registered d-SEE frequency f = 5722 KHz which corresponds to the region where the minimum of intensity between DM and NC_{th} exists. Note, that the time $\tau_{dev} \approx$ 2 s is only slightly less than the time of the AA development for the PW. Similar dynamics is registered at the high frequency edge of DM (f = 5720 kHz). Though, in this case somewhat faster increase of the emission intensity ($\tau_{dev} \approx 1$ s) and the appearance of the overshoot-effect (decrease of the d-SEE intensity while the PW is still operates) is observed. With the decrease of the frequency of the registered emission, the time of growth of the d-SEE intensity after the PW is turned on decreases. Simultaneously, increase the attenuation of the emission intensity due to the overshoot-effect is observed. As a result, very fast enhancement of d-SEE for the frequencies f = 5716 and 5714 kHz (approximately with the times of the FAA development for the PW) with subsequent decrease of the emission intensity with the time ~ 1.5 s takes place. The magnitude of this decrease can be so large, that at the end of the PW pulse and immediately after its switching off, the intensity of emissions appears to be even less than the nondisturbed level of d-SEE. Note, that transition to the nondisturbed level lasts ~ 4 s. It should be mentioned, that the fast stage of the d-SEE response on the switching on of the PW occurring with the FAA development is registered also for higher frequency components. For the frequency f = 5722 kHz as for the frequencies f = 5716 and 5714 KHz for the times ~ 0.1 – 0.8 s it is possible to single out the stage of small increase of the emission intensity. The obtained results demonstrate strong dependence of the variations of the d-SEE intensity on its frequency even within one (DM) emission component. Also, these results once again confirm that the influence of additional heating is complex: at the beginning it leads to the increase of the d-SEE intensity, while for long pumping it can cause the attenuation of d-SEE.

To interpret the data, similar to the discussed experiment, as a basis it is often taken the model in which the determinative factor is the influence of ASSI spectral intensity on variations of d-SEE evolution [Erukhimov et al., 1988; Frolov et al., 1994; Grach et al., 1998; Sergeev et al., 1999a, Sergeev et al., 1999b]. It is assumed that irregularities can spread along the magnetic field lines from the region of their generation near the reflection height of the PW to the height of the d-SEE generation. However, within this way of interpretation of the d-SEE dynamics we meet with certain contradictions while analyzing the obtained results. First, all experiments in which the ASSI properties are investigated, confirm that metre-scale irregularities (which dominate in the irregularity spectrum at the first seconds of pumping [Frolov, 1996; Frolov et al., 1997b]) occupy sufficiently narrow height interval of the order of ~ 10 km [Fialer, 1974; Nasyrov, 1991]. Hence, in our case for $\Delta h \approx 23$ км it is hardly possible that they cause the observed significant influence on the processes of the d-SEE generation. Second, it is difficult to explain why the influence of the ASSI (caused by the AA development) on the d-SEE dynamics is so different in so narrow (less than 10 kHz) frequency range of the generated emissions. Third, time delay that corresponds to the beginning of the d-SEE intensity changes after the PW is turned on and the distance between the reflection heights of the PW and the DW makes it possible to estimate the velocity with which the perturbations (causing the initial growth of d-SEE) propagate along the magnetic field. In our case this time delay was no longer than 0.1 s for the distance $\Delta h \approx 23$ km. So, the transport velocity of perturbations that causes the changes at the level of d-SEE generation after the PW is turned on, definitely should exceed the $2 \cdot 10^7$ cm s^{-1}, or $V_{\parallel} > V_{Te.}$ As it was indicated earlier, this excludes the possibility to explain the fast response of the d-SEE on the switching on of the PW because of the appearance of plasma irregularities near the reflection level of the DW by their spreading from the height of their excitation. At last, as it was

mentioned before, even in case of sufficiently high level of residual turbulence at the periodic heating of plasma by powerful radio wave the ASSI intensity begins to grow only 50 – 200 ms after the next switching on of the PW [Frolov, 1996; Frolov et al., 1997b; Nasyrov, 1991]. Summarizing all mentioned above, it should be considered that the observed variations of the d-SEE intensity are determined by the generation of the secondary turbulence excited by the propagating primary perturbations in the region of interaction of the DW with plasma. As the mechanisms of generation of this secondary turbulence induced by the PW are not completely clear, significant difficulties in interpretation of the variety of the obtained up to now experimental data, like discussed above, exist. The exploration of these mechanisms is one of the main tasks of the investigations, which we carry out.

5.2 Peculiarities of the BUM dynamics at the additional heating. The results of measurements considered in this section were carried out at the Sura heating facility in May 1993 [Frolov et al., 1996] and in March 1995 [Frolov et al., 1997a]. The measurements were performed near the fourth and the fifth harmonics of the electron gyrofrequency. One module of the heating facility radiated continuously the wave of the O-polarization (DW) at the frequency $f_{DW} - nf_{ce} \approx 20 – 60$ KHz (nf_{ce} is the gyroharmonic frequency). In the SEE spectrum for positive frequency shifts $\Delta f \approx$ 15 – 150 kHz the generation of powerful broad-band radiation BUM (broad up-shifted maximum) was observed [Frolov et al., 1996; Frolov et al., 1998; Leyser et al., 1993; Leyser, 2001; Stubbe at al., 1994]. The maximal DW power in these measurements was $P_{eff} \approx 24$ MW. Two other modules radiated the PW with the effective power up to 100 MW at the frequency, which was approximately 300 kHz higher than f_{DW}. The reflection heights of the PW and the DW were ~ 250 km and their difference ~ 3 – 10 km.

Typical for the evening conditions example of DM ($\Delta f = – 9$ kHz) and BUM ($\Delta f = + 23$ kHz) evolution is presented in Figure 3. The frequency of the PW $f_{PW} = 5750$ kHz was approximately 300 kHz above the DW frequency and the additional heating was performed according to the schedule 10 s – on., 10 s – off. The measurements were carried out on May 22, 1993 (T = 18:00 – 20:00 LT). Here and on subsequent presented oscillograms of the SEE signals the moments when the PW was turned on and off in addition are marked by vertical broken lines, as the zeros of the chart recorder pens in different registration channels did not coincide. From Figure 3 it is seen that the switching on of the PW causes an opposite influence on DM and BUM: the attenuation of the DM intensity at approximately 3 db is observed with the characteristic time of decrease and restoration ~ 2 – 3 s. On the contrary, the growth of the BUM takes place with the same as for the DM characteristic growth time, but the relaxation of this PW-induced emission is significantly faster (during the period ≤ 0.2 s). According to the obtained data, the effect of the BUM amplification is stronger emphasized for small deviations of the PW frequency from the harmonic of the gyrofrequency ($f_{DW} - f_{ce} \leq 10 – 40$ kHz), that is in the region where the growth of the second BUM component up to its maximum intensity takes place, but also the generation of its first component still exists [Frolov et al., 1998]. The d-SEE amplification is observed only for sufficiently high levels of the PW power and occurred within the whole spectrum of the BUM except the region of its cut-off ($\Delta f \approx 10 – 15$ kHz), which is characterized by sharp increase of the BUM intensity with the growth of the PW frequency [Leyser et al., 1993; Leyser, 2001]. With the decrease of the additional heating from the total power $P_{eff} \approx 100$ MW to 50 MW this emission is attenuated significantly and it practically disappears for $P_{eff} = 25$ MW. At present it is impossible to confirm which component of BUM (BUM-1 or BUM-2) shows the amplification of its intensity at the additional heating. That is why new purposeful efforts are required.

Fast relaxation of the PW-induced emission in the BUM region is important for clarification of the essence of the observed phenomenon. In the discussed measurements the relaxation time was ≤ 0.2 s. More detailed investigations of the relaxation of such emission performed later in

[Frolov et al., 1997a] have shown that the characteristic time can comprise ~ 60 ms and with the accuracy up to 10 ms no delay in the beginning of relaxation with respect to the moment when the PW is turned off is observed. These measurements as the discussed above were performed in evenings. In such measurements it was obtained that with the decrease of the BUM intensity after the PW was switched off, short (during ~ 500 ms) burst of the DM intensity could be observed. Here we restrict ourselves to the comments mentioned above, because the effects of such kind will be considered in the sixth part of the paper.

The attenuation of the DM presented in Figure 3 can be connected with the growth of scattering from the ASSI of emissions outgoing from the IDV (effect of AA) [Erukhimov et al., 1987; Frolov, 1988; Frolov, 1996; Frolov et al., 1997b]. Taking into account the characteristic times and the results of investigations in which the dynamics of development and relaxation of ASSI with different scales is analyzed [Frolov, 1996; Frolov et al., 1997b; Nasyrov, 1991] we conclude that this additional attenuation should be determined by the amplification of the irregularities with $l_{\perp} \approx 5$ m near the level of interaction of the DW with plasma. Due to the similarity of the time evolution of DW and BUM signals at the turning on of the PW, it would be possible to conclude, that the growth of the emission intensity in the region of BUM could be connected with the amplification of the meter-scale irregularities in the region of its generation. However, fast relaxation of this additional radiation shows that these irregularities are not the direct reason of the observed phenomenon. It should be mentioned that, according to [Frolov et al., 1997a], in daytime conditions the turning on of the PW, on the contrary, caused small amplification of the DM intensity. This demonstrates once again that the ASSI influence on the intensity of SEE thermal components outgoing from the IDV is twofold.

Let us consider the results of measurements near the fifth harmonic of the electron gyrofrequency for different powers of the DW presented in Figure 4. The measurements were carried out on May 23, 1993 in daytime conditions (T = 10:00 – 10:15 LT). The DW was radiated continuously at the frequency 6700 kHz with powers 24, 3 and 1.5 MW (top, middle and bottom panels, respectively). The PW was radiated at the frequency 7000 kHz according to the schedule 3 s – on, 7 s – off with the pulse power 100 MW. It is easy to see that for the full power of the DW (P_{eff} = 24 MW) the DW-induced changes in the emission level of the BUM are insignificant. Even small decrease of its intensity is observed at the moment when the PW is switched on. For P_{eff} = 3 MW, as in the evening conditions, the growth of BUM intensity is observed when the PW is turned on. At the same time fast relaxation of the additional emission when the PW is switched off takes place. However, here the growth of emission is faster and even within the 3 second-pulse of the PW the appearance of the overshoot-effect is observed (the decrease of intensity of the receiving emission with respect to its maximal level).

For the lower level of the DW power, P_{eff} = 1.5 MW the dynamics of the BUM is even more complicated. In this case at least five stages of emission evolution can be singled out:
1) initial attenuation of the emission intensity within the first 0.3 – 0.5 s after the PW is turned on;
2) subsequent amplification of generation of the d-SEE induced by the PW;
3) sufficiently smooth decrease of the emission intensity while the PM is still turned on (overshoot-effect);
4) fast relaxation of additional emission after the PW is turned off. Its level becomes lower than the stationary emission intensity in the absence of the additional heating;
5) subsequent smooth restoration of the BUM intensity up to the stationary level within the period ≥ 7 s.

In these experiments (in contrast to the results of measurements fulfilled in evening conditions presented in Figure 3) sharp and short initial decrease of the BUM intensity is revealed just after

the PW is switched on. As it was shown in some other measurements, this effect manifests itself more clearly for sufficiently short ($\tau_p \approx 1$ s) pulses of the PW and can be accompanied by the burst of emission in the DM region. One may suppose that the schedule of the PW radiation (10 s – on, 10 s – off) for experiments presented in Figure 3 causes the appearance of strong aftereffects and, as a consequence, the disappearance of the minimum in the d-SEE intensity in the first moment after the PW is turned on. Aftereffects cause influence also on peculiarities of the BUM amplification at the additional heating of the ionosphere, when the decrease of pause between pulses of the PW causes the faster development of PW-induced emissions. The latter takes place, first of all, due to diminishing of the delay of their appearance against the background of emissions generated only by the DW in the absence of the additional heating.

As a reason that casuses the effect of BUM amplification at the additional heating of ionospheric plasma by the waves of O-mode polarization it was considered in [Frolov et al., 2002] the influence on BUM generation of electrons accelerated up to suprathermal energies in the region of intensive AIT excited by the PW due to its resonance interaction with plasma. We shall return to the discussion of this problem in the last part of our paper while considering the obtained results.

6. The Effects Observed at Short-Pulse Pumping

In experiments with short-pulse (less than several seconds) pumping the influence of the nonstationary properties of the AIT at the initial stage of its development becomes important. From one side, it can make more complex the interpretation of the observed phenomena. But from the other side, just at the nonstationary stage of the turbulence development often one can clearly see the evolution of processes in plasma. The first results of such purposeful experiments were analyzed in detail in [Frolov et al., 2002]. In this paper it was demonstrated quite convincing that at once after the switching on (or off) of the additional heating, the evolution of the d-SEE had some specific peculiarities. However, not so high (not better than 40 ms) time resolution of the measurements discussed in that paper did not allow resolving with a required accuracy at this stage the characteristic times for the processes of such kind. This was a strong obstacle for the development of empirical models and the interpretation of the observed phenomena.

Below we consider in detail the results of the experiment performed on March 21, 2004 [Frolov et al., 2006]. Among others this experiment was organized in a most detailed form. In this experiment for ionospheric modification short pulses of PW were used and the signals were registered with the time accuracy 5 ms. Some other experiments carried out in the last several years with similar organization practically repeated the obtained results. In the discussed experiment PW with the power $P_{eff} \approx 70$ MW was radiated vertically upwards at the frequency $f_{PW} = 4730$ kHz with pulse duration $\tau_p = 3$, 1, 0.5, 0.2, and 0.1 s and with the repetition period $T_r = 10$ s or with $\tau_p = 0.5$, 0.2, 0, and 0.5 s and $T_r = 1$ s. The DW with the effective radiation power $P_{eff} \approx 5$ or 2.5 MW was radiated continuously at the frequency $f_{DW} = 4300$ kHz. The measurements were performed in very quiet ($K_p < 1$) geomagnetic conditions in the evening (T = 18:20 – 20:30 LT), when the linear absorption in the lower ionosphere was negligible. In the measurements the SEE was registered at the offset 9 kHz with respect to the PW frequency and the d-SEE was registered at the offsets 9 kHz (DM region), 19, and 29 kHz (BC region) with respect to the frequency of the DW. Also we registered amplitudes of the PW and DW reflected from the ionosphere. To construct the graphics presented below the averaging of SEE signals within 10 – 30 pulses of the PW was used. This allowed us to diminish the noise component of the signal. It should be mentioned, that the rise time for the pondermotive narrow continuum emission component, NC_p, [Frolov et al., 2004b] at the frequency f = 4721 kHz ($\Delta f = -9$ kHz with respect to the PW frequency) up to its maximal intensity comprised ~ 50 – 100 ms, and only

for $\tau_p \geq 0.3 - 0.5$ s the development of the thermal (DM и BC) emission components with sufficiently high level was registered. The sequence of development and competition of the pondermotive and the thermal stages of the SEE evolution were explored in detail by the SEE measurements in [Sergeev et al., 1998].

Let us consider the results of measurements when the DW was radiated with the effective power 5 MW and the repetition period for the PW pulses was equal to1 s. The experiment was carried out during the period T = 18:58 – 19:10 LT, when the reflection heights were about 247 for the DW and 257 km for the PW ($\Delta h \approx 10$ km). As an example in Figure 5a the oscillograms for the d-SEE frequency f = 4281 kHz ($\Delta f = -19$ kHz, the region of BC) are shown for different pulse durations of the PW; in Figure 5b the dynamics of the d-SEE for all three registered frequencies is presented for pulse duration of the PW radiation $\tau_p = 100$ ms. These and other data obtained in similar measurements confirm that already 5 – 10 ms after the PW was switched on for the offshifts related to the BC region (but not for DM), the decrease of the emission intensity starts to be registered. This emission with the delay time $\tau_d \approx 20 - 40$ ms relative to the switching on of the PW changes to the growth of the emission intensity for both DM and BC. In these measurements no concrete dependence of the value τ_d on pulse duration of the PW radiation was revealed. The latter at the first glance can appear to be an unexpected result because the off-duty ratio (or its averaged power) changes in the order of magnitude and it would be quite natural to expect that this effect could manifest itself in the changes of the character of the aftereffects (or the storage effects) at the periodic heating of the ionospheric plasma. It follows from the obtained data that for short-pulse pumping with $\tau_p \leq 0.5$ s the intensity of d-SEE achieves its maximal value after some time Δt_{max} already after the end of the PW pulse. The value Δt_{max} does not depend on the duration of the PW radiation and comprises ~ 10 ms for the emission in the region of DM (f = 4291 kHz in the discussed measurements) and ~ 35 – 40 ms for emission in BC (f = 4281 and 4271 kHz). The characteristic relaxation time of the PW-induced additional part of emissions comprises ~ 30 – 40 ms for DM and ~ 80 – 100 ms for BC regardless of the additional heating schedule. Besides such fast relaxation, in some cases slower stage of transition towards the stationary level of d-SEE is singled out. This stationary state is determined only by the d-SEE while the PW is switched off. The duration of this phase comprised ~ 300 – 400 ms. In the discussed series of experiments this duration did not depend on the frequency (component) of the registered emissions and the schedule of the PW radiation.

The discussed above experimental data with $T_r = 1$ s show that for short-pulse additional pumping on plasma of the ionospheric F_2-layer one can single out 4 stages in d-SEE dynamics: 1) the decrease of its intensity beginning immediately after the PW is turned on; 2) the growth of the d-SEE intensity which lasts some time after the PW is turned off; 3) fast relaxation of the PW-induced emissions, and 4) subsequent smooth transition of the d-SEE intensity to the level that corresponds to the situation when only the DW is radiated. The variations of the d-SEE intensity observed at the first three stages we consider as the manifestation of fast processes developing during the interaction of the powerful wave of O-mode polarization with plasma in the ionospheric F_2-region. The data obtained in this experiment have shown that for the repetition period $T_r = 1$ s and pulse durations of the PW $\tau_p \leq 0.5$ s characteristic times of fast variations of the d-SEE intensity are independent from τ_p (though the decrease of d-SEE intensity causes the diminishing of the averaged PW radiation power up to one order of magnitude). Taking into account all mentioned above, one should suppose that the determinative parameters are pulse duration and the on-peak power and not the averaged power of the PW. As this takes place, the fast variations of the d-SEE intensity should be determined not by the development of the thermal (resonance) parametric instability (with characteristic times exceeding 0.3 – 0.5 s [Frolov, 1988; Frolov, 1996; Frolov et al., 1997b]) in the region of interaction of the PW with plasma but they have to be related to the faster processes observed at the stage of pondermotive

parametric instability development near the reflection level of the powerful radio wave [Erukhimov et al., 1982; Vas'kov and Gurevich, 1973].

Let us now consider the results of measurements performed with the PW pulse duration in the range $0.1 \le \tau_p \le 3$ s and the repetition period $T_p = 10$ s. These experiments were performed in the period T = 18:22 – 18:58 LT, when the reflection heights of the DW and the PW were about 253 and 266 km, respectively ($\Delta h \approx 13$ km). The results of measurements are presented in Figure 6 for two d-SEE frequencies: f = 4291 kHz (the region of DM, Figure 6a) and 4281 kHz (the region of BC, Figure 6b). We do not present here the results of measurements at the frequency f = 4271 kHz, because they repeat with slight variations the results of measurements at the frequency f = 4281 kHz. As before, the effective power of the DW radiation was 5 MW. From the presented oscillograms it clearly seen, that the result of additional heating with $\tau_p = 3$ s definitely distinguishes by its characteristics from the results that correspond to shorter radiation pulses of the PW. First of all, it can be seen how the saturation of the d-SEE intensity develops within 3 seconds of additional heating (which manifests itself by the formation of the stationary state of the DM and by the development of the overshoot-effect for BC and the appearance of the minimum in d-SEE intensity after the PW is turned off). All this was not observed for shorter PW pulses. As it was demonstrated in the third part of the paper (where the results ionosphere pumping with long PW pulses were considered) the dynamics of the d-SEE development at the additional heating with $\tau_p = 3$ s can be explained if we take into account that during the PW radiation the ASSI intensity becomes high enough in the region of the DW interaction with plasma. In this case the ASSI cause significant influence on the development of the thermal SEE components, and due to the effect of AA they influence on the emissions outgoing from the IDV.

The detailed processing of the data obtained in this cycle of measurements allowed us to derive the following characteristics for the four stages of the d-SEE evolution that were emphasized before for $T_r = 1$ s

1) For $T_r = 10$ s the minimum of the emission intensity, appearing practically after the PW is switched on, is observed only for BC and only for $\tau_p \le 1$ s, at the same time its depth decreases with the diminishing of the PW pulse duration; for $\tau_p = 3$ s this minimum is not observed for all registered frequencies of the d-SEE.
2) Time delay from the switching on of the PW to the beginning of the visible intensity growth of the d-SEE has maximal values for $\tau_p = 1$ s: ~ 50 ms for DM and ~ 100 ms for BC. These times decrease gradually to 20 and ~ 50 ms, respectively, at the diminishing of τ_p to 0.1 s. Usually this result is connected with the decrease of influence of aftereffects at the periodic heating of the ionospheric plasma. However, it should be mentioned that short time delays were observed for $\tau_p = 3$ s where they comprised ~ 25 ms for DM and ~ 30 – 100 ms for the BC region. This clearly indicates that aftereffects have different origin and can influence in a different manner on the results of measurements. Note, that in the discussed séances of heating with $T_r = 1$ s and $\tau_p = 0.05 – 0.5$ s these delay times for the beginning of the increase of the d-SEE intensity comprised ~ 30 – 40 ms. So, in both cases if $T_r = 1$ or 10 s for $\tau_p \le 0.5$ s the results are similar. This confirms the conclusion made above that not the averaged power of the PW, but the duration of its pulses determines, first of all, the characteristics of the observed phenomena. Second, such short time delays of the beginning of the d-SEE intensity growth after the PW is turned on confirm directly that this effect can not be connected with the spread of the ASSI along the field line from the region of their excitation to the region of the d-SEE generation in the process of the PW interaction with plasma. Indeed, these times are smaller or of the order of the delay with which ASSI begin to grow even in the conditions of the prepared (disturbed by the periodic heating) ionosphere, which comprises ~ 50 –

200 ms for $l_\perp \approx 3 - 10$ m [Frolov, 1988;Frolov, 1996; Frolov et al., 1997b; Nasyrov, 1991].

3) Experiments with $T_r = 10$ s have shown that after the PW was turned off in the conditions of weaker aftereffects, often one could observe not a small gradual growth of the d-SEE intensity (as in the measurements with $T_r = 1$ s), but sharp acceleration of its growth and the formation at such times of the local maximum of the emission intensity which was well singled out. The time interval within which the d-SEE intensity continued to grow up to its maximal value weakly depended on the PW pulse duration for $\tau_p \geq 0.5$ s accounting for ~ 15 – 20 ms for DM and ~ 35 – 50 ms for BC. It is seen that these time values are close to the times within which d-SEE continued to grow for $T_r = 1$ s. In both cases when the PW was turned off, the response on it in DM was faster than in BC. For pulse duration $\tau_p = 0.1$ s ($T_r = 10$ s) these times diminished to ~ 5 – 10 ms for DM and up to ~ 30 ms for BC. The latter can confirm that aftereffects are much weaker for $\tau_p < 0.5$ s.
4) As it was mentioned before, while discussing the measurements with $T_r = 1$ s, in the relaxation of the perturbations of the d-SEE intensity, caused by the PW radiation, as a rule, two stages can be well distinguished: relaxation of PW-induced emissions and subsequent more slow restoration of the d-SEE intensity towards the nondisturbed state, which corresponds to the case when only DW is radiated. According to the results of measurements with $T_r = 10$ s, for all registered off-shifts of d-SEE the decrease of the relaxation time of PW-induced emissions from ~ 0.6 s for $\tau_p = 3$ s to ~ 50 – 100 ms for $\tau_p = 0.1$ s is observed. This result shows that the relaxation process is a nonlinear one and that the level of the induced plasma turbulence determines it. More complicated dependence on the PW pulse duration is observed for transition time towards nondisturbed (stationary) level of the emission intensity when only the DW is radiated. As for the time describing the achievement of maximum, the time dependence for the establishment of the stationary state (t_{ss}) changes at the transition through $\tau_p = 0.5$ s: the value t_{ss} weakly decreases from ~ 4 to ~ 2.5 s with the diminishing of τ_p from 3 to 0.5 s. At the same time, further diminishing of τ_p to 0.1 s leads to sharp decrease of the t_{ss} to ~ 0.5 – 0.7 s. For comparison, in the experiment with $T_r = 1$ s regardless of the pulse duration of the PW, the relaxation time of the additional emissions comprised ~ 30 – 40 ms for DM and ~ 80 – 100 ms for the BC, and the transition time towards the stationary state was ~ 0.3 – 0.4 s for both emission components. It is seen that there is no agreement between the obtained results for different periods T_r of the PW radiation. From this, it can be concluded that the repetition period of the PW pulses causes significant influence on the relaxation of plasma perturbations, for example, by aftereffects.

Comparison of the experimental results with $T_r = 1$ and 10 s allowed us to conclude, that time characteristics of the fast processes are in an agreement only for the shortest pulse durations of the PW radiation. It was also established that for $\tau_p \geq 0.5$ s and $T_r = 10$ s (or, when the pulse duration of the PW exceeded the time required for the development of the fast stage of AA, $\tau_{FAA} \approx 0.3 - 0.5$ s [Frolov, 1988; Frolov, 1996; Frolov et al., 1997b], and the averaged power of the PW exceeded the threshold for generation of the thermal parametric instability and the ASSI generation, $\langle P_{eff} \rangle \approx 0.3 - 0.5$ MW [Erukhimov et al. 1988; Erukhimov et al., 1978; Frolov, 1996]) significant changes in the properties of the fast processes were observed. This effect manifests itself in sharp increase of the characteristic time for the formation of the maximum of d-SEE intensity after the PW is switched off and in the intencification of aftereffects (which cause the increase of the restoration time of the emission intensity towards the nondisturbed level). It can be important, that for pulse durations of the PW less than 0.5 s, fast stage of AA (FAA) does not have enough time for its development. This causes sharp weakening of the ASSI generation by the PW radiation [Frolov, 1988; Frolov, 1996; Frolov et al., 1997b]. The obtained results confirm that characteristics of plasma perturbations at the fast stage of development (due

to aftereffects, the properties of which depend on the pulse duration of the PW radiation, as well as the duration of pause between pulses) are determined by the features of AIT induced by the PW at the development of the thermal (resonance) parametric instability.

The results of measurements for BC presented in Figures 5 and 6 demonstrate that for short pulses of additional heating the characteristic times of the growth/relaxation of d-SEE intensity after the PW is turned on/off are sufficiently close ~ 20 – 40 ms values. These times should be considered as an important characteristic of interaction at the initial stage of the powerful O-mode radio wave with plasma of the ionospheric F-layer (at the stage prior the ASSI development). According to [Erukhimov et al., 1987; Frolov, 1996; Frolov et al., 1997b] these times correspond to the appearance of oscillations (spikes) in the signal reflected from the ionosphere after the end of the pondermotive stage. Assume, that the longitudinal (along the field line of the geomagnetic field) velocity of the perturbations induced by the PW (that determine the dynamics of fast processes) is calculated as the ratio of a distance between the reflection points of the PW and the DW (here ~ 10 km) to the delay time of the d-SEE response on the switching on/off of the PW (≤ 20 – 40 ms). In this case (taking into account the finite time of the turbulence development at the reflection level of the PW, as well as at the level of the d-SEE generation) the obtained values of $V_{\parallel}$ should definitely exceed $(2 – 4)\cdot10^7$ cm s^{-1}. It means that they are higher than the thermal velocity of electrons. Even higher values of $V_{\parallel} \approx (1 – 2)\cdot10^8$ cm s^{-1} are obtained estimating the velocity of perturbations, which accounts for the initial decrease of the d-SEE intensity (related to the BC) 5 – 10 ms later the PW was turned off and also the time describing the response of the DM on the PW switching off. Based on the obtained experimental data, one may conclude that the appearance of fast processes in the d-SEE dynamics is observed for pulse durations of the PW longer than τ_p = 50 ms; the attempts to detect fast processes for shorter pulse durations τ_p = 25 ms were not successful. As the characteristic times of fast processes comprise ~ 20 ms, this testifies that: 1) at the periodic radiation of the PW pulses, the ionosphere pumping within 25 ms is too short for the development of such processes; 2) even for τ_p = 50 ms and T_r= 1 – 10 s the accumulation effect that determines the properties of the initial decrease of the d-SEE intensity just after the PW is turned on should start to show up itself.

Let us briefly discuss some other results obtained in experiments presented above with short pulse pumping. The detailed analysis of these results is beyond the scope of the problems discussed in the present paper.

Comparative measurements of the d-SEE evolution for $P_{DW} \approx 5$ MW, at which the experiments discussed above were performed, and for $P_{DW} \approx 2.5$ MW have shown that at smaller DW power 1) faster increase of the d-SEE intensity after the PW is turned on takes place, 2) more pronounced maximum of the emission intensity after the PW is turned off is observed, and 3) faster relaxation of the PW-induced emissions at practically the same times of the establishment of the stationary d-SEE level takes place. Such distinctions in the d-SEE dynamics quite naturally can be considered as the influence of the increasing level of turbulence (induced by the DW) with the growth of its radiation power. This influence can cause, for example, the growth of the ASSI and the changes in their spectral characteristics at the level of the d-SEE generation, which in turn can cause weakening of the mechanisms that determine the appearance of fast processes. It is clear, that the changes in the ionospheric conditions (e.g., the value of the linear absorption of radio waves in the lower ionosphere or the reflection height of the PW) should cause strong distinctions in the results of different measurements cycles. This is often observed in experiments.

Figure 7 shows the changes in the d-SEE intensity when the frequency of the PW f_{PW}= 4730 kHz was slightly below the critical frequency of the ionospheric F_2-layer $f_{0F2} \approx 4950$ kHz with the

difference in the reflection heights of the PW (h ≈ 278 km) and the DW (h ≈ 260 km) ~ 18 km (left column). The middle column corresponds to the case when the frequency of the PW was of the order of the critical frequency while the difference of the reflection heights for the PW (h ≈ 300 km) and the DW (h ≈ 265 km) was ~ 35 km (f_{0F2} ≈ 4700 – 4750 KHz). The right column corresponds to the case when the frequency of the PW was slightly above the critical frequency. Note, that in the latter case the upper hybrid resonance frequency for the PW was close to the critical frequency (f_{0F2} ≈ 4550 kHz, the reflection height for the DW was 293 km, and the UHR height was 315 – 320 km, right column). The experiments were performed on March 21, 2004 during the period T = 19:43 – 20:30 LT, when the critical frequency of the ionosphere naturally decreased due to the transition from day to night. The schedule of PW radiation was: τ_p = 1 s, T_r = 10 s. The oscillograms are presented for all three registered off-shifts for d-SEE in the regions of the DM and BC. It follows from the data presented in the figure that for $f_{PW} < f_{0F2}$ the growth of the d-SEE intensity starts with the delay no longer than 50 ms after the PW was turned on. After the end of the PW pulse sharp and short-lived growth of the emission intensity was observed. For $f_{pw} \approx f_{0F2}$ significant decrease of influence of additional heating occurred. This effect manifested itself in the diminishing (more than two times) of the d-SEE intensity, in the increase of the delay time up to ~ 200 ms for the beginning of the d-SEE intensity growth, and in the increase of the period within which PW-induced emissions were developed. The d-SEE intensity achieved maximum of its development in ~ 500 ms after the end of the PW pulse without formation of a pronounced maximum in the emission intensity. Such retardation and weakening of the influence of the additional heating can be connected with the growth of the distance between the reflection heights of the PW and the DW up to ~ 35 km, while the PW frequency was approaching the critical frequency of the ionospheric F_2-layer, as well as with possible decrease of the efficient pumping due to partial leakage of the PW through the ionosphere. It cannot be excluded also the influence of some other reasons, connected, for example, with peculiarities of the variations in the d-SEE intensity at the sunset [Kagan and Frolov, 1996]. To separate all these factors without special test measurements is rather complicated. At last, for $f_{PW} > f_{0F2}$ during the PW pulse no growth of the emission intensity was observed. On the contrary, slight decrease of the d-SEE intensity was detected at the frequency 4291 kHz (and somewhat smaller at the frequency 4281 kHz). At the same time the growth of d-SEE intensity was registered after the end of pumping. The time within which the intensity achieved its maximal value (without formation of the sharp, singled out maximum) comprised ~ 1 – 2 s. This time slightly increased with the diminishing of its frequency (with the growth of the negative off-shift). The obtained delay times for the d-SEE response on the switching on/off of the PW correspond to the velocities $V_{\parallel} \geq 10^6$ sm s^{-1}, which in this case also exceeded more than one order of magnitude the thermal velocity of ions and, hence, can not be connected with the processes of the ambipolar diffusion. Based on the results of this experiment it is possible to make the following conclusions. First, it is clearly seen nonlinear dependence of the delay time of the d-SEE response on the height difference between the reflection points of the PW and the DW. From this statement one may conclude that the interaction of the DW with plasma is determined by the development of the secondary turbulence and not the spread of the ASSI from the region of its generation near the reflection height of the PW. Second, the generation of the AIT due to transformation of the PW into UHR oscillations has to occur certain influence on variations of the d-SEE intensity. Third, the results obtained in this experiment clearly demonstrate, that the effects of the additional heating, analyzed in the present paper, are not determined by the influence of the lower ionosphere on the transport of powerful wave energy into the F-region.

7. Discussion of the Results and Concluding Remarks

One of the main goals of investigations, results of which are discussed in the present paper, is the exploration of the peculiarities of the AIT development at the initial stage of interaction of the

powerful HF O-mode radio wave with the upper (F_2-region) ionosphere. The second goal is the investigation of transport along the geomagnetic field lines of plasma perturbations induced by the PW. These perturbations in turn can stimulate the generation of a secondary turbulence. The primary AIT (first of all, high frequency plasma oscillations, fluctuations of plasma density and temperature in different scales, the fluxes of thermal and suprathermal electrons, *etc*) was excited due to the development of different types of instabilities at the resonance interaction of the powerful O-mode radio wave (PW) with ionospheric plasma. In the experiments, discussed in the present paper, the diagnostics of plasma perturbations was performed by the SEE, the properties of which depend on plasma parameters, in particular, on the presence of the ASSI and suprathermal electrons. While considering the evolution of fluctuations in plasma density and temperature of different scales, usually it is assumed that their spreading along the geomagnetic field lines is connected with diffusion and thermodiffusion mechanisms of expanding from the region of intensive generation of perturbations near the reflection level of the PW. This region has small vertical scales compared with the length, determined by the thermal conductivity [Gurevich, 1978; Trakhtengerts et al., 1995; Vaskov et al., 1992; Zhilinsky and Zhendin, 1980]. In this case the velocity with which plasma density perturbations spread along geomagnetic field in the ambipolar approximation (which is usually accepted) should be determined by the diffusion of ions as the slowest (in the mentioned direction) species. This velocity should have the value close to the thermal velocity, that is $V_{\|} \approx V_{Ti} \approx 10^5$ cm s^{-1} for typical experimental conditions in the midlatitude ionosphere at the heights of the F_2 layer. However, the mentioned in the Introduction experiments and the results of the measurements, considered in our paper, have shown that it is not always true.

When the frequency of additional heating of the ionospheric F-region differents from the PW frequency ($f_{PW} \neq f_{DW}$), the measurements have clearly demonstrated, that practically in all registered cases the perturbations (that cause variations of the d-SEE intensity) are transported with velocity sufficiently exceeding the thermal velocity of ions V_{Ti} determined under conditions of measurements. Probably, three different cases should be distinguished: 1) $V_{Ti} < V_{\|} << V_{Te}$; 2) $V_{\|} \approx V_{Te}$, and 3) $V_{\|} >> V_{Te}$. In the first case, when, according to our measurements $V_{\|} \approx (0.7 – 3)\cdot 10^6$ cm s^{-1}, changes in d-SEE intensity are rather smooth and take place with the characteristic time of the order of several seconds. It is quite natural to suppose that this result is connected with the growth of the ASSI intensity in the region of d-SEE generation after the turning on of the PW. Because even in this case $V_{\|} > V_{Ti}$, the amplification of d-SEE can not be the result of spread of plasma irregularities from the region where the PW interacts with plasma (the region of primary turbulence generation) and has to take place directly in the region of the d-SEE excitation. Due to this, the changes in the ASSI intensity induced by the DW should be considered as a result of development of the secondary turbulence, stimulated by primary perturbations propagating in plasma. The results of measurements [Bachmetyeva et al., 1992] of the longitudinal velocity $V_{\|} \approx 10^4 – 2\cdot 10^6$ cm s^{-1}, with which plasma perturbations are transported, should be considered as underestimated. Indeed, these results are influenced significantly by the dynamics of ASSI development [Frolov, 1996; Frolov et al., 1997b; Nasyrov, 1991] as well as the period of their growth up to the registered level. In the second case much faster (at the time ≤ 100 ms) changes in d-SEE level are observed, which are not connected with the ASSI enhancement. Taking into account the perturbation spread velocity $V_{\|} \approx V_{Te} \approx 2\cdot 10^7$ cm/s and the range of heights $\Delta h \leq 30$ km, involved in the process, it is possible to conclude that we deal here with the thermodiffusion processes, determined by the flux of thermal electrons out of the region where resonant interaction of the PW with plasma takes place. Note that similar process were observed in laboratory experiments [Egorov et al., 1988], in which it was shown that thermodiffusion processes can not be considered as one dimensional, because electrons are pushed out mainly along the magnetic field line, while ions are pushed out across the field line. In this case the perturbations of plasma density exist in the volume with the size much more than the horizontal size of the resonant interaction region of the PW with plasma (the

region with primary perturbations of plasma density and temperature) [Kurina, 1998; Voskoboynikov et al., 1989]. These perturbations are accompanied by the appearance of the electric fields and currents in the disturbed and background plasma. At last, in the third case when $V_{\parallel} >> V_{Te}$, most likely that the characteristics of d-SEE are influenced by suprathermal electros accelerated in the plasma resonance region, as it was mentioned in [Frolov et al., 1997a; Frolov et al., 2002]. In any case, due to many reasons discussed in the paper, our measurements clearly demonstrate that for $V_{\parallel} \geq V_{Te}$ the response of d-SEE on the switching on (off) of the PW is not connected with the ASSI influence on the d-SEE generation.

Important results concerning the processes that take place in plasma at the additional heating were obtained in experiments with short-pulse (less than several seconds) pumping in conditions, when the stationary state of the low-frequency AIT is not achieved yet. The performed investigations have shown that in this case in the d-SEE dynamics at least four different stages can be distinguished: 1) fast decrease of the emission intensity that starts practically immediately (in 5 – 10 ms) after the PW is turned on; 2) subsequent growth of the d-SEE intensity within ~ 20 – 40 ms after the PW is turned on, which lasts approximately the same time after the PW is turned off; 3) fast (within ~ 30 – 40 ms) relaxation of PW-induced emissions after the additional heating is turned off, and 4) restoration of the d-SEE intensity to the level, which corresponds to the radiation of DW only. The first three stages of the d-SEE evolution are related to the manifestation of fast processes, which are observed at the initial stage of interaction of the powerful O-mode wave with plasma in the F_2-region of the ionosphere. The phenomena observed at the fourth stage, as aftereffects of different nature, should be referred to slower processes that are determined, first of all, by the evolution of artificial ionospheric irregularities of different sizes. It is important that for fast processes the calculated characteristic velocity $V_{\parallel}$, with which the perturbations propagate along the geomagnetic field lines, is of the order of or higher than the thermal velocity of electrons $V_{Te} \approx 2 \cdot 10^7$ cm s^{-1} found under typical conditions of our experiments in the F_2-layer of the ionosphere. This excludes immediately the possibility to explain the fast variations of the d-SEE by the influence of the low-frequency waves generated in the IDV, because the velocity of such waves do not exceed V_{Te}. Moreover, the performed investigations allowed us to confirm that the amplification of turbulence (that determines the properties of the fast variations of the d-SEE intensity) should take place directly near the reflection height of the DW, and should not be determined by the spread of the ASSI generated in the region of resonant interaction of the PW with plasma. This important from our point of view statement is confirmed by the following facts. The performed in [Frolov, 1996; Frolov et al., 1997b; Nasyrov, 2001] detailed investigations of the ASSI dynamics have shown that even in the preliminary disturbed ionosphere (with sufficiently high level of residual turbulence) the growth of intensity of irregularities with $l_{\perp} \approx 3 – 10$ m in the region of interaction of the PW with plasma takes place with the delay $\Delta t \approx 50 – 200$ ms; the relaxation of these irregularities after the PW is switched off lasts for 1 – 10 s (in both cases larger time intervals correspond to larger irregularity scale lengths). It is seen that time delays for the beginning of the ASSI development exceed characteristic times of fast processes. It is important to mention that even in experiments with two-frequency pumping [Frolov et al., 2000] when the regions of the resonance interaction overlap to a significant extent, not all registered there variations of the DM intensity can be determined by the ASSI influence. Some other mechanisms should be attracted to explain the origins of the effects observed in such experiments. In addition it should be mentioned that the properties of fast processes can not be determined by direct influence of the propagating upwards PW radiation on the characteristics of turbulence excited at the level of the d-SEE generation because they depend on the difference between the reflection heights of the PW and DW and change significantly when the PW starts to leak through the ionosphere.

In [Frolov et al., 1997a] and later in [Frolov et al., 2002] it was supposed that electrons accelerated in the regions with turbulence induced by the PW are involved in the observed

processes. The reason for such supposition was that in some cases $V_{\parallel} >> V_{Te}$, and also that the relaxation times of the variations of d-SEE intensity after the PW was turned off corresponded to the thermolization times of suprathermal electrons. New experimental results obtained at short-pulse pumping confirm that at high powers of PW the fluxes of thermal electrons and electrons accelerated by plasma turbulence can determine to a great extent the observed phenomena. It is reasonable to believe that such short times should be related to the pondermotive and not the thermal mechanisms of the development of plasma instabilities. The behavior of the PW signal reflected from the ionosphere directly testifies it. This behavior shows that the anomalous absorption (AA) of the PW starts (also the ASSI begin to develop) only several hundreds of milliseconds after its switching on. This time exceeds the characteristic times for the fast processes. Also, it should be mentioned that the d-SEE relaxation occurs much faster (within ~ 30 – 40 ms), than the relaxation of the artificial irregularities with $l_{\perp} \approx 1 - 20$ m. The characteristic times for such irregularities comprise several hundred of milliseconds for irregularities of pondermotive nature (excited near the reflection height of the PW) and ~ 0.5 – 20 s for thermal irregularities, excited near the upper hybrid resonance (UHR) level [Bojko et al., 1990; Frolov, 1996; Frolov et al., 1997b]. All these results are of prime importance for clarification of physics of the processes related to the whole complex of problems connected with the excitation and evolution of the secondary turbulence (under the action of plasma perturbations that propagate from the region of their generation where the resonant interaction of the PW with plasma takes place). The solution of this problem is still far from its completion and the prolongation of experimental and theoretical investigations is required.

Above it was supposed that the fluxes of suprathermal electrons accelerated by the turbulence (excited by the PW) determine fast variations of the d-SEE intensity. In this case one may assume that these electrons penetrating into the region of the d-SEE generation cause the growth of the decrement of the UHR oscillations due to Landau damping (as it was shown in [Sergeev et al., 1998]). As a result, after the PW is switched on these electrons determine the appearance in ~ 5 – 10 ms of the initial minimum in the d-SEE intensity. It is important to mention that, according to [Frolov et al., 2002], such minimum is not registered at low levels of the PW radiation power with $P_{eff} \leq 10 - 20$ MW, when the efficiency of electrons acceleration is low. In this case it should be considered that the whole period of time for electron acceleration together with their propagation from the region of acceleration to the region of the d-SEE generation (~ 10 km) should comprise no more than 10 – 20 ms. Note, that the appearance of accelerated (at least up to ~ 4 eV) electrons in the first milliseconds – tens of milliseconds after the PW was turned on was demonstrated in the measurements of artificial optical emissions in green line of atomic oxygen with $\lambda = 5577$Å [Gumerov et al., 1999; Grach et al., 2004]. From the other side these fluxes of suprathermal electrons can stimulate the development of plasma perturbations, which cause the generation of secondary turbulence outside the regions of generation of primary AIT (as, for example, in [Ganguly and Gordon, 1983] the enhancement of plasma perturbations above the F_2 peak height of the ionosphere was revealed). This effect can cause the increase of the d-SEE intensity at the additional heating of plasma by powerful radio wave. According to our measurements, the characteristic time of the development of the secondary turbulence comprises ~ 40 ms. From this one may conclude that this turbulence can be related to high frequency plasma component of AIT induced by the PW near the reflection level of the DW. It is quite natural, that after the PW is turned off, the intensity of the secondary turbulence is supported at high level, at least, during the period of thermolization (~ 10 – 500 ms) of fast electrons (the more, the higher their energy is), providing the stimulation of processes that cause the amplification of the d-SEE generation. This determines the time interval from the moment when the PW is turned off to the moment when the intensity starts to decrease. Taking into account, that at smaller DW power the formation of sharper maximum in the d-SEE intensity is observed, one may assume that the development of the secondary turbulence strongly depends on the level of ASSI excited by the DW. Also, the characteristics of the secondary turbulence should be

influenced by aftereffects of different kind. The decrease for T_r = 10 s of the characteristic time of the d-SEE relaxation with the diminishing of the PW pulse duration can be explained by the decrease of the energy level up to which electrons can be accelerated during the PW pulse and, hence, by their faster thermolization. Faster response of the DM on the turning on (off) of the PW in comparison with the BC and some other distinctions in their evolution at additional heating of the ionospheric plasma can be connected with peculiarities of generation of these AIT components.

Besides the effects mentioned above, the fluxes of thermal and suprathermal electrons directed along the filed lines of the geomagnetic field should cause the appearance of the longitudinal current and solenoidal currents that flow in the disturbed and background plasma. These currents should cause perturbations in plasma parameters far away from the region of the most intensive heating by powerful radio wave. Such development of thermodiffusion processes was observed in laboratory plasma device [Egorov et al., 1988; Golubyatnikov et al., 1988]. Later on in experiments [Tereshchenko et al., 2004] it was shown that the sizes of the IDV with large-scale (tens of kilometers) artificial fluctuations of plasma concentration definitely exceed the horizontal scale of the ionospheric region illuminated by a beam of powerful radio waves.

So, taking into account the influence of the fluxes of thermal and suprathermal electrons, we are able to suggest a consistent explanation of the main observed experimental facts related not only to the fast processes but also to the formation of the IDV in the large-scale part of the spectrum of the artificial fluctuations of plasma density. At the same time it should be mentioned that the absence of clarity in mechanisms of generation of the secondary turbulence restricts significantly the possibility to interpret the results of the measurements discussed in the present paper as well as some other experimental facts. The detailed exploration of the properties of the secondary turbulence is an important part of the performed and the planned our investigations. Without such exploration the construction of the empirical model of the AIT generation can not be considered as complete.

It is clear that in interpretation of the experimental data based on the assumption that the accelerated electrons influence the formation of plasma turbulence in the IDV, an important point is the problem of the acceleration mechanism and the energetic characteristics of the accelerated particles. The theory of multiple acceleration of electrons in the region of plasma resonance (where the development of the modulation instability with the formation of plasma cavitities takes place) was carried out in [Gurevich et al., 1985]. Estimates show that at h ≈ 250 km the time required for the acceleration of electrons up to the energies of several eV and the time of their thermalization should comprise ~ 0.1 – 1 s and ~ 0.1 – 0.3 s, respectively. It is clear that such times certainly exceed the values of the characteristic times of fast variations in the d-SEE intensity observed in experiments after the switching on (off) of the PW. The second mechanism of acceleration (suggested in [Grach et al., 1986]) is based on turbulent retaining of electrons in the region of their acceleration due to the scattering from plasma waves. This effect causes significant growth of time within which electrons are present in the layer with plasma turbulence. Such mechanism provides significantly smaller time of acceleration than in the case of multiple acceleration. However, this mechanism is discussed only in the case of development of thermal parametric instability without taking into account the peculiarities connected with the trapping of plasma waves in plasma irregularities. Additional investigations are required (taking into account new data on the AIT development at the pondermotive and thermal stages, obtained recently in the approximation of strong turbulence) to compare quantitatively experimental results with theory.

The appearance of variations in d-SEE intensity at the additional heating of the ionosphere when the PW frequency exceeds the critical frequency of the ionospheric F_2-layer, but the UHR

frequency is still lower than the critical frequency up to now is not investigated in detail. It is clear that in this case the pondermotive parametric instability (and the whole complex of phenomena connected with this instability) does not develop. But in such conditions the development of the thermal (resonance) parametric instability still can play some role [Leyser, 2001]. According to the results of measurements one may conclude, that the observed d-SEE variations are not the consequence of the ASSI spread from the region of their generation (the region of the resonant interaction of the PW with plasma). Indeed, the height difference between the reflection levels of the PW and the DW in this case is large enough and, also, the calculated value of $V_{\|} \approx 10^6$ cm s^{-1} appears to be one order of magnitude higher than V_{Ti}. It cannot be excluded that in this case the manifestation of the same effects that were observed at the additional heating of the F-region by powerful X-mode radio wave takes place [Frolov et al., 1999]. In any case, these results show that to consider the intensity variations of the d-SEE at the additional heating of the ionospheric plasma and to construct the empirical model of such variations, besides the pondermotive component of the AIT, the influence of the thermal component of turbulence should be taken into account. Without additional investigations it is impossible to give an irrefragable answer to all formulated questions.

After the PW is turned off, the d-SEE relaxates to its nondisturbed level. It is clearly seen that this process can be described as a two-step process. Above we discussed the properties of fast relaxation stage of PW-induced emissions by the action of powerful radio wave on plasma. At the stage of restoration of the d-SEE intensity to the level that corresponds to the nondisturbed state, for thermal emission components the determinative factor is the ASSI dynamics. These irregularities at the turning on of the PW are amplified directly in the region of interaction of the DW with plasma. These irregularities influence also the magnitude of anomalous absorption of the emissions propagating outside of the disturbed region. Considering this stage of the d-SEE dynamics one should take into account possible aftereffects connected with the influence of different components of the residual low-frequency turbulence. As it follows from the data, presented in the paper, these components are strongly amplified at the pulse durations of the PW $\tau_s \geq 0.5$ s and $P_{eff}(PW) \geq 10$ MW, because even at the stage of development of fast AA (FAA) the ASSI intensity reaches high level. This causes stronger influence of the ASSI on subsequent interaction of the PW with plasma. Note, that the "cold start" conditions in the absence of initial level of turbulence can be realized in the region of interaction of the PW with plasma only if the duration of pause between the PW pulses exceeds 10 – 15 min. In this case the relaxation of large-scale artificial plasma irregularities induced by powerful waves takes place, as well as the renovation of plasma in the region of its heating due to natural drift motion. It is clear that such long interval between pump pulses practically can not be utilized in the heating experiments, because in this case even simple programs of measurements would take several hours and, hence, strong day variations of ionospheric conditions would influence significantly the results of measurements.

The carried out investigations demonstrate convincingly that the influence of the additional heating of the ionospheric plasma on the properties of effects observed by d-SEE depends on many factors. Among them the main are the power, relative pulse duration of the PW radiation (by the amplification level of the ASSI intensity and aftereffects); the frequencies of the PW and DW (by their reflection heights, mutual height distribution of the regions of interaction with plasma for these waves and the distance between these regions, and also by gyroresonance effects, when one of the frequencies is close to the harmonic of the electron gyrofrequency); power and schedule of DW radiation (by the spectral composition of d-SEE and its saturation level, and also by the influence of the AIT excited by the diagnostic wave on the interaction of the PW with plasma); the state of the ionospheric plasma and the level of its natural perturbations (by the changes in conditions of interaction of the PW and the DW with plasma in the presence, for example, of photoelectrons, natural small-scale and large-scale plasma density

irregularities). The simultaneous influence of all these factors causes the complexity of manifestation of the observed phenomena and strong variations of their characteristics in somewhat similar ionospheric conditions and even sometimes within the same cycle of observations. This complicates significantly the analysis and interpretation of the obtained results. Sometimes such analysis becomes impossible without special test measurements.

The carried out experiments with the utilization of the additional heating of the ionospheric plasma makes it possible to formulate some conclusions concerning the conditions of their performance (which comprise the basis of this method). First, based on numerous measurements one may prove that the most preferable frequency range for the carrying out of such experiments is the range 5 – 6 MHz, where according to [Frolov et al., 2001; Frolov et al., 2005b] the maximal stationary intensity of the thermal SEE components is observed. In the frequency range $f_{PW} \approx 4.3 - 5$ MHz with the decrease of the PW frequency, the SEE intensity also diminishes. The intensity of the DM decreases faster than the BC intensity. As a result DM becomes less pronounced with respect to BC. Also in this case strong overshoot effect takes place, when the SEE intensity sharply decreases for the DM and BC at the transition to the stationary state of emissions [Sergeev et al., 1999a, 1999b]. All mentioned above makes more difficult to divide the SEE components and to interpret the obtained results. In the region $f_{PW} > 6 - 6.5$ MHz the effects observed at the additional heating as a rule are weak. This is connected with the worsening of the conditions for generation of the SEE due to the growth of thresholds for the generation of the thermal parametric instability [Gurevich et al., 2005]. As a consequence, the intensity of the SEE thermal components strongly decreases. The second moment, to which the attention should be paid, is the dependence of the observed effects on the difference of the reflection heights of the PW and the DW. For $\Delta h < 5$ km it is quite possible that the regions of the resonance interaction of the PW and the DW with plasma overlap. Such situation corresponds more to the case of two-frequency pumping when the conditions for the ionospheric modification and the character of the observed phenomena change substantially due to strong interaction between powerful radio waves and the generated by them plasma turbulence [Frolov et al., 2005a]. From the other side, the carried out experiments confirm that for $\Delta h \approx 30$ km the influence of the additional heating becomes weaker and for $\Delta h \approx 50$ km fast variations of the d-SEE intensity at the switching on of the PW are small and they are registered not always. This can be connected with the fact that the distance between the reflection points of the PW and the DW exceeds characteristic length of thermal conductivity and the mean free path for suprathermal electrons (which comprises at the heights $h \approx 250$ km in the evenings during the measurements ~ 30 km) and also the longitudinal sizes of the ASSI $l_{\parallel} \approx 10 - 20$ km for $l_{\perp} \approx 10$ m [Fialer, 1974; Franz et al., 1999; Nasyrov, 1991]. Hence the optimal for the carrying out of experiments with additional heating should be considered the case when $\Delta h \approx 10 - 20$ km. At last, fast processes are registered fairly well for sufficiently high radiation power of the DW $P_{eff} \approx 3 - 5$ MW. However, for $P_{eff} \geq 10$ MW at cycling turning on of the PW with the usually used pulse duration and repetition period possible aftereffects can cause significant changes in the properties of fast processes and even their disappearance, as it was mentioned in [Frolov, 1996; Frolov et al, 1997a; Frolov et al., 2002]. So, optimal radiation power of the DW should be selected directly during the period of measurements taking into account the formulated tasks, schedules of the PW radiation and ionospheric conditions.

In the present paper we restricted ourselves by the analysis of the results of experiments with additional heating at the stage of stationary development of the d-SEE intensity. However, the existing experimental data shows that the dynamics of the d-SEE development and relaxation can demonstrate significant variations from pulse to pulse of the PW radiation. This effect takes place if the additional heating is produced by the confined sequence of powerful radio pulses, or when the PW pulses are radiated at different stages of the d-SEE evolution after the DW is turned on. Such measurements are closely connected with the exploration of nature of different

aftereffects which cause the determinative influence on the observed phenomena for pulse durations of the PW $\tau_p \geq 1$ s. That is why these measurements are of especial interest. More detailed analysis of the obtained experimental data is beyond the scope of the present paper and will be given in subsequent publications. With the aim to demonstrate the effects of gyroharmonics and the influence of suprathermal electrons on the BUM generation we have briefly discussed in the presented paper some experimental results concerning the case when the DW frequency is close to the gyroharmonic of electrons. We did not touch the results of measurements when the PW frequency was close to the harmonic of the electron gyrofrequency and the characteristics of the AIT excited by the PW demonstrated strong variations at small changes of its magnitude. This, quite naturally, influenced the variations of the d-SEE intensity. The analysis of the obtained data requires a special approach and will be carried out in separate publications. In particular, such measurements make it possible to split pondermotive and thermal mechanisms of the AIT generation and, hence, to consider more in detail the mechanisms of acceleration of electrons, as it was demonstrated, for example, in [Bernhard et al., 2000; Kosch et al., 2002].

Taking into account the data obtained in the last years concerning the influence of additional heating on the AIT properties, it is planned to perform new experiments with the utilization of the X-mode powerful waves for the additional heating (X-heating). In this case the resonance interaction of the PW with plasma is excluded and, hence, a possibility appears to investigate some other mechanisms of the AIT generation (e.g. connected with the ohmic heating of the ionosphere and the generation of large-scale irregularities due to the self-focusing instability, *etc*). The experiments carried out at the heating facility SURA have shown, that the effects observed at the X-heating have complicated and not completely clear nature [Frolov et al., 1999]. In these experiments it was shown that the effects observed at the X-heating manifest themselves also at the O-mode pumping. Though in this case it is more difficult to distinguish such effects at the background of stronger perturbations appearing as a result of parametric instabilities. Nevertheless, their presence can also cause influence on the development of interaction of powerful wave with plasma.

In conclusion it should be mentioned that in the investigation of interaction of powerful radio wave with plasma of the F-region an important problem is the determination of the electro dynamical influence of the conducting E-layer on the processes in the ionosphere. This is one of the new directions of our investigations. The interest to this problem is stimulated by the experimental results obtained in the last time. These results allow us to assume that the F-region modification can cause the appearance of turbulence in the E-region and vice versa, the characteristics of plasma at the heights of E-region can influence the AIT properties excited in the upper ionosphere. Some of these results were mentioned in [Frolov et al., 2004a]. However, for the exploration of the nature of the discussed phenomena more detailed experimental investigations are required that encompass large amount of related problems.

Acknowledgments

The work was supported by the Russian Foundation for Basic Research (grant 05-02-16493), INTAS (grant 03-51-5583), and CRDF (grant PRO-1334-NO-02).

References

Bakhmet'eva, N.V., Yu.A. Ignat'ev, S.A. Dmitriev, and P.B. Schavin (1992), Observation of backscattering from artificial disturbed region at the frequency 1.68 MHz, *Geomagn. Aeron*. (in Russian), *32*, 180.

Berezin, I.V. et al., (1991), Diagnostics of excitation of plasma oscillations by powerful radio wave, *Geomagn. Aeron*. (in Russian), *31(5)*, 874.

Bernhardt, P.A., M Wong, J.D. Huba, B.J. Fejer, L.S. Wagner, J.A. Goldstain, G.A. Selcher, V.L. Frolov, and E.N. Sergeev (2000), Optical remote sensing of the thermosphere with HF pumped artificial airglow, *J. Geophys. Res., 105(A5)*, 10657.

Bernhardt, P.A., J.D. Huba, E. Kudeki, R.F. Woodman, L. Condori, and F. Villanueva (2001), Lifetime of a depression in the plasma density over Jicamarca produced by space shuttle exhaust in the ionosphere, *Radio Sci., 36(5)*, 1209.

Boiko, G.N. et al., (1985), Investigation of radio waves defocusing in the ionosphere under the action of powerful radio waves, *Izv. VUZov Radiofizika*, (in Russian), *28(8)*, 960.

Boiko, G.N., L.M. Erukhimov, and V.L. Frolov (1990), Excitation of small-scale irregularities near the reflection level of the pump wave, *Geomagn. Aeron.* (in Russian), *30*(6), 998.

Egorov, C.V., A.V. Kostrov, and A.V. Tronin (1988), Thermodiffusion and solenoidal currents in magnetized plasma, *Pis'ma JETP* (in Russian), *47*, 86.

Erikhimov, L.M., S.A. Metelev, N.A. Mityakov, and V.L. Frolov (1978), Hysteresis phenomenon at the artificial excitation of irregularities in the ionospheric plasma, *Izv. VUZov Radiofizika* (in Russian), *21(12)*, 1738.

Erukhimov, L.M., S.A. Metelev, N.A. Mityakov, and V.L. Frolov (1982), Experimental investigation of the striction parametric instability in the ionosphere, *Izv. VUZov Radiofizika* (in Russian), *25(5)*, 490.

Erukhimov, L.M., S.A. Metelev, N.A. Mityakov, E.N. Myasnikov, and V.L. Frolov (1987), Artificial ionospheric turbulence (Review), *Izv. VUZov Radiofizika* (in Russsian), *30(2)*, 208.

Erukhimov, L.M., S.A. Metelev, and D.V. Razumov (1988), Diagnostics of ionospheric irregularities with the artificial radio emission. *Radiophys. Quant. Electron. (Engl. Transl.), 31,* 926.

Fialer, P.A. (1974), Field-aligned scattering from a heated region of the ionosphere – observations at HF and VHF, *Radio Sci., 9(11),* 923.

Franz, T.L., M.C. Kelley, and A.V. Gurevich (1999), Radar backscattering from artificial field-aligned irregularities, *Radio Sci., 34(2)*, 465.

Frolov, V.L. (1988), About the problem of anomalous attenuation of radio waves in the disturbed ionospheric region, *Izv. VUZov Radiofizika* (in Russian), *31(10)*, 1164.

Frolov, V.L., G.N. Boiko, S.A. Metelev, and E.N. Sergeev (1994), On the possibility of exploration of the artificial ionospheric turbulence by diagnostic radiation of the ionospheric plasma, *Izv. VUZov Radiofizika* (in Russian), *37(7)*, 909.

Frolov, V.L. (1996), Artificial plasma turbulence in the upper ionosphere excited by powerful HF radiation generated by transmitters situated on the ground. Results of experimental investigations. Doctor thesis, Nizhni Novgorod, 419 p.

Frolov, V.L., S.M. Grach, L.M. Erukhimov, G.P. Komrakov, E.N. Sergeev, B. Thide, and T. Carozzi (1996), Exploration of peculiarities of the board upshifted maximum (BUM) development in the artificial ionospheric turbulence (AIT), *Izv. VUZov Radiofizika* (in Russian), *39(3)*, 352.

Frolov, V.L., L.M. Erukhimov, G.P. Komrakov, E.N. Sergeev, B. Thide, P.A. Bernhardt, L.S. Wagner, J.A. Goldstain, and G.A. Selcher (1997a), On amplification of the BUM generation discovered at the utilization of the scheme of additional heating of ionospheric plasma, *Izv. VUZov Radiofizika* (in Russian), 40(5), 561.

Frolov, V.L., L.M. Erukhimov, S.A. Metelev, and E.N. Sergeev (1997b), Temporal behavior of artificial small-scale ionospheric irregularities: Review of experimental rezults, *J. Atmos. Solar-Terr. Phys., 59(18)*, 2317.

Frolov, V.L., L.M. Erukhimov, L.M. Kagan, G.P. Komrakov, E.N. Sergeev, and P. Stubbe (1998), Two-component nature of the broad upshifted maximum in stimulated electromagnetic emission (SEE) spectra, *Phys. Rev. Lett., 81(8)*, 1630.

Frolov, V.L., L.M. Kagan, E.N. Sergeev, G.P. Komrakov, P.A. Bernhardt, J.A. Goldstein, L.S. Wagner, C.A. Selcher, and P. Stubbe (1999), Ionospheric observations of F-region artificial plasma turbulence, modified by powerful X-mode radio waves, *J. Geophys. Res. 104(A6)*, 12695.

Frolov, V.L., E.N. Sergeev, E.N. Ermakova, G.P. Komrakov, and P. Stubbe (2001), Spectral features of stimulated electromagnetic emissions, measured in the 4.3 – 9.5 MHz pump wave frequency range, *Geophys. Res. Lett., 28(16)*, 3103.

Frolov, V.L., Sergeev, E.N., and P. Stubbe (2002), Exploration of transport processes in the Earth's upper ionosphere with the help of artificial ionospheric turbulence created by the beam of powerful radio waves, *Izv. VUZov Radiofizika* (in Russian), *45(2)*, 121.

Frolov, V.L., and E.N. Sergeev (2004a), Effects observed under modification of semitransparent sporadic E layer of the ionosphere by powerful radio emission, *International J. Geomagnetism and Aeronomy, 4(3)*, 221.

Frolov, V.L., E.N. Sergeev, G.P. Komrakov, P. Stubbe, B. Thide, M. Waldenvik, E. Veszeley, and T.B. Leyser (2004b), The pondermotive narrow continuum (NC_p) component in stimulated electromagnetic emission spectra, *J. Geophys. Res., 109*, A07304, doi:10.1029/2001JA005063.

Frolov, V.L., E.N. Sergeev, B. Thide, and E.A.Shorokhova (2005a), Experimental exploration of the effects observed at the nonlinear interaction of two powerful radio waves in magnetized plasma, *Izv. VUZov Radiofizika* (in Russian), *48(2)*, 110.

Frolov, V.L., D.I. Nedzvetskii, E.N. Sergeev, and P. Stubbe (2005b), About the properties of the thermal narrow continuum component in the spectrum of stimulated electromagnetic emission, *Izv. VUZov Radiofizika* (in Russian), *48(12)*, 1013.

Frolov, V.L., G.P. Komrakov, D.I. Nedzvetskii, V.O. Rapoport, E.N. Sergeev, E.A. Schorokhova, and P Stubbe (2006), About effects observed under the action of powerful

short pulses on the Earth's upper ionosphere, *Izv. VUZov Radiofizika* (in Russian), (accepted for publication).

Ganguly, S., and W.E. Gordon (1983), Heater enhanced topside plasma line, *Geophys. Res. Lett., 10(10)*, 977.

Golubyatnikov, G.Yu., S.V. Egorov, A.V. Kostrov, V.A. Mironov, and Yu.V. Chugunov (1988) Investigation of special dynamics of heating and thermodiffusion of plasma, *Plasma Physics* (in Russian), *14(4)*, 482.

Grach, S.M. (1985), Electromagnetic radiation from artificial ionospheric plasma turbulence, *Radiophys. Quant. Electron., (Engl. Trans.), 28*, 470.

Grach, S.M., N.A. Mityakov, and V.Yu. Trakhtengerz (1986), Acceleration of electrons and additional ionization at the parametric heating of plasma, *Plasma Physics* (in Russian), *12(6)*, 693.

Grach, S.M., M.M. Shvarts, E.N. Sergeev, and V.L. Frolov (1998), Broad continuum feature of stimulated electromagnetic emission. *J. Atmos. Solar-Terr. Phys., 60(12)*, 1233.

Grach, S.M., E.N. Sergeev, A.M. Nasyrov, R.I. Gumerov, R.R. Shaimukhametov, I.A. Nasyrov, and G.P. Komrakov (2004), Simultaneous observations of the 557.7 nm airglow and stimulated electromagnetic emission during HF pumping of the ionosphere with diagnostic schedule: first results, *Adv. Space Res., 34*, 2422.

Gumerov, R.I., V.B. Kapkov, G.P. Komrakov, and A.M. Nasyrov (1999), Artificial airglow of the ionosphere at short-term action of powerful radiation, *Izv. VUZov Radiofyzika* (in Russian), *42(6)*, 524.

Gurevich, A.V. (1978), *Nonlinear phenomena in the ionosphere*, 370 pp., N-Y.: Springer.

Gurevich, A.V., Ya.S. Dimant, G.M. Milikh, and V.V. Vas'kov (1985), Multiple acceleration of electrons in the regions of high-power radio-wave reflection in the ionosphere, *J. Atmos. Terr. Phys., 47(11)*, 1057.

Gurevich, A.V., H. Carlson, A.V. Lukyanov, and K.P. Zybin (1997), Parametric decay of upper hybrid plasma waves trapped inside density irregularities in the ionosphere, *Phys. Lett. A, 231*, 97.

Gurevich, A.V., K.P. Zybin, and H. Carlson (2005), Effect of magnetic zenith, *Izv. VUZov Radiofizika* (in Russian), *48(9)*, 772.

Hedberg, A., H. Derblom, B. Thide, H. Kopka, and P. Stubbe (1983), Observations of HF backscatter associated with the heating experiment at Tromso, *Radio Sci., 18*, 840.

Hedberg, A., H. Derblom, G. Hamberg, B. Thide, H. Kopka, and P. Stubbe (1986), Measurements of HF backscatter cross section for striations created by ionospheric heating at different power levels, *Radio Sci., 21(1)*, 117.

Ignat'ev, Yu.A. (1978), About the action of artificial heating of ionosphere on irregularity structure of the E-region, *Izv. VUZov Radiofizika* (in Russian), *21(3)*, 352.

Kagan, L.M., and V.L. Frolov (1996), Significance of field-aligned currents for F-region perturbation, *J. Atmos. Terr. Phys., 58(13)*, 1465.

Kosh, M.J., M.T. Rietveld, A.J. Kavanagh, C. Davis, T.K. Yeoman, F. Honary, and T. Hagfors (2002), High-latitude pump-induced optical emissions for frequencies close to the third electron gyro-harmonic, *Geophys. Res. Lett., 29(23)*, 2112, doi:10.1029/2002 GL015744.

Kurina, L.E. (1998), About thermodiffusion effects at the heating of electrons in magnetized plasma by the HF field of an electromagnetic source, *Plasma Physics* (in Russian), *24(10)*, 937.

Leyser, T.B., B. Thide, M. Waldenvik, S. Goodman, V.L. Frolov, S.M. Grach, A.N. Karashtin, G.P. Komrakov, and D.S. Kotik (1993), Spectral structure of stimulated electromagnetic emission between electron cyclotron harmonics, *J. Geophys. Res., 98(A10)*, 17597.

Leyser, T.B., B. Thide, M. Waldenvik, E. Veszelei, V.L. Frolov, S.M. Grach, G.P. Komrakov (1994), Downshifted maximum features in stimulated electromagnetic emission spectra, *J. Geophys. Res., 99(A10)*, 19555.

Leyser, T.B. (2001), Stimulated electromagnetic emissions by high frequency electromagnetic pumping of the ionospheric plasma, *Space Sci. Rev., 98*, 223.

Nasyrov, A.M. (1991), *Scattering of radio waves by anisotropic ionospheric irregularities* (in Russian), 149 pp., Kazan University Press.

Sergeev, E.N., V.L. Frolov, G.N. Boiko, and G.P. Komrakov (1998), Results of investigation of the evolution of the Langmuir and upper hybrid resonance plasma turbulence with the help of artificial radio emission from the ionosphere, *Izv. VUZov Radiofizika* (in Russian), *41(3)*, 313.

Sergeev, E.N., S.M. Grach, G.P. Komrakov, V.L. Frolov, P. Stubbe, B. Thide, T.B. Leyser, and T. Carozzi (1999a), Influence of small-scale irregularities on characteristics of the overshoot-effect in the evolution of artificial radio emission from the ionosphere. Part I.The development stage, *Izv. VUZov Radiofizika* (in Russian), *42(7)*, 619.

Sergeev, E.N., S.M. Grach, G.P. Komrakov, V.L. Frolov, P. Stubbe, B. Thide, T.B. Leyser, and T. Carozzi (1999b), Influence of small-scale irregularities on characteristics of the overshoot-effect in the evolution of artificial radio emission from the ionosphere. Part II. The relaxation stage, *Izv. VUZov Radiofizika* (in Russian), *42(8)*, 810.

Stubbe, P., A.J. Stocker, F. Honary, T.R. Robinson, and T.B. Jones (1994), Stimulated electromagnetic emission and anomalous HF wave absorption near electron gyroharmonics, *J. Geophys. Res., 99A*, 6233.

Stubbe, P., and T. Hagfors (1997), The Earth's ionosphere: A wall-less plasma laboratory, *Surveys in Geophys., 18*, 57.

Tereshchenko, E.D., B.Z. Khudukon, A.V. Gurevich, K.P. Zybin, V.L.Frolov, E.N. Myasnikov, N.V. Muravieva, and H.C. Carlson (2004), Radio tomography and scintillation

studies of ionospheric electron density modification caused by a powerful HF-wave and magnetic zenith effect at mid-latitudes, *Physics Letters A, 325*, 381.

Thide, B., H. Kopka, and P. Stubbe (1982), Observations of stimulated scattering of a strong high-frequency radio wave in the ionosphere, *Phys. Rev. Lett., 49*, 1561.

Trakhtengerz, V.Yu., V.O. Rapoport, E.N. Ermakova, G.P. Komrakov, P.A. Bernhardt, L.S. Wagner, and J.A. Goldstein, (1995), Artificial radio emission in the regime of two-frequency heating of the ionosphere, *Geomagn. Aeronom*., (in Russian), *35(6)*, 117.

Utlaut, W.F., and E.J. Violette (1974), A summary of vertical incidence radio observations of ionospheric modification, *Radio Sci., 9(11)*, 895.

Vas'kov V.V., and A.V. Gurevich (1973), Parametric excitation of the Langmuir oscillations in the ionosphere under the action of strong radio waves, *Izv. VUZov Radiofizika* (in Russian), *16(2)*, 188.

Vas'kov, V.V., Ya.S. Dimant, N.A. Ryabova, V.V. Klimenko, and L.M. Duncan (1992), Thermal perturbations in the magnetospheric plasma at the resonant heating of the ionospheric F-layer by the field of powerful radio wave, *Geomagn. Aeronom*., (in Russian), *32(5)*, 140.

Voskoboinikov, S.P., I.Yu. Gurvich, and V.A. Rozhanskii (1989), Non-one-dimensional diffusion in magnetic field, *Plasma Physics* (in Russian), *15(7)*, 828.

Yampolski, Yu.M., V.S. Beley, S.B. Kascheev, A.V. Koloskov, V.G. Somov, D.L. Hysell, B. Isham, and M.C. Kelley (1997), Bistatic HF radar diagnostics induced field-aligned irregularities, *J. Geophys. Res., 102(A4)*, 7461.

Zabotin, N.A., A.G. Bronin, G.A. Zhbankov, V.L. Frolov, G.P. Komrakov, N.A. Mityakov, and E.N. Sergeev (2002), On an anomalous attenuation of extraordinary waves in ionosphere heating experiments. *Radio Sci., 37(6)*, 1102, doi:10.1029/2000RS002609.

Zhilinskii, A.P., and L.D. Tsendin (1980), Collisional diffusion of partly ionized plasma in magnetic field, *Sov Phys. Uspekhi* (in Russian), *131(3)*, 341.

INTERNATIONAL JOURNAL OF GEOMAGNETISM AND AERONOMY
VOL. 5, GI1007, doi:10.1029/2003GI000059, 2004

Ionospheric effects of the magnetic storm on 18–22 August 2003 according to the data of HF sounding of the artificial ionospheric turbulence

V. P. Uryadov[1], G. G. Vertogradov[2], V. G. Vertogradov[2], A. A. Ponyatov[1], and V. L. Frolov[1]

Received 23 December 2003; revised 18 May 2004; accepted 17 June 2004; published 28 July 2004.

[1] The results of the experimental studies of the influence on the HF signals characteristics of the artificial ionospheric turbulence (AIT) created by the impact on the ionosphere of the powerful radioemission of the heating facilities SURA (Nizhny Novgorod region of Russia) are presented. The measurements were conducted on 18–22 August 2003 in the evening time (1600–2000 UT) at the linearly frequency modulated (LFM) sounding paths: Khabarovsk–Rostov on Don, Irkutsk–Rostov on Don, and Inskip (England)–Rostov on Don and also at the Moscow–Rostov on Don path by the reception of signals of the RVM precise time stations. It was found that at the presence of a strong sporadic E layer at the Irkutsk–SURA path, there appeared the conditions for the SW signal propagation through the upper ionosphere at the frequencies exceeding the maximum usable frequency of the standard hop-like propagation through the F region. The presence of these signals was detected by descending of radio waves from F region altitudes to the Rostov-on-Don reception point due to their scatter at artificial small-scale magnetically oriented irregularities. Using the measurements of the Doppler shift of the frequency of the signals scattered at AIT, ionospheric effects of the magnetic storm occurred in the period of the experiment were studied. It is shown that during the magnetic storm the electric field and irregularity drift velocity at F-region heights over the SURA facility reached values of $\sim$8.6 mV m^{-1} and 186 m s^{-1}, respectively, that is, the values typical for the high-latitude ionosphere. The relation of the quasiperiodic oscillations of the Doppler frequency of the scattered signal to propagation of magnetohydrodynamics waves excited during a magnetic storm is considered. *INDEX TERMS:* 2403 Ionosphere: Active experiments; 2471 Ionosphere: Plasma waves and instabilities; 2431 Ionosphere: Ionosphere/magnetosphere interactions; *KEYWORDS:* Artificial ionospheric turbulence; Heating facilities SURA; Ionospheric effects of the magnetic storm.

Citation: Uryadov, V. P., G. G. Vertogradov, V. G. Vertogradov, A. A. Ponyatov, and V. L. Frolov (2004), Ionospheric effects of the magnetic storm on 18–22 August 2003 according to the data of HF sounding of the artificial ionospheric turbulence, *Int. J. Geomagn. Aeron., 5,* GI1007, doi:10.1029/2003GI000059.

1. Introduction

[2] Long-distance propagation of HF radio waves in various geophysical conditions has been considered in a large number of publications [see, e.g., *Gurevich and Tsedilina*, 1979; *Kravtsov et al.*, 1979, and references therein]. The interest in the problem is due, on one hand, to the needs of practical HF radiocommunication and over-horizon radiolocation and, on the other hand, to abilities to study the formation mechanisms of short-wave field at long-distant paths in quiet and disturbed ionosphere. Under natural conditions, there are considerable difficulties in the study of the mechanisms of HF long-distant propagation due to the uncontrolled influence of many factors on the signal characteristics. The total effect of this influence may lead to a very complicated picture of the field formation. We mention here such factors as the presence of the sporadic E layer, traveling ionospheric disturbances (TID), localized disturbances in the regions of particle precipitations, etc.

[3] In the mid-1970s, the creation of investigation facilities in Russia and the United States to study the impact on the ionospheric plasma by powerful decameter radioemission made it possible to study mechanisms of long-distance HF propagation in controlled conditions. This considerably sim-

[1]Radiophysical Research Institute, Nizhny Novgorod, Russia
[2]Rostov on Don State University, Rostov on Don, Russia

1524–4423/04/2003GI000059$18.00

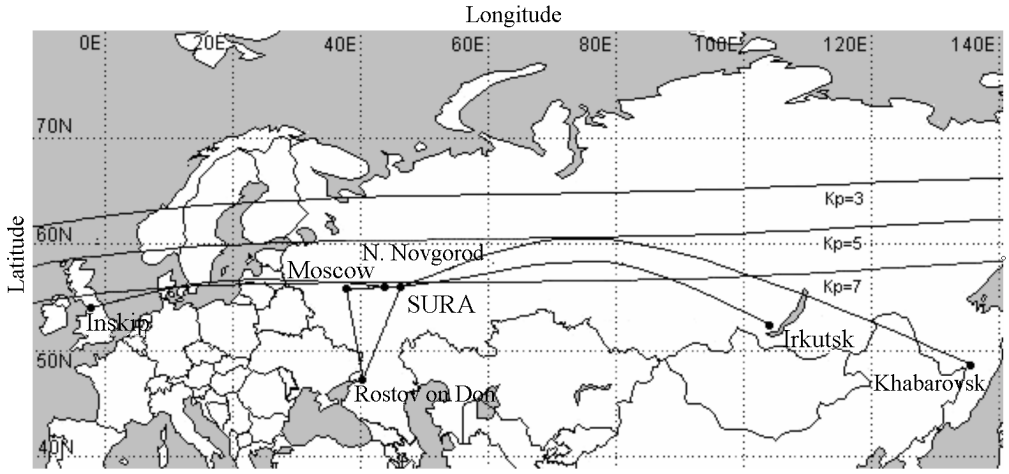

Figure 1. Geometry of the radio paths during the experiment on 18–22 August 2003.

plified the problem of separation and identification of various propagation modes. The first experiments on controlling long-distance HF propagation both at fixed frequencies [*Getmantsev et al.*, 1976] and in the wide frequency band of a linearly frequency modulated (LFM) sounder [*Uryadov et al.*, 1995] showed the efficiency of leading radio waves out of the ionospheric wave channel (IWC) due to the scattering at artificial small-scale magnetically oriented irregularities. In these experiments the heating facilities were used to create controlled disturbances at heights of the ionospheric channel. With the development of the national and global network of LFM sounders, it became possible to carry out wide-scale studies of the impact of artificial ionospheric turbulence (AIT) on short-wave propagation.

[4] In this paper the new results of the study of the AIT influence on the radio wave propagation are presented. The results were obtained using the national and foreign LFM sounders. The AITs were created by the impact on the ionospheric F region of the field of powerful radio waves emitted by the SURA heating facility (Vasil'sursk town, Nizhny Novgorod region, Russia). The diagnostics of AIT was performed by a bistatic Doppler HF radar. The AIT properties were controlled by the artificial radioemission of the ionosphere (ARI). For the properties of ARI, see *Frolov et al.* [2001, and references therein].

[5] The experiment was conducted in the period of a magnetic storm. The storm began on 17 August 2003; its various phases covered the entire period of observations. The magnetic storm considerably influenced the results of the experiment. There are a relatively small number of AIT studies in the conditions of magnetic-ionospheric disturbances, and these studies have been conducted mainly on the basis of the heating facilities in Tromsö [*Blagoveshchenskaya et al.*, 1999]. The results of our experiment showed that the HF sounding can be an effective tool of diagnostics of the ionospheric effects of a magnetic storm at F-region heights in the midlatitude ionosphere.

2. Description of the Experiment

[6] The experiment was carried out on 18–22 August 2003 from 1600 to 2000 LT (LT = UT + 4 hours). The following radio paths were used: Khabarovsk (the geographic coordinates are φ = 47.5°N, λ = 134.5°E) to Rostov on Don (φ = 47.3°N, λ = 39.7°E), Irkutsk (φ = 51.8°N, λ = 104°E) to Rostov on Don and Inskip (England, φ = 53.8°N, λ = 2.8°W) to Rostov on Don. To perturb the ionosphere by powerful HF radioemission, heating facility SURA (φ = 56.1°N, λ = 46.1°E) was used. The facility operated in the following regime: 5 min of emission and 5 min of pause starting from the beginning of each hour. The ordinary polarization wave was emitted at the frequency of the pumping wave f_p close to the critical frequency of the ionosphere f_oF2 ($f_p \leq f_oF2$).

[7] The effective emission power PG was 40 or 80 MW depending on the working frequency f_p. To control the radio wave condition at the Khabarovsk–SURA, Irkutsk–SURA, and Inskip–SURA paths, the reception of LFM signals at the paths Khabarovsk–Nizhny Novgorod (φ = 56.1°N, λ = 44.1°E), Irkutsk–Nizhny Novgorod, and Inskip–Nizhny Novgorod was organized. The LFM sounders in Irkutsk and Khabarovsk operated the first and the second halves of each hour, respectively. The emission of the LFM signals started at 0, 5, 10, ... 55 min of each hour with the following parameters: starting frequency 4 MHz, end frequency 30 MHz, and rate of the frequency returning 100 kHz s^{-1}. On 20 August 2003 when the LFM sounders in Irkutsk and Khabarovsk did not operate, the emission of the LFM sounder from England (Inskip) was received. This sounder operated in the 5-min regime starting from the second minute of each hour with the following parameters: starting frequency 4.2 MHz, end frequency 30 MHz, and rate of the frequency returning 100 kHz s^{-1}. The LFM signals in the Rostov-on-Don reception point were received by the oblique V antenna ori-

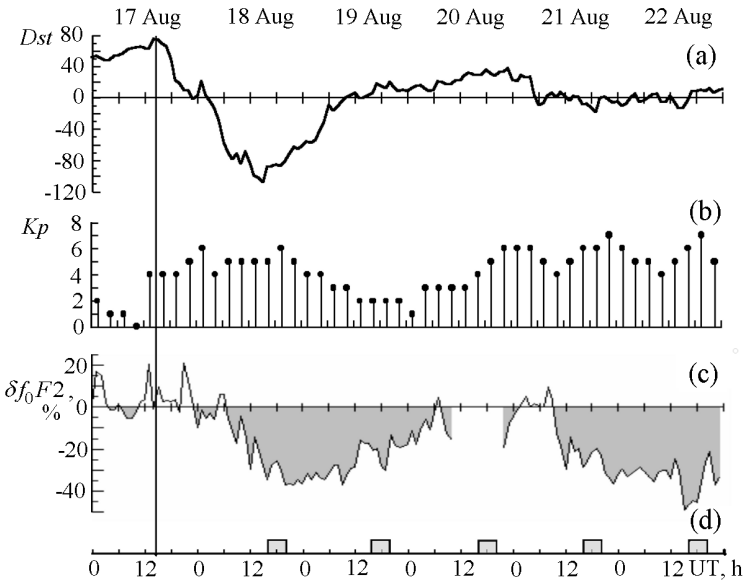

Figure 2. Time behavior of the geomagnetic indices (a) Dst and (b) Kp, (c) relative variations of the f_oF2 critical frequency at the Khabarovsk station and (d) observation intervals on 17–22 August 2003. There are no vertical sounding data at the Khabarovsk station from 1100 to 2000 UT on 20 August 2003.

ented to the SURA heating facility. The same antenna was used to receive the etalon signals of the RVM station at a frequency of 9996 kHz. The RVM transmitter operated in a regime of continuous emission of the carrier from 0 to 8 s and from 30 to 38 s of every hour. During the operation of the SURA facility the RVM transmitter was used as a Doppler HF radar at the RVM sounding path Moscow ($\varphi = 55.3°$N, $\lambda = 38.7°$E) to SURA–Rostov on Don for diagnostics of artificial small-scale magnetically oriented irregularities. In the Nizhny Novgorod reception point the LFM signals were received using the vertical collapsible whip. The geometry of the experiment is shown in Figure 1.

3. Results of the Experiment and Simulation

[8] It has been already mentioned that the experiment was carried out on 18–22 August 2003. This period was characterized by a complicated geophysical situation. Figures 2a and 2b show the time behavior of the geomagnetic indices Dst and Kp, respectively, for the period of the experiment (the data have been obtained from the World Data Center (http://www.wdc.ac.uk)).

[9] The observation intervals are shown in Figure 2e by the cross-hatched rectangles. According to the common classification the storm sudden commencement (SSC) in the form of a sharp increase of Dst at 1400 UT on 17 August 2003 is shown in Figure 2 by vertical line. The maximum value of the Dst variations amplitude equal to −108 nT was registered at 1500 UT on 18 August 2003. On 19–20 August 2003 the Dst variations lied within 0–35 nT. Then on 21 and 22 August the Dst value began to decrease again but slightly, with the maximum Dst amplitude equal to 18. The maximum values of the Kp index during the magnetic storm were 6–7. The detailed picture of the behavior of the horizontal (H) and vertical (Z) component of the magnetic field and the declination D according to the data of the Tromsö ($\varphi = 69.66°$N, $\lambda = 18.9°$E) station for 17–22 August 2003 are shown in Figure 3 (the data have been obtained from http://geo.phys.uit.no/). The beginning of the magnetic disturbance at 1430 UT on 17 August is clearly manifested by the sharp jump of H, Z, and D components of the magnetic field. After that, deep variations of the magnetic field were observed till 0500 UT on 19 August. Later, they changed to relatively smooth variations in its components till 1300 UT on 20 August and then again an increase of strong variations in the geomagnetic field occurred and continued till 23 August.

[10] The magnetic storm in a significant way influenced the conductions of the experiment and its results. For example, from 1600 to 2000 LT on 18 August the critical frequencies of the ionosphere in the SURA facility location were below a frequency of 4.3 MHz, which is the least working frequency of the facility emission. That is why on this day the facility did not operate, and in the reception points, HF signals were received only in the presence of natural ionospheric disturbances. It is known from previous observations that during a magnetic storm, there occurs a broadening of the auroral oval into the midlatitude region. Thin curves in Figure 1 show the position of the equatorial boundary of the auroral oval in the Eurasian longitudinal sector for various values of the Kp index (the data have been obtained from http://sec.noaa.gov). This event was accompanied by an increase in the intensity of the total electron content variations

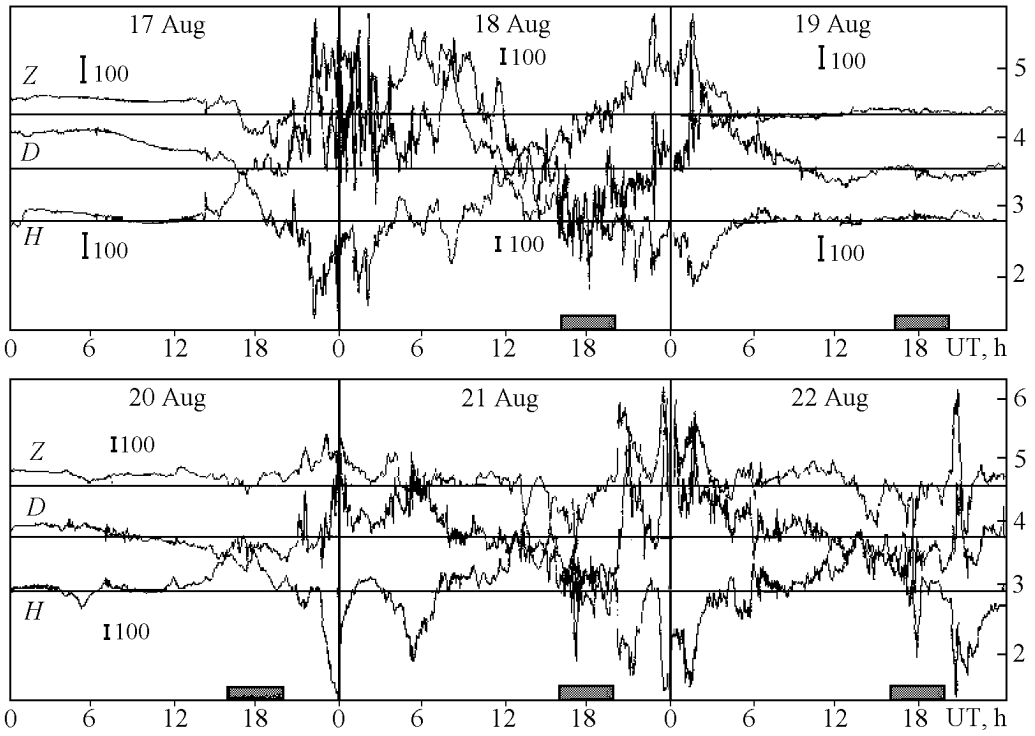

Figure 3. Time behavior of the vertical (Z) and horizontal (H) components of the geomagnetic field and declination (D) for the Tromsö ($\varphi = 69.66°$N, $\lambda = 18.9°$E) on 17–22 August 2003 (the data were obtained at http://geo.phys.uit.no/). The cross-hatched intervals correspond to the time of observations.

[*Afraimovich et al.*, 2003], an increase in the intensity of the small-scale irregularities at middle latitudes responsible for the backscatter of radio waves [*Zherebtsov et al.,* 2002], a depletion of the f_oF2 critical frequency, and an increase of the short-wave absorption in the lower ionosphere [*Brunelly and Namgaladze*, 1988].

[11] The ionospheric effect of the magnetic storm is clearly seen in Figure 2c where the deviations of the f_oF2 critical frequency ($\delta f_oF2(\%) = 100[f_oF2 - \{f_oF2\}]/\{f_oF2\}$) measured at Khabarovsk station on 17–22 August 2003 from the quiet mean values for 11–16 August 2003 are shown. Figure 2c shows that the first phase of the f_oF2 negative disturbance began at 0700 UT on 18 August and the decrease in the critical frequency reached 30–37% in the afternoon of 18 August and in the morning of 19 August. The time of the delay of the maximum deviation of δf_oF2 in the main phase of the magnetic storm on 18 August relative to the maximum magnitude of the Dst index (−108 nT) was 4 hours. The recovery phase began approximately at 2000 UT on 19 August and lasted to 0900 UT on 21 August. Then a secondary strong negative disturbance began with the maximum deviation δf_oF2 reaching 45–49%. The decrease of the maximum usable frequency (MUF), increase in the absorption, and scatter of radio waves during the magnetic storm in the strongest way were manifested at the oblique LFM sounding paths Khabarovsk–Nizhny Novgorod, Irkutsk–Nizhny Novgorod, Khabarovsk–Rostov on Don, and Irkutsk–Rostov on Don. The MUF at these paths decreased by 25–30% and the lower usable frequencies (LUF) increased and that led to a considerable narrowing of the frequency range of the decameter wave channel as compared to quiet conditions.

[12] The most visual effect of the AIT influence on the remote HF propagation was obtained on 19 August at the Irkutsk–SURA–Rostov on Don path. It was manifested in the appearance of an extra signal at frequencies above the maximum observed frequency (MOF) of the F region in the frequency band ∼3–4 MHz during the operation of the heating facility. It is important to note that in this period fairly strong signal was received because of the reflection from the E_s layer with the maximum observed frequency of ∼23–24 MHz. Its appearance could have also been related to ionospheric effects of the storm development. Figures 4a–4d show the sequence of ionograms at the Irkutsk–Rostov on Don paths obtained at 1720–1720 UT on August 19 during the facility operation (with the beginning at 0 and 10 min) and the pause (with the beginning at 5 and 15 min).

[13] The extra signal appearing during the facility operation is marked in Figures 4a and 4b by SS (scattered signal). Figure 4 shows that SS was observed in the frequency interval ∼14–18.5 MHz, whereas MUF at the propagation via the ionospheric F region by the standard hop way was ∼14 MHz. In the pause, there was no scattered signal because its occurrence is due to the radio wave scatter at artificial small-scale irregularities, their lifetime in quiet ionospheric conditions not exceeding a few tens of seconds [*Erukhimov et al.*, 1987]. The ionograms with the scattered signal during the SURA operation were observed from 1700 to 2000 UT on 19 August. On 21 August when the E_s layer was absent at

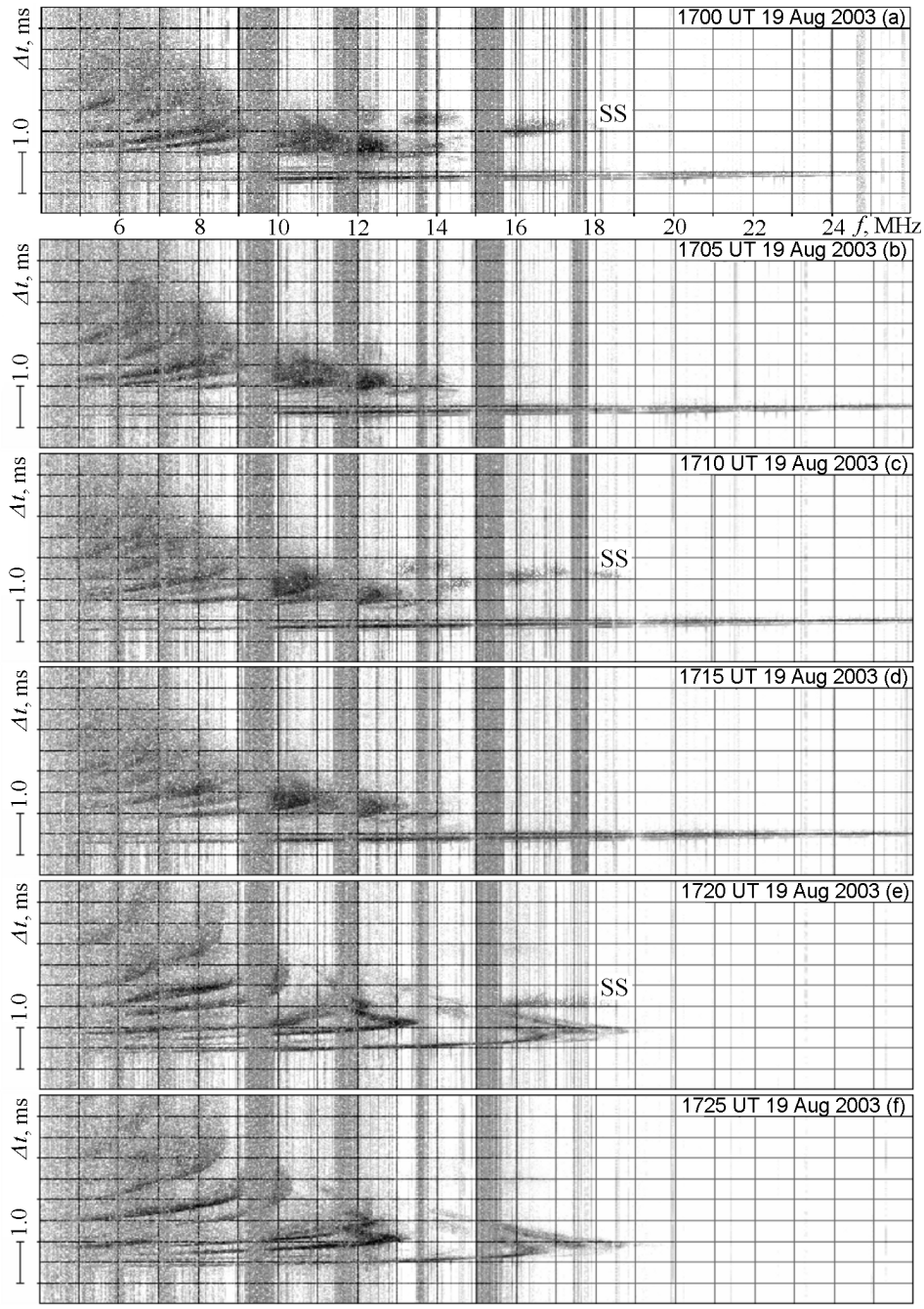

Figure 4. Ionograms of oblique LFM sounding at the Irkutsk–Rostov on Don path: (a, c, and e) during the operation of the SURA heating facilities and (b, d, and f) during the pause. SS is the scattered signal.

the Irkutsk–Nizhny Novgorod and Irkutsk–Rostov on Don paths, the scattered signal was observed during the heating facility operation at the frequencies below MUF for the F region. This situation is shown in Figures 4e and 4f during the facility operation and in the pause, respectively.

[14] During the operation of the LFM sounders at Khabarovsk and Inskip, no extra (scattered) signals (the appearance of which might have been related to the SURA facility) were observed. The most probable cause of that is a small power of these transmitters (200 W in Khabarovsk and 100 W in Inskip) as compared with 1.5 kW of the Irkutsk transmitter.

[15] This factor is especially significant in observation periods with magnetic and ionospheric disturbances when the radio wave absorption at oblique sounding paths increases considerably and the intensity of the scattered signal is be-

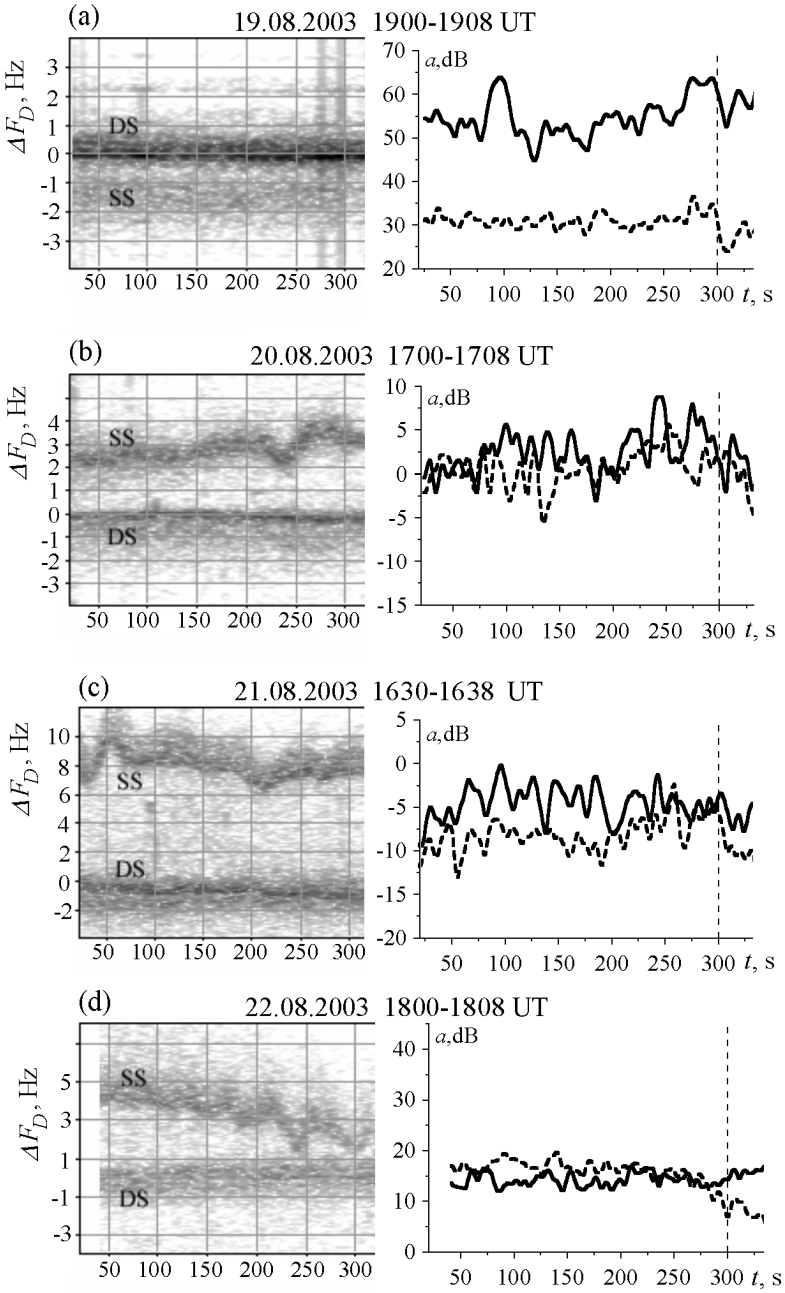

Figure 5. Time dependence of the (left) Doppler frequency shifts and (right) amplitudes of the main (DS) and scattered (SS) propagation modes. The signals of the RVM station at a frequency of 9996 kHz were received in Rostov on Don during the heating of the ionosphere and after its end (300 s after the session beginning). The solid and dashed lines on the right show the main (direct) and scattered signals, respectively. The dashed vertical lines (right) show the time of switching off the heating transmitter.

low the sensitivity threshold of the receiving equipment.

[16] The diagnostics of AIT by the aspect scatter of radio waves was conducted using the bistatic Doppler HF radar at the Moscow–SURA–Rostov on Don path with the reception in Rostov on Don of the standard signals of the precise time RVM signals at a frequency of 9996 kHz. The method of registration and processing of Doppler spectra was described by *Vertogradov et al.* [1994]. Figure 5 (left) shows examples of the variations in the frequency Doppler shift during the operation of the heating transmitter and after its switching off in the conditions of relatively quiet ionosphere (19 August) and during the magnetic storm (20–22 August). The direct and scattered signals are marked as DS and SS, respectively. Figure 5 (right) shows the dependence of the

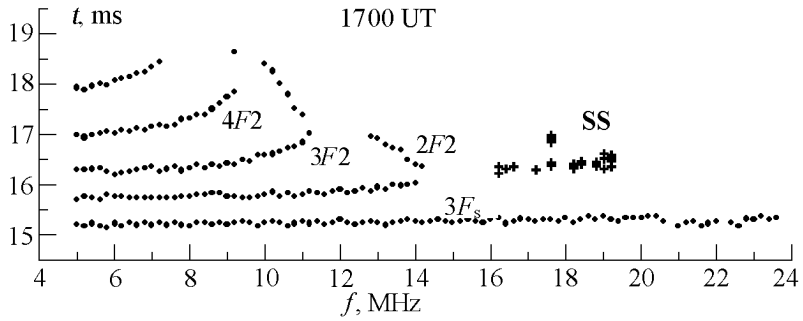

Figure 6. Synthesized ionogram of the oblique sounding at the Irkutsk–Rostov on Don path calculated with taking into account the sporadic E layer and the scattering at artificial small-scale magnetically oriented irregularities generated by the powerful emission of the SURA heating facility. SS is the scattered signal.

amplitudes of the direct and scattered signals on time during the heating and after its end. The dashed vertical lines in Figure 5 (right) show the moments of switching off of the heating transmitter (300 s from the session beginning). Figure 5 (left) shows that the sonograms of the Doppler spectra of the scattered signals obtained in different geophysical conditions differ significantly from each other. For example, in the session at 1900 UT on 19 August (Figure 5a) the Doppler frequency shifts for the direct and scattered signals are close to each other: the difference is ∼1.2 Hz, so the Doppler spectrum of DS is overlapped on the Doppler spectrum of SS. In this case the dependence of the amplitudes on time helps in separating the direct and scattered signals. Figure 5a (right) shows that the amplitude of the scattered signal decreases after the switching off the SURA facility, this fact being caused by the relaxation of scattering irregularities. A similar picture is seen for other sessions shown in Figures 5b–5d (right). Figures 5b–5d (right) show that during the 3 min after the switching off of the heating transmitter the scattered signal did not disappear completely. The latter shows that during geomagnetic disturbances the relaxation time of artificial small-scale irregularities increases. Three minutes after switching off the heating transmitter the sounding transmitter RVM was switched off. That is why we could not follow the evolution of the scattered signal till its complete relaxation after switching off the heating transmitter.

[17] In the period of the magnetic substorm on 20–22 August the Doppler shift of the frequency (DSF) of the scattered signal reached values of ∼8–10 Hz (see Figure 5c, left). It is worth noting that in the magnetically disturbed period sporadically appearing trains of quasiperiodic modulation of DSF of the scattered signal with a period of ∼40–60 s and amplitude reaching 2 Hz (see Figures 5b–5d, left) were observed. In some cases both general increase of DSF (Figure 5b, left) and its depletion (Figure 5d, left) were observed. No quasiperiodic variations were observed in the Doppler spectrum of the scattered signal on a relatively quiet day (19 August, see Figure 5a). It should be noted that no such variations were registered also in the Doppler spectrum of the direct signal in all the days of observation.

[18] Using the Doppler measurements for the bistatic location of the HF radar, one can determine the drift velocity of the irregularities responsible for the aspect scattering of radio waves in the direction orthogonal to the magnetic field along the bisecting line of the angle formed by the directions from the scatter region to the transmitter and receiver of the sounding signal [*Uryadov and Ponyatov*, 2003]:

$$V_{\mathrm{dr}} = (\lambda \Delta F_D)/2 \sin(\theta_s/2) \tag{1}$$

where λ is the wavelength, ΔF_D is the Doppler frequency shift, and θ_s is the scattering angle.

[19] For the given geometry of the location of the radar, depending on the sign of the Doppler frequency shift either southwest (an azimuth A ∼234°) or northeast (A ∼54°) components of the irregularities drift velocity were measured. The estimates show that in the relatively quiet ionosphere (on 19 August) the northeast component of the irregularities velocity was measured and was found equal to ∼20 m s^{-1}. During the magnetic storm (20–22 August) the measured direction of the drift velocity was changed to the southwest one and the velocity magnitude increased up to 186 m s^{-1}, that is up to the values typical to the high-latitude ionosphere [*Boguta et al.*, 1989; *Scali et al.*, 1995]. The evaluations of the electric field based on the velocity of the $\mathbf{E} \times \mathbf{B}$ drift show an increase of the values of the electric field in the upper ionosphere from ∼1 mV m^{-1} in quiet conditions up to ∼8.6 mV m^{-1} during the magnetic storm. The analysis of the experimental data was performed taking into account simulation of radio wave propagation and their scattering at magnetically oriented irregularities concentrated in the region of the interaction of the pumping wave to the ionospheric plasma. The simulation showed that the key role in appearance of the extra signal at frequencies above MUF of the F region at the Irkutsk–SURA path was played by a strong sporadic E layer. Figure 6 shows a synthesized ionogram at the Irkutsk–SURA–Rostov on Don path calculated with the help of the International Reference Model (IRI) taking into account the Es layer at the Irkutsk–SURA path (this part of the path was controlled by the reception of LFM signals in Nizhny Novgorod where ionograms with the propagation mode via E_s were also registered) and the scatter at artificial small-scale magnetically oriented irregularities generated in the upper ionosphere by the powerful emission of the SURA facilities.

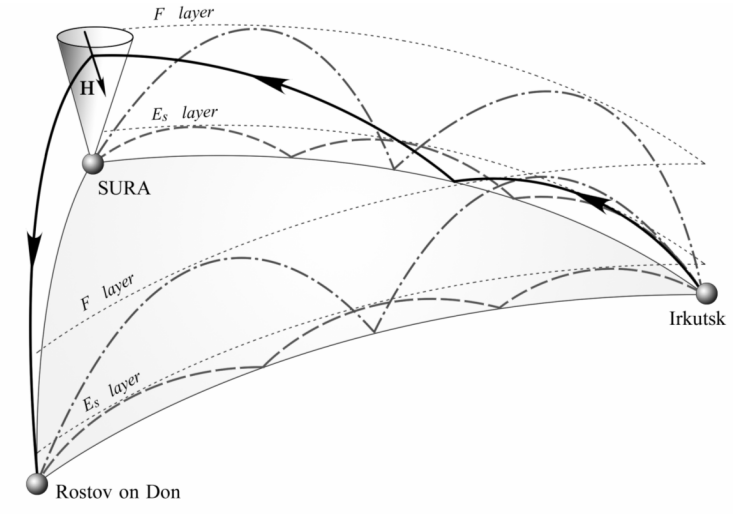

Figure 7. Ray trajectories at the LFM sounding paths.

[20] Comparison of Figures 4a, 4b, and 6 shows their good agreement. The calculations of the ray trajectories (see Figure 7) in the presence of the sporadic E layer show that the trajectories propagating at the first hop via E_s at frequencies above MUF for the F layer are realized at the Irkutsk–SURA path. At the second hop, part of the radio wave energy soaks through the E_s layer and reaches heights of the F region over the SURA heating facility. From there the radio waves are descended to the Earth surface due to the aspect scatter at the artificial small-scale magnetically oriented irregularities. It should be noted that the mechanism of radio wave capturing into the IWC at frequencies above MUF of the F region by other processes (in particular, by the negative gradient of the electron concentration ne) is not realized at this path. The latter is confirmed by the data obtained on 21 August when no E_s layer was observed and in the absence of considerable horizontal gradients of ne the scattered signal at the Irkutsk–SURA–Rostov on Don path was observed at the frequencies below MUF (see Figure 4e).

4. Discussion

[21] The studies showed that the wide-band oblique sounding of the modified ionospheric region with artificially created small-scale irregularities is an effective tool for studies of mechanisms of propagation and formation of the HF signal field. For example, for the first time at a long-distant midlatitude path in the absence of considerable horizontal gradients of the electron concentration the determining influence of the sporadic E layer on formation in the upper ionosphere of the radio wave field propagating at frequencies exceeding MUF (of the standard hop mechanism via the F region) was shown. It is evident that to obtain more complete data on the AIT influence on the remote propagation of short radio waves a continuation of the studies in various geophysical conditions is needed.

[22] As for the diagnostics of the artificial ionospheric turbulence by the method of aspect scattering of testing HF signals, the relation of the characteristics of the Doppler spectrum of the scattered signals to the magnetic activity level was established. According to the data obtained, in relatively quiet ionospheric conditions, DSF of SS is ∼0 to ±2 Hz, and there are no quasiperiodic variations in DSF. During the magnetic storm DSF reached values of ∼8–10 Hz, and sporadic trains of quasiperiodic variations in DSF with the period of ∼40–60 s and the amplitude modulation of ∼0.5–2 Hz were registered.

[23] To interpret the experimental data, the data on the solar wind and interplanetary magnetic field (IMF) were used because it is known [*Nishida*, 1980] that variations of these parameters play the key role in the development of a magnetic storm. Figure 8 shows for the period of the experiment the behavior of the solar wind V, B_z component, latitudinal (θ) and azimuth (φ angles of IMF (in the solar-ecliptic coordinate system), and the electromagnetic power of the solar wind (ε) incoming into the magnetosphere (the data were taken from the Advanced Composition Explorer (ACE) satellite Web site http://hiraiso.crl.go.jp/). Figure 8 shows that at approximately 1340 UT on 17 August, a jump of the wind velocity and the magnitude of the B_z component occurred. This sharp increase may be identified with the shock wave and its impact on the magnetosphere. At 0100 UT on 18 August, there occurred a sharp change of the orientation of the IMF B_z component from the northward to the southward and this level of the B_z magnitude (about −17 nT) stayed till 0600 UT. Simultaneously, the rate of the energy income into the magnetosphere ε strongly increased up to 8 TW. The second increase of ε but with lower values of ∼1–3 TW occurred from 1600 UT on 20 August to 1600 UT on 22 August. It is known [*Blagoveshchensky and Zherebtsov*, 1987] that when the IMF B_z component turns southward, the large-scale convection electric field is intensified and this leads to a generation of magnetospheric substorms. The effect of the main phase of the magnetic storm was manifested in strong variations of the geomagnetic field in Tromsö and negative disturbance of the critical frequency in Khabarovsk

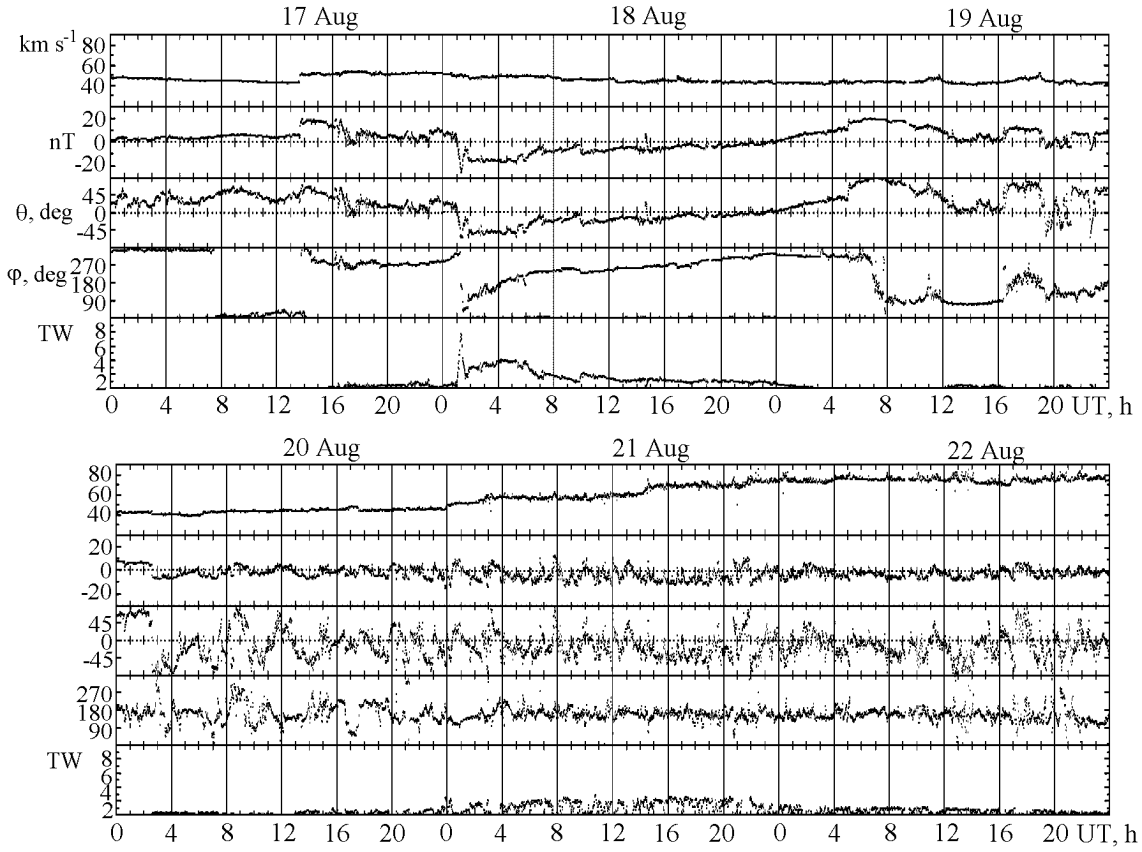

Figure 8. Variations of the solar wind and interplanetary magnetic field parameters (V is the wind velocity, B_z is the IMF southward component, θ is the latitudinal angle, φ is the azimuth angle, and ε the electromagnetic energy of the solar wind incoming to the magnetosphere in terawatts (1 TW = 1019 erg s^{-1}) during the magnetic storm on 17–22 August 2003). The data were obtained from the Advanced Composition Explorer (ACE) satellite data (available at http://hiraiso.crl.go.jp/).

(see Figures 2 and 3). After 0600 UT on 18 August the southward component of B_z smoothly decreased and since 0000 UT on 19 August changed sign to the northward direction ($B_z > 0$). Approximately from 1920 UT on 19 August and later on 20, 21, and 22 August there occurred numerous changes of the B_z component sign from the northward to southward and back. This might have generated a sequence of magnetospheric substorms [*Brunelly and Namgaladze*, 1988]. The change of the B_z sign was also manifested in the behavior of the magnetic field in Tromsö and variations of the critical frequency in Khabarovsk. The variations of the IMF vector rotation southward and back northward and also of the magnitude of the southward component ($B_z < 0$) itself were accompanied by variations of the value of the latitudinal angle θ which on 20–22 August fluctuated within the $\pm 45^\circ$ interval with a small shift toward negative values. Comparing Figures 8 and 3, one can see a correlation of the variations in the geomagnetic field components in Tromsö to the changes of the solar wind electromagnetic energy power incoming into the magnetosphere and also to the behavior of the IMF B_z component. The southward direction of the latter ($B_z < 0$) determines a development of magnetospheric disturbances. Figures 2c and 8 show that the negative disturbance of the electron concentration correlates well (but with some delay) to the same parameters.

[24] During a magnetic storm a formation of the magnetosphere–ionosphere current systems occurs, causing an increase of the electric fields at ionospheric heights. It is worth noting here that according to the *Basu Sun et al.* [2001] data the magnetospheric electric fields penetrating into middle latitudes during a magnetic storm may be responsible for the ionospheric effects, leading to fluctuations of the total electron content and blinking of radio signals of navigation satellite systems. According to our data obtained on the basis of the measurements of HF signals scattered at artificial small-scale magnetically oriented irregularities the electric field at F-region heights increased during the magnetic storm up to the values of $\sim$8.6 mV m^{-1} as compared

with the value of ∼1 mV m^{-1} in quiet conditions. This led to the increase of the irregularities drift velocity up to values of ∼186 m s^{-1} typical for the high-latitude ionosphere. The trend (close to a linear one) in the form of the DSF increase (Figure 5b, left) and DSF decrease (Figure 5d, left) may be due to the variations in the electric field vector (both by the magnitude and direction) at F-region heights during the development and recovery phases of the ionospheric effects of the magnetic storm.

[25] The occurrence of trains of quasiperiodic variations in DSF of the HF signals in the magnetically disturbed period manifests a presence of wave processes in the region containing artificial small-scale irregularities. Since at the scattering at strongly stretched magnetically oriented irregularities ($L_\parallel \gg L_\perp$, where $L_\parallel$ and $L_\perp$ are the scales of the irregularities along and across the magnetic field, respectively) only the component of the drift velocity perpendicular to the magnetic field is measured [*Nasyrov*, 1991], one can conclude that the wave processes responsible for the DSF variations have the lateral to the geomagnetic field lines component of charged particle motion. This effect may be caused by the lateral magnetohydrodynamics waves playing the determining role in the activity of the natural pulsations of the geomagnetic field [*Gul'el'mi and Troitskaya,* 1973].

[26] The problems of registration and interpretation of the quasiperiodic variations in DSF of the testing signal scattered at the artificial small-scale magnetically oriented irregularities were considered by *Sinitsin et al.* [1999] and *Blagoveshchenskaya and Troshichev* [1996]. *Sinitsin et al.* [1999] considered the relation of the DSF variations to the plasma drift in the electric field of the geomagnetic pulsations. *Blagoveshchenskaya and Troshichev* [1996] considered the influence of the traveling ionospheric disturbances generated by powerful decameter radioemission of the heating facility or caused by the natural acoustic gravity waves on the Doppler measurements results.

[27] By they periodicity (∼40–60 s) the observed variations in DSF are close to the geomagnetic pulsations of the Pc3–4 type and also to the irregular oscillations of the Pi2 type [*Saito,* 1969]. It should be noted that the quasiperiodic variations in DSF were not observed on 19 August at the recovery phase under positive value of the IMF B_z component. At the same time on 20, 21, and 22 August when IMF had almost radial direction (the azimuth angle φ was $\sim 180^\circ$ and the latitudinal angle θ fluctuated around 0°, that is, numerous reorientation of the B_z component from the southward to the northward directions took place) quasiperiodic oscillations of DSF of the scattered signal were registered. In the same way the activity of trains of the Pi2 geomagnetic pulsations is manifested. The pulsations are usually generated during a magnetospheric substorm. Its expansion phase is preceded by reorientation of the IMF B_z component from the northward to southward direction [*Gul'el'mi and Troitskaya*, 1973]. The energy coming in from the solar wind in the reconnection process on the daytime side of the Earth and also the energy of the magnetic field in the magnetosphere tail released in the reconnection process may be the energy sources of the magnetic pulsations.

[28] Assuming that the quasiperiodic pulsations of the DSF of the scattered signal are due to the wave processes related to the propagation of the lateral MHD waves generated during a magnetic substorm, we evaluate the magnetic field variations providing the observed values of the Doppler oscillations amplitudes. For the lateral oscillations of the field lines frozen into the plasma the relation between the plasma motion velocity and variations of the magnetic field in the linear approximation is given by the following expression [*Frank-Kamenetsky*, 1964]:

$$\delta\nu \simeq \delta H/(4\pi\rho)^{1/2} \tag{2}$$

where $\rho = \Sigma m_i N_i$ is the plasma density, and m_i and N_i are the ion mass and concentration, respectively.

[29] At heights of the F region, ions of atomic oxygen predominate, i.e., $n_e \sim N_i \sim N(\mathrm{O}^+)$ [*Fatkullin et al.,* 1981]. From equations (1) and (2) for the values $\lambda = 3 \times 10^3$ cm, $\delta F_D = 1 - 2$ Hz, and $N(\mathrm{O}^+) = 5 \times 10^5$ cm^{-3} we obtain $\delta H \sim (0.6 - 1.2)$ nT. Such values of the amplitudes of the geomagnetic field pulsations agree with the experimental data [*Gul'el'mi and Troitskaya*, 1973]. Some trains of the quasiperiodic variations in the geomagnetic field with an amplitude of a few tens of nanoteslas registered in Tromsö one can see, for example, in Figure 3 on 22 August within the 0700–0800 UT interval. Comparing the experimental and calculated values of the geomagnetic field, one should introduce a correction for the different location of Tromsö (69.66°N) and the SURA facility (56.1°N). According to *Saito* [1969] the pulsation amplitudes increase with latitude. The performed calculations and the data comparison are of an estimation character. A detailed comparison requires magnetogram recordings with high amplitude and temporal resolution directly in the vicinity of the SURA facility. To confirm the mechanism of quasiperiodic oscillations of the Doppler spectrum of the scattered signal related to propagation of the MHD waves generated during a magnetic substorm, coordinated radiophysical studies of AIT combined with measurements of the geomagnetic pulsations in the place of location of the heating facility are needed.

[30] At the same time, the data available on the relation of the variations in the DSF of the scattered signal to the geophysical situation in the period of the experiment indicate to the natural source of the MHD waves responsible for the quasiperiodic oscillations of the Doppler frequency shift of the scattered signal observed during the magnetic storm.

5. Conclusions

[31] 1. Ionospheric effects of the magnetic storm determined by the Doppler measurements of the signals scattered by AIT correlate well to the behavior of the southward B_z component of the interplanetary magnetic field and variations in the geomagnetic field on the Earth. It is found that at heights of the F region of the midlatitude ionosphere in undisturbed conditions the electric field and the drift velocity of irregularities corresponded to the typical values ∼1 mV m^{-1} and 20 m s^{-1}, respectively. During the magnetic storm these values increased up to values of

$\sim$8.6 mV m^{-1} and 186 m s^{-1}, respectively, the latter values better corresponding to the values typical for the high-latitude ionosphere.

[32] 2. The comparison of the appearance of sporadic trains of the quasiperiodic variations in DSF of HF signals to the behavior of the interplanetary magnetic field and variations of the magnetic field components on the Earth as well as the estimates of δH of the geomagnetic field based on the Doppler measurements lead to the conclusion that the oscillations of the Doppler shift of the scattered signal frequency are due to the wave processes related to the propagation of lateral magnetohydrodynamic waves intensified during a magnetic storm.

[33] 3. Using the diagnostics of the ionospheric channel with the help of the aspect scattering of radio waves at artificial small-scale magnetically oriented irregularities, the conditions of formation of the HF signal field in the upper ionosphere in the presence of a sporadic E layer are studied. It is demonstrated that at distant paths the E_s layer may play an important role in formation in the upper ionosphere of the radio wave field at frequencies exceeding MUF of the standard hop propagation via the F region of the ionosphere.

[34] In conclusion, we note that in parallel to the measurements of the aspect scatter of radio waves at the magnetically oriented small-scale irregularities of the plasma, in the period from 9 August to 23 August we conducted studies of the characteristics of the artificial radioemission of the ionosphere (ARI) at the reception point located in 1.5 km from the SURA facility. The observation period covered both quiet (before 17 August) and disturbed (18–23 August) ionospheric conditions. A detailed discussion of the results obtained is out of the scope of this paper and will be presented in a separate publication. Here we only mention briefly that according to the preliminary processing of the experimental data obtained, in magnetically disturbed conditions an increase by 4–8 dB in two main components of the emission is detected [*Frolov et al.,* 2001]: DM (downshifted maximum, the main spectral maximum in the ARI spectrum shifted down by 10–15 kHz from the pumping frequency) and BUM (broad upshifted maximum, the wide-band maximum of the emission at frequencies above the pumping wave frequency the generation of which is observed when the frequency of the powerful wave exceeds the frequency of the harmonics of the electron gyrofrequency in the region of its interaction to the ionospheric plasma). This may indicate to a considerable influence of ionospheric disturbances on the conditions (mechanisms) of ARI generation. For more detailed consideration of the nature of such influence we plan in future to conduct new experimental studies.

[35] **Acknowledgments.** The authors thank V. I. Kurkin and S. V. Rosanov for their help in organization the operation of the LFM sounders in Irkutsk and Khabarovsk and for the data of the vertical sounding in Khabarovsk. The work was supported by the Russian Foundation for Basic Research (projects 02-05-64383 and 02-02-17475) and by the grant CRDF-RPO-1334-NO-92.

References

Afraimovich, E. L., O. S. Lesyuta, and I. I. Ushakov (2003), The relation of the auroral oval dynamics, intensity of ionospheric irregularities, and failures in phase measurements in the GPS system, IX International Scientific and Technical Conference "Radiolocation, Navigation, and Communication", Voronezh State University, Voronezh, Russia.

Basu Sun, et al. (2001), Ionospheric effects of major magnetic storms during the International Space Weather Period of September and October 1999: GPS observations, VHF/UHF scintillations, and in situ density structures at middle and equatorial latitudes, *J. Geophys. Res., 106*(A12), 30,389.

Blagoveshchenckaya, N. F., and O. A. Troshichev (1996), Ionospheric phenomena produced by modification experiments, *J. Atmos. Terr. Phys., 58*(1–4), 397.

Blagoveshchenskaya, N. F. et al. (1999), Phenomena observed by HF long-distance tools in the HF modified auroral ionosphere during magnetospheric substorm, *Radio Sci., 34,* 715.

Blagoveshchensky, D. V., and G. A. Zherebtsov (1987), *High-Latitude Geophysical Phenomena and Forecasting of HF Channels* (in Russian), 272 pp., Nauka, Moscow.

Boguta, H. M., Yu. V. Noga, and V. P. Uryadov (1989), Spectral characteristics of HF signals scattered at irregularities of the F region of the sub-polar ionosphere, *Geomagn. Aeron.* (in Russian), *29*(4), 678.

Brunelly, B. E., and A. A. Namgaladze (1988), *Physics of the Ionosphere* (in Russian), 527 pp., Nauka, Moscow.

Erukhimov, L. M., S. A. Metelev, E. N. Myasnikov, N. A. Mityakov, and V. L. Frolov (1987), Artificial ionospheric turbulence, *Radiophysics* (in Russian), *30,* 208.

Fatkullin, M. N. et al. (1981), *Empirical Models of the Midlatitude Ionosphere* (in Russian), 256 pp., Nauka, Moscow.

Frank-Kamenetsky, D. A. (1964), *Lectures on Plasma Physics* (in Russian), 283 pp., Atomizdat, Moscow.

Frolov, V. L. et al. (2001), Spectral features of stimulated electromagnetic emission, measured in the 4.3–9.5 MHz pump wave frequency range, *Geophys. Res. Lett., 28*(16), 3103.

Getmantsev, G. G. et al. (1976), Aspect scattering of HF signals at artificial ionospheric irregularities, *Radiophysics* (in Russian), *19,* 1909.

Gul'el'mi, A. V., and V. A. Troitskaya (1973), *Geomagnetic Pulsations and Diagnostics of the Magnetosphere* (in Russian), 208 pp., Nauka, Moscow.

Gurevich, A. V., and E. E. Tsedilina (1979), *Superdistant Propagation of HF Radio Waves* (in Russian), 249 pp., Nauka, Moscow.

Kravtsov, Yu. A., M. B. Tinin, and Yu. N. Cherkashin (1979), Possible mechanisms of excitation of ionospheric wave channels (a review), *Geomagn. Aeron.* (in Russian), *19*(5), 769.

Nasyrov, A. M. (1991), *Scattering of Radio Waves by Anisotropic Ionospheric Irregularities* (in Russian), 150 pp., Kazan' Univ. Publ. House, Kazan', Russia.

Nishida, A. (1980), *Geomagnetic Diagnosis of the Ionosphere* (in Russian), 299 pp., Mir, Moscow.

Saito, T. (1969), Geomagnetic pulsations, *Space Sci. Rev., 10*(3), 319.

Scali, J. L., B. W. Reinisch, C. J. Heinselman, and T. W. Bullet (1995), Coordinated digisonde and incoherent scatter radar F region drift measurements at Sondre Stromfjord, *Radio Sci., 30*(5), 1481.

Sinitsin, V. G. et al. (1999), Ionospheric conductivities according to Doppler radar observations of stimulated turbulence, *J. Atmos. Sol. Terr. Phys., 61,* 903.

Uryadov, V. P., and A. A. Ponyatov (2003), Over-horizon LFM HF radar for diagnostics of ionospheric irregularities, IX International Scientific and Technical Conference "Radiolocation, Navigation, and Communication", Voronezh State University, Voronezh, Russia.

Uryadov, V. P., N. V. Ryabova, and V. A. Ivanov (1995), The investigation of long-distanse HF propagation on the basis of a

chirp sounder, *J. Atmos. Terr. Phys., 57*(10), 1263.

Vertogradov, G. G., Yu. P. Myatezhnikov, V. P. Uryadov, and S. V. Rozanov (2004), Coordinated experimental evaluation of the characteristics of HF wave propagation at midlatitude paths of different length and orientation, *Radiophysics* (in Russian), *47*(1), 15.

Zherebtsov, G. A. et al. (2002), Irkutsk incoherent scatter radar, *Radiotech. Electron.* (in Russian), *47*(11), 1339.

G. G. Vertogradov and V. G. Vertogradov, Rostov on Don State University, Rostov on Don, Russia.

V. L. Frolov, A. A. Ponyatov, and V. P. Uryadov, Radiophysical Research Institute, 25 Bolshaya Pecherskaya Str., Nizhny Novgorod 603600, Russia.
(vf@nirfi.sci-nnov.ru, ur@nirfi.sci-nnov.ru)